The Molecular Basis of Activity-Dependent Somatosensory Cortex Development

Ruth Fiona Deighton

Presented for the degree of Doctor of Philosophy

The University of Edinburgh

2007

Declaration

This work was carried out in the School of Biomedical Sciences and the Department of Neuroscience at the University of Edinburgh. I have composed this thesis and the work and data presented is my own, except where stated below:

1) Biochemical purification of the PSD and PPW was performed in collaboration with Ruth Phillips, an honours student I supervised in the laboratory.
2) Immunoelectron microscopy (Figures 3.10 and 4.7) was performed in collaboration with Dr Tom Gillingwater.
3) Slice Stimulation experiments were set up in collaboration with Jo Konkel, an MSc student I supervised in the laboratory.
4) Tissue Culture stimulation experiments were set up together with Anne Petrie, another PhD student in the laboratory.
5) The protein phosphorylation screens (Figures 5.6 and 5.7) were performed by Kinexus^{TM} Bioinformatics Corporation.
6) The affymetrix gene array presented in Chapter 5 was performed by a postdoc in Professor Stanley McKnight's laboratory.

The work in this thesis has not been submitted for any other degree or professional qualification.

Ruth F. Watson

February 2007

Acknowledgements

I'd like to say a HUGE thank you to several significant groups of people and individuals that have supported me throughout my PhD. First of all, thank you to all the past and present members of the Kind Lab: Mark Barnett, Louise Dunn, Anne Petrie, Lasani Wijetunge, Mark Hillen, Sally Till and Aoife MacMahon. I've really valued your friendship and willing team spirit over the past three years. I'll certainly never forget the Kind lab – the lab has quite literally scarred me for life as a result of 200mph paintballs!

Secondly, a massive thank you to my principal supervisor Peter Kind, a constant source of encouragement, right from persuading me to do a PhD in 2003 (!), to publishing several papers, and finally submitting this thesis. You've been an inspiration as a scientist and a friend throughout.

Thanks also to my second supervisor Mike Cousins, who has always been willing to help out when needed, and has let me use his laboratory on numerous occasions for performing biochemical fractionations. In addition, thanks to Linda Wilson and Trudi Gillespie for their help capturing images of the barrelfield on the confocal microscope.

And last, but not least, I'd like to say a big thank you to my husband, Matthew and to the rest of my immediate family. Thank you for all of your love and support throughout the ups and downs of PhD life!

Abbreviations

°C	Degrees Celsius
µg	Microgram
µM	Micromolar
5-HT	5-hydroxytryptamine
5-HTT	5-hydroxytryptamine transporter
AC	Adenylyl cyclase
AKAP	A-kinase anchoring protein
AMPA	Alpha-amino-3-hydroxy-5-methyl-4-isoxazolepropionic acid
AS	Anterior Snout
ATP	Adenosine triphosphate
Bp	Base pairs
BSTC	Brainstem trigeminal complex
CamKII	Calcium/Calmodulin-dependent kinase II
cAMP	Cyclic adenosine monophosphate
Cdh	Cadherin
cDNA	Complimentary deoxyribonucleic acid
CNS	Central Nervous System
CO	Cytochrome Oxidase
DAB	Diaminobenzadine
DAG	Diacylglycerol
dH_2O	Deionised water
DIV	Days in vitro
DNA	Deoxyribonucleic acid
dNTP	Deoxynucleoside triphosphates
E	Embryonic day
EM	Immunoelectron microscopy
EPSC	Excitatory postsynaptic current
ER	Endoplasmic reticulum
ERK	Extracellular signal-related kinase
ES	Embryonic stem

G	Gram
g	Gravitational force
GAPDH	Glyceraldehyde-3-phosphate dehydrogenase
GluR	AMPA receptor subunit
H	Homogenate
ION	Infraorbital nerve
IP_3	Inositol 1,4,5-triphosphate
KO	Knockout
LTD	Long Term Depression
LTP	Long Term Potentiation
M	Molar
MAGUK	Membrane-associated guanylate kinase
MAO	Monoamine oxidase
MAPK	Mitogen-activated protein kinase
MeOH	Methanol
Mg	Milligram
mGluR	Metabotrophic glutamate receptor
ml	millilitre
mM	millimolar
MRI	Magnetic Resonance Imaging
mRNA	Messenger ribonucleic acid
NMDA	N-methyl-D-aspartate
NMDAR	N-methyl-D-aspartate receptor
NR	N-methyl-D-aspartate receptor subunit
NRC	NMDA-receptor complex
nVc	Nucleus caudalis
nVi	Nucleus interpolaris
nVo	Nucleus oralis
nVp	Nucleus principalis
OD	Ocular Dominance
P	Postnatal day
PBS	Phosphate buffered saline
PCPA	Parachlorophenylalanine

PCR	Polymerase chain reaction
PFA	Paraformaldehyde
PH	Pleckstrin homology domain
PIP_2	Phosphatidyl inositol 4,5-bisphosphate
PKA	Protein kinase A
PKC	Protein Kinase C
PLC	Phospholipase C
PMBSF	Posteromedial barrel subfield
PP	Protein phosphatase
PPW	Presynaptic particle web
PrV	Principal trigeminal nucleus
PSD	Postsynaptic density
RNA	Ribonucleic acid
rpm	Revolutions per minute
RT-PCR	Reverse transcriptase polymerase chain reaction
S	Synaptosomes
S1	Primary somatosensory
SERT	Serotonin Transporter
SynGAP	Synaptic GTPase activating protein
TCA	Thalamocortical axons
TGC	Trigeminal ganglion cell
TTX	Tetrodotoxin
WT	Wildtype
VMAT	Vesicular Monoamine transporter
VpM	Ventral posterior medial nucleus

Abstract

The murine primary somatosensory cortex (S1) contains discrete cytoarchitectonic units in layer IV called "barrels" that accurately recapitulate the pattern of the mystacial whisker follicles on the facepad. Presynaptic serotonergic and postsynaptic glutamatergic neurotransmission are known to play a crucial role in development of the barrel cortex since mice lacking *Nr1* or *Mglur5* genes fail to form barrels and excessive activation of 5Ht1b receptors disrupts barrel formation. However the intracellular mechanisms by which receptor activation is translated into alterations in neuronal phenotype during cortical development are just beginning to be elucidated. The recent characterisation of the major constituents of the postsynaptic density (PSD) from adult rat forebrains (Walikonis et al., 2000; Husi et al., 2000) has highlighted potential pathways downstream of glutamate receptors (mGluR5 and NMDARs) for mediating cortical development. Targeted molecules are now being screened for a role in barrel development and include Protein Kinase A (PKA) and Synaptic Ras GTPase activating protein (SynGAP).

Mice that lack Adenylyl Cyclase1 (AC1), a Ca^{2+}/calmodulin sensitive adenylyl cyclase that can be regulated by 5HT1B, mGluR and NMDA receptors are "barreless", lacking both TCA and cellular segregation in layer 4. *Adcy1*$^{-/-}$ (*barreless*) mutants also have deficits in LTP/LTD at TCA/layer4 synapses and decreased GluR phosphorylation and association with the PSD (Lu et al., 2003). These results led to the hypothesis that LTP/LTD type synaptic plasticity may be required for barrel development (Lu et al., 2003). cAMP-dependent Protein Kinase A (PKA) is a major downstream target of AC1, implicating a possible role for PKA in barrel development. In Chapter 3, I show that while barrels are present in *Prkar2β*$^{-/-}$ mice, they show significantly reduced cell density ratio between barrel walls and barrel hollows compared to wild-type animals, but normal thalamocortical afferent segregation in the posteromedial barrel subfield. Immunoelectron microscopy confirms that R2β protein is selectively localised to dendrites and dendritic spines. Biochemistry experiments also show that R2β associates with the postsynaptic density in a calcium dependent manner. These data clearly show a role for postsynaptic PKA signaling pathways in barrel development and suggest that PKA may not be the principle target downstream of cAMP generated by adenylyl cyclase

type 1 (AC1). Furthermore *Prkar2β*$^{-/-}$ mice show a defect in GluRA insertion into the PSD of developing TCA synapses, however GluRA, GluRB and GluRC KO mice develop normal barrels, indicating that this process is not necessary for barrel formation. These data suggest that mechanisms of synaptic plasticity can be dissociated from barrel formation.

SynGAP is a Ras GTPase Activating Protein that associates with NMDARs and regulates dendritic development and plasticity (Vasquez et al., 2004; Komiyama et al., 2002). In Chapter 4, I show that *Syngap*$^{-/-}$ mice display defects in barreloid segregation in VpM and only partial segregation of TCAs in layer IV into rows rather than whisker-related patches; layer IV neurons fail to segregate into barrels. *Syngap*$^{+/-}$ mice however display normal barreloid development and TCA segregation, but barrel soma show reduced segregation compared to WT controls. SynGAP is not expressed in brainstem and is not required for barrelette development. Immunoelectron microscopy reveals that in layer 4, SynGAP is selectively expressed in dendrites and postsynaptic densities (PSDs). Moreover SynGAP associates with the PSD in a PSD95-independent manner.

Chapter 5 describes research designed to further elucidate the glutamatergic pathways and cellular processes downstream of PKAR2β- and SynGAP- mediated barrel formation. Several experimental approaches have been evaluated. First, pharmacological manipulation of cortical slices and tissue culture was employed to specifically examine the regulation of extracellular-regulated-kinase (ERK) in PKAR2β and SynGAP mutant mice upon glutamate receptor stimulation. Preliminary results demonstrate that PKAR2β and SynGAP regulate ERK upon glutamate receptor stimulation. Second, the use of large-scale protein phosphorylation screens was investigated to identify downstream targets of PKAR2β. A number of phosphorylation sites are regulated in *Prkar2β*$^{-/-}$ mice and bioinformatics is helping to identify kinases that act at these sites. Third, transcriptional regulation in *Prkar2β*$^{-/-}$ mice was analysed using a commercialised gene array. A list of genes that are regulated in *Prkar2β*$^{-/-}$ mice has been identified and is providing a useful tool for focussing future research into the molecular mechanisms of somatosensory cortical development.

Table of Contents

Chapter 2: Materials and Methods

Chapter 3: The role of PKAR2β in mouse somatosensory cortex development

CHAPTER 1:
Introduction

The mammalian cerebral cortex is arranged into discrete cortical domains that process different aspects of sensation, movement and cognition. The anatomist Korbinian Brodmann was the first to describe this cortical regionalisation (early in the 20th century) when he mapped the human brain according to differences he observed in cellular architecture and proposed that each anatomical "cortical area" would correspond to a unique and specific function. Subsequent research has confirmed Brodmann's anatomical data and functional hypothesis, and has furthered understanding by refining the divisions of anatomical and functional areas using more parameters such as input and output connections, cell size and packing density and distributions of various neurotransmitter receptors. In addition, modern brain imaging techniques such as functional MRI have helped to define the unique functional domains of the cortex.

It is now well established that genetic programs coordinate the establishment of the gross anatomy of these areas, in part, by allowing axons to find their correct pathways and correct targets. But sensory-driven activity plays a crucial role in creating the final synaptic pattern by refining synaptic connections during critical periods in early childhood. Over the last several decades, the role of activity in cortical development has been a focus of intense research. The interest stemmed from the work of Hubel and Wiesel in 1963, who demonstrated that an animal's early visual experience altered the anatomy and physiology of ocular dominance columns in the visual cortex (Wiesel & Hubel, 1963a,b). It has now become clear that many anatomical and functional features of the developing cortex can be permanently and extensively modified during sensitive periods early in development in response to activity.

Recent advances in molecular and biochemical techniques have permitted the elucidation of the molecular basis of experience dependent developmental plasticity. Model systems commonly used to study this aspect of neuronal development and plasticity, include hippocampal long-term-potentiation (LTP) and long-term-depression (LTD), ocular dominance (OD) columns in the visual system and "barrels" in the rodent somatosensory cortex. The rodent primary somatosensory (S1) cortex is the focus of all the experiments presented in this thesis. It is an

excellent system for studying the role of neural activity in differentiation of the neocortex because it displays unique cytoarchitectonic modules in layer 4 of S1 that allow for easy assay of the effects of manipulating individual genes. In this introductory chapter I will first briefly review embryonic cortical development. I will then focus on organisation of the rodent somatosensory cortex and will discuss the role of neural activity and more specifically the postsynaptic second messenger pathways downstream of glutamate neurotransmission that are involved in barrel development.

1.1 Development of the Neocortex

1.1.1 Corticogenesis

The brain originates from embryonic ectoderm that thickens at approximately embryonic day 7.5 (E7.5) in mice and rats (all steps occur slightly earlier in mice than rats) to form the neural plate. The neural plate then invaginates by E11 to form the neural tube. Even before the posterior portion of the tube is closed, the most anterior portion of the neural tube undergoes rapid cell proliferation and expansion into three primary vesicles: forebrain (prosencephalon), midbrain (mesencephalon), and hindbrain (rhombencephalon). Subsequently the prosencephalon is subdivided into two secondary vesicles: the diencephalon, which develops into the thalamus, epithalamus, hypothalamus, retina and optic tracts, and the telencephalon, which gives rise to the cerebral cortex, hippocampus, amygdala, basal ganglia and olfactory lobes (Gilbert, 2000; Price and Wilshaw, 2000). More specifically the dorsal telencephalon develops into the neocortex, paleocortex (piriform cortex) and archicortex (hippocampus), while the ventral telencephalon differentiates into the basal ganglia (Bayer & Altman, 1991; Price & Wilshaw, 2000; Gotz & Sommer, 2005)

Most neurons of the mouse cerebral cortex are generated in the ventricular zone of the lateral ventricle between E12 and E17. The ventricular zone is an epithelial layer of progenitor cells that are undergoing cell division. When the first postmitotic

neurons leave the cell cycle, they accumulate below the pial surface and form a new layer called the preplate. Then subsequent precursor neurons migrate out from the ventricular zone to form the cortical plate, which splits the preplate into the superficial marginal zone and a deep subplate (reviewed by Rice and Curran, 2001). Two populations of progenitor cell are important in neurogenesis: [1] radial glial cells (apical progenitors) (Malatesta et al, 2000; Parnavelas & Nadarajah, 2001; Gotz et al., 2002) and [2] basal progenitors (Guillemot, 2005). Radial glial cells appear early in neurogenesis (E12-E13 in the mouse) and give rise, directly or indirectly by generating basal progenitors, to most projection neurons of the cerebral cortex. Most radial glial cells divide asymmetrically at the ventricular surface and generate a radial glial cell and either a neuron, which migrates through the intermediate ventricular zone (IVZ) into the cortical plate (CP), or a basal progenitor, which moves to the subventricular zone (SVZ) and divides symmetrically to generate two neurons (Guillemot, 2005). The cortical plate gradually differentiates as more neurons are "born" from the ventricular zone and becomes organised into well-defined layers in a deep to superficial, or "inside-out" manner (Gilles & Price, 1993). Cells that migrate from the ventricular zone and exit the cell cycle at early stages in neurogenesis give rise to neurons that settle in the deepest layers of the cortex, layers 6 and 5. In contrast, cells that leave the ventricular zone and exit the cell cycle at progressively later stages migrate over longer distances, past early-born neurons, and settle in more superficial layers of the cortex, layers 4, 3 and 2 respectively. The marginal zone cells then form layer 1 (Gilles & Price, 1993). This migration of neurons to their appropriate destinations takes place over a period of several days, beginning at approximately E14 in the mouse and continuing throughout the first postnatal week of postnatal life, when barrels develop (described later in section 1.2.2).

It is now known that the above scheme of corticogenesis and radial migration only applies to pyramidal neurons, the excitatory projection cells of the neocortex (Parnavelas, 2000; Chan et al., 2001; Anderson et al., 2002). Most GABAergic cortical interneurons arise in the ganglionic eminence (GE), the primordium of the basal ganglia in the ventral telecephalon (Anderson et al., 1997, 2002; Lavdas et al., 1999; Wichterle et al., 2001). Tracer-labeling studies have shown that these

interneurons round the corticostriatal notch and follow multiple tangentially orientated paths to enter the cortex (Nadarajah & Parnavelas, 2002; Marin & Rubenstein, 2003). Most interneurons traverse through the intermediate zone (IZ), but some subsets of neurons migrate through the MZ or at the interface of SVZ and IZ (Nadarajah et al., 2002). Recent research has also shown that subsets of interneurons actively migrate towards the cortical VZ upon reaching the dorsal telencephalon, a process that has been termed 'ventricle-directed migration' (Nadarajah et al., 2002). Real-time imaging has shown that these interneurons migrate into the cortical VZ, pause and then resume radial migration in the direction of the pial surface to reach their final destinations in the cortical plate (Nadarajah et al., 2002). This ventricle-directed migration is currently hypothesised to be a method by which these cells can seek information, possibly relating to their laminar fate, from the cortical VZ.

1.1.2 Cortical Lamination

The adult mouse neocortex consists of six distinct layers that are defined by cell density and cell morphology (McConnell, 1995). The layered organisation of the cortex aids function and provides an efficient way of organising the inputs and outputs of neocortical neurons (Kandel et al., 2000). For example neurons in different layers of the neocortex project to different parts of the brain (corticocortical connections arise primarily from neurons in layers 2 and 3, and projections to subcortical regions arise mainly from layers 5 and 6). The layers are generated in an inside-out pattern during development (as described above; section 1.1.1) with a strong correlation between a neuron's birthday and its normal laminar position. This close correlation between cell birthday and laminar fate has enabled transplantation studies to analyse the timing of commitment to specific laminar phenotypes during development. Transplantation of early progenitors, normally destined to give rise to layer 6 neurons, into the brains of older hosts at the time of upper-layer neurogenesis has revealed that the laminar fate of early progenitors is determined just prior to a neuron's final mitotic division within the ventricular zone (McConnell and Kaznowski, 1991). Progenitors transplanted early in the cell cycle, during S-phase, are multipotent, generating neurons that migrate to the upper cortical layers together

with the host neurons. In contrast, progenitors transplanted late in the cell cycle, shortly before mitosis, remain committed to migrating to layer 6 in the older host brains (McConnell and Kaznowski, 1991). This restriction in laminar fate potential occurs over time in a progressive manner (Desai and McConnell, 2000).

Several regulatory genes such as Tbr-1, SCIP, Id2, Otx1 and Otx2 are also expressed in specific layers during development and are thought to play a role in controlling cortical lamination (Bulfone et al., 1995; Frantz et al., 1994; Neuman et al., 1993). Furthermore, cell surface and extracellular molecules including cadherins, semaphorins, Eph receptors and ephrin ligands and chondroitin and heparan sulfate proteoglycans have been found to be expressed in a lamina-specific fashion postnatally and might account for some of the molecular differences between layers that result in the termination of thalamocortical afferents that provide input to the cortex (Suzuki et al., 1997; Redies et al., 1993; Skaliora et al., 1998; Polleux et al., 1998; Donoghue & Rakic, 1999; Mackarehtschian et al., 1999; Oohira et al., 1994; Watanabe et al., 1996).

1.1.3 Cortical Regionalization

Cortical regionalization is determined by a combination of intrinsic and extrinsic factors. Several studies have shown that during embryonic development, broad cortical regions are intrinsically created by gene gradients or restricted expression of area-specific genes. These genes include locally secreted molecules such as Wnts 2b, 3a, 5a and 7a, Shh, Fgf8 and BMPs 2, 4, 6 and 7, adhesion molecules such as LAMP, Latexin, Cadherin 6 and Cadherin 8, and transcription factors such as Emx1, Emx2, Tbr1 and Pax6 (Lopez-Bendito and Molnar, 2003). The involvement of distinct gene expression patterns has been demonstrated in part by altering or abolishing the normally graded expression of signaling molecules and transcription factors across the cortical surface (Bishop et al., 2000, 2002, 2003; Fukuchi-Shimogori and Grove, 2001, 2003; Hamasaki et al., 2004). For example, the transcription factors Emx1 and Emx2 are normally expressed in high caudomedial to low rostrolateral gradients in the neocortex, and the transcription factor Pax6 is expressed in an opposing low caudomedial to high rostrolateral gradient. Loss of

Emx expression results in a caudomedial shift of cortical areas and loss of Pax6 results in a contrasting rostrolateral shift (Bishop et al., 2000). In addition a study by Fukuchi-Shimogori and Grove (2001) provided direct evidence for the secreted signaling molecule Fgf8 in patterning the neocortex. Electroporation mediated gene transfer was used to express Fgf8 in varying amounts and in ectopic locations in mouse embryos, and then barrelfield location was assessed in postnatal mice. The expansion or reduction of endogenous Fgf8 source in the anterior telencephalon shifted the barrel field posteriorly or anteriorly, respectively. Furthermore a second Fgf8 source introduced into the posterior cortical primordium, resulted in a mirrored duplication of the somatosensory barrelfield (Fukuchi-Shimogori and Grove, 2001). Studies of Mash1 and Gastrulation Brain Homeobox 2 (Gbx2) knockout mice (Miyashita-Lin et al., 1999; Hevner et al., 2002; Wassarman et al., 1997) have also supported the notion that the cortex is regionalized in part, early in neurogenesis. Neither Mash1, or Gbx2 are expressed in neocortex, but mice that lack these genes fail to develop correct thalamocortical projections to the cortex. However although cortices from Mash1 and Gbx2 knockouts lack thalamic innervation, general cortical regionalization develops normally at least defined by regional boundary markers such as Cad6, Cad8, Cad11, Emx1, Lhx2 and Id2.

There is also evidence however that cortical regionalization is induced by innervation of afferent thalamocortical axons (TCAs) (Creutzfeld, 1977). For example, barrels do not form in the cortex unless thalamocortical afferents innervate the cortex with appropriate patterning. Additional evidence comes from experiments where presumptive embryonic (E17-18) rat visual cortex was grafted onto P0 somatosensory cortex, and patterned afferents from the host thalamus induced the grafted tissue to develop characteristics of somatosensory cortex (Schlaggar and O'Leary, 1991). These transplantation experiments by Schlaggar and O'Leary (1991) have frequently been cited as a definitive demonstration of pluripotentiality in the developing cortex. However many other experimenters have carried out similar transplantation techniques and have found ambiguous and contradictory results. For example, Alla Katnelson from our laboratory repeated the transplantation experiment in mice and observed re-specification in only three out of one hundred and twenty four (2.4%) transplants that exhibited good graft integration (Katnelson, 2002). In

addition, work from the laboratory of Michel Roger, (Ebrahimi-Gaillard et al., 1994; Ebrahimi-Gaillard and Roger, 1996; Garnier et al., 1997; Frappe et al., 1999; Gaillard and Roger, 2000), that used similar transplantation techniques as those employed by the O'Leary group, repeatedly demonstrated results that were contradictory to the results of Schlaggar and O'Leary (1991). Roger and colleagues showed that embryonic tissue (E16) heterotopically transplanted into neonatal animals maintains the characteristics of its site of origin, based on projections to and from the explant (Gaillard and Roger, 2000). Furthermore, based on their results, the Roger laboratory suggests that a moderate degree of cortical area specification exists by E16, even with respect to orientation (mediolateral versus lateromedial) within a single cortical area (Garnier et al., 1995). However cortical progenitors can change their fate upon heterotopic transplantation at E12 (Gaillard et al., 2003). Interestingly, Garnier et al., (1995) found a very small percentage of cases in their transplantation work (E16) where the tissue re-specified; however, the majority did not and they concluded that the identity of the tissue was largely unchangeable by the time of transplantation. It is interesting to note that while Schlaggar and O'Leary (1991) stated they performed the procedure on eight litters of rat pups, they did not state how many of those animals formed barrels. In summary, all of the above transplantation experiments suggest that re-specification of cortical tissue is actually quite limited in the late stages of embryonic development and that broad areal specification is determined, at least in part, early on in development. However, as previously mentioned, barrels cannot form in the cortex unless thalamocortical afferents innervate the cortex. Therefore, it is likely that more specific specialisation of cortical areas does require thalamic input.

1.2 The rodent barrel cortex and trigeminal neuraxis

Thomas Woolsey and Hendrik Van der Loos (1970) were the first to describe the unique structure and organisation of the mouse primary somatosensory cortex (S1). Discrete cytoarchitectonic units called "barrels" are found in layer 4 of mouse S1 that represent individual facial vibrissae on the sensory periphery in an isomorphic relationship. In nissl stained sections cut tangential to the pial surface, barrels are

seen as cell-dense rings (barrel "walls") that surround cell-sparse regions (barrel "hollows"). Also individual barrels are clearly separated by relatively acellular areas (barrel "septa"). In contrast, nissl stained coronal sections (cut perpendicular to the pial surface) depict barrels as cellular columns that span layer 4 and taper at both the top and the bottom. Coronal sections therefore reveal the three-dimensional nature of barrels and the bowed cylinder shape that originally led to the term barrel being used to describe their anatomy (Woolsey & Van der Loos, 1970). The posteromedial barrel subfield (PMBSF) is a subdivision of S1 that receives input from the main facial vibrissae and has markedly large and well-defined barrels (Woolsey & Van der Loos, 1970). In this region barrels are arranged in a highly organised pattern of five rows that precisely recapitulates the 5 rows of mystacial vibrissae found on the contralateral side of the rodent's snout. Also, each barrel in the PMBSF is connected to a single whisker through subcortical relay stations. This one-to-one mapping is not found elsewhere in the barrelfield; the small anterior barrels in rodent S1 receive input from one or more small whiskers on the anterior snout as well as hindlimb and forelimb. Whisker-related patterns are not unique to S1, but are reiterated at each level of the trigeminal neuraxis sequentially: in brainstem (Ma and Woolsey, 1984), thalamus (Van der Loos, 1976) and S1 cortex (Woolsey and Van der Loos, 1970). The development of this sensory signaling pathway from whisker to cortex is described below.

1.2.1 Brainstem and thalamus

Trigeminal ganglion cells (TGCs) invade the developing whisker pad and innervate each whisker follicle according to size and location; the large caudal vibrissae are densely innervated and the small rostal vibrissae are less densely innervated (Welker & Van der Loos, 1986). These bipolar TGCs fire action potentials in response to whisker deflection and cause the release of glutamate at brainstem synapses. TGCs project centrally and extend collaterals to four distinct nuclei in the caudal brainstem trigeminal complex (BSTC) (Hayashi et al., 1980). Most of the excitation produced from whisker movement is received by neurons in the principal trigeminal nucleus (nVp), however excitation is also received by the subnucleus interpolaris (nVi) and

subnucleus caudalis (nVc). In each of these three brainstem nuclei, both the incoming axons and the cell bodies cluster, and accurately recapitulate the ipsilateral whisker pattern observed on the snout (Bates and Killackey, 1985; Ma and Woolsey, 1983, 1984). The cytoarchitectonic structures formed are called "barrelettes". The development of barrelettes has been studied in detail using several staining methods including Nissl staining, cytochrome oxidase histochemistry, and Golgi-impregnation (Ma, 1993). Barrelettes are first evident in the mouse on postnatal day (P) 0 using cytochrome oxidase histochemistry (a label of high metabolic activity), and appear well segregated by P1 (Ma, 1993). However the development of cytoarchitectural barrelettes lags behind "histochemical" barrelettes and Nissl staining has shown that the cells only begin to aggregate on P1 and complete segregation into 5 rows by P4 (Ma, 1993). At the next level of the trigeminal neuraxis, brainstem neurons project their axons across the midline of the brain to the ventral posterior medial thalamus (VpM). In VpM, axon terminals and cell bodies again cluster and replicate the whisker pattern in cytoarchitectonic units termed "barreloids" (Van der Loos, 1976). Barreloids are first seen using cytochrome oxidase histochemistry at P3 (Yamakodo, 1985). Another feature of barreloids observed at P5, is that dendrites of the VpM neurons selectively project towards the incoming brainstem axons resulting in a dense plexus of synapses in the centre of each barreloid (Brown et al., 1995; Zantua et al., 1996). However this confinement of dendritic arbors to single barreloids is not maintained into adulthood and by P18 dendrites are seen extending into adjacent barreloids (Brown et al., 1995; Zantua et al., 1996).

1.2.2 S1 cortex: the 4 stages of barrel development

There are four main cellular processes that contribute to barrel development in layer 4 of S1: presynaptic TCA segregation (Rebsam et al., 2002), postsynaptic cellular aggregation (Rice & Van der Loos, 1977), selective dendritic orientation into the barrel hollow (Woolsey et al., 1975) and the formation and strengthening of TCA/layer 4 synapses and spines within each barrel (Crair and Malenka, 1995). Each distinct process is described below.

[1] TCA segregation

VpM barreloid neurons project to cortex, terminating in layer 4 of the primary somatosensory cortex by P0. Initially TCAs are found uniformly distributed across layer 4, with axons spanning one to two prospective barrel diameters (Rebsam et al., 2002). However during the first 3 postnatal (P0-P2) days in mouse, the thalamic afferents segregate into broad rows that correspond to the principal whisker rows of the muzzle. By P3-P4 the afferents segregate further into whisker-related patches that display the somatotophic map of the contralateral whisker pad (Rebsam et al., 2002). By P7, TCA arbors are found almost exclusively within a single barrel. The TCAs from VpM project mainly into the barrel hollows (Killackey, 1973; Rebsam et al., 2002) and only a few into the interbarrel region or septa (Pierret et al., 2000). The mechanism of TCA segregation involves retraction of inappropriately located afferents and the selective elaboration of appropriately placed afferents (Rebsam et al., 2002).

[2] Cellular aggregation

A unique feature of rodent S1 is that the layer 4 cells recapitulate the whisker pad pattern, as well as the incoming TCAs. At P3 layer 4 cells are seen by Nissl to be evenly distributed, but between P4 and P7 the cells aggregate to form the anatomical units termed barrels that consist of cell-dense barrel walls that surround each segregated TCA patch and cell-sparse barrel hollows left in the regions of TCA innervation. A full barrel field is clearly visible by P7 and septa are also present at P7, but barrel segregation appears most distinct between P10-P14 (unpublished observations, P. Kind). The postsynaptic cell-clustering event to form barrels is almost certainly dependent upon the segregation of presynaptic TCA terminals. However analysis of transgenic mice that show normal TCA segregation but fail to form cellular barrels demonstrates that TCA segregation is not sufficient and that these two processes are genetically dissociated (Hannan et al., 2001). The barrel system can therefore be used as a tool to provide strong indication between pre- and post- synaptic events involved in cortical differentiation.

[3] Dendritic orientation

Another feature of barrels is the selective orientation of layer 4 cell dendrites into the barrel hollows where they synapse with incoming TCAs from VpM (Woolsey et al., 1975). The exact timing of this process is not yet clear, however it is thought that it results from a selective pruning of inappropriate branches outwith the associated TCA patch combined with an elaboration of appropriate branches located within each barrel hollow (Greenough & Chang, 1988). Unlike the transient dendritic orientation in VpM, layer 4 cell dendrites remain selectively orientated throughout development and into adulthood (Woolsey et al., 1975).

[4] Synapse formation and strengthening

Appropriate anatomical and functional development of synapses in layer IV is crucial for the transfer of information from thalamic afferents to the cortex and the formation of barrels. In P4 rodent S1 cortex, the density of total synapses is about 15-25% that of the adult, and postsynaptic densities can be clearly identified under an electron microscope (Micheva and Beaulieu, 1996; Spires et al., 2005). Also in P4 mouse PMBSF, De Felipe et al (1997) have shown that both asymmetrical (putatively excitatory) and symmetrical (putatively inhibitory) synapses are present. In adult animals, 85% of synapses in the rodent barrel cortex are glutamatergic (Micheva and Beaulieu, 1995). However between P4 and P8, the period of barrel formation, 57% of synapses are excitatory and 43% are inhibitory (identified by GABA staining; De Felipe et al., 1997). The developmental profile of asymmetrical (excitatory) synapse density has been characterised in sections through layer 4 as follows: synapse density increases rapidly between P6 to P8, slowly from P9 to P12 and sharply between P13 and P14, correlating with the onset of patterned whisking (White et al., 1997). In layer 4, 20-25% of the synapses develop from the thalamic (VpM) afferents making asymmetrical contact onto the stellate cells, and on other neurons with processes in layers 4 (White, 1979). Importantly, even at early postnatal ages (P3) when TCAs are segregating, functional TCA synapses can be detected using electrophysiological methods (Lu et al., 2003). Glutamate neurotransmission is important early in postnatal development with NMDAR-dependent synaptic plasticity (LTP/LTD) induced only in a narrow time window between P3 and P7 in TCA/layer 4 synapses (Crair and Malenka, 1995; Lu et al.,

2003). Interestingly the ratio of NR2B to NR2A-containing NMDA receptors has also been shown to decrease over a similar, but not identical, time-course (Lu et al., 2001). This developmental transition of the NR2 subunit also parallels a change in the NMDAR current kinetics from slow to fast at thalamocortical synapses. To examine if NMDAR subunit composition correlates with NMDAR current kinetics and critical period plasticity, Lu et al. (2001) examined NR2A knockout mice. Their study reveals that NR2A containing NMDARs are responsible for accelerating NMDAR kinetics in situ but do not close the critical period, since the critical period remains unchanged in *Nr2A*$^{-/-}$ mice (Lu et al., 2001).

1.3 Cellular Theories of Barrel Development

The cellular mechanisms responsible for barrel differentiation have not yet been deduced. However several theories as to how cell-dense barrel walls are generated exist (see figure 1.1). First, neuronal cell death might occur selectively in the area of TCA innervation, leaving this area "cell-sparse" and the barrel walls comparatively "cell-dense". Cell death studies in developing S1 however have shown that most neuronal cell death occurs in the second or third postnatal week (Heumann and Leumann, 1983; Heumann et al., 1978; Finlay and Slattery, 1983; Al-Goul and Miller, 1989), well after the emergence of the barrel pattern and also that apoptotic nuclei are not seen preferential to any region across layer 4 (Miller 1995). Second, layer 4 cells may be passively displaced to form the barrel wall as a result of neuropilar elaboration in the areas of cortical input from the thalamus. However this possibility also seems unlikely because Hannan et al. (2001) showed that mutant mice lacking *Plcβ1* lack layer 4 cortical barrels but exhibit normal axonal segregation and Upton et al. (in preparation) showed normal dendritic complexity and orientation in these mice. Third, neurons may actively migrate away from the incoming thalamocortical afferents that segregate into whisker-related patches in layer 4 (currently no evidence for or against this hypothesis yet exists). Fourth, differential cell adhesion across layer 4 regulated by signals from invading TCAs and simultaneous radial cortical expansion during the first postnatal week might cause a barrel pattern to develop. Cadherin-8 and Tenascin-C are two adhesion molecules

that are expressed in S1 cortex during the first week of postnatal life and downregulated in response to activity (Gil et al., 2002; Steindler et al., 1995; Cybulska-Klosowicz et al., 2004), but there is currently no direct evidence to support this hypothesis. It is still to be determined however if any of these processes are in fact involved in barrel formation.

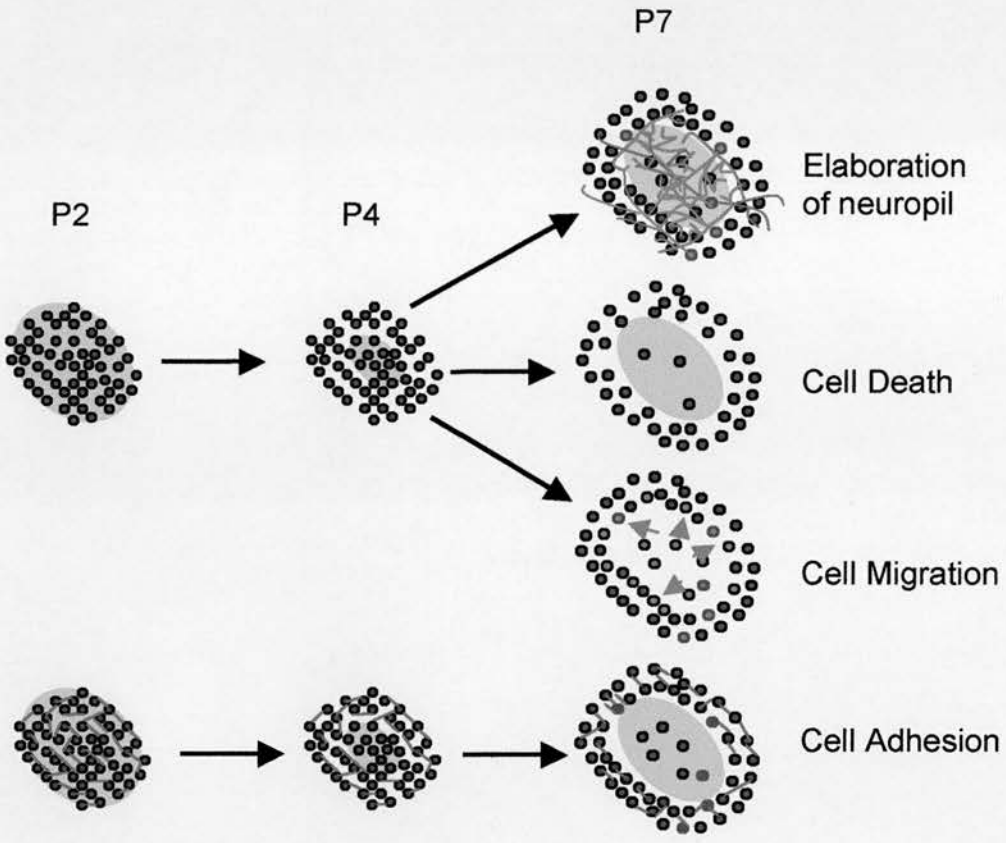

Figure 1.1: Schematic diagram showing four cellular mechanisms that could cause layer 4 cells to segregate into barrels. The theories are: [1] Massive elaboration of neuropil (axon terminals and layer 4 cell dendrites) causes a passive displacement of layer 4 cortical neurons to form a cell-dense barrel wall and a cell-sparse barrel-hollow; [2] Selective cell death occurs in the region of TCA innervation; [3] Active cell migration of layer 4 cell bodies occurs away from the incoming TCAs; and [4] Differential cell adhesion takes place in combination with cortical expansion: cell adhesion molecules could be downregulated in the region of TCA innervation leaving only cells on the edge of the TCA patch tightly bound. As the cortex grows a barrel would emerge due to tightly bound high-density regions around the TCA patch and loosely bound, low-density regions in the TCA patches (barrel hollows).

1.4 Cortical Plasticity and Sensitive Periods

During development certain sensory areas of the cortex exhibit a time period of heightened plasticity in response to alterations in the sensory environment. The time frame of this developmental plasticity is specific to cortical area and cortical layer and is referred to as a "sensitive period". Hubel and Wiesel (1963) were the first to demonstrate experience-dependent synaptic plasticity in the cerebral cortex, using the developing cat visual system. The cat primary visual cortex is organised into ocular dominance columns in which cells from one column respond preferentially to input from one eye, and cells in an adjacent column respond preferentially to input from the other eye. Hubel and Wiesel (1963) performed monocular deprivation experiments, where they deprived kittens of input from one eye by lid-suture straight after eye-opening (at P10-P12) and then conducted single-cell recordings in the primary visual cortex after three months of deprivation. They found that monocular deprivation in early life caused the visual cortex to develop connections heavily biased towards the non-deprived eye at the expense of the deprived eye.

Similar deprivation experiments have now been performed in rodent primary somatosensory cortex. Van der Loos and Woolsey (1973) lesioned row C follicles on the mystacial whiskerpad at birth (P0) and then examined the permanent effects on the cortical barrel map. Row C follicle ablation at P0 caused the loss of discrete row C barrels in layer IV. Instead row C afferents fused into a thin band and patches in adjacent rows B and D appeared to take over the territory usually innervated by row C. Layer IV cortical cells also rearranged to form a "megabarrel" around the fused row of afferents in row C (Van der Loos and Woolsey, 1973) and layer IV dendrites selectively orientated into the megabarrel with the fused TCA plexus (Steffan and Van der Loos, 1980; Harris and Woolsey, 1981). These cortical alterations to peripheral follicle lesion only occur during a sensitive period however. The degree of anatomical disruption to the cortex from follicle lesioning decreases over the first few post-natal days of life, and there is no effect by P5 (Woolsey and Wann, 1976).

Physiological changes in the rodent barrel cortex can still be recorded after the anatomical sensitive period has ended at P5. LTP (Crair and Malenka, 1995; Isaac et al., 1997) and LTD (Feldman et al., 1998), both physiological measures of activity dependent synaptic plasticity can be induced at thalamocortical synapses in layer IV between P3 and P7 in rat thalamocortical slices. These results suggest that there is a physiological sensitive period in layer IV barrel cortex between P3-P7. Work done by Fox (1992) however reports a slightly different physiological plasticity time period. Fox (1992) recorded from layer II, III and IV neurons in the barrel cortex of adult rats in which all but one whisker (D1) was trimmed at P0, P2, P4, or P7. The whiskers were allowed to re-grow before recording and plasticity assessed by recording responses to D1 whisker stimulation in cortical cells located within D1, and cells located within surrounding barrels. The trimming technique was employed by Fox because Hand (1982) and Simons and Land (1987) showed that trimming vibrissae instead of lesioning follicles could cause changes in the physiological organisation of the cortex by changing the balance of activity in the pathways from the vibrissae to the cortex, without affecting the anatomical organisation of the cortex, a phenomenon similar to monocular deprivation. Trimming vibrissae allows the study of experience dependent plasticity without the complicating effects of nerve degeneration, cell death and primary afferent regeneration (Waite and Cragg, 1982; Hamori et al., 1986; Rhoades et al., 1987) that confound follicle lesion experiments. In animals trimmed at P0, an increased response to stimulation of the D1 whisker was seen in the "deprived" barrels surrounding the D1 barrel. This plasticity in layer IV decreased however to a basal state in P4 and P7 trimmed animals. In contrast plasticity remained high in layers II and III of animals whose whiskers were trimmed at P7, demonstrating that developmental sensitive periods differ between cortical layers and that plasticity in supragranular layers continues well into postnatal life (Fox, 1992). The distinction between sensitive periods is thought to result from differences in the maturation of thalamocortical and intracortical connections (O'Leary et al., 1994). For example intracortical connections are mostly in layers II/III of S1 barrel cortex and exhibit a very late sensitive period. If the infraorbital nerve (ION) is transected at P7, barrels form as usual but local intracortical connections diminish in number and extent (McCasland et al., 1992).

Recent research has also identified several sharply defined sensitive periods of structural plasticity during the second postnatal week of barrel cortex development. Lendvai et al. (2000) used time-lapse two-photon microscopy to show that layer 2/3 dendritic spines and filopodia are highly motile throughout barrel development. However if whiskers are trimmed one to three days before imaging, during a sensitive period from P11-P13, a reduction in protrusive motility is observed in the deprived regions of barrel cortex. Surprisingly spine density, length and shape remain unchanged, but layer 2/3 receptive field properties are degraded (Lendvai et al., 2000). In addition, Maravall et al. (2004) demonstrated that there is a sensitive period for branching of secondary dendrites of layer 2/3 cells in the barrel cortex between P10 and P14. This period of heightened dendritic plasticity shares a sensitive period with receptor field plasticity just like the sensitive period of spine motility, and interestingly correlates with the onset of patterned whisking (see figure 6.1 in Chapter 6 for more details).

1.5 The role of neural activity in barrel development

Although an intact sensory periphery is crucial for the normal differentiation of the cerebral cortex, there has been a great deal of controversy concerning the roles of neural activity in pattern formation. In developing visual cortex, the segregation of thalamocortical inputs into eye-specific stripes is disrupted by manipulations that perturb or abolish neural activity (reviewed by Constantine-Paton et al., 1990). However in developing rodent S1, the segregation of thalamocortical afferents into whisker-related patterns is not disrupted by P0 blockade of action potentials using TTX (Chiaia et al., 1992) or NMDA receptor activity with APV or MK801 (Henderson et al., 1992; Schlaggar et al., 1993), indicating that neither patterned nor spontaneous activity is required for S1 differentiation. An important limitation of all these pharmacological activity blockade experiments however is that thalamocortical axons have already reached the cortex by P0, so activity blockade conducted at this stage in development could be too late to cause an effect. To address this question Chiaia et al. (1994), applied TTX to newborn hamsters. Hamsters also form barrels, but are born with a relatively immature trigeminal system because they have a

shorter gestation period (16 days) compared to mice or rats (21 days) (Jacquin and Rhoades, 1987). The results, examined by various histochemical stains, showed no qualitative or quantitative effects upon thalamocortical segregation in the PMBSF of hamsters treated with TTX (Chiaia et al., 1994). Cellular segregation in layer IV was not examined.

Fox et al. (1996) re-examined whether activity is required for barrel development by blocking cortical activity during the anatomical sensitive period of barrel development and assaying the receptive field properties of individual neurons in the barrel cortex weeks later. Fox and colleagues demonstrated that although crude thalamocortical segregation does not appear to be affected by activity blockade, both NMDA and non-NMDA receptor blockade significantly disrupt the receptive field properties of thalamocortical afferents. A role for activity in the barrel cortex has also been shown by the fact that TTX and APV block barrelfield plasticity that is induced by neonatal row C ablation (Schlaggar et al., 1993). Furthermore, whisker trimming in early postnatal life effects single-neuron responses in the cortex, even though somatotopic patterning of thalamocortical afferents is not affected (Fox, 1992). All of these studies show that neural activity does in fact play a role in refining thamocortical connections in barrel development. Dissociation between TCA segregation and cortical segregation appears to exist however and activity seems to play a more significant role in cortical refinement.

There are several different types of activity; the two main subdivisions being spontaneous and sensory evoked activity. Recently it has been proposed that sensory-evoked activity is not required for barrel map formation and that spontaneous activity (either patterned or random) might be sufficient for the normal development of S1 cortex (Van der Loos and Woolsey, 1973). This spontaneous activity could be instructive, taking the form of patterned waves of correlated activity across the thalamus to establish the distinct neuronal structures in the barrelfield, or permissive, merely taking on a certain threshold level that is sufficient for the normal development of barrels. It is not yet clear which is the case. However, neurotransmitter activity is known to play an essential role in conferring the presynaptic patterns of the TCAs to the postsynaptic cells in layer IV. The analysis

of transgenic animals, with gene deletions in various neurotransmitters and signaling molecules has shown two main subdivisions of neurotransmitter receptor activity involved in S1 differentiation: presynaptic serotonergic activity (at neuromodulatory synapses from raphecortical projections onto TCA terminals) and postsynaptic glutamatergic activity (excitatory synapses between TCAs and cortical neurons) (Gaspar et al., 2003; Erzurumlu and Kind, 2001).

1.5.1 Presynaptic serotonergic activity

Mice deficient of the gene encoding for monamine oxidase A (MAOA), an enzyme that decatalyses the oxidative deamination of monoamines such as catecholamines and serotonin (5HT), first demonstrated a role for 5HT in barrel development. MAOA knockout mice were found to contain excessive levels of 5HT (700-900%) during the neonatal period and lacked both TCA and cellular segregation in layer IV despite normal whisker-related patterning in the thalamus and brainstem nuclei (Cases et al., 1996). Pharmacological inhibition of MAOs in wildtype mice during the first postnatal week generated a similar phenotype (Vitalis et al., 1998). However early pharmacological inhibition of 5HT synthesis in MAOA knockout mice, using parachlorophenylalanine (PCPA) rescued the mutant phenotype indicating that normal serotonin levels are crucial for barrel development. Conversely inhibition of catecholamine synthesis did not restore barrel development (Vitalis et al., 1998).

The analysis of 5HTT knockout mice also provided evidence for a role of 5HT in barrel formation (Bengel et al., 1998; Persico et al., 2001). Developing thalamic neurons normally express 5HTT (the serotonin transporter; SERT) that allows the uptake of exogenous 5HT from the synaptic cleft of raphe neurons into TCA terminals. Barrel formation was almost completely disrupted in 5HTT knockout mice, with the exception of a few large and most caudal whisker barrels. At lower levels of the trigeminal neuraxis, barrelettes were well segregated but barreloids appeared less well-defined, as seen in MAOA knockout mice. The significant difference between the 5HTT-ko model and the MAOA-ko mice though, was that the 5HTT-ko mice could not take up 5HT into the TCA terminals (Cases et al., 1998;

Persico et al., 2001). Therefore the 5HTT-ko phenotype indicated that accumulation of 5HT in the extracellular space and not the thalamic afferents caused the abnormal segregation of the axon terminals (Persico et al., 2001; Salichon et al., 2001). In addition the increase of 5HT levels in the brain of 5HTT-ko mice was not as large as that found in the MAOA-ko mice, likely because of feedback mechanisms that reduced 5HT synthesis (Ravary et al., 2001). These less extreme levels of 5HT could explain why 5HTT-ko mice display a slightly less severe phenotype than MAOA-ko mice, with a few of the largest barrels in the PMBSF developing.

In addition to the serotonin transporter (5HTT), thalamic neurons express the vesicular monoamine transporter (VMAT2) that allows for storage of 5HT taken up from the raphe neurons (Lebrand et al., 1996) and 5HT1B receptors that modulate neurotransmitter release, transiently between P0-P10 (Bennett-Clarke et al., 1993). 5HT itself is not synthesised in the thalamic neurons, but expression of the above serotonin-related genes in the thalamocortical afferent terminals causes a transient barrel-like 5HT pattern to form in layer 4 of S1 cortex of mice early in postnatal development. Serotonergic afferents from raphe nuclei are present in layer IV of the barrel cortex one day after TCA innervation (Luo et al., 2003).

The 5HT1B receptor was shown to be important for barrel formation using a double knockout (dko) strategy. Work examining MAOA/5HT1B dko and 5HTT/5HT1B dko mice showed that barrels are restored in each of these double transgenic mice. Furthermore, barrels formed in MAOA/5HTT/5HT1B triple knockout mice, even though brain serotonin levels remained high (Salichon et al., 2001). These results (restoration of barrel formation) indicated that the high 5HT levels present in MAOA knockout and 5HTT knockout mice disrupted barrel formation via the excessive activation of 5HT1B receptors. Subsequently the possible mechanisms (trophic or activity-dependent) through which 5HT1B receptors could mediate their effect on barrel formation were investigated. Laurent et al. (2002) showed that in P5-P9 thalamocortical (TC) slices, 5HT and the activation of 5HT1B receptors reduces monosynaptic TC ESPCs evoked by low frequency internal capsule (IC) stimulation. Also the effect of 5HT is caused by a presynaptic action on the release of glutamate by the TCAs in layer IV (Laurent et al., 2002). It is possible therefore that increased

5HT levels in MAOA ko mice over-activates 5HT1B receptors and causes alterations in thalamocortical glutamate neurotransmission that disrupts TCA segregation.

1.5.2 Postsynaptic glutamatergic activity

The first demonstration that glutamate neurotransmission was necessary for axon segregation within the trigeminal system came from analysis of *Nr1*$^{-/-}$ (the essential subunit of NMDARs) mice that showed normal axonal projections from the whisker pad but failed to develop barrelettes (Li et al. 1994). *Nr1*$^{-/-}$ mice die within a day after birth, so pattern formation could not be examined at higher relays in the trigeminal pathway. However NMDA receptor-mediated neural activity was examined along the ascending somatosensory pathway, by introducing ectopic expression of two different levels (high and low) of an NR1 transgene (Iwasato et al., 1997) that rescued the lethality of the *Nr1*$^{-/-}$. High levels of the transgene expression rescued the formation of the whisker related patterns in the brainstem, thalamus and cortex, but low levels did not (Iwasato et al., 1997). Also recently, Rudhard et al. (2003) generated a transgenic mouse to investigate the importance of NMDA receptor coincidence detection properties and calcium signaling in cortical development. An N598R mutation was introduced into NR1 resulting in functional NMDARs that are Mg^{2+} insensitive and Ca^{2+} impermeable. Whisker-related pattern formation was impaired in these mice that lacked coincidence detection properties and calcium signaling, showing that one or both of these properties of NMDARs are important in refinement of synaptic connectivity. Interestingly though, Binschtok et al. (2006) just showed that the predominant type of NMDAR in wildtype TCA/layer 4 glutamatergic synapses in S1 cortex are NR2C-subunit containing NMDARs that are relatively insensitive to voltage-dependent Mg^{2+} blockade (Monyer et al., 1992, 1994; Farrant et al., 1994; Momiyama et al., 1996). All of these results however have indicated a role for NMDARs in mediating pattern formation in the trigeminal somatosensory system, but they have not able to determine whether or not the lack of differentiation in layer IV in *Nr1*$^{-/-}$ results primarily from the absence of subcortical patterning.

To address whether cortical NMDARs were crucial for barrel development Iwasato et al. (2000) then generated conditional transgenic mice in which deletion of the *Nr1* gene was restricted to excitatory cortical neurones (Cx*Nr1*$^{-/-}$ mice). These Cx*Nr1*$^{-/-}$ mice developed normal barrelettes and barreloids but failed to form cellular aggregates in layer 4 even though TCAs segregated, albeit with decreased TCA patch size in the posteromedial barrel subfield (PMBSF). The Cx*Nr1*$^{-/-}$ mice therefore showed that postsynaptic NMDAR activation is vital in communicating the periphery-related senory patterns from TCAs to barrel cells. Iwasato et al. (2000) also examined the effects of peripheral Row C lesions in P1 Cx*Nr1*$^{-/-}$ mice on the patterning of whisker-related TCA patches. In contrast to NMDAR pharmacological blockade (Schlaggar et al., 1993), Cx*Nr1*$^{-/-}$ mice showed normal lesion-induced plasticity in TCA segregation (Iwasato et al., 2000). One explanation for the discrepancy has been thought to reside in the presence of NMDA-mediated activity in GABAergic cells in the Cx*Nr1*$^{-/-}$ mutant. Cortex specific NR1 deletion (in Cx*Nr1*$^{-/-}$ mice) was achieved using an Emx1 promoter, but GABAergic cells originate in the ganglionic eminence where Emx1 is not expressed. Therefore despite NR1 deletion in the cortex, residual NMDAR activity in the unaffected cells could mediate the apparent effects on cortical development. Alternatively, the discrepancy between receptor deletion and acute receptor blockade could result from the disruption of associated downstream molecules in knockout animals (Husi and Grant, 2001).

In addition, Hannan et al. (2001) later reported that mice with a deletion of metabotropic glutamate receptor 5 (*Mglur5*$^{-/-}$) also fail to form whisker-related cellular aggregates, despite partial TCA segregation into rows in the PMBSF (more details below in section 1.7.1). Wijetunge et al. (in preparation) have shown by immunoelectron microscopy that mGluR5 is postsynaptic in layer 4 of S1. Analyses of both the Cx*Nr1*$^{-/-}$ and *Mglur5*$^{-/-}$ mutants, has convincingly demonstrated that postsynaptic neurotransmitter receptor activation is vital in communicating the peripherally related sensory patterns from TCAs to barrel cells (reviewed by Erzurumlu & Kind 2001; Kind & Neumann 2001). However it is not yet known how activation of these postsynaptic glutamate receptors results in the changes in neuronal morphology that is required to form barrels. The intracellular signaling

pathways downstream of these glutamate receptors that regulate cortical development are just beginning to be elucidated (more details in section 1.7).

1.6 The postsynaptic density / NMDARcomplex

Postsynaptic glutamate receptors that mediate excitatory synaptic transmission in the mammalian brain are clustered at synapses in the postsynaptic spine in the postsynaptic density (PSD). Under electron microscopy the PSD appears as a dense mass just beneath the postsynaptic membrane and contains multiple receptors and their multi-protein complexes (Kennedy, 1993; Kennedy, 1997). The NMDAR complex (NRC) is a subcomplex within the PSD that has provoked a lot of interest because it has been shown to be involved in various forms of synaptic plasticity in both the hippocampus and the cortex (Malenka and Nicoll, 1993; Bliss and Collingridge, 1993; Bear and Malenka, 1994).

Recent large-scale purification and characterisation of the *in vivo* NMDAR complex (NRC) (Husi & Grant, 2000, 2001) and the entire postsynaptic density (PSD) of excitatory synapses (Walikonis et al., 2000; Peng et al., 2004) by mass spectrometry and immunoblotting from adult rodent forebrain, has provided a large framework of candidate molecules involved in signal transduction pathways downstream of NMDAR and mGluR5 activation. Initially, 77 molecules were found to co-immunoprecipitate with the NMDA receptor (Husi and Grant, 2000). To date, approximately 200 molecules have been shown to associate with the NRC/MASC and over 800 molecules have been discovered to associate with the PSD (personal communication, Seth Grant). The PSD contains several glutamatergic receptors (NMDARs, mGluRs and AMPARs), adaptor proteins (such as PSD95), signaling enzymes (including protein kinases and phosphatases) and cell-adhesion and cytoskeletal molecules (Husi and Grant, 2000). Moreover the complex contains sets of molecules constituting many known signaling pathways, for example, Ras, Raf, MEK, SynGAP and Mitogen-activated protein kinase (MAPK). It appears from the composition of the complex therefore, that synaptic activity via the glutamate receptors could integrate and affect downstream second messenger pathways. This

would result in processes such as transcriptional and translational regulation, AMPA receptor trafficking, and cytoskeletal changes, which are all involved in plasticity and could cause the alterations in neuronal phenotype that occur during barrel development.

1.7 Postsynaptic Intracellular Signaling Pathways involved in barrel formation

An on-going approach taken by Dr Peter Kind's laboratory to elucidate the glutamate receptor dependent intracellular pathways underlying barrel development is to perform targeted screens of transgenic mice with genetic deletion of genes encoding PSD proteins. So far, the targeted screen approach has identified one signaling molecule, phospholipase C-β1 (PLC-β1) (Hannan et al., 2001) to play a role in barrel formation. In chapters 3 and 4 of this thesis I am going to examine 2 more potential candidates for a role in barrel development: PKA (Chapter 3; Watson et al., 2006) and SynGAP (Chapter 4; Barnett et al., 2006). Reasons for focussing on each of these particular molecules are explained below. I also hypothesise that ERK could play a role downstream of these signaling molecules in barrel formation.

1.7.1 mGluR5-PLCβ1

PLC-β1 is one of four PLC-β family members that are part of a larger family of phosphoinositide (PI)-specific PLCs. The β subfamily are G-protein-coupled and, of the PLC-βs, β1 is the most highly expressed in the neocortex. The PI-specific PLCs hydrolyse phosphatidylinositol 4,5-bisphosphate (PIP2) into two second messengers, diacylglycerol (DAG) and 1,4,5-inositol triphosphate (IP3). Subsequently, DAG activates Protein Kinase C (PKC) and IP3 activates the IP3 receptor (IP3R) to release intracellular Ca^{2+} from the endoplasmic reticulum (ER).

A role for G-protein coupled phospholipases in developing cortical neurons was first suggested when Dudek and Bear (1989) found that mGluR-mediated PI hydrolysis

paralleled the sensitive period in visual cortex. PLC-β1 was subsequently isolated from a screen designed to identify molecules selectively expressed in the developing cat visual cortex (Kind et al., 1994, 1997) raising the possibility that PLC-β1 was a primary target of phosphoinositide-coupled (i.e. group 1) mGluR signaling during cat visual cortical development. Interestingly Kind et al (1997) found that PLC-β1 is highly expressed in intermediate-compartment-like organelles called botrysomes, located selectively near the roots of, and within, dendrites. These findings led to the hypothesis that PLC-β1 might regulate protein trafficking to dendrites in response to mGluR activation and hence may be a key regulator of activity-dependent dendritic development.

In support of a role for PLC-β1 in cortical development, Hannan et al. (1998, 2001) showed that PLC-β1 levels are high in layers 2-4 of rodent S1 in the first two postnatal weeks, corresponding spatially and temporally with barrel formation and dendritogenesis. Furthermore, genetic deletion of *Plc-β1* disrupted the cytoarchitectural differentiation of barrels, but did not affect the pattern, distribution or size of TCA patches (although the structure and size of individual TCA axons has not been examined). Group 1 mGluR-mediated PI-hydrolysis was dramatically reduced in neocortex of young *Plc-β1*$^{-/-}$ mice supporting the hypothesis that mGluR5 activation of PLC-β1 regulates cellular aggregation in layer 4. The normal pattern of TCAs in *Plc-β1*$^{-/-}$ mice compared with the disrupted pattern in *Mglur5*$^{-/-}$ mice, however, indicates that mGluR5 regulation of TCA segregation may be mediated by a PLC-β1-independent mechanism. MGluR5, but not PLC-β1 is expressed at high levels in the somatosensory thalamus (Munoz et al., 1999; Watanabe et al., 1998) suggesting that mGluR5 in VpM neurons may regulate TCA segregation. However, the defects in TCA segregation do not appear to result from a loss of segregation at lower levels in the trigeminal pathway since barreloid development, as revealed by cytochrome oxidase histochemistry, appears normal in both *Mglur5*$^{-/-}$ and *Plc-β1*$^{-/-}$ mice (Wijetunge and Kind, unpublished observations). These findings suggest that mGluR5 may regulate TCA segregation by controlling the release of retrograde signals from layer 4 in a similar manner to NMDARs (Iwasato et al., 2000) although a direct role in the TCAs cannot be ruled out.

To directly test the hypothesis that PLC-β1 regulates activity-dependent dendritic rearrangements during cortical development, dendritic complexity and orientation of layer 4 neurons in *Plc-β1*$^{-/-}$ mice has recently been examined using Rapid Golgi staining (Upton et al., in preparation). In contrast to the *CxNr1*$^{-/-}$ (Datwani et al., 2002), no significant difference in total dendrite length, dendrite number and number of branch points of layer 4 neurons was observed between *Plc-β1*$^{-/-}$ and wild type mice. In addition layer 4 neuronal dendrites were normally oriented toward TCA patches. This study indicates 1) that PLC-β1 is not regulating dendritic complexity and orientation of layer 4 neurons and 2) selective dendritic elaboration within TCA patches is not sufficient to form barrels. These differences between *Plc-β1*$^{-/-}$ and Cx*Nr1*$^{-/-}$ mice indicate that multiple pathways activated by glutamate receptors are not simply converging to regulate cortical development. Instead different combinations of pathways are likely needed to differentially regulate aspects of cortical differentiation such as barrel development, dendritic complexity and dendritic orientation. Recent spine density analysis however has shown that *Plc-β1*$^{-/-}$ mice have an increase in spine density in the barrel cortex compared to wildtype mice (Upton et al., in preparation) similar to Cx*Nr1*$^{-/-}$ mice, indicating that there may also be convergence of pathways.

Interestingly, Spires et al. (2005) demonstrated a reduced symmetric/asymmetric synaptic ratio within the barrel cortex at P5 in *Plc-β1*$^{-/-}$ mice, possibly resulting in an imbalance in excitatory and inhibitory circuitry. Spine morphology of layer 5 pyramidal neurons passing through layer 4 also showed a reduction in mushroom type spines compared to age-matched wildtypes indicating a disruption in spine maturation. These observations correlate well with findings in the hippocampus that the stimulation of group 1 mGluRs causes spine elongation (Vanderklish & Edelman, 2002) and that calcium release from intracellular stores affects spine morphology (Harris, 1999). In conclusion, PLC-β1 signaling appears to be important in the development of cortical connectivity by regulating spine shape, density and synapse formation, but not dendritic complexity, or dendritic orientation.

Although the cellular mechanisms regulated by PLC-β1 are beginning to be elucidated, the biochemical pathways through which mGluR5 activation of PLCβ1 regulates these cellular processes remains largely unknown. One hypothesis proposed by Spires et al. (2005) is that PLCβ1 could affect spine morphology through its interaction with Homer proteins. Homer proteins are encoded by 3 genes (Homers1-3) and are multidomain, scaffolding molecules that link mGluR5/PLCβ1 to the IP3R. They also link mGluR5 with the NMDAR complex (Xiao et al., 2000; Fagni et al., 2002) by binding to Shank, another scaffolding molecule that associates with the guanylate kinase-associated protein GKAP/PSD95 complex. Homers have previously been shown to be involved in regulating the morphology of dendritic spines (Sala et al., 2003) and one splice variant Homer1a has been shown to regulate spine formation in an activity-dependent manner (Sala et al., 2003). In collaboration with Professor Paul Worley our lab has examined the barrel cortex of individual Homer null mutant mice and Homer triple mutants (*H1*$^{-/-}$*H2*$^{-/-}$*H3*$^{-/-}$). Nissl staining showed normal cellular segregation of layer 4 neurons into barrel walls and barrel septa also appeared normal (Watson, unpublished observations). Therefore the mechanisms by which PLC-β1 controls barrel development are likely to be Homer-independent. These findings suggest that IP3-stimulated release from the ER is not a crucial step in barrel development. However, it may be that a limited release of Ca^{2+} from the ER, that is not dependent on a close association of mGluR5 with the IP3 receptor, may be sufficient to drive barrel formation, or Homers may not be the only molecules that tether IP3 receptors to mGluR5 receptors. Alternatively, DAG activation of PKC or direct regulation of PIP2 levels by PLC-β1 may be the crucial step to barrel development. A role for PKC in spine plasticity via its interaction with Rac and Rho has been shown (Pilpel & Segal, 2004). It is important to note that no-one has yet examined whether Homers are critical for PLC-β1 dependent spine and synapse development. Further work will be necessary to determine the cellular mechanism regulated by PLC-β1 that underlie barrel formation and spine maturation.

1.7.2 cAMP-dependent Protein Kinase A

cAMP-dependent Protein Kinase A signaling has been shown to play an important role in numerous forms of synaptic plasticity, for example, learning and memory in Aplysia and Drosophila (Greenberg et al., 1987), hippocampal LTP (Frey et al., 1993) and ocular dominance shifts in rodents (Reid et al., 1996; Fischer et al., 2004). This thesis (Chapter 3) examines whether cAMP/PKA signaling is also crucial for mechanisms of barrel development. A detailed description of PKA and discussion about cAMP/PKA signaling can therefore be found in Chapter 3. However in brief, PKA has been targeted and hypothesised to play a role in barrel development because a spontaneous "barrelless" mutant described by Welker et al. (1996) was found to lack the gene Adenyl Cyclase 1 (AC1) (Abdel-Majid et al 1998). Adenylyl cyclases convert ATP into cAMP and a major downstream target of cAMP is PKA. AC1 has furthermore been shown to associate with 5HT1B, mGluR5 and NMDA receptors (Kind and Neumann, 2001) that have all been shown to play a role in TCA/layer 4 synapses for barrel development.

The cAMP-dependent protein kinase (PKA) family of enzymes is assembled from the products of four regulatory (R1α, R1β, R2α, R2β) and two catalytic (Cα and Cβ) subunit genes. These PKA subunits have distinct expression patterns across various mammalian tissues but are notably all expressed in neurons (Cadd and McKnight, 1989). In general, α subunits are expressed ubiquitously and β subunits are tissue-specific; for example, R1β expression is restricted to neurons and R2β expression is high in brain and adipose tissue (Brandon et al., 1997). In addition to the unique tissue expression patterns, PKA subunits have different subcellular distributions. Research has shown that R2- containing holoenzymes are localised via scaffolding molecules called A-kinase anchoring proteins (AKAPs) to particulate fractions of tissue homogenate (Glantz et al., 1992; Ludvig et al., 1990), and R1-containing holoenzymes are delocalised in the cytoplasmic fraction of tissue homogenate (Skalhegg et al., 1994). In Chapter 3, I examine the expression of different PKA subunits in barrel cortex and explore if PKA could play a role downstream of AC1 in barrel development.

1.7.3 SynGAP

SynGAP is a brain-specific Ras-, Rab-, or Rap- GTPase Activating Protein (Kim et al., 1998). It is highly expressed in the postsynaptic density of excitatory glutamatergic synapses and binds PSD-95 *in vivo*, suggesting that it is involved in NMDA-receptor activity-mediated signaling (Kim et al., 1998). Since NMDARs are known to be crucial for barrel development, SynGAP makes an excellent candidate for a role in barrel formation downstream of NMDARs and is examined in chapter 4 of this thesis. Therefore detailed discussion about SynGAP and its signaling pathways can be found in Chapter 4. Interesting to note here though is that SynGAP is known to act as a molecular switch to negatively regulate the ERK/MAPK pathway via its GAP domain (Kim et al., 1998; Kim et al., 2003). In response to NMDAR activation, SynGAP binds the active GTP-bound form of Ras (or other small G-protein), which stimulates its intrinsic GTPase activity and causes rapid hydrolsis of GTP to GDP, returning Ras to its inactive form (Scheffzek et al., 1998) and thereby regulating ERK. The ERK/MAPK pathway has been shown to be involved in many cellular processes that could be important for the mechanisms of barrel formation (see below; section 1.7.4).

1.7.4 ERK and barrel development

It has previously been proposed that a primary role for extracellular-regulated kinase (ERK) may be to integrate signals initiated from a variety of sources to produce coordinated cellular events (Rosenblum et al., 2000; Cancedda et al., 2003; Adams and Sweatt, 2002). Since multiple receptors (mGluR5 and NMDARs), signaling via numerous intracellular pathways (PLC-β1, SynGAP and PKA) may be necessary for barrel development, it is tempting to hypothesize that ERK may be acting to integrate these signals to mediate barrel formation. In support of this notion, mGluR5 signaling has been shown to activate the ERK pathway (Gallagher et al., 2004; Berkeley & Levey 2003; Choe & Wang 2001) as can PKA (Cancedda et al., 2003) and PKC activity (Sweatt, 2004). In addition, deleting SynGAP has been shown to increase ERK activity (Komiyama et al., 2002), and blocking ERK activation using MEK inhibitors has been shown to prevent ocular dominance plasticity to monocular

deprivation and LTP in visual cortex and hippocampus (Di Cristo, 2001; Sweatt, 2001). Our laboratory hypothesizes that there may be a critical band of ERK activity necessary for normal neuronal development and that disruption of any single signaling pathway could alter ERK activity to such an extent that barrel development is disrupted.

A role for ERK signaling in barrel development is also interesting because ERK has been shown to control numerous developmental processes such as cell migration and neuronal structural plasticity as well as proliferation and differentiation that were described when ERKs were first identified (reviewed by Sweatt, 2001). Many studies in different systems have used MAPK signaling pathway inhibitors, such as the MEK inhibitor PD98059 that prevents ERK activation and have shown that ERK signaling plays a role in regulating cell motility (Klemke et al., 1997; Rigot et al., 1998; Nguyen et al., 1999; Krueger et al., 2001; Ho et al., 2001). Potentially, ERK activation could play a similar role downstream of NMDARs and mGluR5s in influencing cell migration of layer 4 cells in S1 cortex to form barrels. In addition, studies using MEK inhibitors and ERK activity agonists have demonstrated that ERK activity is required for structural alterations in spine morphogenesis and changes in spine density on hippocampal neurons (reviewed by Thomas and Huganir, 2004). In this way ERK could affect barrel formation via synaptogenesis, affecting the level of integration of TCA signal to the surrounding layer 4 cells, as previously described in *Plcβ1*$^{-/-}$ mice.

1.8 Summary of the present thesis

1.8.1 Aim 1: To determine the role and locus of cAMP-dependent Protein Kinase (PKA) subunit RIIβ in barrel development

To further elucidate the intracellular pathways downstream of neurotransmitter activity that are required for barrel formation, I have focussed research on the potential candidate molecule, cAMP-dependent Protein Kinase A (PKA). PKA is hypothesised to play a role in barrel formation because it is a major downstream

target of AC1 and mice that lack AC1 are "barreless" (Abdel-Majid et al., 1998). Preliminary studies examining PKA subunit specific mutants were conducted prior to me joining the laboratory and found that *Prkar2β*$^{-/-}$ mice have a qualitative impairment in barrel segregation. To determine the precise role of PKAR2β in barrel development, I carried out detailed analysis of the barrel phenotype in chapter 3. Barrels were assessed quantitatively and segregation found to be reduced. In addition the site of action of the R2β subunit of PKA in developing somatosensory cortex was investigated to aid understanding of the signaling pathways involved in barrel development. Finally I have demonstrated a role for PKAR2β in AMPA receptor insertion and have investigated whether the process of AMPA receptor trafficking is a mechanism crucial for barrel formation, as previously hypothesised by Lu et al. (2003).

1.8.2 Aim 2: To determine the role of SynGAP in pattern formation in the trigeminal system of mice

To further elucidate the second messenger pathways that translate thalamocortical activity into cortical differentiation in the barrel cortex, I have focussed research on the potential candidate molecule, SynGAP. SynGAP is hypothesised to play a role in barrel formation because it is highly abundant in excitatory glutamatergic synapses and has been shown to associate with NMDARs via MAGUK scaffolding molecules. Furthermore SynGAP has been shown to negatively regulate ERK and ERK has been shown to regulate numerous cellular processes such as cytoskeletal rearrangements, synaptogenesis, dendritic morphology, and cellular migration (Ho et al., 2001; Adams and Sweatt, 2002) that could be crucial for barrel development. Preliminary studies examining *Syngap*$^{-/-}$ mutants were conducted prior to me joining the laboratory and were qualitatively screened for a barrel phenotype. Chapter 4 of this thesis examines in greater detail the role of SynGAP in gross cortical development and also patterning of the trigeminal system by analysing the sensory-periphery related patterns in each ascending relay in the somatosensory pathway. In addition the site of gene action of SynGAP in barrel development was examined. SynGAP was found to be associated to the PSD in a PSD95 independent manner.

Finally a link between SynGAP and PKARIIβ signalling in barrel development was investigated.

1.8.3 Aim 3: To determine the intracellular pathways through which PKARIIβ and SynGAP mediate barrel formation

Screening targeted transgenic mice is a useful 'first step' for identifying molecules involved in barrel development. However the transgenic approach taken in Chapters 3 and 4 provides little information about the signaling pathways though which these molecules act to mediate barrel formation. To address the glutamatergic pathways and cellular processes downstream of PKAR2β- and SynGAP- mediated barrel formation, three different approaches: a pharmacological approach, a proteomic phosphorylation approach, and a genomic approach using gene arrays were carried out and are discussed in Chapter 5. Quite a few difficulties and limitations were experienced with each of these approaches and are explained in Chapter 5. However some molecules are highlighted as potential candidate downstream targets and are discussed for further experimentation.

CHAPTER 2:

Materials and Methods

2.1 Tissue Preparation for Biochemistry

2.1.1 Dissection of Barrel Cortices

Mice were sacrificed at the appropriate developmental stage for analysis by cervical dislocation (P7-adult mice) or decapitation (P0-P7 mice). Brains were then rapidly removed from the animal's skull and placed into either ice-cold phosphate buffered saline (pH7.4 PBS, NaCl 137mM, KCl 2.7mM, NaH_2PO_4 1.4mM, Na_2HPO_4 4.3mM) or an ice-cold 320mM sucrose solution (pH 7.4, containing 1mM EDTA and 5mM Tris) for synaptosome preparation. The two cerebral hemispheres were separated using a new razor blade and dissection of the barrel cortex performed on each hemisphere. Each hemisphere was placed on its medial surface and two coronal cuts were made: an anterior cut where the olfactory tubercle joins the piriform cortex, and a posterior cut where the hippocampus extends medial-lateral but has not started to curve ventrally. Then a third cut was made at the clear divide between the archicortex and neocortex. Finally a fourth cut was made at a 40° angle from the previous cut. The small block of extracted tissue was placed pial surface down, and all subcortical tissue removed using curved forceps. Particular attention was taken to ensure that all striatum was removed, because any striatum would contaminate the barrel cortex sample with earlier expression of many NRC component genes. The "barrel cortex" dissections obtained via this dissection protocol contain all six cortical layers and are pieces of tissue approximately 2.5-3mm square and 1-1.5mm thick depending upon age. Previous work has also shown that these dissections contain approximately 70-80% enrichment of the barrelfield in layer IV (Katnelson, 2002). Dissections were snap frozen on dry ice and stored in eppendorf tubes at -70° prior to analysis.

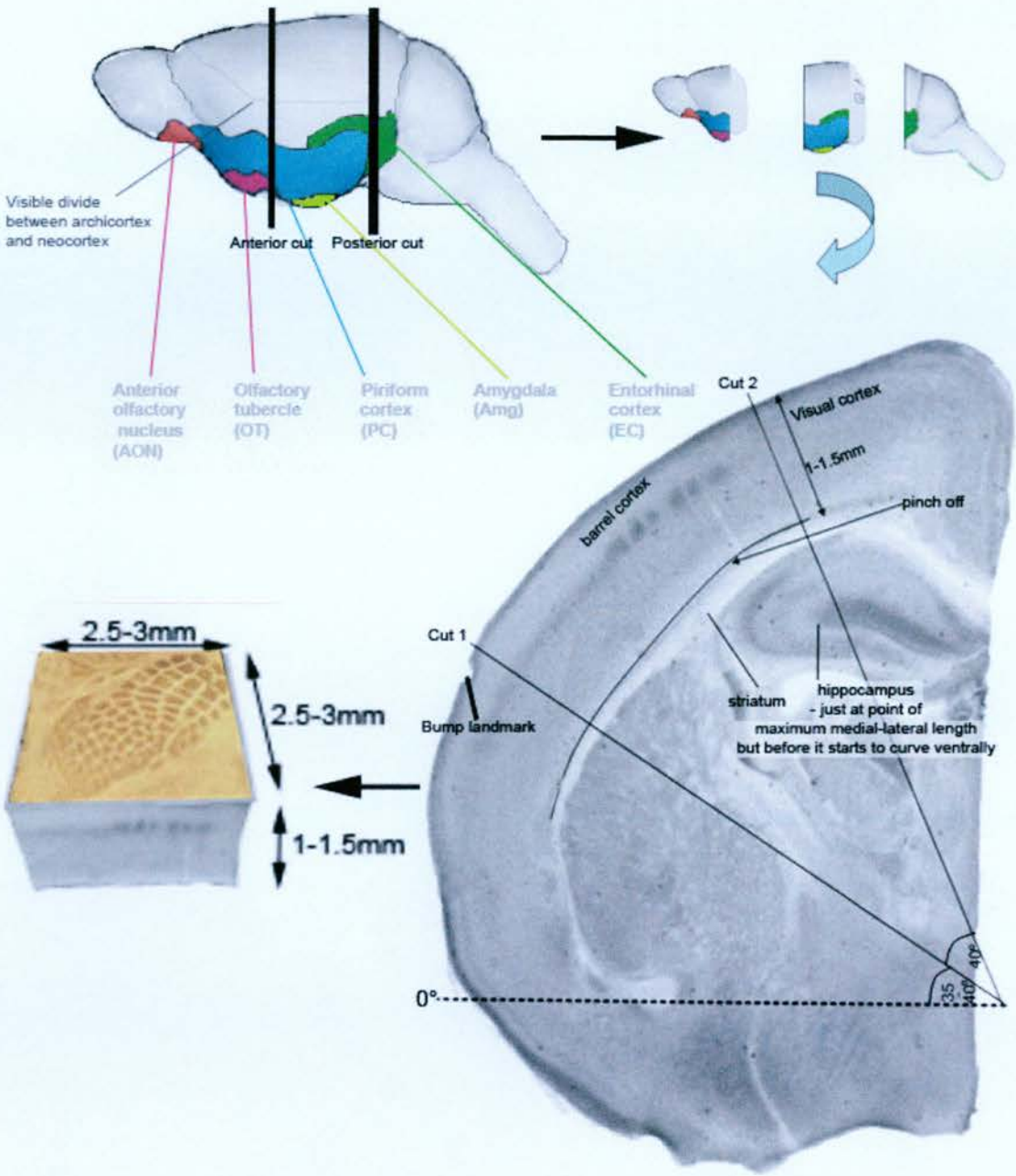

Figure 2.1: Barrel Cortex Dissection. Each brain hemisphere is placed on its medial surface and two coronal cuts are made: an anterior cut where the olfactory tubercle joins the piriform cortex, and a posterior cut where the hippocampus extends medial-lateral but has not started to curve ventrally. The central section of the brain is then laid anterior surface down and a third cut made at the divide between the neocortex and the archicortex. A final cut is made at a 40° angle from the third cut. The small block of tissue remaining is placed pial surface down, and all subcortical tissue removed using curved forceps. (Diagram by Mark Hillen; Hillen, 2006)

2.2 Biochemistry

2.2.1 Barrel Cortex Homogenisation

Barrel cortices from individual mice were homogenised for western blot analysis using a Teflon-glass homogeniser in 200µl of lysis buffer (containing 50mM HEPES pH7.5, 1% Triton X-100, 50mM NaCl, Protease Inhibitors (Roche) and Phosphatase Inhibitor cocktails I and II (Sigma P2850 and P5276)) on ice. Protein concentration in the homogenate was determined by carrying out a Lowry Assay (using the Biorad Protein Assay kit) using a BSA protein standard curve.

2.2.2 Synaptosome and PSD preparation

Synaptosomes were prepared according to the methods of Dunkley et al. (1986). Multiple barrel cortices were combined for each synaptosome preparation (to provide enough working material) and strongly homogenised in an ice-cold 320mM sucrose solution (pH 7.4, containing 1mM EDTA and 5mM Tris) using a Teflon glass homogeniser at 700rpm. The homogenate was then layered onto percoll gradients (3ml layers of 24, 10 and 3% percoll) and centrifuged for 12 minutes at 15,000rpm at 4°C. Synaptosomes were removed from between the 24 and 10% percoll layers and centrifuged for 40 minutes at 15000rpm in ice-cold 320mM sucrose solution. The resulting pellet was resuspended in cold Krebs buffer (lacking Ca^{2+}, but containing NaCl, KCl, $MgSO_4$, glucose, $Na_2HPO_4.12H_20$, and HEPES) and centrifuged at 4°C for 10 minutes at 15000rpm, twice in succession. The final pellet of synaptosomes was then treated with lysis buffer ((containing 50mM HEPES pH7.5, 1% Triton X-100, 50mM NaCl, Protease Inhibitors (Roche) and Phosphatase Inhibitor cocktails I and II (Sigma P2850 and P5276)). The PSD fraction was obtained by two further successive centrifugations at 36,800 x g for 45 minutes (Walikonis et al., 2000).

2.2.3 Western Blotting

Samples for SDS-polyacrylamide gel electrophoresis were prepared by boiling in Laemmli sample buffer containing 5% β-mercaptoethanol (Sigma, UK), and loaded onto a 7% or 10% SDS-minigel (according to the molecular weight of the protein of interest) with a 4% stacking gel. Gels were run at constant current in buffer (Tris, glycine, SDS and dH_20). The protein gels were then electroblotted onto nitrocellulose membranes (biorad) in transfer buffer (Tris, glycine, methanol and dH_20) for 2 hours at a constant current. After transfer, the nitrocellulose was stained in 0.1% Amido Black, followed by several washes in distilled water, to confirm visually that equal amounts of protein were loaded in comparable lanes. The nitrocellulose membranes were then probed with primary antibody overnight at room temperature. The membranes were rinsed in dH_20, and TBS:0.2%Triton followed by two 5 minute washes in TBS:0.2%Triton, before a 1.5hour incubation in appropriate secondary antibody (HRP-conjugated or fluorescent 698 or 800 anti-mouse or anti-rabbit antibodies). Blots were washed as above and the signal detected using either an ECL plus kit (Amersham or Pierce, Rockland) and Kodak XAR autoradiographic film, or by drying the nitrocellulose blots and scanning them with the Licor Odyssey imaging system. Densitometry was performed using either the BioRad GS710 imager using the BioRad Quantity One imaging software or the Licor Odyssey imaging system and then using NIH ImageJ software.

2.3 Tissue Preparation for Histology

2.3.1 Brain Perfusion

Animals were deeply anaesthetized with a lethal dose of sodium pentobarbital (0.1ml of 60mg/ml Sagatal/Pentoject, AnimalCare Ltd, Dunnington, York, UK) injected intraperitoneally. When all reflexes had subsided the animals were then transcardially perfused with 0.1 M phosphate-buffered saline (PBS; pH7.4) followed by 4% chilled paraformaldehyde in 0.1 M phosphate buffer (pH7.4; $NaH_2PO_4.2H_20$, Na_2HPO_4). Brains were removed from the skull and postfixed for at least 24 hours in

the same fixative, and stored at 4°C. Prior to sectioning on a freezing microtome the brains were placed in 30% sucrose in PB to equilibrate overnight.

2.3.2 Tissue for immunohistochemistry

Brain tissue was sectioned at 48μm on a freezing microtome at -20°C (with the exception of sections for immunoelectron microscopy) either coronally to reveal the cortical layers and thalamic nuclei or tangential to the pial surface to reveal a full barrel field. Prior to performing tangential sections through the cortex, curved forceps were used to remove all the tissue beneath the cortex including thalamus, hippocampus and striatum, in order to flatten the cortical sheet. The flattened cortex was then placed pial surface up on a freezing microtome stage using a glass slide to ensure a level surface. The glass slide was kept in place until the cortex froze to ensure sections were cut in the tangential plane. For coronal sections, the cerebellum was removed and the brain mounted posterior end down on a freezing microtome stage, with the brain's midline at a 90° angle to the stage.

2.3.3 Tissue for immunoelectron microscopy

Brain tissue was perfused as above (2.3.1) except that 0.1% gluteraldehyde was included in the fixative. Tissue was then sectioned at 50μm on a vibrotome at room temperature and placed in primary antibody overnight at 4°C in the absence of detergent. Immunohistochemistry was performed on the sections as described below (2.4.3) except that no triton was used in any step of the protocol to protect cellular ultrastructure. Control sections however, were incubated in antibody containing triton.

2.4 Histological Techniques

2.4.1 Cytochrome Oxidase Staining

Brain sections were mounted on chromealum coated slides and left to dry overnight. Mounted sections were then placed in cytochrome oxidase solution (0.5mg/ml DAB, 0.1M PB, 0.2mg/ml cytochrome C (sigma), 40mg/ml sucrose (sigma)) for 4-5hours at 37°C. Sections were then thoroughly washed in PB before dehydrating though an alcohol series (1 minute consecutively in 70%, 90%, 95%, 100% and 100% ethanol (EtOH)), defatting in Xylene and coverslipping in Depex.

2.4.2 Nissl Staining

Brain sections were mounted on chromealum coated slides and left to dry overnight. Then sections were briefly re-hydrated in dH_20 and placed in thionin solution (nissl stain) for 20minutes. Thionin staining solution was made up fresh from three stock solutions: [A] 1g thionin /100ml dH_20; [B] 0.1M glacial acetic acid; and [C] 0.1M Na acetate. Thionin solution contained 90mls [B] + 10ml [C] and 2.5ml [A]. Once stained, sections were differentiated in 95% ethanol containing acetic acid (1:1000). Then sections were dehydrated through a series of graded alcohols (70%, 90%, 95%, 100% and 100% EtOH), defatted in xylene and coverslipped in Depex.

2.4.3 DAB immunohistochemistry

Free-floating sections were placed in primary antibody diluted in DMEM (containing 5% fetal calf serum, 0.2% azide and 0.2-0.5% triton X-100) overnight at room temperature on a shaker. Sections were then washed twice for 5 minutes in PBS before being placed in either anti-mouse or anti-rabbit biotinylated secondary antibody, diluted in DMEM (containing 5% fetal calf serum, 0.2% azide and 0.2-0.5% triton X-100) for 2 hours. Once again sections were washed twice for 5 minutes in PBS and sections were placed in biotinylated HRP mix (Vectastain ABC kit) for 30 minutes. Visualisation was performed using DAB (1tablet dissolved in 5ml dH_2O; Sigma) containing H_2O_2.

2.4.4 Fluorescent Immunohistochemistry

Sections were incubated in primary and secondary antibodies as described above. Visualisation was performed however, by incubating the free-floating sections in a streptavidin fluorecent epitope (488 or 568), for 30 minutes. Following this, the sections were washed twice for 5minutes in PBS and then placed in 9:1 glycerol:PBS solution overnight to clear. To double label with Topro to mark cell nuclei, Topro was added (1:1000) to the 9:1 glycerol:PBS solution. Sections were mounted on un-subbed slides using Mowoil mounting medium (containing: Glycerol, dH_2O, Tris, 1,4-Diazobicyclooctane (DABCO) (Sigma) Antifade and Mowoil (Poly Vinyl Alcohol, BDH)) before examination using a confocal microscope.

2.5 Neuronal Primary Cell Culture

2.5.1 Preparation of dissociated cortical cell cultures

Timed pregnancies were set up and pregnant females sacrificed when their embryos reached E18.5. E18.5 embryos were dissected out of the sacrificed adult mice using sterile tools and placed into a petri dish containing ice-cold L15 (Leibovitz) solution (Gibco). Individual brains were then removed from their skulls and their cortices dissected out in fresh ice-cold L15 solution. The hippocampus and other subcortical tissue as well as the meninges were removed. Dissected cortices were then placed in E1 solution ((120mg papain (calbiochem), 20mg cysteine (Sigma), 200µl EDTA solution, 40µl B-mercaptoethanol solution (Sigma) dissolved in 20ml HEBSS (Gibco) at 37°C and sterile filtered)) on ice. Once all the embryos were dissected, cortices were chopped in E1 solution and placed in an incubator at 37°C for 30 minutes. After 30 minutes the reaction was stopped by adding equal volumes of E2 solution ((20mg trypsin inhibitor and 2mg DNAse (both Sigma) dissolved in HDMEM (Gibco) and sterile filtered)) and growth medium (100ml BME, 5ml Horse Serum, 1ml Pen-strep, 1.6ml of 32.5% glucose solution, 1ml 100mM sodium pyruvate and 1ml N2 supplement (all Gibco), sterile filtered) to the chopped cortices in E1. The mixture was gently shaken and the cells spun down in a centrifuge for 5

minutes at 1200rpm. The supernatant was removed and discarded and 1ml of growth medium added to the pellet of cells. The tissue was then triturated using graded, fire polished Pasteur pipettes until no clumps were visible. Finally the density of cells was calculated using a haemocytometer and the cell suspension diluted to an appropriate concentration for plating in a 6-well plate (approximately 500,000 cells per well). The plates were pre-coated in poly-L-lysine (1:200 dilution of 10mg/ml PLL; Sigma for 2 hours) and washed once with dH_2O before use.

2.5.2 Maintenance of cortical cell cultures

24 hours after plating the dissociated cortical cells, the culture media was changed, replacing the old media with fresh, 1.5 ml of serum-free growth media (100ml BME, 1ml Pen-strep, 1.6ml 32.5% glucose solution, 1ml Na pyruvate, 1ml N2 supplement, 2ml B27 supplement; Gibco). Subsequently, half the volume of old media was changed twice a week for fresh serum-free growth media to keep the cultures healthy. Cells were maintained until 14 days in vitro (DIV).

2.5.3 Harvest of cortical cell cultures

Cortical cell cultures were harvested for biochemistry at the appropriate day in vitro for experimental analysis. Growth media was removed from the cultures and the cells briefly washed in PBS at room temperature. Then ice-cold lysis buffer (containing 50mM HEPES pH7.5, 1% Triton X-100, 50mM NaCl, Protease Inhibitors (Roche) and Phosphatase Inhibitor cocktails I and II (Sigma P2850 and P5276)) was added to each well and the cells scraped off into the lysis buffer. The cell suspension was removed into a fresh eppendorf tube and snap frozen on dry ice.

2.6 Real Time RTPCR

2.6.1 Isolation of mRNA from barrel cortices

A Qiagen RNeasy mini kit was used to isolate mRNA from barrel cortices. First, barrel cortices were homogenised in Qiagen RLT lysis buffer containing β-mercaptoethanol (10μl β-mercaptoethanol/1ml lysis buffer). This homogenisation was performed by repeatedly pipetting up and down the thawed brain tissue in RLT buffer and then by drawing and expelling the mixture through a 0.2mm diameter syringe needle five times. Then the manufacturers instructions were followed in order to extract total RNA (Qiagen). The optional 15minute Rnase-free Dnase digestion step (Qiagen) was included in the protocol.

2.6.2 RNA quality assessment

Quality of RNA samples was tested before proceeding to cDNA synthesis. 1μl of RNA sample was run out on a 1% agarose gel made with 1xTBE buffer (100mM Tris, 90mM boric acid and 1mM EDTA, dH_2O) containing ethidium bromide (EtBr: 1μl/100ml) for visualisation. Samples were run in an "RNA only" gel tank and run at 80volts for 15minutes before imaging the resultant gel. Good quality RNA was recognised by (1) two distinct bands that represent 60S and 40S RNA and (2) a 60S band that displayed twice the intensity of the 40S band. If the RNA was smeared or the 60S band did not show greater intensity than the 40S band, the samples were re-run on a fresh gel, and if the characteristics of the mRNA remained the same, they were then discarded because the samples appeared to be degraded.

2.6.3 Reverse Transcription of messenger RNA

1μg of mRNA was added to 21.1μl of double distilled water in an Rnase-free 0.5ml PCR eppendorf tube. This RNA mixture was heated to 75°C in a PCR block for 5minutes and then immediately cooled on ice and stored until required. A cDNA mastermix solution was prepared that contained 3.3μM random hexamers

(Amersham), 3mM $MgCl_2$ (Invitrogen), 500μM of NTPs (Promega), 1 unit/μl Rnase inhibitor (Invitrogen) and 1x PCR buffer (Invitrogen). For each cDNA synthesis, 77.9μl of cDNA mastermix solution was added to the diluted mRNA samples and placed in a PCR block at 42°C for 5minutes. 2μl of MMLV-RT enzyme (Invitrogen) was then added to each tube before incubating them at 42°C for 1 hour, and 95°C for 5 minutes. The cDNA was stored at -20°C.

2.6.4 SYBRgreen RTPCR Primer Design

Primer pairs were designed for qRT-PCR according to the following guidelines:

1. amplicon size must have between 80-200bp
2. the primers must span an intron
3. the primer sequences must pass a BLAST test so that primers have homology to only the gene of interest
4. the primers must produce a single specific DNA product

2.6.5 Relative Gene Expression Quantification

qRTPCR data was normalised against two housekeeping genes, glyceraldehyde-3-phosphate dehydrogenase (GAPDH) and 18S. The reason for normalising the data to housekeeping genes was to compare the data between (1) different primer pairs and (2) repeated runs of PCR on the same gene. Housekeeping genes should ideally be expressed at levels that remain constant in proportion to the total RNA in each sample, causing variation in the total RNA added to each cDNA synthesis reaction to be normalised. Housekeeping genes should also not change between genotype (Suzuki et al., 2000).

2.6.6 SYBRgreen qRT-PCR linearity tests

Two serial dilution series of either WT or KO P7 cDNA were performed for every primer pair in every qRT-PCR run in order to test the linearity of each PCR reaction. The dilution series tested for both cDNA quality and pipetting accuracy and also

tested for any differences in rate of cDNA amplfication between sample concentration that should not occur.

CHAPTER 3:

The role of PKAR2β in mouse somatosensory cortex development

3.1 Introduction

The signaling molecule cAMP-dependent protein kinase A (PKA) has been shown to play an important role in numerous forms of synaptic plasticity. It has recently been demonstrated that pharmacological blockade of PKA disrupts postsynaptic mechanisms such as long-term potentiation (LTP) and long-term depression at developing TCA synapses (Lu et al., 2003) and that PKA plays an essential role in ocular dominance plasticity in the developing visual cortex (Beaver et al., 2001; Fischer et al., 2004). PKA is a holoenzyme composed of two regulatory (R1α, R1β, RIIα and RIIβ) and two catalytic subunits (Cα and Cβ). cAMP binds to the regulatory subunits and results in the liberation of the active catalytic subunits. Different PKA-holoenzymes are targeted to various subcellular loci both pre- and post- synaptically, mediated by the interaction of R-subunits with different A-kinase anchoring proteins (AKAPs) (Colledge & Scott, 1999; Rubin, 1994).

PKA was first postulated to play a role in barrel development when "barrelless" (*brl*) mice (Welker et al., 1996) were found to have a defect in the Adenyl Cyclase 1 (AC1) gene (Abdel-Majid et al., 1998). *Barrelless* mice have normal gross topological organisation of S1 but no segregation of TCAs or layer 4 cells, similar to 5-HT over-expressing mice (Gaspar et al., 2003). AC1 is a Ca^{2+}/calmodulin dependent adenylyl cyclase that converts ATP into cAMP to increases in intracellular calcium. The most studied target of cAMP is PKA. PKA is a ubiquitously expressed enzyme present in both the presynaptic axon terminals and postsynaptic densities of thalamocortical synapses and can be regulated by presynaptic 5-HT1B and postsynaptic NMDA and mGluR5 receptors (Kind and Neumann, 2001). 5HT1B, NMDA and mGluR5 are all neurotransmitter receptors known to play an important role in barrel formation (see Chapter 1). The lack of TCA segregation in *brl* mice suggested that PKA via AC1 could affect barrel development in the presynaptic axon terminal, possibly downstream of the 5HT1B receptor reducing glutamate release (Abdel-Majid et al., 1998; Laurent et al., 2002). Overactivation of the 5HT1B receptor by excessive 5HT in MAOA knockout mice has been shown to reduce monosynaptic TC EPSCs (Laurent et al., 2002). However whether AC1 acts via PKA or another cAMP dependent target is not known. This

chapter examines whether PKA is a downstream target of AC1 in presynaptic terminals in barrel development. Alternatively, PKA has been hypothesised to play a post- synaptic role in barrel formation (Kind and Neumann, 2001).

Previous pharmacological studies using PKA inhibitors have not been able to distinguish between the effects and loci of different PKA-holoenzymes in barrel development because these inhibitors abolish all types of PKA. However recent advances in transgenic technology have created a useful tool for investigating the role of PKA in barrel formation in detail. Prior to me joining the lab, mutant mice lacking each of the PKA subunits were generated (Brandon et al., 1995, 1998; Howe et al., 2002; Amieux et al., 2002; Skalhegg et al., 2002) and their barrel cortices screened for defects using Nissl stain, with the exception of RIα, as *Prkar1α*$^{-/-}$ mice were found to die in utero (Amieux et al., 2002). Normal segregation of layer 4 cells was observed in each of the PKA subunit specific knockouts generated apart from the *Prkar2β*$^{-/-}$ mutants in which qualitative assessment of segregation was impaired (Figure 3.1). This chapter examines the barrelfield morphology of *Prkar2β*$^{-/-}$ mutant mice in greater detail, determines the site of action where PKAR2β plays its role in barrel formation and investigates whether or not the molecular mechanisms through which PKAR2β affects barrel development are the same as those involved in synaptic plasticity.

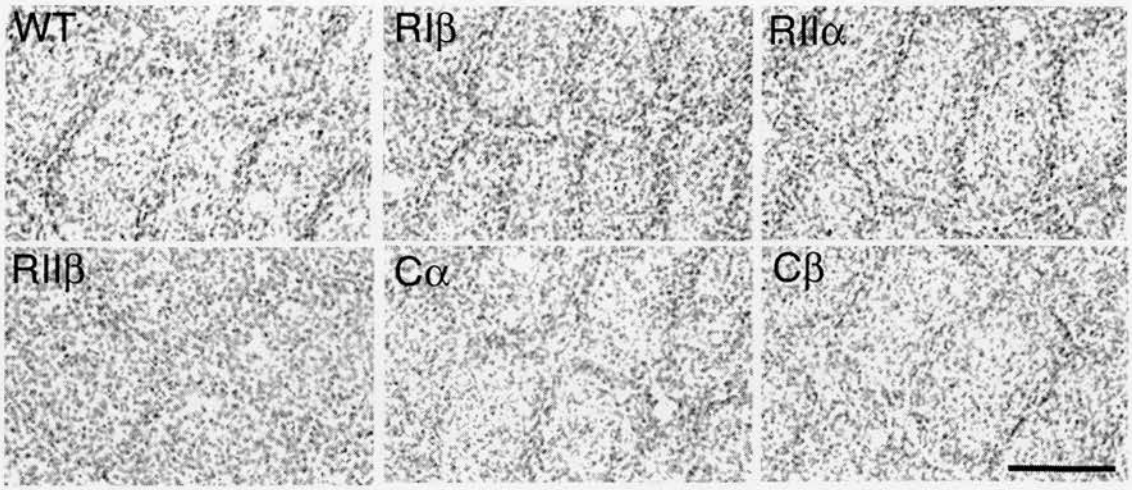

Figure 3.1: Nissl stained tangential sections through layer 4 of S1 of adult wild-type (WT) and PKA subunit specific knockout mice lacking RIβ, RIIα, RIIβ, Cα and Cβ. Barrels are present in each PKA-subunit specific knockout generated however *Prkar2β*$^{-/-}$ mice show less well defined barrels. Scale bar, 200μm. (Watson et al., 2006 – included as Appendix 1)

3.2 Methods

3.2.1 Animals

Initial generation of *Prkar2β*$^{-/-}$ mice has been described previously (Brandon et al., 1998). In brief, *Prkar2β*$^{-/-}$ mice were created by whole animal gene targeting, introducing genetically manipulated ES cells into the germ line of chimeric mice. Newly derived ES cells were manipulated using an R2β targeting vector that has a neomycin cassette that substitutes for 2kb of genomic sequence, which includes exon 1 and the translational start site (Brandon et al., 1998). *Prkar2β*$^{-/-}$ mice were obtained from the University of Washington, Seattle and maintained at the University of Edinburgh on a C57BL/6J background. *Prkar2β*$^{-/-}$ mice were also bred onto the B6/129 and MF1 genetic backgrounds to screen for barrel phenotypes. GluRA KO (Zamanillo et al., 1999), GluRB and GluRC KO brains were obtained from Dr Rolf Sprengel (Max-Planck-Institut fur medizinische Forschung, Heidelburg, Germany).

3.2.2 Genotyping

Tails biopsies were digested overnight with a proteinase K solution, and the DNA extracted using a Macherey-Nagel Nucleospin kit (ABgene). R2β genotyping was then performed by RTPCR using the following primers and Taqman probes: R2β_for 5'-CACGGGCAGGATGAGCAT-3', R2β_Rev 5'-TCAGCACCTCCACCGTGAA-3', neo_for 5'-ATGGCCGCTTTTCTGGATT-3', neo_rev 5'-GCCAAGCTCTTCAGCAATATCA-3', R2β hyb 6-FAM-CTCACGGAGCTGCT-TAMRA, and neo hyb VIC-CGGACCGCTATCAGG-TAMRA. A full description of the genotyping protocol can be found in Appendix 2.

3.2.3 Histology and immunohistochemistry

Postnatal day 4, 7 and 14 animals were killed and perfused as described in Chapter 2, postfixed overnight in 4% paraformaldehyde and then equibrilated overnight in 30% sucrose. Brains were sectioned on a freezing microtome at 48μm, either coronally to reveal cortical layers and thalamic nuclei or tangentially to reveal a full barrel field (more details can be found in Chapter 2). Sections were then mounted on chromealum coated slides and stained with thionin to reveal cellular distribution or placed in primary antibodies, free floating overnight, to reveal the localisation of PKAR2β, serotonin transporter (SERT), GluRA, GluRB/C or GluRD. Immunohistochemistry was performed as described in Chapter 2 using the following primary antibodies: rabbit anti-mouse PKAR2β (1:600 – 1:2000; Santa Cruz Biotechnology), goat anti-rabbit SERT (1:2000; Calbiochem), goat anti-rabbit GluRA (1:250; Upstate Biotechnology), goat anti-rabbit GluRB/C (1:250; Upstate Biotechnology) or goat anti-rabbit.GluRD (1:250; Upstate Biotechnology), followed by biotinylated anti-rabbit antibodies. Protein localisation was visualised using a Vectastain ABC kit (Vector laboratories) and DAB as the chromogen. All sections were subsequently dehydrated into xylene and coverslipped. For cell counts, 48μm tangential sections were immunolabeled for SERT (as above), but visualised using an Alexafluor 488 streptavidin epitope (1:200; Invitrogen). These free-floating sections were then counterstained with Topro (1:1000, Invitrogen) diluted in PBS-glycerol

(9:1) to reveal the cell nuclei. Sections were mounted on non-subbed slides and coverslipped using Mowoil (see Chapter 2). To examine thalamic nuclei, coronal sections were mounted on chromealum subbed slides and then reacted with cytochrome oxidase (see Chapter 2).

3.2.4 Area measurements

Tangential sections stained with anti-SERT antibody were used to calculate measurements of TCA patch, PMBSF area and total S1 cortex area. Images were captured at magnifications of 31.25X (S1 cortex area), 62.5X (PMBSF area), and 125X (C1 barrel area) using a Leica DMLB microscope, Leica 480 digital camera, and the Leica DMLB Image Manager version 4.0 program. Image Tool software was used to measure areas of interest on these digital images and the measurements calibrated using a 1mm graticule.

3.2.5 Cell Counts

Cells counts were performed on tangential sections fluorescently labelled with anti-SERT antibody and Topro. All sections were examined and then the sections with the most well-segregated barrels were chosen and the position of C2 determined. Confocal images of C2 and its neighbouring barrels were obtained at 7μm intervals through each of these sections using the 10 and 20X objectives. For each series of optical sections, the section containing the most qualitatively segregated (cell-dense barrel wall versus cell-sparse barrel hollow) barrel of interest was chosen to begin the analysis and then the two adjacent sections (upper and lower) were also used. The selected sections were converted to black and white to increase contrast, and 5-8 rectangular boxes placed in the barrel wall, determined by the edge of the TCA patch stained by SERT antibody, and in the barrel hollow at the centre of the TCA patch. The density of Topro-stained nuclei in each rectangle was calculated and from all this data the average density of Topro-stained nuclei in the walls and hollow of the chosen barrel was calculated in both WT and *Prkar2β*$^{-/-}$ animals.

3.2.6 Immunoelectron microscopy

P14 WT mice were perfused as described in Chapter 2 but 0.1% gluteraldehyde was added to the 4% paraformaldehyde fixative. Brains were sectioned coronally at 50μm using a vibrotome and then placed in anti- R2β antibody (1:200) overnight at 4°C in the absence of detergent to protect cellular ultrastructure. Sections were reacted for DAB histochemistry as described in Chapter 2 but triton was omitted from every step of the protocol. They were then post fixed in 1% osmium in 0.1M phosphate buffer for 45 minutes. Following dehydration through an ascending series of ethanol solutions and propylene oxide, and in collaboration with Dr Tom Gillingwater, all sections were embedded on glass slides in Durcupan resin. Under a dissecting microscope, regions of barrel cortex (approximately 1 x $1mm^2$) were then cut out using a scapel blade and glued onto a resin block for sectioning. Ultrathin sections (70nm) were cut and collected on Formvar-coated grids (Agar Scientific, Stansted, UK). These were stained with uranyl acetate and lead citrate in a LKB-Wallac (Gaithersburg, MD) Ultrostainer, and then assessed in a Philips CM12 transmission electron microscope. Negatives taken in the microscope were scanned onto an Apple Macintosh G5 computer using an Epson 4870 photo flat-bed scanner at 1200 dots per inch. Finally images were prepared for presentation using Adobe Photoshop software (Adobe systems).

3.2.7 Synaptosome and PSD preparations

Animals ranging in age from P4 to adult were killed and their brains dissected for S1 cortex in ice-cold 320mM sucrose solution (see Chapter 2). Synaptosomes were then prepared according to the methods of Dunkley et al. (1986) and as previously described in Chapter 2. It is important to note that a strong homogenisation step was used, resulting in little if any membrane remaining attached to the postsynaptic density; therefore the synaptosomes used here contain a presynaptic terminal and only postsynaptic proteins associated with the PSD. Synaptosomes were then centrifuged at 36,800 x g for 45 minutes twice in succession (Walikonis et al., 2000) to pellet the PSD fraction. This was performed in the presence or absence of Ca^{2+} (100μM).

3.2.8 PPW and PSD separation

The presynaptic particle web (PPW) and PSD were initially purified according to the methods of Phillips et al. (2001). In brief, synaptosomes were extracted with 1% triton at pH6.0 and then 1% triton at pH8.0. Synaptosomes were diluted 1:10 with ice-cold 0.1mM $CaCl_2$ and then brought to a final concentration of 20mM Tris, pH6.0 and 1% triton and left on ice for 30 minutes to extract membranes. The insoluble material was then pelleted by centrifugation at 40,000 x g for 30 minutes. The supernatant was decanted and proteins precipitated using 10 volumes of acetone at -20°C and recovered by centrifugation at 15,000 x g for 30 minutes. The remaining pellet was resuspended in 1% triton solution at pH6.0 and reextracted, precipitated and pelleted as above (saving an aliquot for gel electrophoresis). The insoluble pellet was then resuspended in 20mM Tris and 1% triton at pH8.0 and extracted, centrifuged and the supernatant reprecipitated as above. This was repeated several more times in the hope of isolating pure PPW and PSD fractions. Protein concentrations were then calculated in all pellet and recovered supernatant fractions and samples prepared for western blot analysis.

3.2.9 Western Blotting

Immunoblot analysis was performed on P4 to adult barrel cortex homogenate, synaptosome and PSD preparations as described in Chapter 2. The following primary antibodies were used: GluRA (1:1000, Upstate Biotechnology), R2β (1:600, Santa Cruz Biotechnology), PKA R1 (1:500, BD Transduction Labs), PKA C (1:1000, BD Transduction labs). PKA R2α (1:1000, BD Transduction labs), SAP102 (1:5000, Chemicon) and PSD95 (1:20,000, Upstate Biotechnology).

3.3 Results

3.3.1 Defects in the cortical barrelfield of *Prkar2β*$^{-/-}$ mutant mice

To investigate the role of PKAR2β in barrel formation, I first examined the expression of R2β protein through development. Immunostaining for R2β in coronal sections shows strong expression in layer IV of the cortex of WT mice at P4 and P7 (Fig. 3.2 A,B respectively), the time when barrels are forming. The staining appears as diffuse neuropilar patches through layer IV. R2β immunohistochemistry on a tangential section through layer IV at P7 (Fig. 3.2 C) confirms that these patches correspond to the barrels, showing high expression in S1 in a clear whisker-related pattern. No reaction product is visible in brains from *Prkar2β*$^{-/-}$ mice (Fig. 3.2 E, F), confirming that the R2β antibody used is specific.

The precise morphology of the barrel defect present in *Prkar2β*$^{-/-}$ mutants was then examined at P7 (previous preliminary analysis was performed on adult brains). Nissl-stained sections of P7 WT and *Prkar2β*$^{-/-}$ mice (Fig. 3.2 G-J) show that *Prkar2β*$^{-/-}$mice have reduced cellular segregation in layer IV, similar to that seen in adult KOs. Barrels can be seen in the PMBSF of *Prkar2β*$^{-/-}$mice but they appear much less well defined compared to those present in WT mice. In the anterior snout (AS) region however, no barrels are visible. To investigate the possibility that the plane of section missed the anterior snout region, adjacent sections were examined through each brain (Figure 3.2).

The *Prkar2β*$^{-/-}$ barrel phenotype described above is relatively subtle compared to barrelless mice and was examined on a C57/BL6 genetic background (Fig. 3.2 I, J). Previous work on *Mglur5*$^{-/-}$ mice has shown that background strain can affect the degree of severity of a barrel phenotype (Hannan et al., 2001). To determine whether *Prkar2β*$^{-/-}$ mice have a stronger phenotype on another background the R2β null mutation was examined on two more backgrounds, MF1 and B6/129 (Fig. 3.3 A-D). By qualitative assessment, the *Prkar2β*$^{-/-}$ mice display similar barrel phenotypes on all three backgrounds (C57/BL6, MF1 and B6/129). Since a stronger

phenotype was not found on another strain, it was decided that all further experiments should continue on the C57/BL6 strain of mice.

Since *Prkar2β*$^{-/-}$ mice appear to show impairment in layer IV cellular segregation in PMBSF, and not a complete lack of barrels, quantitative analysis of cellular segregation was performed in both WT and *Prkar2β*$^{-/-}$ mice in order to further assess the barrel defect found in *Prkar2β*$^{-/-}$ mice. The cell densities of barrel walls and barrel hollows were calculated in WT and *Prkar2β*$^{-/-}$ mice (Fig. 3.4 A–F) from tangential sections double labelled by Topro that stains the cell nuclei, and SERT immunohistochemistry that stains the TCA patches. The same barrel (in this case, C2) was identified in each animal, and nuclei counts performed on 7μm optical sections through this barrel, obtained using the confocal microscope (Fig. 3.4 A-F). The blind analysis revealed a significant decrease in the wall-to-hollow cell density ratio in the *Prkar2β*$^{-/-}$ mice ($n = 5$) compared to the WT controls ($n = 5$) (1.32 ± 0.03 vs 1.76 ± 0.05, respectively; $p = 0.0001$) (Fig. 3.5). Importantly, a change in overall density of cells in layer IV was not found, suggesting that cell death is unlikely to be responsible for the *Prkar2β*$^{-/-}$ phenotype, although stereology was not used so calculation of the overall numbers of cells is not possible.

3.3.2 Role of R2β in TCA segregation

To determine whether R2β plays a role in TCA segregation, SERT staining was performed on tangential sections through layer IV. Qualitatively a normal whisker related pattern is visible in the PMBSF of WT and *Prkar2β*$^{-/-}$ mice (Fig. 3.6 A, B respectively). Both patch size and distribution of TCAs in the PMBSF also appear similar between WT and *Prkar2β*$^{-/-}$ mice. This result was in distinct contrast to the diffuse termination of TCAs in layer IV of *brl* (AC1 KO) mutant mice (Welker et al, 1996), suggesting that PKAR2β might not be the downstream target of AC1 as previously hypothesised. Measurements of individual patch area and overall PMBSF size were performed in order to confirm the qualitative assessment. No difference in individual patch area or overall PMBSF size is found between WT and *Prkar2β*$^{-/-}$ mice (Fig. 3.6 C and Appendix 3). Differences in SERT staining are observed

however in the anterior snout (AS) region of the *Prkar2β*$^{-/-}$ barrelfield (Fig. 3.6 B). In *Prkar2β*$^{-/-}$ mice TCA patches are more difficult to define within the AS region due to reduced segregation. To confirm that this observation did not simply result from the differences in flattening and sectioning the cortex, three adjacent sections through layer IV were examined in several *Prkar2β*$^{-/-}$ mice compared to three adjacent sections in wild type animals (Fig. 3.7). Each *Prkar2β*$^{-/-}$ mouse examined shows reduced segregation in the AS region compared to the segregation found in a WT (Fig. 3.7). The boundaries between the AS region and other subregions of S1 are still clearly evident in each *Prkar2β*$^{-/-}$ though (Fig. 3.6 B and Fig. 3.7 B-D), indicating that the loss of R2β does not effect general TCA pathfinding, but causes reduced TCA segregation solely in the AS region. The anterior snout phenotype in *Prkar2β*$^{-/-}$ mice, consisting of a lack of cortical barrels despite partial TCA segregation, is similar to the phenotypes found in phospholipase C-β1 (PLCβ1), mGluR5 (Hannan et al., 2001) and cortex specific NR1 knockout mice (Iwasato et al., 2000) and agrees with a postsynaptic role for PKA in barrel formation.

To further assess a possible presynaptic role for R2β, I examined its expression pattern in the thalamic ventral posterior medial (VpM) nucleus, which projects to S1, and barreloid formation. At P7, immunohistochemistry for R2β shows diffuse staining throughout the thalamus, with strongest staining in the inter-barreloid regions in VpM (Fig. 3.8 C) and cytochrome oxidase staining shows that barreloid segregation is indistinguishable between WT and *Prkar2β*$^{-/-}$ mice (Fig. 3.8 A, B). These results reveal that R2β is not crucial for barreloid formation and support the hypothesis that cortically expressed R2β is required for barrel development.

3.3.3 Postsynaptic expression of R2β

PKA holoenzymes are targeted to discrete subcellular structures via scaffolding molecules called A-kinase anchor proteins (AKAPs) (Colledge & Scott, 1999). In adult brain, AKAP79/150 and Yotiao are known to bind to the R2β subunit of PKA and localise it to NMDA receptors. To determine whether R2β selectively associates with the PSD in developing thalamocortical synapses, two different experimental

approaches were carried out: biochemical isolation of PSD from P10 barrel cortex tissue and immunoelectron microscopy (EM) of layer IV of P14 barrel cortex.

PSD purification

In CNS synapses the PSD is very tightly adhered to the presynaptic particle web (PPW), a presynaptic specialization important for the docking of vesicles (Phillips et al., 2001). The strong interaction that exists between the PSD and PPW results from adhesion molecules such as cadherins, neuroligin-B, neurexin, ephrins and eph receptors spanning the synaptic cleft (Abbas, 2003). "Classic" biochemical PSD preparations, described in Chapter 2 and literature from other laboratories (Walikonis et al., 2000; Peng et al., 2004), contain enriched PSD proteins but also some presynaptic membrane associated proteins resulting from the strong pre- and post-synaptic adhesion. Therefore a "classic" PSD preparation (Walikonis et al., 2000) cannot be used to confirm the pre- or post- synaptic localisation of a particular protein. Phillips et al. (2001) however demonstrated a sensitivity of the PPW to small changes in pH and established that synaptosomes extracted using detergent at pH8.0 caused PPW to disintegrate and become soluble, leaving behind an insoluble fraction that EM revealed to be PSD. At pH6.0, this phenomenon did not occur and the presynaptic specialisation remained insoluble and attached to the PSD. The initial biochemical approach taken to determine the pre- and/or post- synaptic localisation of R2β was to recreate this result found in Phillips et al. (2001) in younger (P10) cortex and isolate "pure" PSD and PPW preparations that could be used to determine localisation of synaptic proteins, including R2β. To assess the purity of the PSD (P2) and PPW (S2) fractions isolated by this pH extraction protocol (see Methods), each fraction was separated by gel-electrophoresis and stained with presynaptic markers Dynamin and Munc-18, and postsynaptic marker PSD95. Following extraction at pH8.0, Dynamin and Munc-18 are both enriched in the PPW insoluble fraction and PSD95 is enriched in the PSD fraction as expected (Fig. 3.9 B). However Dynamin and Munc-18 are still found present in P2 and PSD95 in S2 indicating that while both fractions are enriched in their appropriate synaptic proteins, the PSD and PPW are not completely isolated from one another. As a consequence the protocol was adapted, and further extraction steps introduced in order to increase the stringency of the purification (see Methods). A western blot

of the fractions produced by these multiple extraction steps (Fig. 3.9 C) shows that postsynaptic markers PSD95 and GluR1 are found consistently in each insoluble pellet (P1, P2, P3 and P4). No major decrease in the levels of these proteins can be seen between pellet fractions P1 and P4 and neither proteins were present in the soluble supernatant fractions S3 and S4, indicating that PSD95 and GluR1 are well-retained in the PSD fraction, P4. In contrast, Munc-18 and Dynamin are gradually lost from the subsequent pellet fractions, as expected because they are both presynaptic proteins. Munc-18 and Dynamin are not detected in the presynaptic soluble fractions though, likely due to dilution of the sample and although protein precipitation was attempted, acetone precipitation was insufficient to concentrate the sample. The protein profiles of these presynaptic markers (P1/S1 to P4/S4) (Fig. 3.9 C, D) clearly demonstrate an enrichment of the PSD and PPW fractions, but the presence of Munc-18 and Dynamin at low levels in the final PSD fraction P4 shows that the PSD and PPW fractions have not been purely isolated. These preps could not be used therefore to confirm the localisation of R2β.

However we did use the biochemical fractions (P1/S1 to P4/S4) to examine enrichment of R2β. Surprisingly we did not detect any R2β in the very first pellet PSD fraction. Instead R2β appeared completely associated with the first supernatant PPW fraction. We realised at this point in the study however, that Ca^{2+} was present in the PPW-PSD separation protocol buffers compared to the buffers normally used for our "classic PSD" preparation. In adult mouse brain, R2β has been shown to associate with the PSD in a calcium dependent manner (Colledge et al., 2000; Snyder et al., 2005). To test whether this calcium dependent association of R2β to the PSD also occurs in developing barrel cortex, PSDs were isolated from P7 barrel cortex in the presence or absence of 100μm Ca^{2+} (Fig. 3.10 G). In the presence of Ca^{2+}, R2β is found in the soluble supernatant fraction (dissociated from the PSD), and in the absence of Ca^{2+} R2β is found in the pellet fraction (associated with the PSD).

Immunoelectron Microcopy

Light microscopic analysis of R2β immunostaining cannot elucidate whether R2β is localised to presynaptic axon terminals or postsynaptic dendrites in layer IV. Therefore immunoelectron microscopy (EM) of layer IV of P14 barrel cortex was performed in collaboration with Dr Tom Gillingwater to determine the localisation of R2β. R2β was visualised using DAB reaction product that appears as patches of dense black staining on the EM images. R2β is present in some, but not all, dendrites and dendritic spines containing postsynaptic densities (seen in orange Fig. 3.10 B) and is never seen localised to axons or presynaptic terminals (seen in blue Fig. 3.10 B), characterised by the presence of synaptic vesicles. The absence of R2β at some of the layer IV synapses does not appear to result from poor antibody penetration because immunopositive dendrites are often seen close to the immunonegative synapses (Fig. 3.10 E, F). DAB reaction product is particularly black and dense within the PSD, indicating that R2β is mainly targeted to the PSD.

3.3.4 Lack of compensation by other PKA subunits

Compensation for the loss of R2β by other PKA subunits was investigated in order to determine whether the differences seen in phenotype between the *Prkar2β*$^{-/-}$ and barrelless mouse resulted from an increase in the expression of other PKA subunits. First, western blot analysis of synaptosome preparations from developing barrel cortices was used to show which PKA subunits are present at synapses during barrel formation (Fig. 3.11 A). All PKA subunits are present in synaptosomes that consist of presynaptic terminals with attached PSD, from P4, P7, P14, P21 and adult barrel cortex. Between P4 and P21, the expression of all the PKA subunits increase (Fig. 3.11 A), correlating with the rapid onset of synaptogenesis that occurs during this time (White et al., 1997; Spires et al., 2005). In support of this biochemistry data, we examined mRNA for each PKA subunit in developing barrel cortex and found all of them to be present at each age examined (Appendix 4). To examine compensatory changes in PKA subunit expression in *Prkar2β* mice, barrel cortex homogenate from P7 WT and *Prkar2β*$^{-/-}$ mice was analysed by western blot. No difference is detected in the level of other PKA regulatory subunits in a *Prkar2β*$^{-/-}$. However the level of

catalytic subunits detected using a pan-catalytic subunit antibody that recognises both Cα and Cβ is reduced by 35% in *Prkar2β*$^{-/-}$ mice compared to WT mice, but this reduction is not significant [720 optical density units (ODU) ± 116, n=4 vs 1107 ODU ± 180, n=4; t-test, p = 0.12] (Fig. 3.11 B). It has been reported by other groups that PKA catalytic subunits are reduced in both adult forebrain (Brandon et al., 1995, 1998) and P11 somatosensory cortex of *Prkar2β*$^{-/-}$mice (Inan et al., 2006). The apparent lack of compensation by other PKA subunits in this study and trend of lower catalytic subunit levels in *Prkar2β*$^{-/-}$ mice agrees with work done by Dr G Stanley McKnight that shows that total PKA activity is reduced by 40% in S1 of P7 *Prkar2β*$^{-/-}$ mice compared to WT controls (Appendix 5). It has previously been described that a decrease in PKA activity in *Prkar2β*$^{-/-}$ mice (Brandon et al., 1997) could be due to the degradation of catalytic subunits that occurs in the absence of a regulatory subunit (Amieux et al., 1997; Brandon et al., 1998). Higher basal activity was also found (by Dr G Stanley McKnight) in *Prkar2β*$^{-/-}$ mice (Appendix 5). One explanation for this is that catalytic subunits no longer have R2β to bind to and therefore are free and constitutively active in the cell before degradation (Niswender et al., 2005).

3.3.5 PKAR2β and AMPARs

PKA activity has been shown by several other laboratories to contribute to synaptic plasticity in part by regulating GluRA trafficking at the postsynaptic membrane (Esteban et al., 2003; Malinow and Malenka, 2002). In addition *brl* mice exhibit a reduction in PKA-phosphorylated GluRA suggesting that GluRA could be a major downstream target of AC1/PKA signaling at thalamocortical synapses. Lu et al. (2003) hypothesised that AMPAR trafficking might be the crucial mechanism underlying barrel formation as well as mechanisms of synaptic plasticity such as LTP and LTD. GluRA is present throughout S1 cortex at P7 (Fig. 3.12 C). Immunohistochemistry for GluRA in wildtype brains shows staining in each cortical layer and labels neuronal soma and neuropil, indicating synaptic localisation. Staining is reduced in layer IV compared to other layers, however neuronal and neuropilar staining is still clearly evident (Fig. 3.12 D). No staining is seen in

GluRA KO animals, which confirms the specificity of the GluRA antibody (Fig. 3.12 A, B). GluRA is also expressed in P7 VpM but at lower levels than in cortex and the rest of the thalamus (Fig. 3.12 E). Western blot analysis of WT homogenate and synaptosome preparations from S1 cortex also confirms that GluRA is expressed thoughout S1 development (Fig. 3.12 F).

To determine whether R2β plays a role in regulating the insertion of GluRA into the PSD during barrel formation, I examined the level of GluRA in synaptosomes from P7 WT and *Prkar2β*$^{-/-}$ S1 cortex (Fig. 3.13 A). Densitometry performed on western blots reveals a significant reduction in GluRA expression at the synapse in *Prkar2β*$^{-/-}$ mice compared to WT mice (Fig. 3.13 B). No change however is seen in the expression level of Sap102 in synaptosomes or GluRA levels in S1 homogenate from P7 WT and *Prkar2β*$^{-/-}$ mice (Fig. 3.13 A). To investigate if this defect in GluRA insertion into the PSD in *Prkar2β*$^{-/-}$ mice was a key mechanism for barrel formation and the reason for the barrel phenotype found in *Prkar2β*$^{-/-}$ mice, the barrelfield of GluRA KO mice was examined. Nissl-stained tangential sections through layer IV of GluRA KO mice show clear, well-segregated barrels in the PMBSF and the anterior snout region, similar to WT controls. To rule out the possibility of a subtle phenotype and confirm barrel formation to be normal in GluRA KO mice, I next quantified the degree of barrel segregation in GluRA KO mice, performing the same cell count analysis that was used to assess the *Prkar2β*$^{-/-}$ barrel phenotype. Tangential sections through layer IV were double-labeled with Topro (to stain nuclei) and SERT immunohistochemistry (to stain TCAs and thereby define the barrel hollow area), and nuclei were counted in images of 7μm optical sections (Fig. 3.13 E-G). No significant difference is found in the cell density ratio of barrel walls relative to barrel hollows in GluRA KO mice versus WT controls (1.58 ± 0.05 vs 1.6 ± 0.05, respectively; $p = 0.784$) (Fig. 3.13 H).

To look at compensation by other AMPAR subunits and further investigate a role for AMPA receptors in barrel development I examined the expression of AMPAR subunits, GluRB, GluRC and GluRD through P7 S1 cortex. Immunohistochemistry for GluRD shows a lack of staining throughout S1 cortex, in contrast to heavy

staining in the hippocampus, indicating that GluRD is not expressed in developing S1 cortex (Fig. 3.14 D and E respectively). In agreement, western blot analysis of S1 homogenate does not detect any GluRD either. GluRB and GluRC were examined using an antibody that recognised both subunits. GluRB/C staining can be seen throughout P7 S1 cortex (Fig. 3.14 A). Interestingly patches of staining are evident through layer IV that might correspond to a barrel pattern. To determine whether R2β also plays a role in GluRB/C insertion in S1 cortex, I examined the level of GluRB/C in synaptosomes from P7 WT and *Prkar2β*$^{-/-}$ S1 cortex (Fig. 3.14 A). Western blots reveal a reduction in GluRB/C expression in synaptosomes from *Prkar2β*$^{-/-}$ mice compared to WT mice (Fig. 3.14). A PKA phosphorylation site has not yet been identified in either GluRB or GluRC, however the data showing a GluRB/C insertion defect into the PSD, led me to perform a preliminary analysis of the barrelfields of GluRB and GluRC KO mice. Nissl stained tangential sections through layer IV in both GluRB and GluRC KO mice appear normal with clear barrel segregation in both PMBSF and the anterior snout region (Fig. 3.15). Compound GluRA/C double mutants were also examined to question the possibility of compensation between AMPAR subunits. GluRA/C mutants also appear under qualitative assessment to develop qualitatively normal barrels, with well-segregated cell dense barrel walls and cell sparse barrel hollows.

3.4 Discussion

The R2β subunit of PKA is highly expressed in layer IV of developing mouse somatosensory cortex in a whisker related pattern. Preliminary work performed prior to my joining the laboratory, suggested that mice that lack *Prkar2β* showed reduced segregation of cortical barrels compared to WT controls and four other viable PKA subunit-specific knockout mice examined. I have furthered this qualitative assessment and confirmed that *Prkar2β*$^{-/-}$ mice do form barrels but they are poorly defined due to a reduction in the ratio of cell density in barrel sides relative to barrel hollows. Defects in TCA segregation were seen in the anterior snout region, but in the PMBSF TCA segregation appeared normal. Lower in the trigeminal system, R2β

was found to be expressed throughout VpM but barreloids are well segregated in *Prkar2β*$^{-/-}$ mice. In addition, immunoelectron microscopy supported a postsynaptic role for R2β in barrel formation, showing that R2β is specifically localised to dendrites and dendritic spines in developing S1. Furthermore R2β has been found to associate with the PSD in S1 in a calcium dependent manner. Finally, R2β has been shown to regulate GluRA insertion into the PSD of P7 S1 cortex. However the reduction of GluRA found in the PSD of *Prkar2β*$^{-/-}$ mice does not appear to regulate barrel development, since GluRA KO mice form normal, well-segregated barrels. Together all of these results demonstrate that postsynaptic PKA signaling pathways are required for barrel formation and give insight into the pathways by which NMDA and mGluR5 receptors may be regulating barrel development.

3.4.1 Does PKA play a pre- or post- synaptic role in barrel development?

PKA is a major target of cAMP and cAMP signaling was demonstrated to play a crucial role in barrel development when the *barrelless* mutant was reported to have a spontaneous mutation in the AC1 gene (Welker et al., 1996; Abdel-Majid et al., 1998). *Brl* mutant mice lack both TCA and cortical cell segregation in layer IV indicating a presynaptic role for AC1 in barrel development. Recently a cortex-specific *Adcy1*$^{-/-}$ has been examined in which TCAs and cortical cells segregate as normal. This concluded that the site of gene action of AC1 is presynaptic in somatosensory cortex (Iwasato et al., 2005). A presynaptic role for AC1 has also been observed in retinal ganglion cell projection (Nicol et al., 2006; Ravary et al., 2003). Low AC1 activity in presynaptic terminals, either because of a loss-of function of AC1 mutation or possibly through increased stimulation of 5HT1B serotonin receptors, results in the loss of barrels perhaps by suppressing glutamate transmission (Abdel-Majid et al., 1998; Salichon et al., 2001; Gaspar et al., 2003).

PKA has previously been hypothesised to lie downstream of AC1 in barrel development, but no evidence has yet been found to suggest that PKA is the primary target of AC1 in somatosensory cortex. Individual PKA subunit specific KOs of R2α, R1β, Cα and Cβ made by Professor Stanley McKnight show normal patterning

of mouse S1 cortex (Watson et al., 2006) and mice lacking R2β show reduced cellular segregation but normal TCA segregation unlike *Adcy1*$^{-/-}$ mice. The lack of barrel phenotypes in these animals could be explained by compensation between PKA subunits, a mechanism that has been found in other tissues (Brandon et al., 1995, 1997, 1998; Amieux et al., 2002) but in this study no compensation for R2β was found in *Prkar2β*$^{-/-}$ mice. Alternatively R1α could be the key regulatory subunit downstream of presynaptic AC1 in barrel development but *Prkar1α*$^{-/-}$ mice could not be analysed for a barrel phenotype because they die in early embryonic development (Amieux et al., 2002; Watson et al., 2006).

Immmunoelectron microscopy data in this chapter provided evidence that PKAR2β is postsynaptic in developing thalamocortical synapses in S1. Biochemistry also demonstrated that PKAR2β associates with PSDs from P7 S1 cortex in a calcium dependent manner. AKAP79/150 is a scaffolding molecule known to bind regulatory subunits of PKA and target PKA holoenzymes to specific subcellular localisations. AKAP79/150 is recruited to glutamate receptors through its association with membrane-associated guanylate kinase scaffolding (MAGUK) molecules, and in this way tethers R2β-containing holoenzymes to the NMDA receptor in the postsynaptic density (Colledge et al., 2000). Loss of R2β could therefore theoretically result in altered or constitutive PKA activity. Work performed by Professor Stanley McKnight found a small increase in basal PKA activity and a large 40% decrease in stimulated levels of PKA activity in P7 *Prkar2β*$^{-/-}$ mice (Watson et al., 2006). These results indicated an increase in free catalytic subunits but overall reduction in catalytic subunit concentration in *Prkar2β*$^{-/-}$ mice. Expression levels of catalytic subunits in P7 *Prkar2β*$^{-/-}$ barrel cortex homogenate were not found significantly reduced in this chapter, however Inan et al., 2006 did find a reduction in P11 barrel cortex homogenate.

3.4.2 Synaptic plasticity (LTP/LTD) versus barrel formation

A potential mechanism downstream of postsynaptic PKA in barrel formation is AMPAR trafficking. Lu et al. (2003) reported a reduction in GluRA phosphorylation

and GluRA surface expression levels in *brl* (*Adcy1*$^{-/-}$) mutant mice and hypothesised that this regulation of GluRA could cause the loss of plasticity at thalamocortical synapses and affect barrel development by consolidating some synapses and eliminating others to refine the cortical map. Recent work in the layer IV to II/III pathway in adult barrel cortex has also shown that the GluRA subunit of AMPARs is important for postsynaptic neocortical plasticity (Hardingham & Fox, 2006). Less GluRA was found in the PSD of P7 S1 cortex from *Prkar2β*$^{-/-}$ mice than in WT animals showing a role for R2β in AMPA receptor insertion and synaptic plasticity in developing thalamocortical synapses (Lu et al., 2003). This data supports recent work by Inan et al. (2006) showing that there is a decrease in GluRA phosphorylation at the PKA dependent site Ser 845 and a lack of LTP at developing layer IV synapses in *Prkar2β*$^{-/-}$ mice. It also agrees with experiments carried out in the visual cortex showing that PKA is required for ocular dominance plasticity (Beaver et al., 2001) and that GluRA phosphorylation at Ser 845 regulates GluRA insertion into the PSD in visual cortex (Heynen et al., 2003). However the finding that GluRA KO mice develop normal barrels, assessed by the cell density ratio in barrel walls relative to barrel hollows, indicates that although R2β plays a role in both GluRA insertion and barrel development, the mechanisms of synaptic plasticity and barrel formation can be genetically dissociated or are not causally linked (Fig. 3.16).

The cytoplasmic tail of GluR4 is also known to contain a PKA phosphorylation site and PKA activity has previously been shown to drive the synaptic insertion of GluRD in rat hippocampus (Esteban et al., 2003). However significant levels of GluRD were not detected in S1 cortex during barrel development, which is consistent with previous findings (Catania et al., 1995). Therefore barrelfield examination of GluRD KO mice was excluded from this chapter's analysis. Also, no evidence for the phosphorylation of GluRB or GluRC by PKA has yet been reported, so GluRB/C has not been examined in detail. However preliminary data has shown that despite GluRB/C expression through layer IV during barrel development and a reduction in GluRB/C levels in the PSD of P7 *Prkar2β*$^{-/-}$ S1 cortex, barrel formation is normal in GluRB and GluRC KO mice. The trafficking of AMPAR subunits does not therefore appear to affect barrel development (Fig. 3.16). However KO mice of

multiple AMPAR subunits need to be examined in order to rule out the possibility of compensation by other subunits. So far, only GluRA/C double mutants have been examined but these appear to form normal barrels. Dissociation of barrel development from mechanisms of synaptic plasticity does agree however with some previous findings. One example is that a "megabarrel" forms in animals with row C follicle ablation (Van der Loos and Woolsey, 1973). The layer IV cells cluster around the fused row of TCA afferents despite the lack of appropriate follicles, suggesting that patterned sensory-evoked glutamatergic activity, required for synaptic plasticity is not important for regulating barrel formation. Also it has been shown that mice that exhibit delayed barrel formation due to the early overexpression of 5HT, develop barrels even in the absence of whisker follicles (Rebsam et al., 2005).

3.4.3 Alternative PKAR2β signaling pathways in barrel formation

NMDA and mGluR5 glutamate receptors can both activate PKA (Kind and Neumann, 2001). Moreover, PKAR2β is a PKA-holoenzyme that associates with the PSD in a Ca^{2+} dependent manner, and therefore highly likely to be activated by one or both of these glutamate receptors. NMDA receptors could regulate PKAR2β through Ca^{2+}/calmodulin dependent adenylyl cyclases AC1 or AC8 that are expressed in layer IV neurons in the NRC (Husi et al, 2000) during barrel development (Nicol et al., 2005). However barrel formation appears to be normal in both *Adcy8*$^{-/-}$ mice (Abdel-Majid et al., 1998) and cortex-specific *Adcy1*$^{-/-}$ mice (Iwasato et al., 2005). Either compensation occurs between these adenylyl cyclases, or they do not lie upstream of PKAR2β in regulating barrel formation. Consistent with the idea that R2β could be dissociated from AC1 and AC8 in barrel development, R2β has been shown to play a key role in visual cortical plasticity, but ocular dominance plasticity (ODP), LTP and LTD all remain intact in *Adcy1/Adcy8*$^{-/-}$ mice (Fischer e al., 2004).

It is also possible that mGluR5 receptors could regulate PKAR2β through the release of Ca^{2+} from intracellular stores via the activation of PLCβ1 and subsequent IP3

production (Hannan et al., 2001). The *Prkar2β*$^{-/-}$ barrel phenotype shows similarities to the phenotype found in *PLCβ1*$^{-/-}$ mice, suggesting that R2β could indeed lie downstream of mGluR5 activation of PLCβ1 in barrel formation. There are also other adenylyl cyclases that are regulated by mGluR5 that could activate PKA and thereby mediate barrel development. Both AC4 (Defer et al., 2000) and AC9 (Antoni et al., 1998) are expressed in cortical neurons and are regulated by the principal G-protein, Gq that is associated with mGluR5. Alternatively, PKA may be activated by a cAMP-independent mechanism. Recently a cAMP-independent form of type II PKA activation was identified (Ma et al., 2005) and has provided a new concept that PKAR2β could be regulating barrel development entirely independent of adenylyl cyclases.

The molecular mechanisms downstream of PKAR2β in barrel development still require elucidation but they appear to be different from those that regulate synaptic plasticity. There are several well-characterised signaling cascades through which PKA, downstream of mGluR5 or NMDARs, could signal during development of the barrel cortex. A signaling pathway from cAMP/PKA to mitogen-associated protein kinase (MAPK) was first described in PC12 phaeochromocytoma cells (Vossler et al., 1997) and then also illustrated in hippocampal neurons in vitro (Grewal et al., 2000). The activation of PKA induces the association of two small G-proteins, Rap1 and B-Raf. Rap1 can phosphorylate B-Raf that phosphorylates MAPK/ERK kinase (MEK), which then phosphorylates MAPK. MAPK is subsequently able to activate transcription factors such as Elk1 and CREB. Alternatively PKA can directly or indirectly phosphorylate CREB via CamKIV or can act through a Ras-MAPK signaling pathway via the Raf1 kinase that acts as mediator between Ras and the MEK/MAPK cascade (reviewed by Waltereit & Weller 2003). It has previously been shown that PKA, ERK and CREB are intrinsically linked, playing a role during experience-dependent development of the visual cortex (Cancedda et al., 2003). This has highlighted that this pathway could also be important in development of the somatosensory cortex.

3.4.4 Isolation of the PSD and PPW: technical limitations

Biochemical purification of the PSD and PPW as described by Phillips et al., 2001 was attempted in order to determine the synaptic localisation of R2β. Enrichment of PSD and PPW proteins was observed in the appropriate pellet (PSD) or supernatant (PPW) fraction. However there were several limiting factors that prevented this method from being a reliable assay for determining the localisation of synaptic proteins in developing S1 cortex. Firstly, different synaptic proteins were found to bind the PSD or PPW with different binding affinities. Secondly, calcium was present in all the buffers throughout the protocol and we have shown that some proteins such as PKAR2β are postsynaptic but only associate with the PSD in the absence of calcium. Thirdly, protein precipitation of the supernatant fraction using acetone did not recover the proteins present in the PPW and lastly, considerable variability between preparations was observed. To localise synaptic proteins biochemically, a more efficient, less variable protocol must be established, perhaps created by varying the pH slightly or the calcium concentration compared to that Phillips et al., 2001 used to separate the PPW from the PSD in adult rat cortex. In addition a more vigorous protein precipitation reagent such as TCA might retrieve the PPW associated proteins.

3.4.5 Future Work

This chapter has established that R2β-containing PKA holoenzymes are key players downstream of glutamate neurotransmission in barrel development. It has also shown that R2β plays a role in regulating GluRA insertion and synaptic plasticity, but that the segregation of layer IV cortical cells into barrels is unlikely to depend upon these changes in synaptic strength. Initial future aims are to identify the R2β activator, the relevant phosphorylation substrates and the molecular mechanism(s) through which R2β influences barrel development. Barrels have been hypothesised to form as a result of either: [1] neuropilar elaboration, [2] cell death, [3] cell migration, or [4] cell adhesion (see Chapter 1) and PKA has been shown in other systems to play a role in some of these processes (Howe et al., 2004; Tojima et al., 2003). Identification of targets of R2β in S1 cortex with roles in any of these cellular

processes could provide insight into the cellular mechanisms of barrel formation. Several experimental approaches have begun to address identification of the activator(s) and targets of PKAR2β and are written about in Chapter 5.

Secondly it would be interesting to examine the role of R2β in other key developmental processes such as dendritogenesis and synaptogenesis. Analysing the dendritic orientation and spine density of layer IV spiny stellate cells in the *Prkar2β*$^{-/-}$ mice could provide further insight into the cellular processes of barrel formation disrupted in these mice. Recent work by Inan et al. (2006) examined the orientation bias of layer IV cell dendrites in *Prkar2β*$^{-/-}$ mice and concluded that they exhibit significantly less selective orientation of their dendrites towards the TCA patch compared to those in WT mice. However the analysis performed was flawed because it did not take into account the location of each neuron analysed within the barrelfield. In WT mice, cells in each barrel wall show selective dendritic orientation into the appropriate barrel hollow, but cells in the barrel hollow display no orientation bias. In *Prkar2β*$^{-/-}$ mice that have poorly segregated barrels, fewer cells are located within the barrel walls and therefore a much larger proportion of cells, that were chosen for dendritic analysis by Inan et al. (2006) because TCA patches were not defined, would be expected to show a lack of dendritic orientation bias.

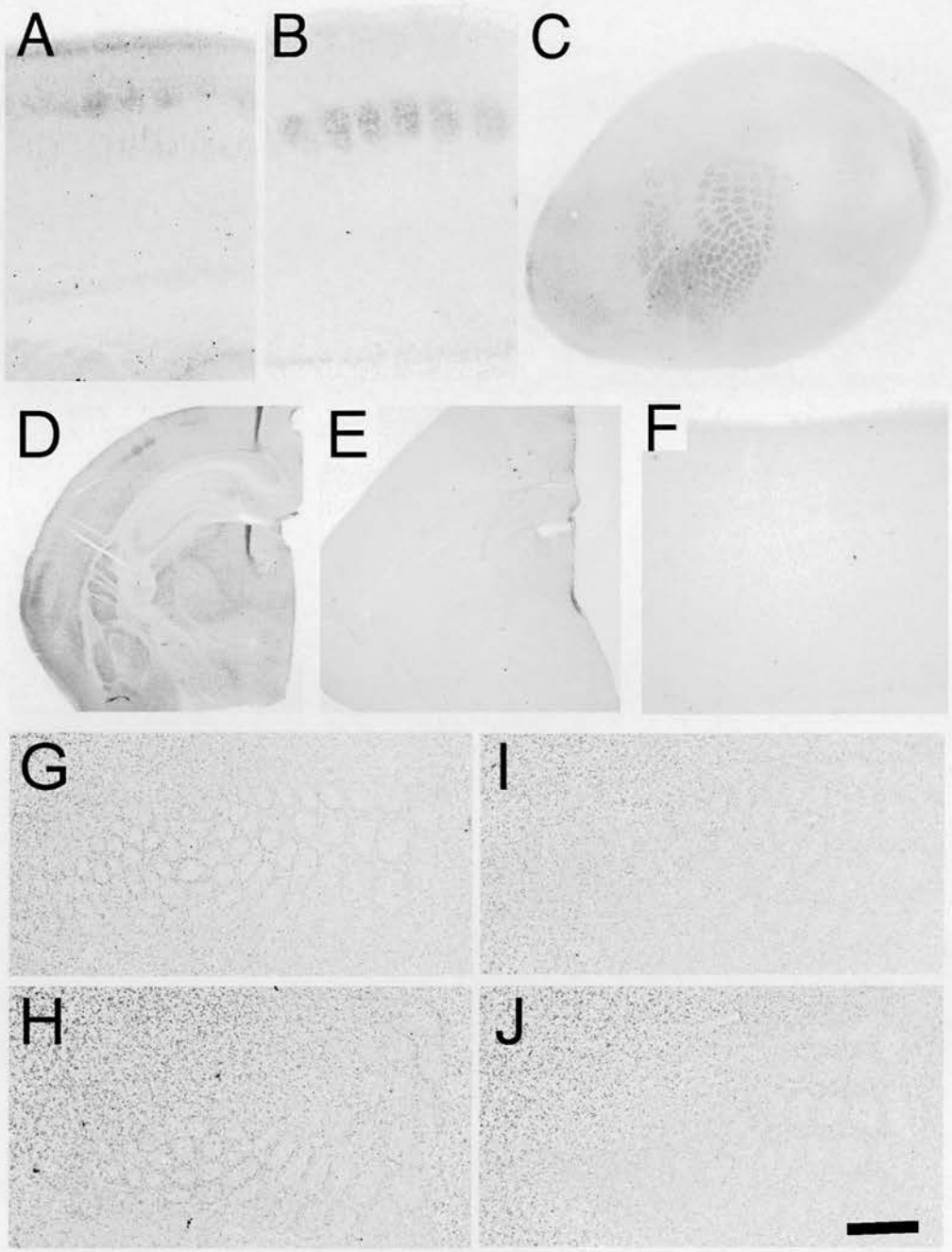

Figure 3.2: R2β protein expression and defects in cellular segregation in *Prkar2β*$^{-/-}$ mice. **A, B,** Immunostaining for R2β in coronal sections shows high levels of the protein in layer IV of S1 cortex in WT mice at P4 (**A**) and P7 (**B**). **C,** Immunostaining for R2β in a tangential section through layer IV of P7 WT mice shows that R2β expression corresponds to barrel hollows. **D, E, F,** Specificity of the R2β antibody is shown by a lack of reaction product in P7 *Prkar2β*$^{-/-}$ coronal sections immunoreacted for R2β (**E, F**) compared to WT P7 brain sections (**D**). **E - H**, Digitized images of pairs of adjacent Nissl-stained sections through layer IV of S1 in P7 WT (**G, H**) and *Prkar2β*$^{-/-}$ (**I, J**) mice are shown. In *Prkar2β*$^{-/-}$ mice, barrels are visible in PMBSF but the cells appear less well segregated and few barrels can be seen in the anterior snout region. Scale bar: (in **J**) **A, B,** 250μm; **C,** 750μm; **D, E,** 1320μm; **F,** 250μm; **G-J,** 200μm.

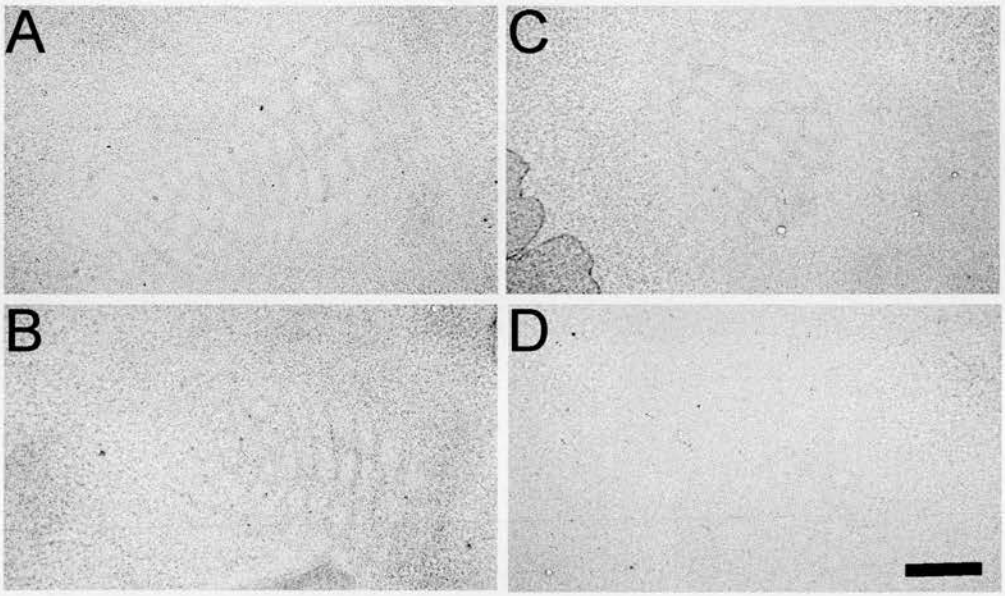

Figure 3.3: Cellular segregation in the barrel cortex of *Prkar2β*$^{-/-}$ mice on different genetic backgrounds. **A - D,** Digitized images of pairs of adjacent Nissl-stained sections through layer IV of S1 in P7 *Prkar2β*$^{-/-}$ mice on an MF1 background (**A , B**) and a B6/129 background (**C, D**). *Prkar2β*$^{-/-}$ mice that have been bred onto an MF1 or B6/129 background, display barrels in PMBSF but cellular segregation appears poor and few barrels can be seen in the anterior snout region. Scale bar (in **D**): **A-D**, 200μm.

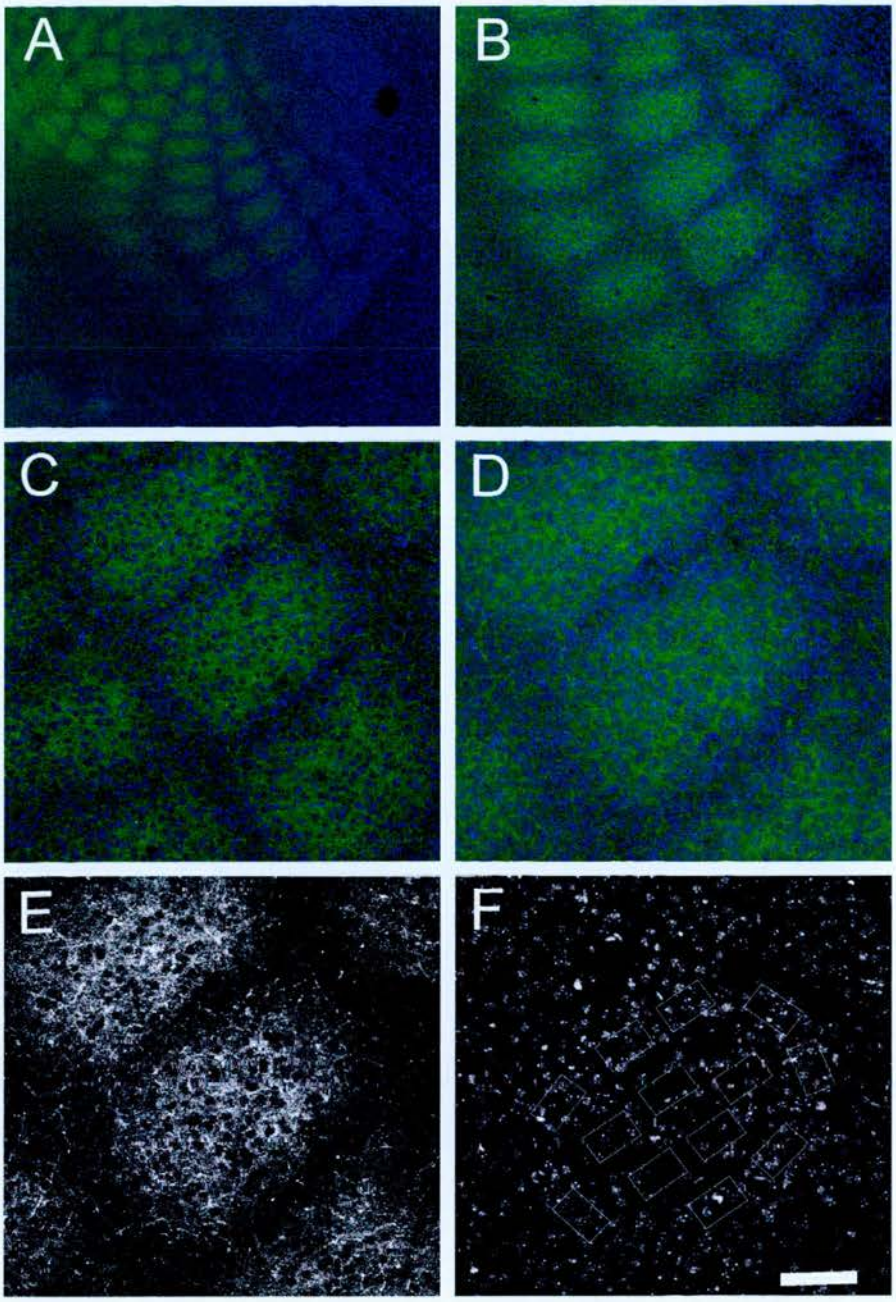

Figure 3.4: Cell count methodology: images through WT S1 cortex demonstrate the quantification method used to calculate the degree of cellular segregation in the PMBSF of WT and KO mice. **A - D**, Tangential sections through layer IV of P7 WT and *Prkar2β*$^{-/-}$ mice were stained with Topro to label nuclei and immunostained using anti-SERT antibody to label TCAs. Confocal images were taken of the barrelfield (always including barrel C2) at X5 (**A**), X10 (**B**), X20 (**C**) and X20zoom1.7 (**D**) magnifications. **E,** A digitized image through layer IV that shows the TCA patch in barrel C2 immunolabelled by anti-SERT antibody and converted to black and white for increased contrast. **F,** A digitized image through layer 4 that shows Topro stained nuclei and appropriately placed boxes counts of cell density in the barrel wall and barrel hollow of barrel C2. Scale bar: (in **F**) **A,** 360μm; **B,** 180μm; **C,** 90μm; **D - F,** 66μm.

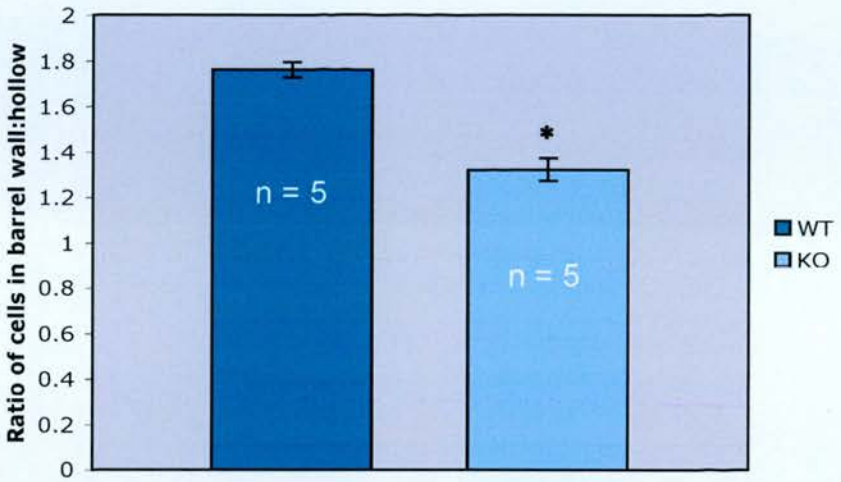

Figure 3.5: Decreased cellular segregation in PMBSF of *Prkar2β*$^{-/-}$ mice. Blind analysis of the cell densities of barrel walls and hollows showed a significant decrease in the wall-to-hollow ratio in *Prkar2β*$^{-/-}$ mice relative to that of WT mice (1.32 ± 0.03 vs 1.6 ± 0.05, repectively; p = 0.0001, 2-sample *t* test).

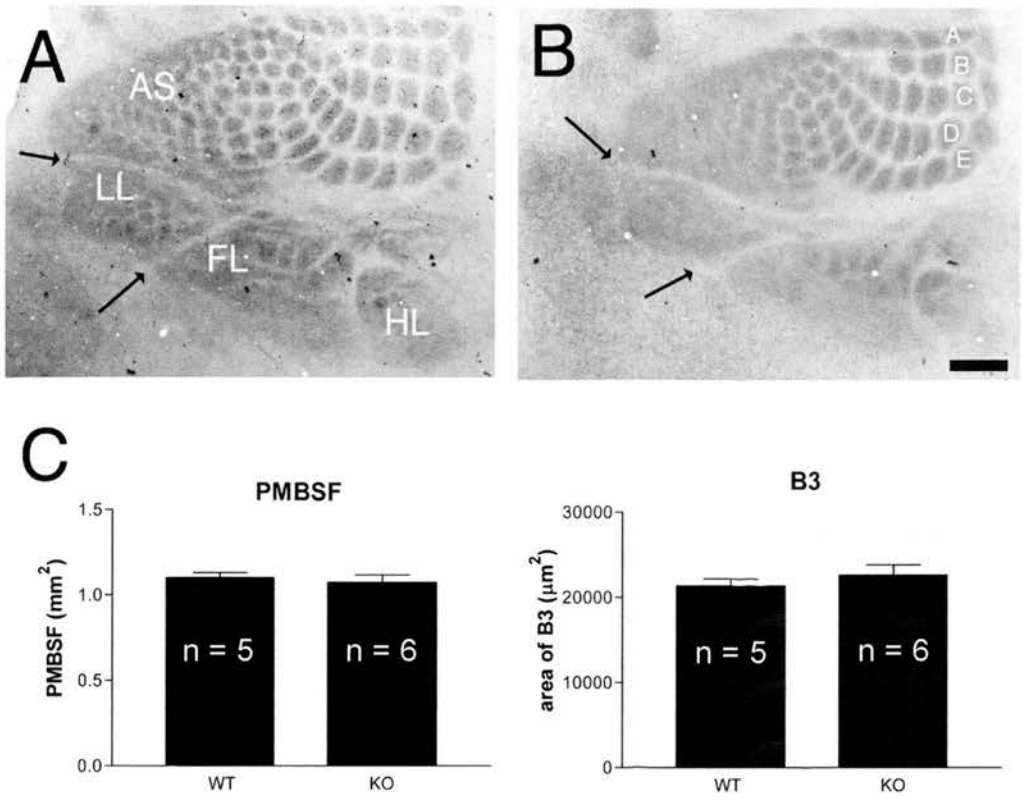

Figure 3.6: TCAs segregate into whisker-related patches in PMBSF but not in anterior snout regions in *Prkar2β*$^{-/-}$ mice. **A, B,** SERT immunohistochemistry performed on tangential sections through layer IV of S1 at P7 reveals clear TCA patches in PMBSF in WT (**A**) and *Prkar2β*$^{-/-}$ (**B**) mice. In *Prkar2β*$^{-/-}$ mice, staining appears more diffuse in the AS regions with just the largest, most dorsomedial patches being visible. The demarcations between different subregions (arrows) of S1 are clearly visible in both WT and *Prkar2β*$^{-/-}$ mice, indicating that the loss of segregation within AS is not as a result of a general TCA pathfinding problem in this region. LL, Lower lip; FL, forelimb; HL, hindlimb. The five main rows of barrels that represent the five rows of facial mystacial vibrissae are labeled as A-E in **B**. **C,** To quantitatively examine TCA segregation in the PMBSF of *Prkar2β*$^{-/-}$ mice, areal measurements of PMBSF and individual TCA patches (B3 above and B2, C2, C3, D2 and D3 shown in appendix 3.3) were carried out blind to genotype. No significant differences in any of the measurements were observed (PMBSF, $p = 0.66$; B3, $p = 0.43$). Scale bar: (in **B**) **A, B,** 200μm.

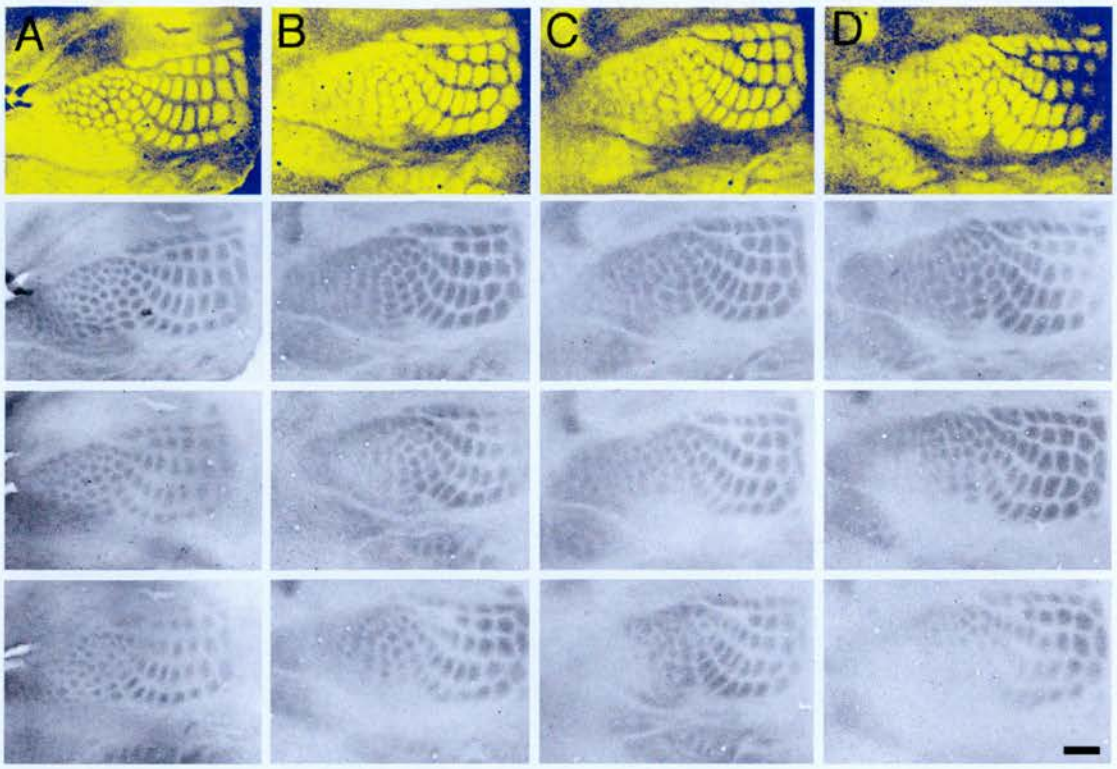

Figure 3.7: TCAs show reduced segregation in anterior snout regions of *Prkar2β*$^{-/-}$ mice. The top row of images **A - D** are blue/yellow gradient maps of SERT immunostaining in flattened tangential sections through layer IV in a WT (**A**) and 3 different *Prkar2β*$^{-/-}$ mice (**B - D**). The sections that displayed the best segregation in the anterior snout region were used and are shown in row 2. Each digital image was acquired using identical luminance levels and digital images were processed identically using Adobe Photoshop. Rows 3 and 4 show adjacent sections above and below the sections in Row 2. Scale bar: (in **D row 4**) **A - D** all rows, 200μm.

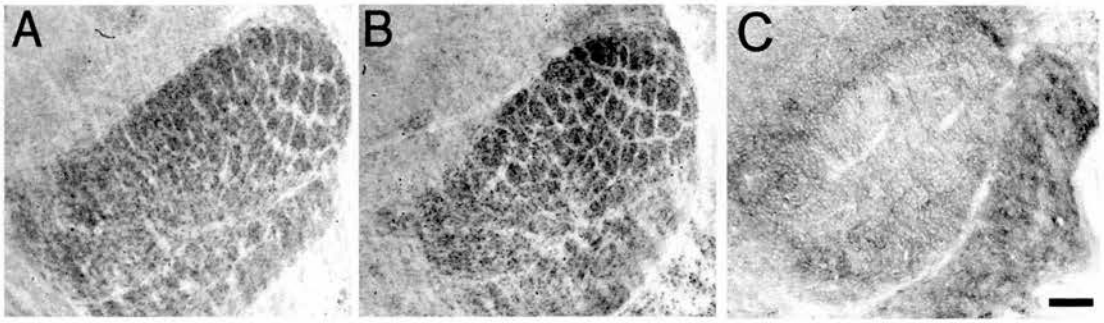

Figure 3.8: Barreloid formation appears normal in VpM of *Prkar2β*$^{-/-}$ mice. **A, B,** Cytochrome oxidase staining of coronal sections through the VpM nucleus of P7 WT (**A**) and *Prkar2β*$^{-/-}$ (**B**) mice shows clear barreloids even in the regions that represent the anterior snout whiskers. **C,** R2β immunostaining of the thalamus reveals low level R2β expression thoughout the VpM with highest levels in the inter-barreloid regions. Scale bar: (in **C**) **A - C,** 80μm.

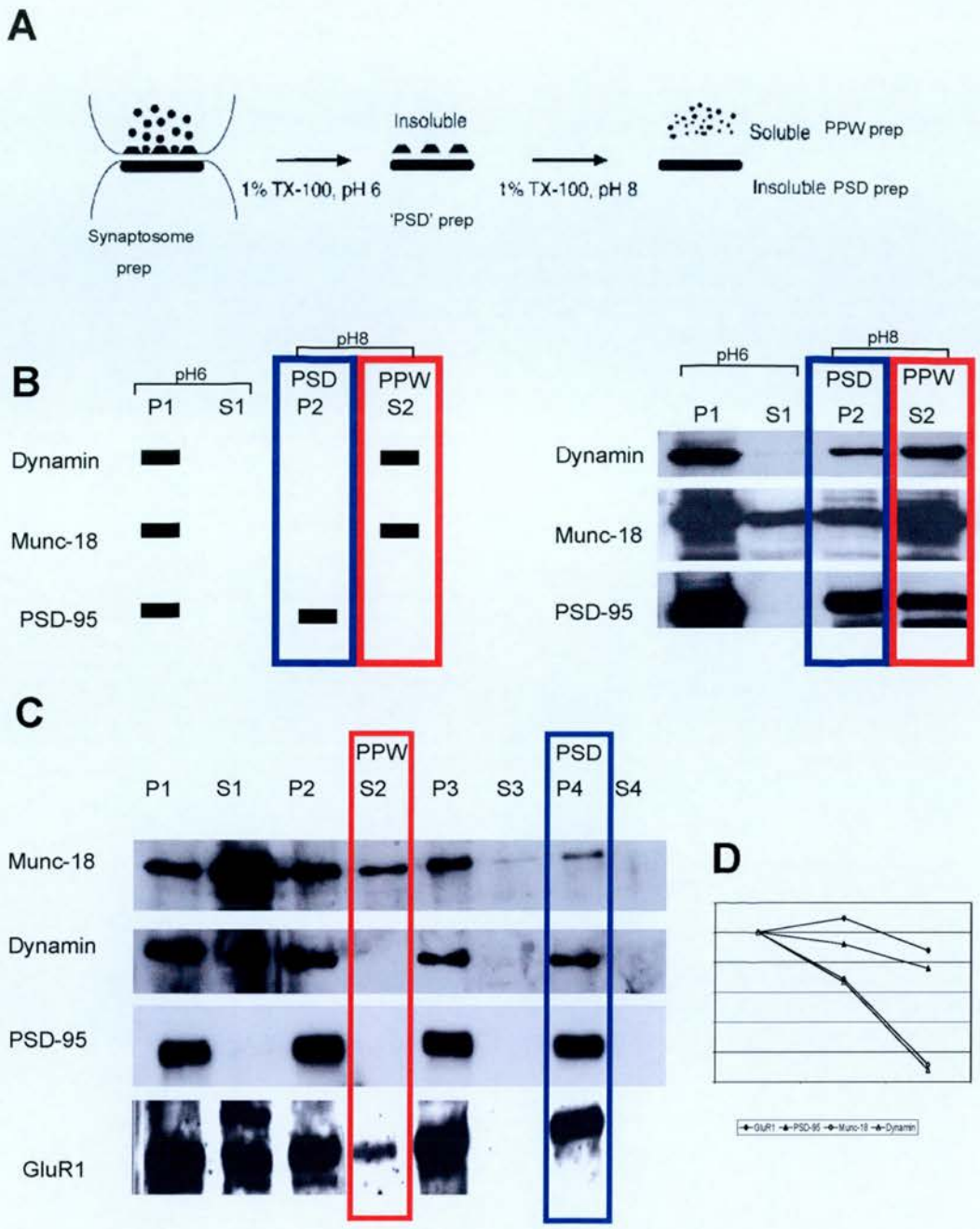

Figure 3.9: Biochemical purification of the postsynaptic density. **A,** Diagram illustrating the sensitivity of the PPW to pH, plus separation of the PPW from the PSD (taken from Phillips et al., 2000). **B,** Hypothetical and real western blot results, obtained from performing the Phillips et al., 2000 protocol on synaptosomes from P10 WT cortex. Dynamin and Munc-18 (presynaptic) and PSD95 (postsynaptic) were used as markers to assess isolation of the PPW from the PSD. **C,** Biochemical fractions isolated from an adapted protocol where further extraction steps were included. To assess biochemical purification, Dynamin and Munc-18 (presynaptic) and PSD95 and GluR1 (postsynaptic) markers were used. **D,** Western blot results in **C** graphed: Munc-18 and Dynamin levels decrease in successive pellet fractions but PSD95 and GluR1 levels remain high in all pellet fractions extracted indicating gradual purification of the PSD. The PSD (P4) however still contains some Munc-18 and Dynamin, so is not completely purified.

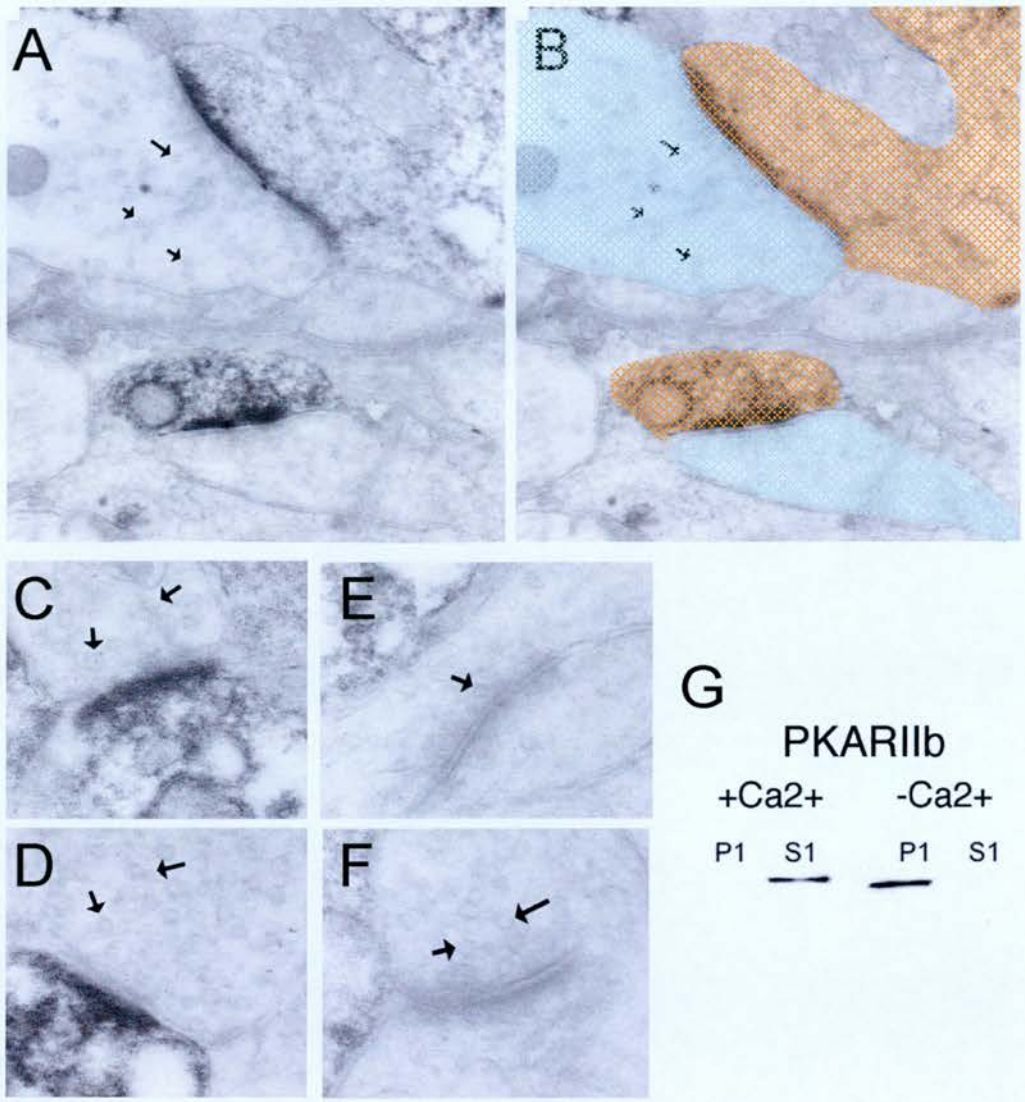

Figure 3.10: R2β is postsynaptic in developing S1 cortex. **A - D,** Electron micrographs of layer 4 of P14 barrel cortex reveal dark immunoreactive product within postsynaptic densities and dendrites (**A - D**), but not in presynaptic terminals. PSDs and dendrites are marked in orange and presynaptic terminals marked in blue in **B**. Synapses can be identified by the presence of presynaptic vesicles (arrows) opposite an electron dense PSD. **E, F,** Not all synapses in layer 4 are labeled; however the presence of DAB reaction product in adjacent dendrites (asterisks) indicates that the absence of staining is not because of a lack of penetration of the antibody. **G,** Western blot analysis demonstrates that the association of R2β with the PSD is regulated by Ca^{2+}. In the presence of 100μm calcium, R2β is found in the soluble (S) fraction of synaptosome preparations. In the absence of Ca^{2+}, R2β is in the particulate (P) fraction and therefore associated with the PSD.

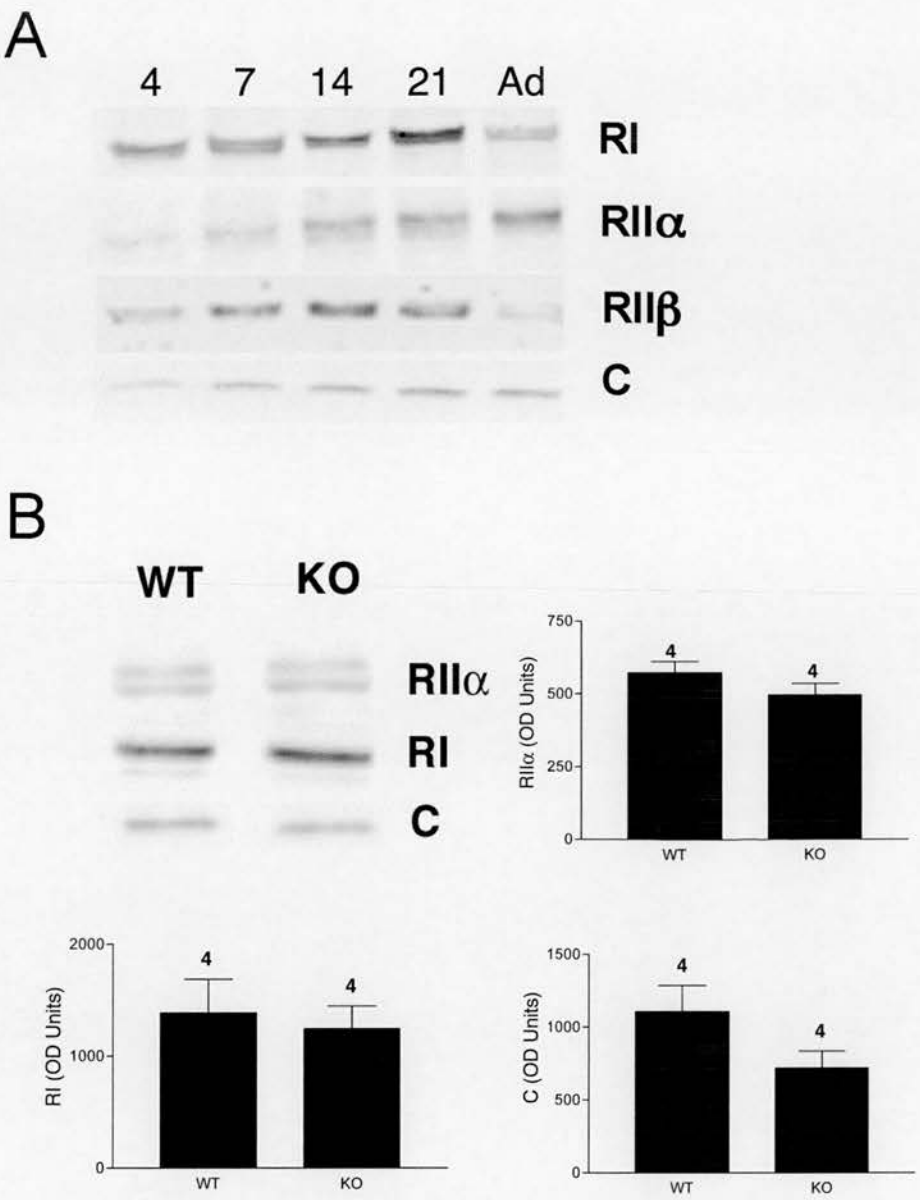

Figure 3.11: Protein expression of other PKA subunits in developing S1 cortex. **A,** Western blot developmental expression profiles show that R1, R2α, R2β and C subunits are all present in developing S1. Although antibodies specific for each of the R1 and C subunits were not used, the results reveal that several different holoenzymes are present at synapses throughout postnatal development of the barrel cortex. **B,** R2α, R1 and C subunit expression in S1 cortical homogenate of P7 *Prkar2β*$^{-/-}$ mice reveals no significant difference in the levels of other PKA subunits in *Prkar2β*$^{-/-}$ mice compared to WT mice. Measurements of protein density expressed as optical density units confirmed the qualitative assessment and is presented in graph form in **B**.

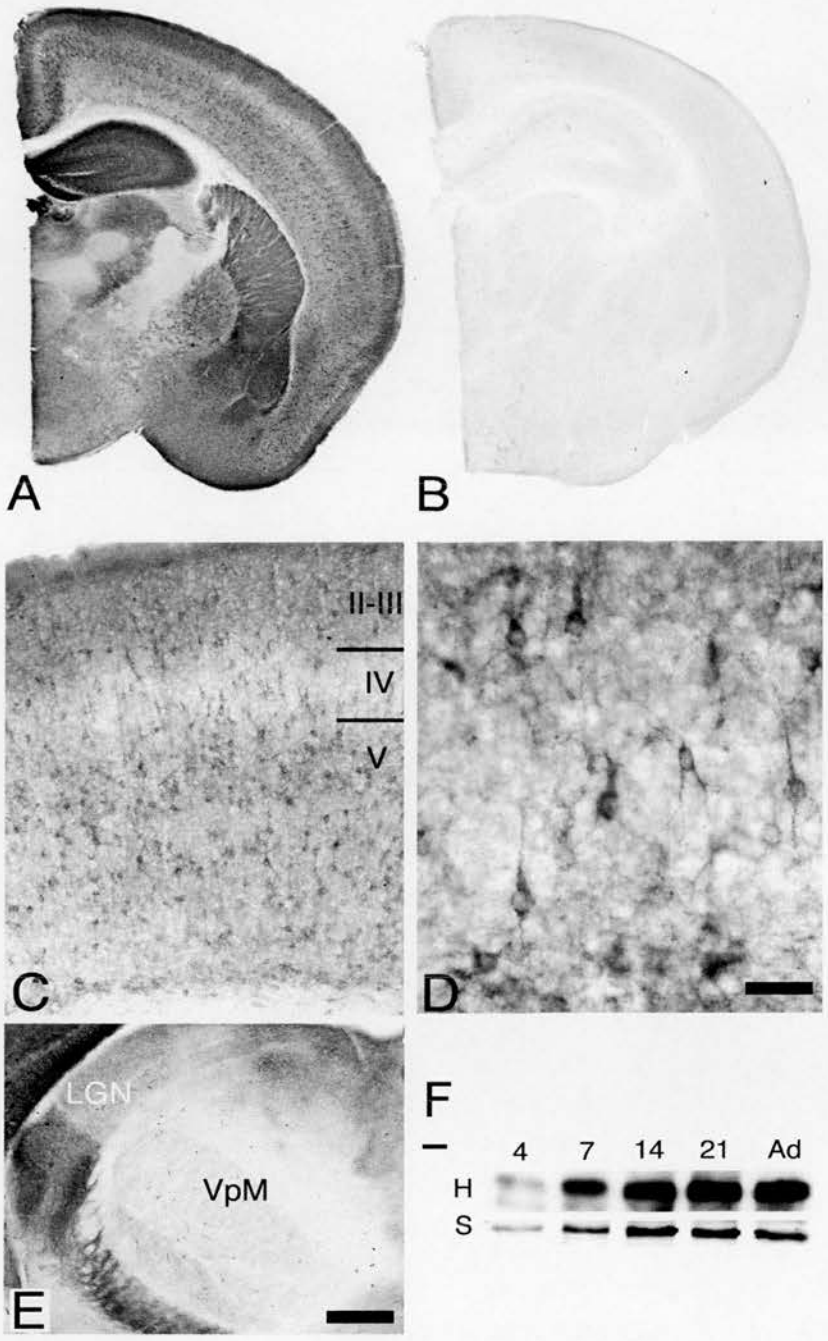

Figure 3.12: GluRA protein expression in developing S1 cortex. **A, B,** Immunostaining for GluRA in coronal sections through P7 WT (**A**) and GluRA KO (**B**) brains demonstrates specificity of the anti-GluRA antibody used. **C,** GluRA immunolocalisation in S1 of P7 mice shows staining throughout the cortex with highest levels in layers II/III and V. **D,** Higher magnification images through layer IV show clear immunopositive neurons and diffuse neuropilar staining. **E,** GluRA staining is also present throughout P7 thalamus with lowest levels in VpM. **F,** Western blot analysis demonstrated a rapid increase of GluRA levels in homogenates (H) and synaptosome (S) preparations during the first postnatal week, consistent with the rapid increase in synapses during this period. Scale bar: (in **E**) **A, B,** 950μm; **C,** 140μm; **D,** 35μm; **E,** 250μm.

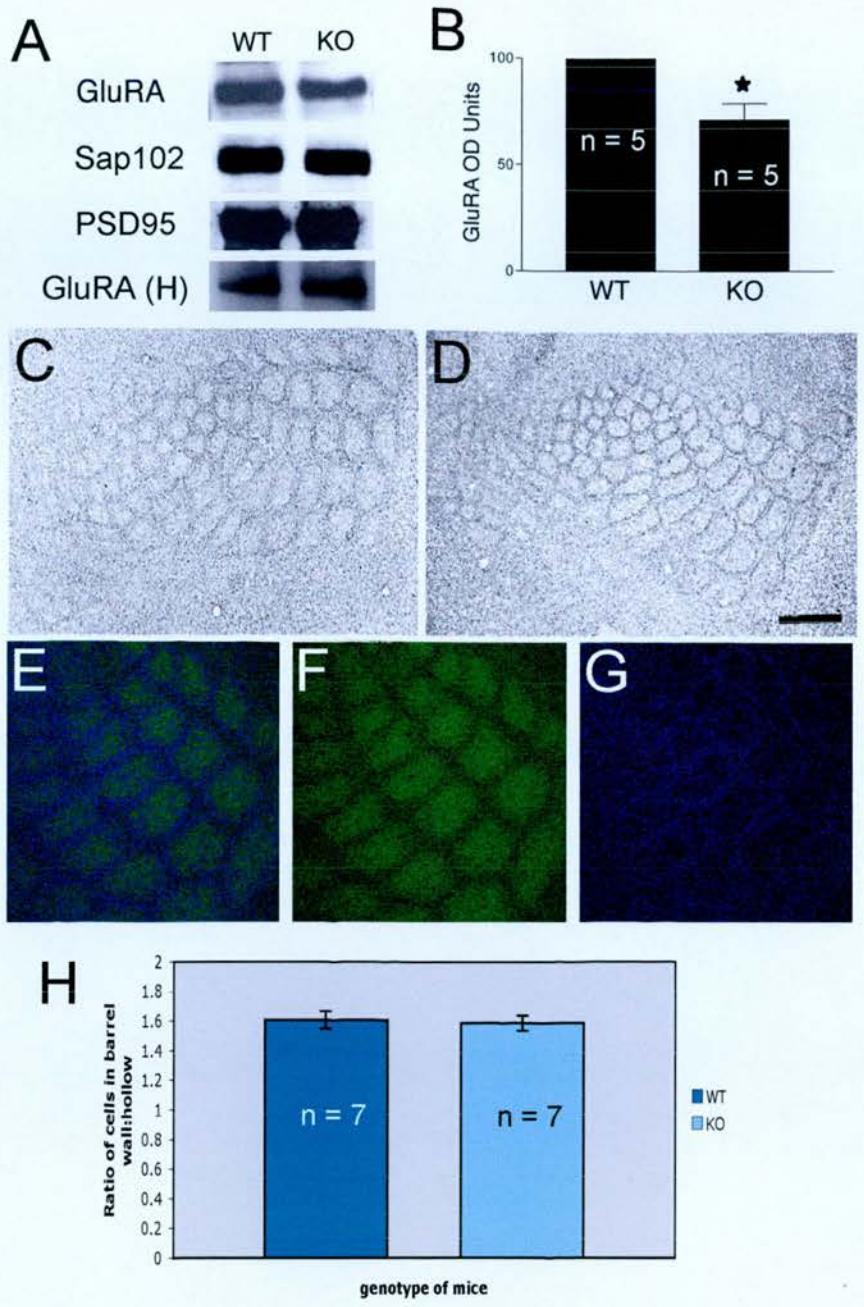

Figure 3.13: R2β regulates GluRA insertion independent of barrel formation. **A,** To determine whether R2β is necessary for the insertion of GluRA into the PSD, Western blot analyses of synaptosome preparations from S1 P7 WT and *Prkar2β*$^{-/-}$ mice were performed. In each experiment, GluRA levels in *Prkar2β*$^{-/-}$ mice are normalised to WT levels. Western blots of Sap102 and PSD95 in synaptosomes and GluRA levels in homogenate (H) from S1 P7 WT and *Prkar2β*$^{-/-}$ mice are controls **B,** *Prkar2β*$^{-/-}$ mice have significantly less GluRA (74.4% ± 6.8; n = 5; 1-sample *t* test, p = 0.006) in synaptosomes than WT mice (n = 5; 100%). No differences in Sap102 (**A**) or PSD95 levels (**A**) or GluRA levels in homogenates (**A**) were seen, indicating that the decrease in GluRA was not simply caused by a general decrease in PSD components in *Prkar2β*$^{-/-}$ mice. **C, D,** Nissl staining through layer IV of adult WT (**C**) and GluRA KO (**D**) mice reveals clear cellular segregation into barrels in both PMBSF and the anterior snout region in GluRA KO mice. **E, F,G,** For cell counts in barrel walls and hollows, tangential sections through layer IV of WT and GluRA were stained with Topro to label cell nuclei and SERT antibody to label TCA patches. **H,** No significant different was found in the cellular segregation in GluRA KO mice compared to WT animals. Scale bar: (in **D**) **C, D,** 200μm.

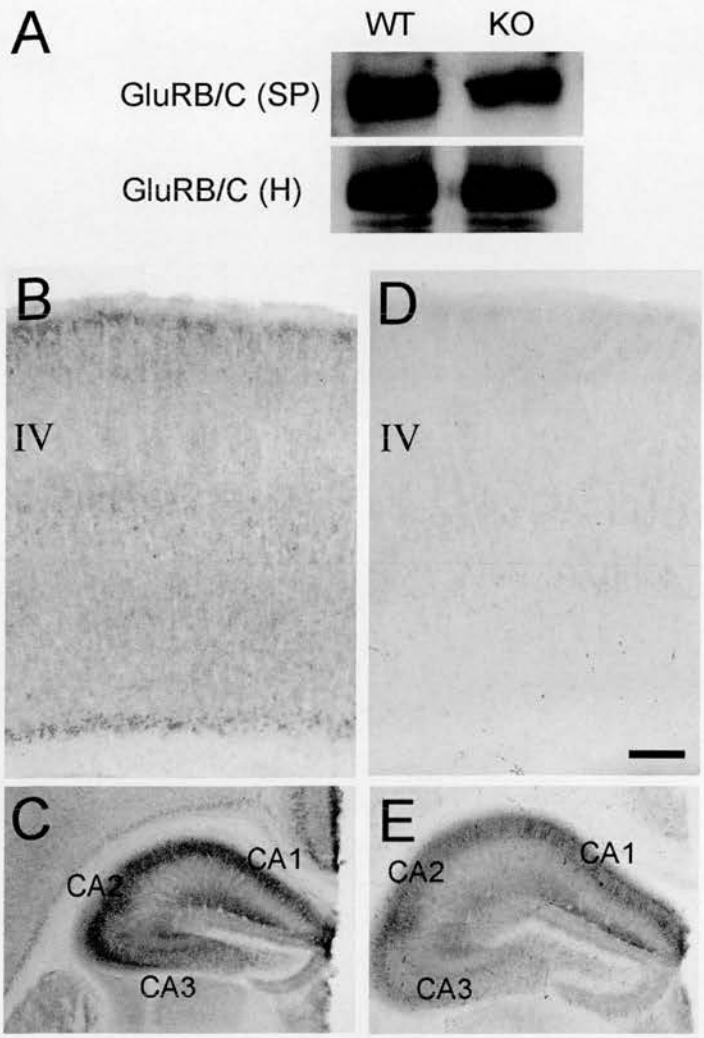

Figure 3.14: GluRB/C and GluRD protein expression in developing S1. **A,** Western blot analysis of GluRB/C levels in P7 synaptosome preparations (SP) and homogenate (H) in *Prkar2β-/-* and WT animals reveals that R2β also regulates GluRB/C insertion into the PSD (n=2). **B, C,** Immunostaining of GluRB/C in S1 cortex (**B**) and hippocampus (**C**) shows expression throughout all layers of the cortex with patchy staining throughout layer IV, and intense staining throughout layers of the hippocampus. **D, E,** Immunostaining of GluRD in S1 cortex (**D**) and hippocampus (**E**) shows an almost complete lack of staining thoughout the entire cortex, but high staining in the hippocampus indicates that the lack of cortical staining is not due to a penetration problem or problems with the anti-GluRD antibody. Scale bar: (in **D**) **B, D,** 140μm.

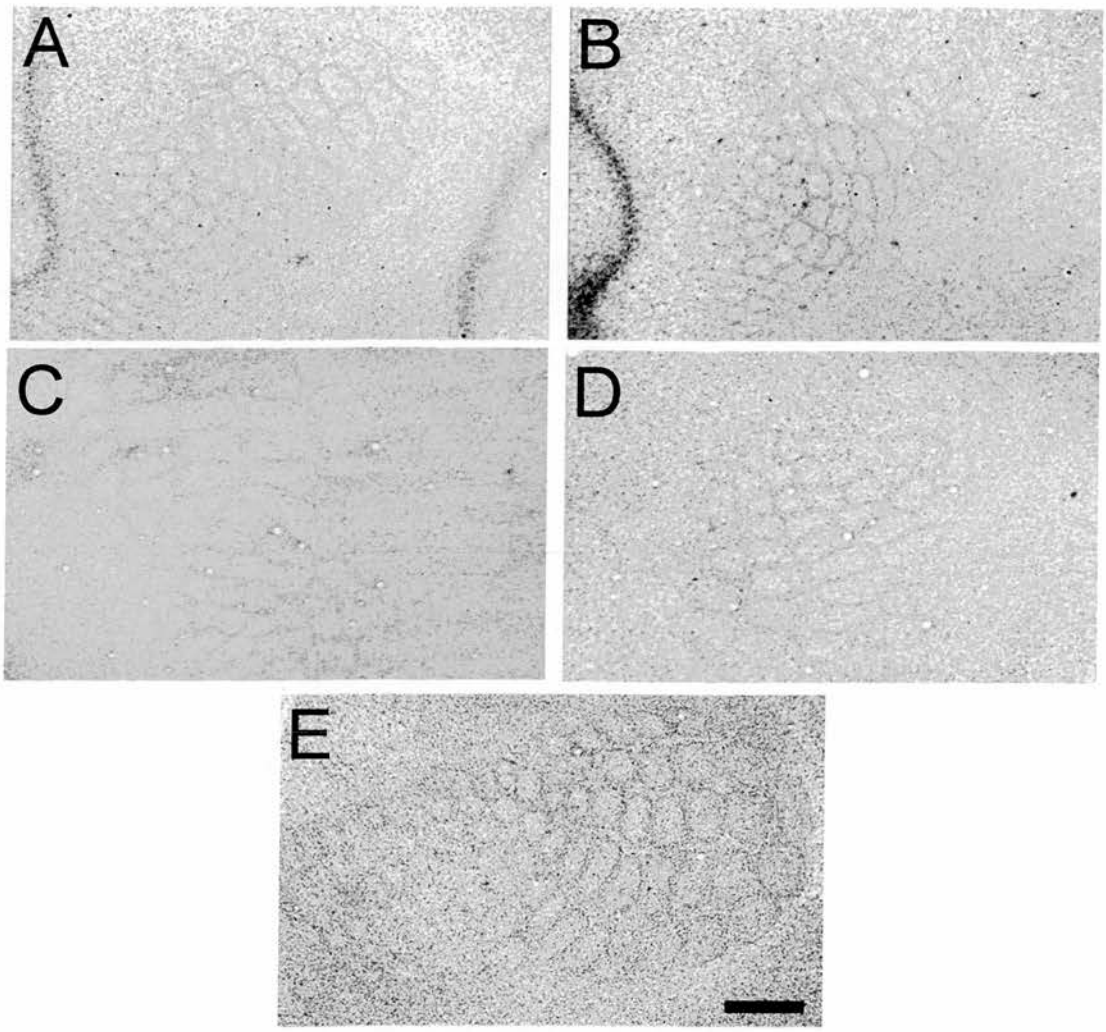

Figure 3.15: GluRB, GluRC and GluRA/C KO mice develop cortical barrels. **A, B,** Adjacent nissl stained tangential sections through layer IV of GluRB KO mice show clear cellular segregation throughout P7 barrel cortex. **C, D,** Adjacent nissl stained sections through layer IV of P14 GluRA/C KO mice also show distinct cellular segregation into barrels. **E,** In addition a nissl stained flattened tangential section through P7 GluRC KO barrel cortex shows cellular segregation throughout PMBSF and anterior snout regions of layer IV (**E**). Scale bar: (in **E**) **A - E,** 200μm.

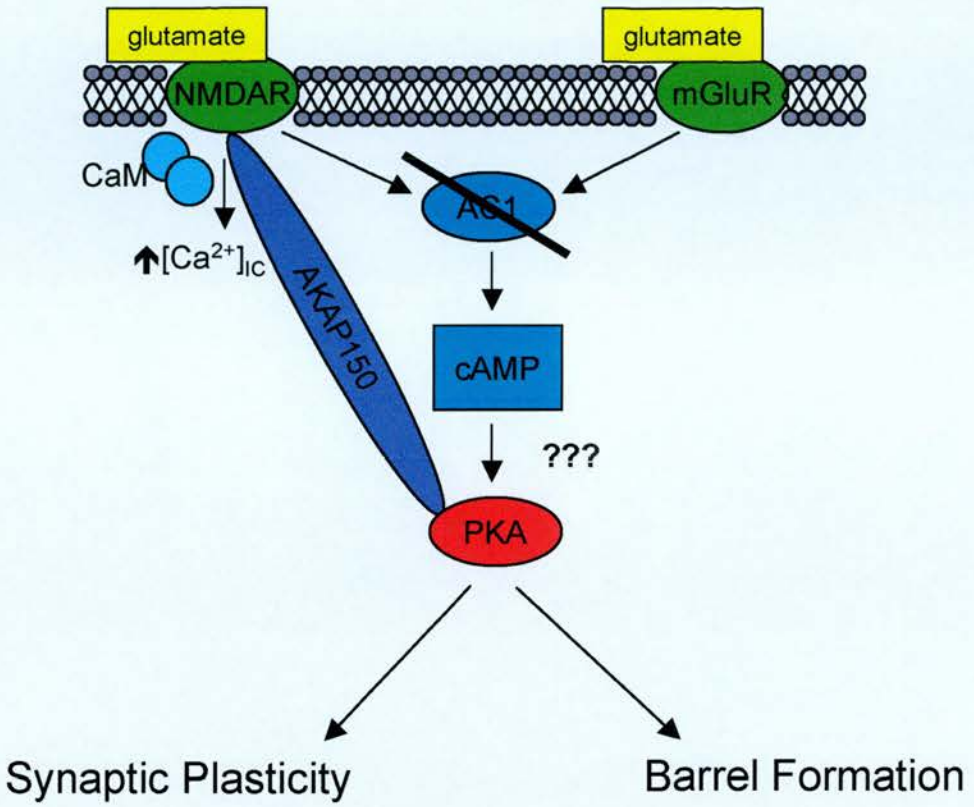

Figure 3.16: Working Model. PKAR2β is postsynaptic in layer IV/TCA synapses during barrel development and could lie downstream of either NMDAR or mGluR5 receptors. Initially PKA was hypothesised to lie downstream of AC1 in barrel development but this has since been found not to be the case (refer to 3.4.1). It is not yet clear whether cAMP or a cAMP-independent mechanisms activate PKAR2β in barrel development. PKAR2β has been shown however to play a role in AMPAR trafficking and barrel formation but these two processes seem to be genetically distinct from one another since GluR subunit specific knockout mice develop barrels in layer IV like WT animals.

CHAPTER 4:

Pattern formation in the trigeminal system of mice requires SynGAP

4.1 Introduction

Recent isolation and characterisation of the NMDAR complex and the postsynaptic density (PSD) has provided a useful list of candidate proteins that are associated with glutamate receptors and could mediate glutamate receptor dependent signaling that underlies barrel formation (Husi et al., 2000; Walikonis et al., 2000). One such candidate protein is SynGAP, a synaptic GTPase activating protein that can regulate small G-proteins (Ras, Rab, and Rap) (Chen et al., 1998; Kim et al., 1998; Krapivinsky et al., 2004; Tomoda et al., 2004). SynGAP is highly enriched in excitatory glutamatergic synapses and has been shown to bind NMDARs via membrane associated guanylate kinases (MAGUKs) such as PSD95 and Sap102 (Chen et al., 1998; Kim et al., 1998). SynGAP negatively regulates the extracellular-regulated-kinase (ERK) signaling cascade (Komiyama et al., 2002; Rumbaugh et al., 2006), a signaling pathway that plays a role in numerous forms of synaptic plasticity, including ocular dominance plasticity in the visual cortex, long-term-potentiation (LTP), and learning and memory (Di Cristo et al., 2001; Adams and Sweatt, 2002). Furthermore ERK regulates cellular processes such as cytoskeletal rearrangements, synaptogenesis, dendritic morphology, and cellular migration (Ho et al., 2001; Adams and Sweatt, 2002), processes that may be required for barrel formation (see Chapter 1). Therefore SynGAP could provide an important link between NMDARs and the downstream intracellular pathways that regulate barrel development.

Previous work from Kennedy's laboratory has shown that SynGAP is involved in several other developmental events. *Syngap*$^{-/-}$ neurons prematurely form spines and functional synapses in culture and develop much larger mature spines compared to wild type neurons (Vasquez et al., 2004). These larger spines demonstrate a precocious incorporation of PSD proteins relative to wild type spines indicating that SynGAP plays an important role in regulating spine formation and maturity. Also more recently, SynGAP has been shown to regulate neuronal apoptosis (Kneusel et al., 2005). Measurements of caspase-3 activation in *Syngap*$^{-/-}$ brains show that significantly more neurons in the hippocampus and the cortex undergo apoptosis at P0/P1 compared to wildtype animals (Kneusel et al., 2005). Also, *Syngap* conditional knockout mutants, that begin to lose SynGAP expression in forebrain

pyramidal neurons at 1-2weeks of age, show higher levels of caspase3 activation in these neurons than age-matched controls. Furthermore by examining conditional ko mice that express different levels of *Syngap*, the level of neuronal apoptosis was shown to correlate with the level of SynGAP protein present, and that this apoptosis only occurs in neuronal types where the Syngap gene is lost (Kneusel et al., 2005)

This chapter examines the role that SynGAP plays in the development of the mouse trigeminal system. Prior to me joining the lab, preliminary data demonstrated that both *Syngap*$^{-/-}$ and *Syngap*$^{+/-}$ mice display defects in barrel formation. This chapter substantiates and furthers this datum by showing that *Syngap*$^{-/-}$ mice display a complete lack of cortical cell barrels (Barnett et al., 2006 – in Appendix 6) and further investigates a role for SynGAP in TCA segregation and the segregation of whisker related patterns in thalamic and brainstem nuclei of the trigeminal neuraxis. In addition the chapter examines the expression and localisation of SynGAP during barrel cortex development and the expression of molecules that tightly associate with SynGAP during postnatal development. Finally, whether PKAR2β and SynGAP signal via common or distinct intracellular signalling pathways in barrel development is investigated.

4.2 Methods

4.2.1 Animals

Initial generation of SynGAP knockout mice has been described previously (Komiyama et al., 2002). In brief, targeting constructs were electroporated into embryonic stem (ES) cells and southern blots used to confirm homologous recombination before injecting targeted cells into pseudopregnant mice to generate chimeras. The targeting vector used deleted exons encoding the C2 and GAP domains of SynGAP and introduced an HA-IRES-lacZ-neo cassette. SynGAP mutant mice were obtained from Professor Seth Grant and maintained at the University of Edinburgh on a mixed MF1/129 background. SynGAP heterozygous mating pairs were used to generate wild-type (+/+), heterozygous (+/-), and

homozygous (-/-) pups for experimental analysis. To genotype the animals, genomic DNA was extracted from tail tissue using a Macherey-Nagel Nucleospin kit (Abgene) and then genomic PCR was performed by Anne Petrie as described previously (Komiyama et al., 2002). *Prkar2β$^{-/-}$/SynGAP$^{+/-}$* mice were generated on a mixed C57Bl/6/129/MF1 background (50% C57Bl/6, 25% 129 and 25% MF1) by several generations of matings between the PKAR2β colony (see Chapter 3) and the SynGAP colony (described above).

4.2.2 Histology and Immunohistochemistry

Postnatal day 4, 7 and 14 animals were killed and perfused as described in Chapter 2, postfixed overnight in 4% paraformaldehyde and then equibrilated overnight in 30% sucrose. Brains were sectioned on a freezing microtome at 48μm, either coronally to reveal cortical layers and thalamic nuclei or tangentially to reveal a full barrel field (more details can be found in Chapter 2). Sections were then either mounted onto chromealum-coated slides before staining with thionin or cytochrome oxidase or they were incubated free floating in primary antibody overnight. Thionin (nissl) and cytochrome oxidase (CO) staining was performed as described in Chapter 2 and described previously (Hannan et al., 2001). Immunohistochemistry was performed as described in Chapter 2, to reveal the localisation of 5–HT, 5HTT, Calretinin, PKAR2β and SynGAP, using the following primary antibodies: rat anti-mouse 5-HT (1:10-1:20; Harlan Sprague Dawley), rabbit anti-mouse 5-HTT (1:2000; Calbiochem), goat anti-rabbit calretinin (1:3000; Swant antibodies), rabbit anti-mouse PKAR2β (1:600 – 1:2000; Santa Cruz Biotechnology) and rabbit anti-mouse pan-SynGAP (1:600; Affinity Bioreagents). In all the above cases, mounted sections were dehydrated into xylene and coverslipped. For cell counts, 48μm tangential sections were immunolabeled for SERT (as above), but visualised using an Alexafluor 488 streptavidin epitope (1:200; Invitrogen). These free-floating sections were then counterstained with Topro (1:1000, Invitrogen) diluted in PBS-glycerol (9:1) to reveal the cell nuclei. Sections were mounted on non-subbed slides and coverslipped using Mowoil (see Chapter 2).

4.2.3 Measurements of cortical and layer thickness

All analysis was done blind to genotype. Mice aged between P5 and P7 were combined into one age group for analysis because no difference in cortical thickness or neocortical area was found amongst these animals. Cortical thickness measurements were obtained in the posterior medial barrel subfield (PMBSF) from thionin (nissl) stained 48μm coronal sections equivalent to between –1.82 and –1.94 mm posterior and between 2.8 and 3.2mm lateral to bregma (Franklin and Paxinos, 1997). In the anterior snout region of the barrelfield, cortical thickness measurements were obtained from 48μm coronal sections equivalent to between –0.94 and –1.06 mm posterior and between 3.0 and 3.4mm lateral to bregma. To confirm the location of all the measurements performed in either PMBSF or the anterior snout region, 5-HTT immunohistochemistry was carried out on adjacent sections. Layer 4 and layer 5/6 thickness measurements were obtained in identical sections stained with anti-PKAR2β and anti-calretinin antibodies, respectively. All area measurements were obtained from tangential sections stained with anti-5HT or anti-5-HTT antibodies. Images were analysed at a final magnification of 40X (S1 cortex area), 80X (PMBSF), and 160X (C1 barrel area, cortical thickness, and cortical layer thickness measurements) using a Leica DMLB microscope and the Leica DMLB Image Manager version 4.0 program. All linear and area measurements were performed using the image Tool software and each image was calibrated using a 1mm graticule.

4.2.4 Synaptosome and PSD preparation

P7 mice were killed and their brains dissected for S1 cortex in ice-cold 320mM sucrose solution (see Chapter 2). Dissections were then pooled according to genotype and synaptosomes prepared according to the methods of Dunkley et al. (1986) and as previously described in Chapter 2. To obtain the PSD fraction, synaptosomes were centrifuged at 36,800 x g for 45 minutes, twice in succession (Walikonis et al., 2000).

4.2.5 Western Blotting

Immunoblot analysis was performed on P4 to adult barrel cortex homogenate, synaptosome or PSD preparations as described in Chapter 2. The following primary antibodies were used to incubate the blots overnight: calcium calmodulin-dependent protein kinase II (CamKII) (1:1000; Promega), PSD95 (1:20,000; Upstate Biotechnology), pan-SynGAP (1:4000; Affinity Bioreagents), SynGAPa (1:2000; Upstate Biotechnology), Sap-102 (1:5000; Santa Cruz Biotechnology, Chemicon, Alomone labs or Synaptic systems), NR2A (1:2000; Chemicon), NR1 (1:10,000; Santa Cruz Biotechnology). The blots were then placed in secondary antibody (anti-mouse IgG 1:10,000, anti-rabbit IgG 1:25,000, anti-goat IgG 1:50,000;Sigma) coupled to HRP for 1-2hours, and the proteins then visualised using ECL reagents (Amersham Biosciences) and XAR Kodak autoradiographic film.

4.2.6 Immunoelectron Microscopy

P14 WT mice were perfused as described in Chapter 2 but 0.1% gluteraldehyde was added to the 4% paraformaldehyde fixative. Brains were sectioned coronally at 50μm using a vibrotome and then placed in anti-pan-SynGAP antibody (that recognises all SynGAP isoforms) at a 1:200 dilution, overnight at 4°C in the absence of detergent. Sections were reacted for DAB histochemistry as described in Chapter 2 but with the exception that triton was omitted in each step of the protocol. Sections were then prepared for immmunoelectron microscopy as described in Chapter 3.

4.2.7 Cell Counts

Cell counts were performed on tangential sections through PMBSF of P7 *Prkar2β*$^{-/-}$ */Syngap*$^{+/+}$ and *Prkar2β*$^{-/-}$*/Syngap*$^{+/-}$ mice, fluorescently labelled with anti-SERT antibody and Topro. The average density of Topro-stained nuclei in the walls and hollow of C2 barrel was calculated in both genotypes above using the same methodology as described in Chapter 3.

4.3 Results

4.3.1 SynGAP mutant mice display normal cortical lamination

Syngap$^{-/-}$ mice have been generated by several laboratories and have previously been reported to die within 48hours of birth (Komiyama et al., 2002; Vasquez et al., 2004), except for one report that showed they could live as late as P7 (Kim et al., 2003). In the colony that was used for experiments in this chapter, it was observed that *Syngap*$^{-/-}$ mice had a particular tendency to die soon after birth when part of a large litter. If competition was reduced by either a naturally small litter being born or by deliberate culling of littermates, homozygous knockout mice could be maintained until P7. It was also observed that *Syngap*$^{-/-}$ pups were often considerably smaller in body size during the first postnatal week than their age matched littermates. A reduction in body weight and brain size in *Syngap*$^{-/-}$ mice has previously been reported (Kim et al., 2003; Vasquez et al., 2004) and has raised the possibility that general ill health or defects in brains development might explain the defects in barrel development in these animals. We find this possibility highly unlikely though. General ill health does not prevent TCA or barrel segregation (Vongdokmai, 1980). For example, *TrkB*$^{-/-}$ mice show reduced body and brain weight, and similar to *Syngap*$^{-/-}$ mice, die during the first postnatal week. However, despite their general ill health, TCAs segregate normally in layer 4 of *TrkB*$^{-/-}$ mice, and barrels are indistinguishable from wildtype controls (Vitalis et al., 2002).

To first determine if SynGAP plays a role in general development and lamination of the cortex, I examined the expression of several layer-specific markers including 5-HTT, PKAR2β, and calretinin in the barrel field of P5-P7 *Syngap*$^{-/-}$, *Syngap*$^{+/-}$, and *Syngap*$^{+/+}$ mice (Figure 4.1). Qualitatively, no difference was observed in the laminar expression patterns of these proteins in *Syngap*$^{+/-}$ or *Syngap*$^{-/-}$ mice relative to littermate *Syngap*$^{+/+}$ control animals. However to confirm this qualitative assessment, appropriately matched digital images were chosen and then used to perform the following cortical measurements: (1) cortical thickness in coronal nissl sections through both PMBSF and the anterior snout whisker regions; (2) radial thickness of TCA terminals in coronal sections labelled with 5-HTT in sections through both PMBSF and the anterior snout whisker regions; and (3) radial thickness

of layers 1-4 and 5-6 in calretinin-labeled sections through both PMBSF and the anterior snout whisker region (Fig. 4.1m). No significant difference was found in cortical lamination between *Syngap*$^{+/+}$ and *Syngap*$^{+/-}$ mice, with respect to the measurements done, indicating that the cortex develops normally in these mice. However a small reduction was found in the cortical thickness of PMBSF and the anterior snout whisker region in *Syngap*$^{-/-}$ mice compared to *Syngap*$^{+/+}$ and *Syngap*$^{+/-}$ mice. Individual thickness assessment of layers 1-4, layers 5-6 and TCA patches revealed that all layers were affected in *Syngap*$^{-/-}$ mice (Fig. 4.1m). The data therefore (summarized in Table 4.1) is in good agreement with the fact that *Syngap*$^{-/-}$ mice have a reduction in overall brain size (Kim et al., 2003; Vasquez et al., 2004).

4.3.2 Barrel formation is disrupted in *Syngap* +/- and -/- mice

Preliminary data before I joined the lab indicated that SynGAP plays a role in cellular segregation into barrels in layer 4. To confirm this data, I examined the distribution of TCAs and layer-IV cell soma in several additional *Syngap*$^{+/+}$ (n=4) and *Syngap*$^{-/-}$ (n=5) mice. Nissl stained tangential sections through layer IV of P6/7 *Syngap*$^{-/-}$ mice reveal a complete loss of cellular segregation into barrels in layer IV (Fig. 4.2b). To provide further evidence that *Syngap*$^{-/-}$ lack barrels, I examined three adjacent nissl-stained sections through layer IV of additional *Syngap*$^{-/-}$ animals. No barrels can be seen in any section (Fig. 4.4 a-c) indicating that the result cannot be an artefact of the difficulties in cutting flattened tangential sections to view a full barrelfield. *Syngap*$^{+/+}$ littermate controls show qualitatively normal cellular segregation into barrels in layer IV (Fig. 4.2a).

Next I examined the distribution of TCAs in *Syngap*$^{-/-}$, *Syngap*$^{+/-}$ and *Syngap*$^{+/+}$ mice using 5-HTT immunohistochemistry (Lebrand et al., 1996; Lebrand et al., 1998) (Fig. 4.2 c-e). Coronal sections immunoreacted with 5-HTT-antibody demonstrate that TCA termination in the PMBSF region of P6/P7 mice is restricted to layer IV in all three genotypes (Fig. 4.1 g-i). However tangential sections through layer IV of *Syngap*$^{-/-}$ mice show a striking defect in TCA segregation, revealing rows instead of individual whisker-related patches (fig. 4.2 e and Fig. 4.4 d-g). It is clear that this defect in TCA segregation within S1 does not reflect a general defect in TCA

pathfinding since segregation between cortical areas (V1, S1, S2 and A1) appears normal. Furthermore subregions within S1 such as PMBSF and the anterior snout, lower lip, forepaw, and hindpaw areas are easily identifiable. To further asssess these findings I quantitatively examined the areas of neocortex, S1, and PMBSF in flattened sections labelled with 5-HTT. A small decrease in the size of S1 and PMBSF was found in *Syngap*$^{-/-}$ animals compared to *Syngap*$^{+/+}$ and *Syngap*$^{+/-}$ animals, however this reduction was very small and not significant with respect to the area of S1. The decrease in area of S1 and/or PMBSF does not therefore seem a likely explanation for the loss of TCA segregation seen in *Syngap*$^{-/-}$ mice (Fig. 4.2F).

In contrast, *Syngap*$^{+/+}$ and *Syngap*$^{+/-}$ littermates show normal TCA segregation into whisker-related patches in layer IV (Fig. 4.2 c,d). To confirm these findings I quantitatively examined the area of B1-B3, C1-C3, and D1-D3 barrels in *Syngap*$^{+/+}$ and *Syngap*$^{+/-}$ animals (Fig. 4.2 f and Fig. 4.3). No significant difference was found in the TCA areas of individual whisker-related patches between *Syngap*$^{+/+}$ and *Syngap*$^{+/-}$ mice (Fig. 4.3).

A complete lack of cortical barrels, despite partial TCA segregation in *Syngap*$^{-/-}$ mice suggested a role for SynGAP in the cortex during barrel formation. To investigate this hypothesis further, Dr Tania Vitalis analysed the *Syngap*$^{+/-}$ mice in more detail (Appendix 7). Histology performed by Tania shows that despite normal TCA segregation, P8 *Syngap*$^{+/-}$ mice demonstrate reduced cellular segregation in PMBSF compared to *Syngap*$^{+/+}$ littermate controls. Quantification of this defect confirms a significant decrease in cell density barrel wall-to-hollow ratio in *Syngap*$^{+/-}$ mice (1.25 ± 0.13) ($p<0.01$) compared to *Syngap*$^{+/+}$ mice (1.76 ± 0.16) (Appendix 7; Barnett et al., 2006). No difference is calculated however in the total number of cells in layer 4 indicating that the reduced barrel wall-to-hollow ratio results from a decrease in the number of neurons in the barrel wall and an increase in the number of neurons in the barrel hollow due to poor segregation. Importantly, this reduction in barrel segregation has been observed in *Syngap*$^{+/-}$ mice at all ages, so it does not reflect a delay in barrel formation (personal communication, Dr Peter Kind).

4.3.3 Segregation of barreloids is reduced in *Syngap-/-* mice

Whisker-related patterns also form in the rodent brainstem and thalamus and are called barrelettes and barreloids respectively. To determine whether the loss of segregation cortically results from a loss of *Syngap* at the level of the thalamus, I examined barreloid formation in VpM of the thalamus by CO histochemistry. *Syngap*$^{-/-}$ mice show reduced segregation of barreloids in comparison to *Syngap*$^{+/+}$ littermates at both P4 and P7 (Fig. 4.5 c,f and a,d respectively). Patches of CO label can be seen in the dorsolateral region of *Syngap*$^{-/-}$ VpM corresponding to the large facial vibrissae, but they are not as distinct as the patches observed in *Syngap*$^{+/+}$ or *Syngap*$^{+/-}$ animals, and no segregation is apparent in the regions that receive input from the anterior snout whiskers in *Syngap*$^{-/-}$ animals. In contrast, P7 *Syngap*$^{+/-}$ mice display clear barreloid segregation that is indistinguishable from *Syngap*$^{+/+}$ mice. However at P4, *Syngap*$^{+/-}$ mice display barreloid segregation throughout VpM, but the segregation is not as well-defined as in *Syngap*$^{+/+}$ mice where inter-barreloid regions are clear, suggesting that there could be a slight delay in barreloid segregation in *Syngap*$^{+/-}$ mice.

CO histochemistry was also used to examine barrelette formation in *Syngap*$^{-/-}$ and *Syngap*$^{+/-}$ mice. Qualitative assessment of the staining reveals that barrelettes form normally in both the principal nucleus (Fig. 4.5 g,h) of the trigeminal complex (PrV) and the subnucleus interpolaris (SpI) (Fig. 4.5 i,j). These results are in good agreement with the complete lack of SynGAP expression in developing brainstem nuclei (Porter et al., 2005).

4.3.4 SynGAP expression during barrel development

A temporal and spatial requirement for SynGAP throughout development is indicated by the disruption of various whisker related patterns in the trigeminal system of SynGAP mutant mice. To identify the cells that express SynGAP, Porter et al., (2005) examined the spatiotemporal expression profile of SynGAP in *Syngap*$^{+/-}$ mice, taking advantage of the presence of the insertion of the gene encoding β-galactosidase (β-gal) into the SynGAP locus (Komiyama et al., 2002)

(see Appendix 8; Barnett et al., 2006). In brief, X-gal staining (reflecting the expression of SynGAP mRNA) is seen throughout cortical and thalamic development in a dynamic temporal and spatial profile. At birth, X-gal staining is high thoughout the dorsal thalamus but is not present in the ventral thalamus indicating that SynGAP expression is selective to the projection nuclei of the thalamus. X-gal staining remains high in the dorsal thalamus at P4, increases dramatically in VB by P8 and peaks at P14 before decreasing by P21. In adult, thalamic X-gal staining is no longer visible. In cortex, X-gal staining always appears in a pattern consistent with neuronal localisation, being absent in white matter and failing to co-localise with GFAP, an astrocytic marker (Barnett et al., 2006). In S1 at birth, X-gal staining can only be seen as a thin dense band at the bottom of the cortical plate. However by P4, SynGAP expression can be observed through the granular and supragranular layers, but not in the infragranular layers. Then during the second postnatal week X-gal staining spreads throughout the entire cortex and particularly high levels of staining can be seen in layer IV in bands corresponding to barrel walls. Finally by P35 and adulthood, overall X-gal staining is reduced but two thin bands in upper layer 3 and at the layer 4/5 boundary remain (see Appendix 8).

To complement the X-gal histochemistry performed by Karen Porter, Peter Kind and Tania Vitalis, which reflects *Syngap* mRNA rather than protein, I examined the localisation of SynGAP protein in early postnatal development. Immunohistochemical distribution of SynGAP protein in S1 cortex and VpM is in good agreement with the results obtained for X-gal staining (Fig. 4.6). Immunostaining for SynGAP in P7 coronal sections shows that this protein is expressed throughout S1 cortex with particularly high levels of staining in layer IV and the supragranular layers. In layer IV, staining appears as diffuse neuropilar patches that correspond to barrels (Fig. 4.6 d). In thalamus, SynGAP expression is visible within VpM (Fig. 4.6 a,c), which is in good agreement with the previously shown role for SynGAP in barreloid development.

Despite strong immunohistochemical staining in patches through layer IV that correspond to barrels, it is not clear whether SynGAP is localised to presynaptic TCA terminals or postsynaptic layer IV dendrites. To determine the subcellular

localisation of SynGAP in barrel cortex, I performed immunoelectron microscopy (EM), on layer IV dissected from P14 S1 cortex. The EM images obtained show regions of dense black staining that is DAB reaction product, in postsynaptic densities abutting presynaptic terminals containing synaptic vesicles (Fig. 4.7). However no reaction product can be seen in any axons or presynaptic terminals. These results suggest that SynGAP has an exclusive postsynaptic localisation in developing thalamocortical synapses and is in agreement with previous findings showing SynGAP association with PSDs in cultured hippocampal neurons (Chen et al., 1998; Kim et al., 1998; Krapivinsky et al., 2004; Petralia et al., 2005).

4.3.5 SynGAP associates with the PSD independent of PSD95

MAGUK proteins are scaffolding molecules that interact with NMDA receptors and tether signaling molecules to the PSD. The family of MAGUKs include PSD95, PSD93/Chapsyn110, and SAP102. All of these proteins contain 3 PDZ domains, of which the first two bind to the C termini of NR2 subunits. The third PDZ domain of PSD95 and Sap102 then bind to the C-terminus of SynGAP. If PSD95 were the key MAGUK responsible for regulating SynGAP, one would expect to find a defect in barrel formation in *Psd95*$^{-/-}$ mice. However a normal barrelfield is evident in P7 and adult *Psd95*$^{-/-}$ mice (see Appendix 9; Barnett et al., 2006). The lack of a barrel phenotype in *Psd95*$^{-/-}$ mice raised the possibility that SynGAP could be associating with the PSD in a PSD95 independent manner. To examine this possibility I isolated PSDs from *Psd95*$^{-/-}$ and wild-type S1 cortex and then used western blot analysis to determine the presence of SynGAP protein in each fraction. A 135kDa band corresponding to pan-SynGAP protein was clearly visible in PSD fractions from wildtype and *Psd95*$^{-/-}$ S1 cortex (Fig. 4.8 b).

To gain further insight into the dynamics of the PSD during barrel development I examined the developmental expression profiles of other PSD constituents in S1 homogenates and in synaptosomes prepared from P7 S1 cortex (Fig. 4.8). In summary, the western blots show two different general trends of protein expression throughout development. SynGAP, NR1, SAP102 and αCamKII, a Ca^{2+}/calmodulin dependent kinase known to phosphorylate SynGAP, all steadily increase in their

expression levels from P0 into adulthood, correlating with the normal development and maturation of synapses (synaptogenesis). NR2A, SynGAPα and PSD95 however, show larger increases in their expression levels with age, increasing rapidly at P14. NR2A appears hardly detectable at P7, but increases dramatically between P7 and P14 and continues to increase in expression level into adulthood. PSD95 is a very abundant protein in barrel cortex homogenate and is expressed throughout the first postnatal week and increases dramatically at P14 into adulthood. Two dilutions of PSD95 antibody were used to clearly analyse the lower and higher spectrums of PSD95 expression because of the substantial increase at P14. A 1:20,000 dilution of PSD95 antibody shows that PSD95 is expressed at birth and gradually increases with age over the first postnatal week (P0, P4 & P7), however due to the large increase between P7 and P14, levels of expression are saturated on this blot from P14 into adulthood. Therefore to examine the expression profile of PSD95 in the second postnatal week, a 1:40,000 dilution of antibody was used. The 1:40,000 dilution blot shows that PSD95 is highly expressed and remains constantly expressed from P14 into adulthood. Figure 4.8b shows that PSD95 is also found highly enriched in synaptosomes from P7 barrel cortex, but as previously described the presence of PSD95 is not required for SynGAP to associate with the PSD. PSD95 does not therefore appear crucial for SynGAP-dependent barrel formation. Instead SAP102 (or another MAGUK) may play this role in normal development or at least be able to compensate for the loss of PSD95. High expression of SAP102 in barrel cortex homogenates during the first postnatal week is in good agreement with this possibility.

To address whether the MAGUK-dependent association of SynGAP to the PSD is necessary, the developmental expression profile of SynGAPα1 was also examined by biochemistry. SynGAPα1 is the C-terminal splice variant reported to contain the QTRV sequence necessary for binding to the PDZ domain of PSD95. I compared the expression profile of SynGAPα1 against the expression profile of total SynGAP (using a pan-SynGAP antibody that recognises all SynGAP isoforms because the epitope lies in the GAP domain), to determine the relative abundance of SynGAPα1 protein in developing barrel cortex. Expression levels of both pan-SynGAP and SynGAPα1 increase considerably during the second postnatal week, however in the

first postnatal week SynGAPα1 is barely detectable. This expression data suggests that the forms of SynGAP present during barrel development are not those that directly bind MAGUKs, indicating that during early postnatal development SynGAP may be associating with the PSD and regulating barrel development in a MAGUK-independent manner (see discussion).

4.3.6 SynGAP and PKAR2β in barrel development

In chapter 3, I showed that PKAR2β plays an essential role in postsynaptic signaling pathways involved in barrel formation. Subsequently I have shown that SynGAP is required in S1 cortical cells to mediate barrel development. I have also demonstrated by immunoelectron microscopy that both of these molecules localise to dendrites and PSDs in layer 4 of developing S1 cortex. To explore a potential link between PKAR2β and SynGAP in the mechanisms regulating barrel formation, I took a double transgenic approach, generating *Prkar2β*$^{-/-}$/*Syngap*$^{+/-}$ double transgenic mice in order to examine their barrel phenotype compared to single *Prkar2β*$^{-/-}$ and *Syngap*$^{+/-}$ mutant mice. I reasoned that there could be three potential outcomes of the *Prkar2β*$^{-/-}$/*Syngap*$^{+/-}$ barrel phenotype and that any of these would provide further insight into the different signaling possibilities of PKAR2β and SynGAP in barrel formation:

Potential Outcome 1: barrel cortex looks like a *Syngap*$^{+/-}$

Potential Outcome 2: barrel cortex looks like a *Prkar2β*$^{-/-}$

Potential Outcome 3: barrel cortex looks worse than either of the single mutants

Nissl stained sections through layer IV of *Prkar2β*$^{-/-}$/*Syngap*$^{+/-}$ mice reveal only a few barrels that are very poorly segregated (Fig. 4.9a-d); a phenotype that appears qualitatively worse than the barrelfield in *Prkar2β*$^{-/-}$ (Fig. 4.9 d,e) or *Syngap*$^{+/-}$ mice. To determine whether the degree of cellular segregation is reduced in *Prkar2β*$^{-/-}$ /*Syngap*$^{+/-}$ mice compared to *Prkar2β*$^{-/-}$ mice, I performed cell counts on both genotypes (when C2 was visible in the double knockout mice), on tangential sections through layer IV co-labelled with Topro and SERT, labelling cell nuclei and TCA patches respectively (Fig. 4.9g,h). The cell density ratio of barrel wall: barrel hollow in barrel C2 is significantly reduced in *Prkar2β*$^{-/-}$/*Syngap*$^{+/-}$ mice (1.178 ± 0.04)

compared to *Prkar2β*$^{-/-}$ mice (1.356 ± 0.1). Interestingly the degree of reduced cellular segregation in the *Prkar2β*$^{-/-}$/*Syngap*$^{+/-}$ mice (1.178 ± 0.04) is very similar to that previously reported in *Syngap*$^{+/-}$ mice (1.2 ± 0.13; Barnett et al., 2006). However these mice are on different genetic backgrounds so a direct comparison cannot be made. Unfortunately cell density counts could not be obtained in *Syngap*$^{+/-}$ mice from this double transgenic colony because an outbreak of MHV in the colony required culling of the appropriate animals. Therefore these experiments are ongoing. However despite similar degrees of cellular segregation of barrel C2 in *Prkar2β*$^{-/-}$/*Syngap*$^{+/-}$ mice compared to the previously analysed *Syngap*$^{+/-}$ mice, qualitative observation of the barrelfield reveals fewer visible barrels compared to *Syngap*$^{+/-}$ mice, indicating that the barrel phenotype is worse.

PKA does not appear to regulate barrel formation by regulating AMPAR trafficking (see Chapter 3). PKA has been shown by other laboratories however to regulate the activity of transcription factors, for example MEF2 (Wang et al., 2005; Waltereit & Weller, 2003). To investigate whether PKA regulates barrel formation by gene transcription, I began by examining expression levels of SynGAP protein in synaptosomes from S1 cortex in *Prkar2β*$^{-/-}$ and wild-type mice. SynGAP levels are dramatically reduced to approximately 40% in *Prkar2β*$^{-/-}$ synaptosomes (n=3; Fig. 4.10 a). mRNA levels were also examined using RT-PCR with primers specific to the conserved GAP domain. Preliminary RTPCR data shows a high degree of variability. One experiment (n=1) demonstrates that pan-SynGAP mRNA levels are reduced in a P7 *Prkar2β*$^{-/-}$ compared to wild-type S1 cortex, in agreement with the biochemical data (Fig. 4.10 b). However a second experiment performed to validate this result does not show any difference in pan-SynGAP mRNA levels between P7 *Prkar2β*$^{-/-}$ and wildtype S1 cortex (n=1). Finally, western blot analysis shows that levels of SynGAP protein are further reduced in *Prkar2β*$^{-/-}$/*Syngap*$^{+/-}$ mice compared to *Prkar2β*$^{-/-}$ mice (Figure 4.10c).

4.4 Discussion

NMDA receptors are crucial for the normal development of S1 somatotopy (Schlaggar et al., 1993; Fox et al., 1996; Iwasato et al., 2000; Datwani et al., 2002). Now the intracellular pathways that mediate NMDAR signals and initiate the morphological changes required for barrel formation are beginning to be elucidated. This chapter shows a clear role for SynGAP, likely downstream of NMDARs in barrel development. SynGAP is a component of the mature NMDAR complex (Chen et al., 1998; Kim et al., 1998, 2003; Komiyama et al., 2002) and is also present in developing PSDs where it plays a role in regulating S1 cortical development. *Syngap*$^{-/-}$ mice fail to form barrels, have TCAs segregated into rows rather than whisker related clusters and display partial barreloid segregation in VpM. *Syngap*$^{+/-}$ mice also show reduced barrel segregation but their TCA patches and barreloids develop normally. SynGAP can associate with the PSD in P7 S1 cortex in mice lacking *Psd95*, a MAGUK scaffolding molecule; this result suggests that PSD95 is not crucial for barrel development and agrees with the normal barrel formation found in *Psd95*$^{-/-}$ mice. Lastly, a potential link between SynGAP and PKAR2β in barrel formation may exist in S1 cortex since *Prkar2β*$^{-/-}$*/Syngap*$^{+/-}$ mice show a qualitatively worse barrel phenotype than *Prkar2β*$^{-/-}$ or *Syngap*$^{+/-}$ mice. In addition, SynGAP and PKAR2β likely signal via different pathways in VpM, since barreloids form normally in *Prkar2β*$^{-/-}$ mice. In summary, these data demonstrate an important role for SynGAP in patterning the trigeminal system of mice and show heterogeneity in the intracellular pathways used by different brain regions at different developmental stages.

4.4.1 Heterogeneity of signaling pathways in the trigeminal system of mice

Barrel formation in layer IV of S1 requires NMDA receptors (Iwasato et al., 2000), PKAR2β (Chapter 3; Watson et al., 2006) and SynGAP. However all of these molecules demonstrate different spatiotemporal profiles in postnatal development and are not all required for the development of whisker-related maps in the brainstem

and thalamus of the trigeminal pathway. In VpM of the thalamus, barreloid formation requires NMDA receptors (Iwasato et al., 1997) and SynGAP but not PKAR2β (Chapter 3; Watson et al., 2006). In the brainstem nuclei however, barrelette formation requires NMDA receptors (Li et al., 1994; Iwasato et al., 1997) but not PKAR2β or SynGAP. These observations indicate that the mouse trigeminal system uses different signaling molecules in different neuronal populations to pattern the sensory periphery and attain similar cellular outcomes, for example the segregation of presynaptic afferents and postsynaptic cells.

4.4.2 Is SynGAP pre- or post-synaptic in barrel formation?

Immunoelectron microscopy data confirmed that SynGAP protein is expressed in dendrites and postsynaptic spines, but not in axons or presynaptic terminals in layer IV of developing somatosensory cortex. In agreement biochemistry showed that SynGAP is localised to postsynaptic densities in P7 S1 cortex. It is clear therefore that SynGAP plays a postsynaptic role in cellular segregation in layer IV in barrel formation. However it is not clear whether the incomplete segregation of TCAs into rows in *Syngap*$^{-/-}$ mice is due to the loss of SynGAP in the cortex or the thalamus. Previous work on *CxNr1*$^{-/-}$ mice has shown that cortically derived signals are able to regulate TCA elaboration, because these mice exhibit smaller TCA patches and demonstrate a significant decrease in TCA complexity within layer IV (Lee et al., 2005). Therefore it is possible that NMDA receptors could be regulating TCA segregation via SynGAP-regulated release of a retrograde signal. However loss of SynGAP in the thalamus could also generate a cell-autonomous defect in thalamic neurons that prevents normal TCA terminal segregation in the cortex. To distinguish between these two possibilities, a cortex-specific *Syngap*$^{-/-}$ mouse is required for analysis.

However, two observations in the targeted *Syngap* mutant mice have indicated a postsynaptic cortical role for SynGAP during barrel formation. First, *Syngap*$^{+/-}$ mice displayed reduced segregation of layer IV neurons despite normal TCA segregation. Second, *Syngap*$^{-/-}$ mice lacked cortical barrels of any description, despite partial segregation of TCAs into rows. This result contrasted with formation of a

"megabarrel", a large barrel where layer IV cells cluster around the row of TCAs, previously described to form in WT mice after cauterisation of row C follicles (Van der Loos and Woolsey, 1973). A large barrel would have been expected to form in *Syngap*$^{-/-}$ mice if barrel formation was independent of cortically expressed SynGAP. In addition, a previous study that reported splice variant SynGAPα2 to localise to axons in cultured cerebellar axons (Tomodo et al., 2004), led Dr Mark Barnett from the laboratory to investigate whether SynGAPα2 is present in developing VpM and hence could localise to TCAs. SynGAPα2 is not found in VpM cells during barrel development (Barnett et al., 2006) providing additional evidence that SynGAP is postsynaptic in barrel formation.

4.4.3 Is SynGAP signaling dependant upon MAGUKs?

SynGAP has previously been shown to associate with NMDARs in mature PSDs via PSD95 (Chen et al., 1998; Kim et al., 1998). *Psd95*$^{-/-}$ mice however develop normal barrels (Barnett et al., 2006) and I have shown that the interaction between SynGAP and PSD95 is not required to maintain the association of SynGAP with developing PSDs. Instead, SynGAP may preferentially associate with NMDARs via SAP102 during development. SAP102 is another member of the membrane-associated guanylate kinase (MAGUK) family and has more recently been reported to interact with SynGAP (Kim et al., 2005). Furthermore NR2B containing NMDARs predominantly associate with SAP102 and are abundant during neonatal development, declining into adulthood. In contrast NR2A containing NMDARs associate with PSD95 and are expressed later in development, perhaps displacing NR2B/SAP102 complexes from the PSD (Shi et al., 1997; Sans et al., 2000; Yoshii et al., 2003; Van Zundert et al., 2004). Analysis of *Nr2A*$^{-/-}$ mice has shown that NR2A is not necessary for barrel formation (Lu et al., 2001). In S1, I found high levels of PSD95 and SAP102 in P7 PSDs and the expression profiles of both proteins increased over a developmental stage series correlating well with synaptogenesis in rodent S1 (Micheva and Beaulieu, 1996; White et al., 1997; Spires et al., 2005). Interestingly though, PSD95 levels increase more dramatically with age revealing a more similar developmental expression profile to NR2A. Therefore during barrel

development, SynGAP could be associating with the PSD via NR2B/SAP102 complexes rather than through PSD95.

Alternatively SynGAP could associate with developing PSDs in a MAGUK independent manner, as previously found in tissue culture (Vasquez et al., 2004; Rumbaugh et al., 2006). In agreement with this possibility Dr Mark Barnett in the laboratory has analysed the C-terminal isoforms of SynGAP in layer IV and found several SynGAP splice variants present without MAGUK-binding consensus sequences (Li et al., 2001). SynGAP-β has previously been reported by Li et al. (2001) to have a distinct binding specificity for CamKII, a key NRC component. Strong protein–protein interactions between these two molecules could drive SynGAP-β to the PSD. All SynGAPs also contain a pleckstrin homology domain (PH) and a C2 domain both of which could be involved in localising SynGAP to the synapse. PH domains are small B-sandwich modules of approximately 100 amino acids that bind phosphoinositides embedded in the lipid membrane bilayer with varying degrees of specificity and affinity. They are strongly electrostatically polarised structures and therefore attraction between their positive charged faces and the negatively charged surface of the membrane may substantially contribute to their membrane targeting (Lemmon et al., 1997; Lemmon & Ferguson, 2001). C2 domains are protein modules that bind Ca^{2+} and phospholipids (Rizo & Sudhof, 1998), and most mediate Ca^{2+}-dependent phospholipids binding.

4.4.4 What are the potential signaling pathways downstream of SynGAP?

SynGAP has been shown in hippocampal slices to regulate activation of the ERK-mitogen-activated protein kinase (MAPK) signaling pathway (Komiyama et al., 2002). SynGAP can regulate ERK-MAPK through its role as a Ras-GAP (Chen et al., 1998; Oh et al., 2004), acting as a molecular switch that negatively regulates Ras (a small GTP-ase) via its GAP domain (Kim et al., 1998; Kim et al., 2003). Upon CamKII activation, SynGAP binds the active form of Ras, which stimulates its weak intrinsic GTPase activity and causes rapid hydrolysis of GTP to GDP, returning Ras to its inactive form (Scheffzek et al., 1998). In this way SynGAP regulates the

MAPK pathway in response to NMDA receptor activation (Kim et al., 1998). The MAPK pathway is just one of several potential pathways downstream of Ras (Cullen & Lockyer, 2002), but it is particularly interesting, because as mentioned in the introduction, it has been shown to be important in regulating many developmental processes including cell proliferation, differentiation, survival, migration and neuronal plasticity (Orban et al., 1999; Gille and Downward, 1999; Sweatt, 2001; Di Cristo et al., 2001; Adams and Sweatt, 2002; Sweatt, 2004). These findings all suggest that SynGAP may regulate barrel formation by signaling via the ERK-MAPK pathway. Furthermore this hypothesis is supported by recent findings including a role for ERK-MAPK in visual cortex development and NMDAR-dependent LTP in visual cortex and hippocampus (Di Cristo et al., 2001; Winder et al., 1999) and performance on spatial learning tasks (Bozon et al., 2003). A role for the ERK-MAPK pathway in all of these processes indicates conservation of signaling pathways between ages and developmental stages.

However it is important to note that SynGAP could be regulating barrel development independently of ERK. For example, SynGAP could be regulating Ras-dependent, but ERK-independent pathways or Ras-independent pathways. In support of an ERK-independent mechanism, *Syngap*$^{+/-}$ mice show defects in LTP induction using pairing protocols and 100Hz stimulation (Komiyama et al., 2002), two forms of LTP induction that are ERK independent in wild-type slices (Winder et al., 1999; Watabe et al., 2000). Also, several ERK-independent signaling cascades have been described downstream of Ras in response to NMDA receptor activation (Cullen & Lockyer, 2002) including the Ras-PI3K pathway (Cullen & Lockyer, 2002). PI3K is a major effector of Ras and has been shown to be involved in cytoskeletal remodelling and is necessary for NMDAR-stimulated delivery of AMPARs to the neuronal surface, a mechanism of synaptic plasticity (Man et al., 2003; Opazo et al., 2003). Recent studies have also revealed that SynGAP can act as a Rab-GAP (Tomoda et al., 2004) and a Rap-GAP (Krapivinsky et al., 2004). While SynGAP bares closest homology to other RasGAPs, Krapivinsky et al. (2004) found that for *in vitro* hippocampus, SynGAP has more efficient GAP activity for Rap than it does for Ras. Krapivinsky et al. (2004) also showed that dephosphorylated SynGAP that is dissociated from its complex with MUPP1 and CaMKII, causes an inactivation of

Rap and subsequent increase in p38MAPK activity. Therefore p38MAPK is another potential signaling cascade through which SynGAP might regulate barrel formation. Finally, Tomoda et al. (2004) showed that SynGAP regulates Rab5 activity, whose activity regulates the actin cytoskeleton during "circular ruffle" formation and cell migration (Lanzetti et al., 2004). It is possible therefore, that other small non-Ras G-proteins are crucial effectors of SynGAP during barrel development.

4.4.5 Convergence of PKAR2β and SynGAP barrel signaling pathways

There are four potential hypotheses that could link PKAR2β and SynGAP in barrel development (demonstrated by diagrams in figure 4.11): (1) PKAR2β lies upstream of SynGAP within the PSD, and regulates SynGAP activity; (2) SynGAP lies upstream of PKAR2β within the PSD and regulates PKAR2β activity; (3) PKAR2β regulates gene expression that affects SynGAP or vice versa; and (4) PKAR2β and SynGAP signal via two distinct pathways but converge, for example on ERK to affect barrel formation. Alternatively there may be no interaction between PKAR2β and SynGAP but both affect barrel formation by regulating different mechanisms. To provide further insight into the above possibilities, I examined the barrel phenotype of *Prkar2β*$^{-/-}$/*Syngap*$^{+/-}$ mice and reasoned that the three potential outcomes described in results section 4.3.6 would indicate the following different signaling possibilities:

Potential Outcome 1: barrel cortex looks like a *Syngap*$^{+/-}$ - this result would indicate that PKAR2β lies upstream of SynGAP within the PSD, and regulates SynGAP activity **(Hypothesis 1)**; or that PKAR2β regulates gene expression that affects SynGAP **(Hypothesis 3)**.

Potential Outcome 2: barrel cortex looks like a *Prkar2β*$^{-/-}$ - this result would indicate that SynGAP lies upstream of PKAR2β within the PSD and regulates PKAR2β activity **(Hypothesis 2)**.

Potential Outcome 3: barrel cortex looks worse than either of the single mutants - this result would indicate that PKAR2β and SynGAP signal via two distinct pathways but converge on a common target to affect barrel

formation **(Hypothesis 4)**; or that PKAR2β regulates gene expression that affects SynGAP **(Hypothesis 3)**.

Cellular segregation, quantified within barrel C2, was found significantly reduced in *Prkar2β*$^{-/-}$/*Syngap*$^{+/-}$ mice compared to *Prkar2β*$^{-/-}$ mice. In addition, qualitative observation of the barrelfield in *Prkar2β*$^{-/-}$/*Syngap*$^{+/-}$ mice revealed fewer visible barrels compared to Syngap$^{+/-}$ mice. This preliminary phenotypic data has indicated that the barrelfield is more disrupted in *Prkar2β*$^{-/-}$/*Syngap*$^{+/-}$ mice than either *Prkar2β*$^{-/-}$ or Syngap$^{+/-}$ mice (Potential Outcome 3). Western blot analysis also showed that SynGAP protein levels are reduced in *Prkar2β*$^{-/-}$ mice compared to wildtype controls and even further reduced in *Prkar2β*$^{-/-}$/*Syngap*$^{+/-}$ animals. If substantiated by further experimentation, the qualitatively worse phenotype found in the *Prkar2β*$^{-/-}$ /*Syngap*$^{+/-}$ mice and reduced SynGAP levels on combining *Prkar2β*$^{-/-}$ and Syngap$^{+/-}$ mice suggests that SynGAP and PKAR2β signal via two independent barrel development pathways that converge on a common factor (Hypothesis 4; Figure 4.11).

4.4.6 Future Work

This chapter has established that SynGAP is a key regulator of barrel development, likely downstream of glutamate neurotransmission. A question that now remains, is how does SynGAP mediate glutamate signaling to cause the morphological changes that occur during barrel formation? As discussed above, there are several candidate signaling pathways that could play a role in barrel formation downstream of SynGAP, however the ERK/MAPK pathway is probably the most studied and heavily implicated. Chapter 5 investigates whether or not SynGAP signals via the ERK/MAPK cascade upon synaptic stimulation in cortical cultures.

Further analysis of the PKAR2β-SynGAP double transgenic mice could also provide greater insight into the postsynaptic pathways involved in barrel development. Interestingly, work by another group has recently provided a link between PKA and SynGAP in another developmental process. PKA has been shown to phosphorylate a

transcription factor called MEF2 (Wang et al., 2005) that subsequently regulates SynGAP and suppresses excitatory synapse numbers (Flavell et al., 2006). Synapse formation and strengthening is a crucial process for barrel formation (see Chapter 1 for details). It would be interesting to investigate if a PKA-MEF2-SynGAP pathway exists in S1 cortex and whether disruption of this pathway affects barrel formation.

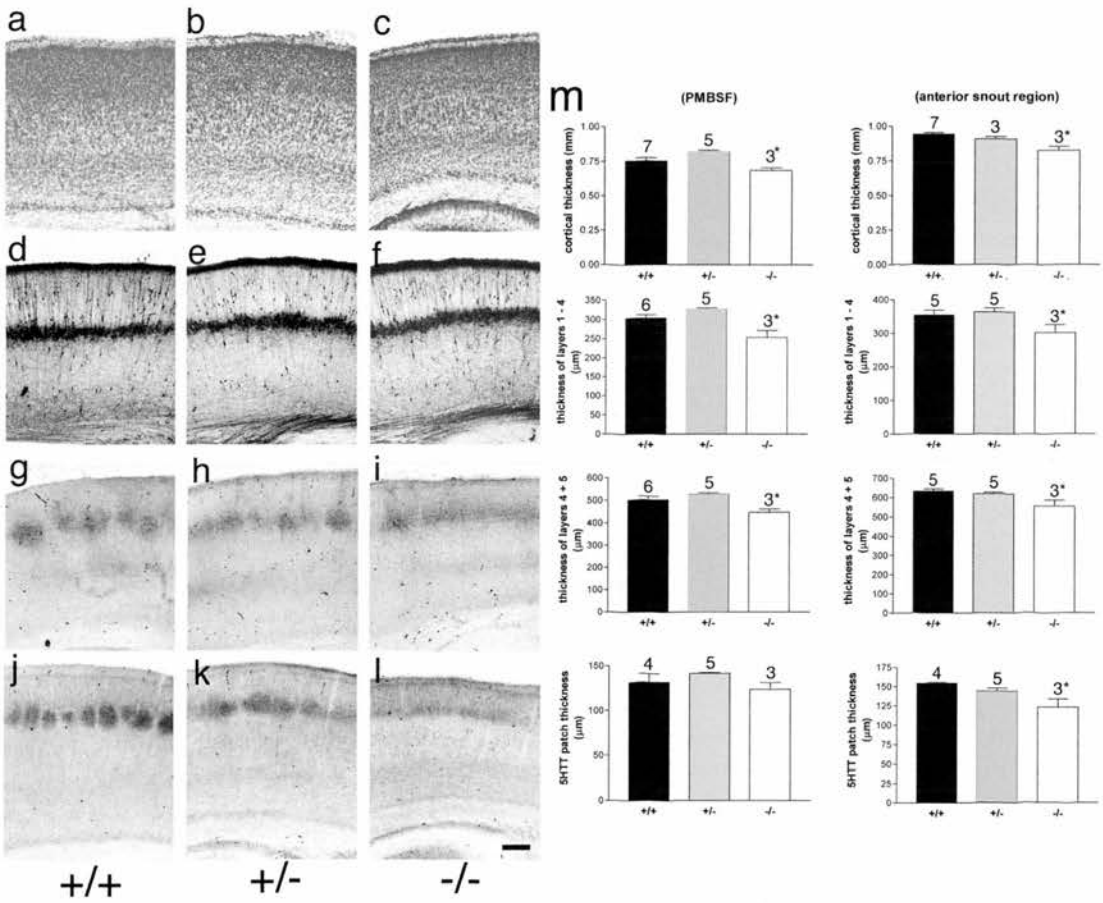

Figure 4.1: Cortical lamination is normal in *Syngap*$^{+/-}$ and *Syngap*$^{-/-}$ mice. Cortical sections through S1 cortex of P6/7 *Syngap*$^{+/+}$ (**a,d,g,j**), *Syngap*$^{+/-}$ (**b,e,h,k**), and *Syngap*$^{-/-}$ (**c,f,i,l**) mice stained with thionin (nissl) (**a-c**), calretinin (**d-f**), 5HTT (**g-l**), and PKAR2β (**j-l**). No qualitative difference is seen between genotypes with the exception of the lack of TCAs seen in the *Syngap-/-* mice. Quantitative analysis of cortical thickness, radial thickness of TCA terminals, layer 5/6 thickness, and layer 1-4 thickness was also calculated (**m**). In all cases, no significant difference was found between *Syngap*$^{+/+}$ and *Syngap*$^{+/-}$ animals. There was a significant decrease in *Syngap*$^{-/-}$ compared with *Syngap*$^{+/+}$ and *Syngap*$^{+/-}$ mice in all parameters measured except 5-HTT terminal zone thickness in PMBSF. Scale bar: (in **l**) **a - l,** 250µm. Error bars represent standard errors.

	WT/HET MEAN	KO MEAN	% DIFF.	P VALUE
Thickness of layers 1-6 (PMBSF) in mm	0.78 ± 0.017	0.68 ± 0.020	12.60	0.020
Thickness of layers 1-6 (AS) in mm	0.93 ± 0.010	0.83 ± 0.028	11.36	0.001
Thickness of layers 1-4 (PMBSF) in μm	314 ± 6.12	252 ± 17.90	19.75	0.001
Thickness of layers 1-4 (AS) in μm	360 ± 18.95	303 ± 23.73	15.83	0.018
Thickness of 5HTT patch (PMBSF) in μm	137 ± 4.33	123 ± 7.56	10.22	0.142
Thickness of 5HTT patch (AS) in μm	149 ± 2.67	123 ± 10.62	17.45	0.006
Area of neocortex in mm^2	23.4 ± 0.35	20.7 ± 1.19	11.54	0.011
Area of S1 in mm^2	4.69 ± 0.10	4.41 ± 0.16	5.97	0.192
Area of PMBSF in mm^2	0.93 ± 0.016	0.86 ± 0.023	7.82	0.045

Table 4.1: Quantification of layer thickness and cortical area in *Syngap*$^{+/+}$, *Syngap*$^{+/-}$ and *Syngap*$^{-/-}$ mice.

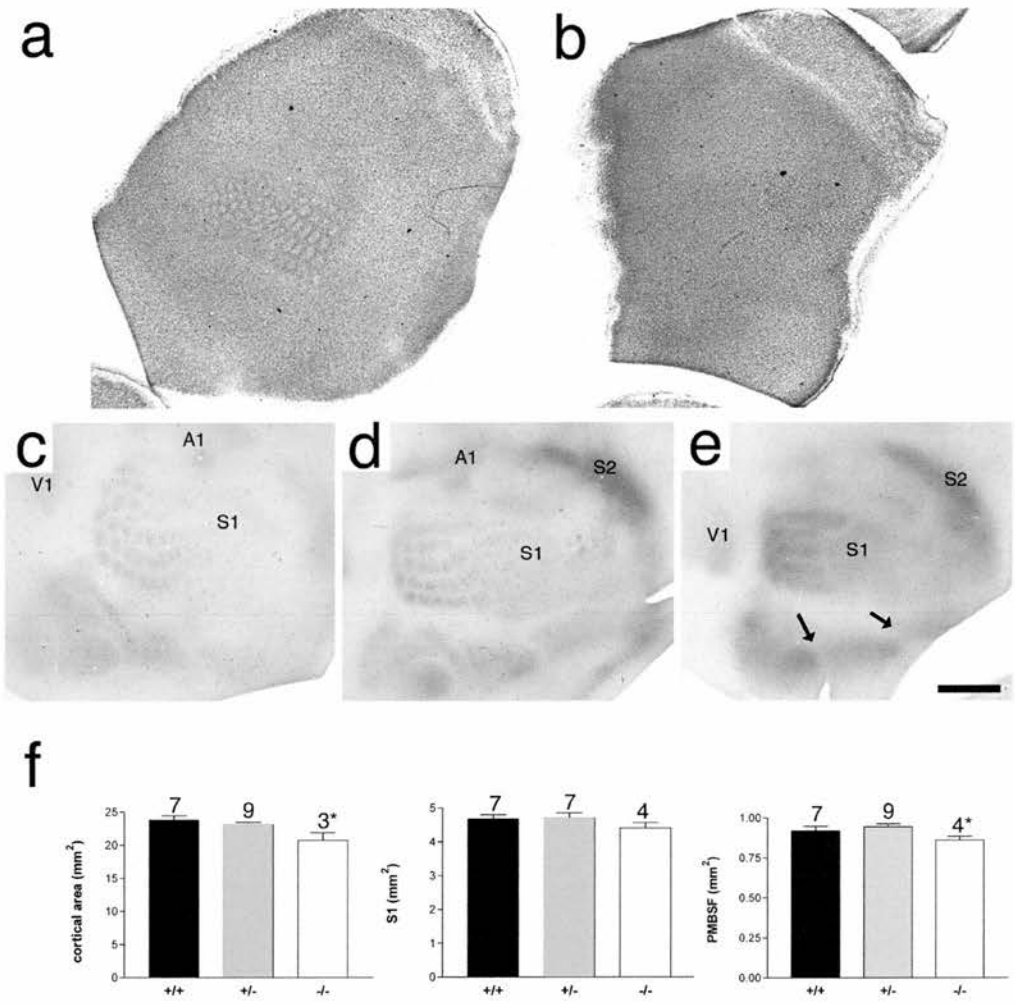

Figure 4.2: *Syngap*$^{-/-}$ mice lack cortical barrels. **a, b,** Nissl stained tangential sections through layer IV of P6.5 *Syngap*$^{+/+}$ (**a**) and *Syngap*$^{-/-}$ (**b**) mice show a complete lack of cellular segregation in *Syngap*$^{-/-}$ mice. **c, d, e** Immunostaining of 5HT in flattened tangential sections through layer IV of *Syngap*$^{+/+}$ (**c**), *Syngap*$^{+/-}$ (**d**), and *Syngap*$^{-/-}$ (**e**) mice to reveal the distribution of TCAs. In all three genotypes clear segregation between cortical areas: primary visual (V1), somatosensory (S1), auditory (A1), and secondary sensory (S2) can be seen, indicating that there is no general defect in TCA pathfinding in *Syngap* mutants. Subregions of S1 are also clearly defined (arrows). However within the AS region no TCA segregation is visible and within PMBSF, TCAs can be seen segregating into rows instead of patches seen in WT animals. **f,** Quantification of neocortex, S1 and PMBSF area in *Syngap*$^{+/+}$, *Syngap*$^{+/-}$, and *Syngap*$^{-/-}$ mice (graphical representation of the data shown in table 4.1) Scale bar: (in **e**) **a, b,** 1mm; **c - e,** 800μm.

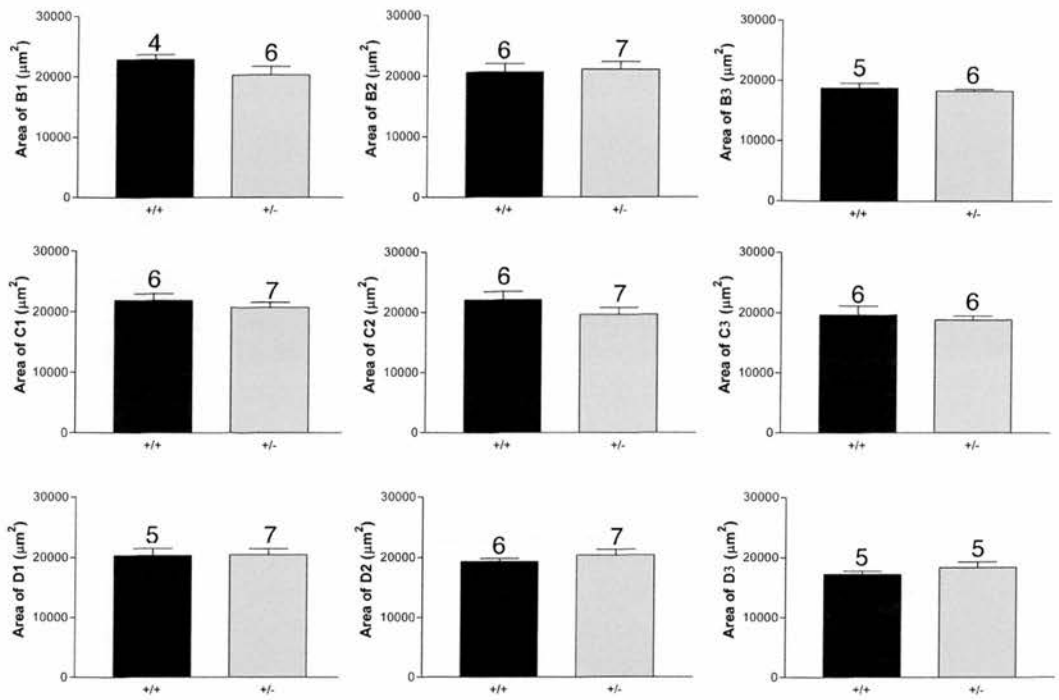

Barrel	WT (mean area, μm²)	HET (Mean area, μm²)	P VALUE
B1	22900 ± 792 n=4	20230 ± 1393 n=6	0.1879
B2	20670 ± 1402 n=6	21160 ± 1259 n=7	0.7979
B3	18800 ± 805 n=5	18290 ± 326 n=6	0.5437
C1	21854 ± 1133 n=6	20701 ± 856 n=7	0.427
C2	22110 ± 1378 n=6	19670 ± 1122 n=7	0.1923
C3	19650 ± 1525 n=6	18810 ± 673 n=6	0.6272
D1	20300 ± 1202 n=5	20470 ± 1000 n=7	0.9151
D2	19280 ± 529 n=6	20380 ± 963 n=7	0.3610
D3	17230 ± 533 n=5	18360 ± 944 n=5	0.3306

Figure 4.3: Quantification of TCA patch size in PMBSF of *Syngap*$^{+/+}$ and *Syngap*$^{+/-}$ animals. No significant difference in TCA segregation is found between *Syngap*$^{+/+}$ and *Syngap*$^{+/-}$ mice.

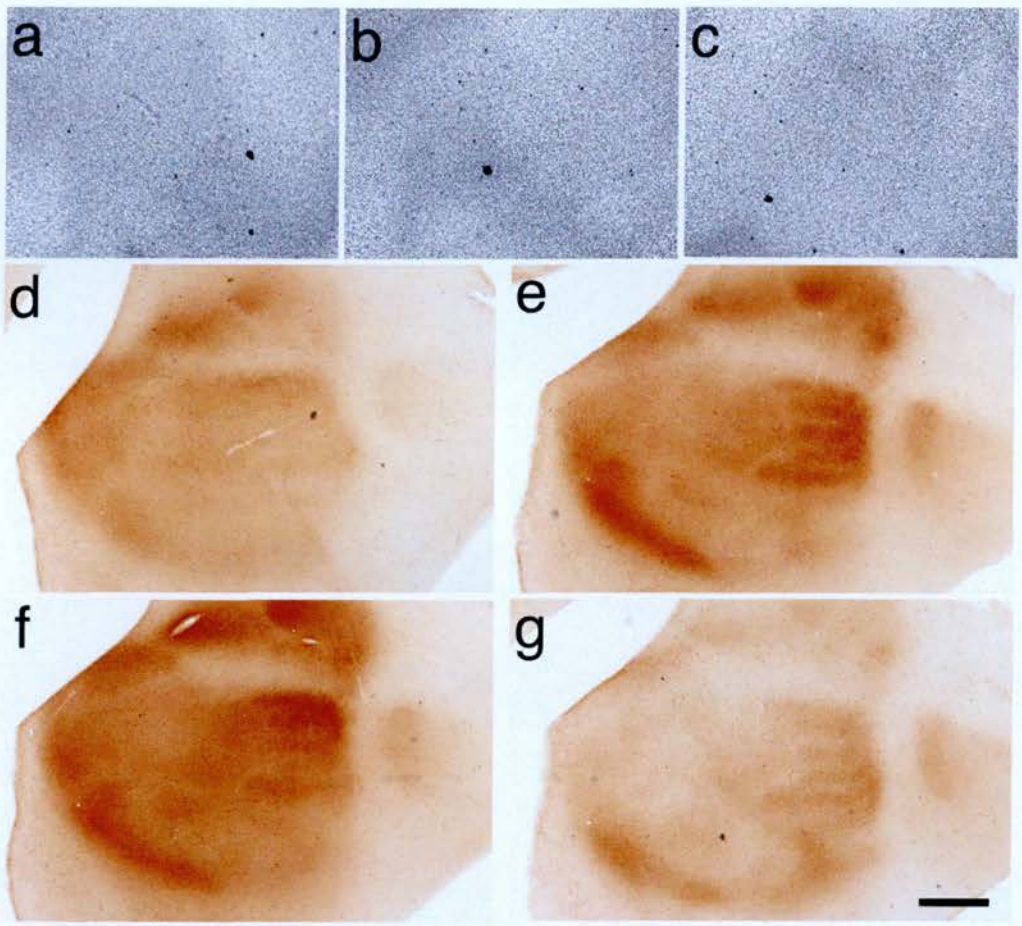

Figure 4.4: *Syngap*$^{-/-}$ mice completely lack cellular segregation in layer 4 and their TCAs segregate into rows, not individual patches. **a - c,** Three adjacent nissl stained tangential sections through layer IV of a P6 *Syngap*$^{-/-}$ animal shows a complete lack of cellular segregation into barrels in these animals. **d - g,** Four adjacent sections through layer IV immunostained for SERT to reveal distribution of the TCAs. Section **e** shows the mostly clear segregation of TCAs and reveals that TCAs segregate into rows in *Syngap*$^{-/-}$ mice. Scale bar: (in **g**) **a - c,** 300μm; **d - g,** 800 μm.

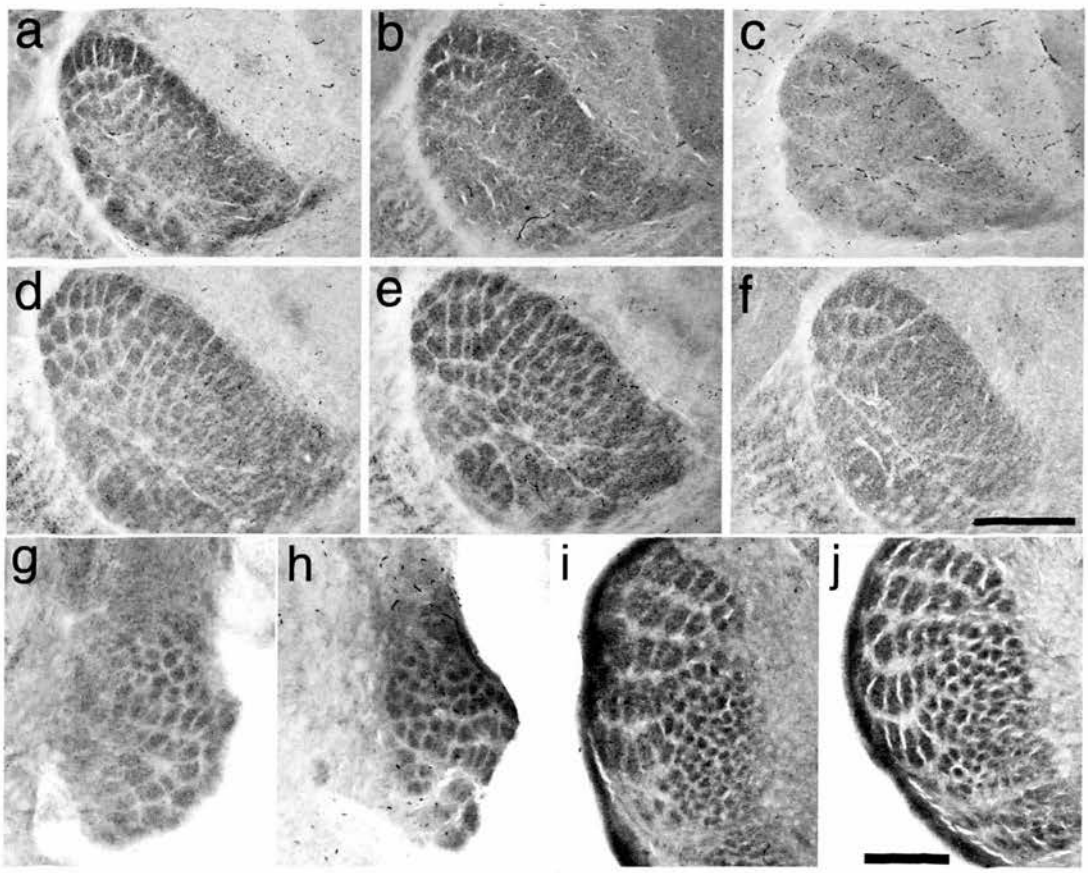

Figure 4.5: Reduced barreloid segregation in *Syngap*$^{-/-}$ mice. **a - f,** Cytochrome oxidase staining in VpM of thalamus to show barreloids in *Syngap*$^{+/+}$ (**a, d**), *Syngap*$^{+/-}$ (**b, e**), and *Syngap*$^{-/-}$ (**c, f**) mice at P4 (**a - c**) and P7 (**d - f**). Barreloids can be seen in all genotypes at both ages (P4 and P7); however reduced segregation in observed in *Syngap*$^{-/-}$ mice (n = 3) at both ages relative to *Syngap*$^{+/+}$ (n = 4) and *Syngap*$^{+/-}$ (n = 5) mice, especially in the region that represents the anterior snout whiskers. **g - j,** Cytochrome oxidase staining on coronal sections through the brainstem trigeminal complex in P3/P4 *Syngap*$^{+/+}$ (**g, i**; n = 5) and *Syngap*$^{-/-}$ (**h, j**; n=4) mice show normal barrelette formation in PrV (**g, h**) and SpI (**i, j**). Scale bars: (in **f**) **a - f,** 350μm; (in **j**) **g, h,** 225 μm; (in **j**) **I, j,** 250μm.

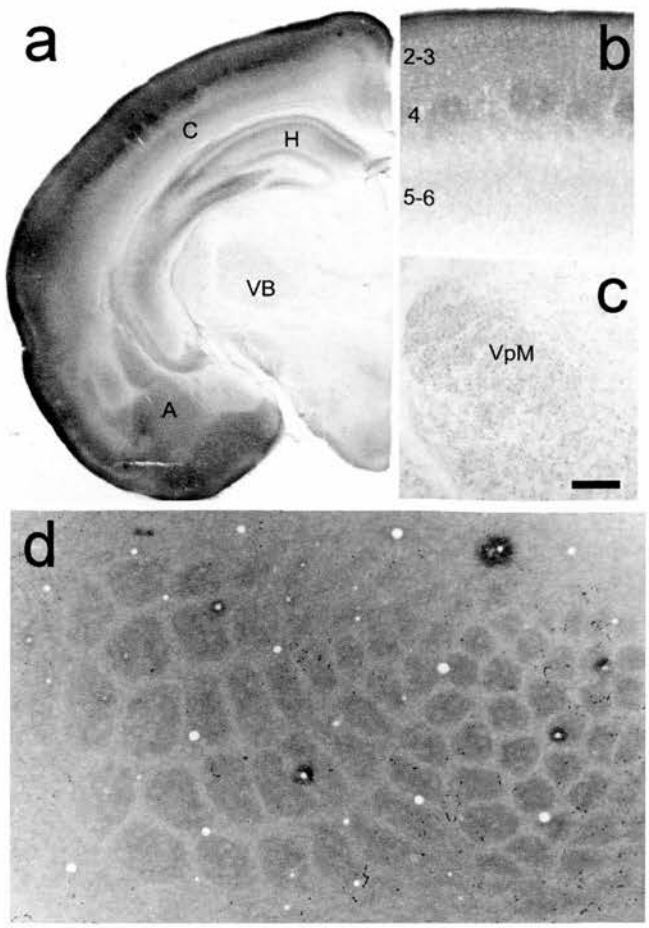

Figure 4.6: SynGAP protein expression in developing S1 cortex and thalamus. **a - d,** Immunolocalisation of SynGAP protein using a pan-SynGAP antibody that recognises all SynGAP isoforms. Low power images (**a**) show high levels of SYnGAP in the cortex (C), hippocampus (H), and amygdaloid complex (A) with lower levels in the VB of the thalamus. S1 cortex (**f**) shows that SynGAP expression is highest in layer IV, and the supragranular layers and barrel patches can be seen. In thalamus (**c**), SynGAP is expressed thoughout VB including VpM. **d,** SynGAP immunohistochemistry on tangential sections through layer IV shows that SynGAP is immunolocalised to barrels because a whisker related pattern is clearly evident (**d**). Scale bar: (in **c**) **a,** 775μm; **b,** 150μm; **c,** 275μm; **d,** 95μm.

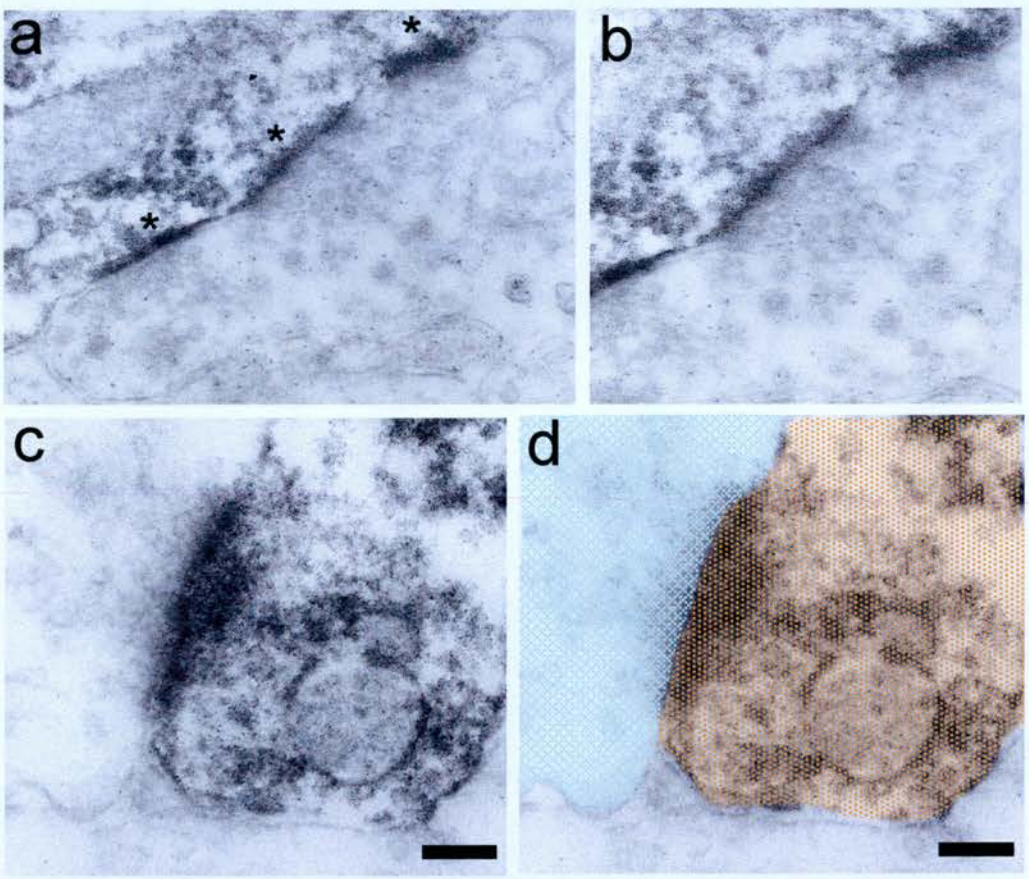

Figure 4.7: SynGAP is postsynaptic in developing S1 cortex. **a - d,** Electron micrographs of layer IV of P14 barrel cortex reveal dark immunoreactive product within postsynaptic densities (asterisks) opposite presynaptic terminals containing synaptic vesicles, and dendrites (**a - d**). In **a,** three PSDs are clearly visible on the shaft of a dendrite. **b,** a higher magnification image of the middle synapse that is seen in **a** - it clearly shows a concentration of presynaptic vesicles opposite the SynGAP-positive PSD. **d,** duplicate of image **c,** labeling the presynaptic terminal in blue and the postsynaptic terminal in orange. Scale bar: (in **c, d**) **a,** 250nm; **b,** 175nm; **c**, **d,** 100nm.

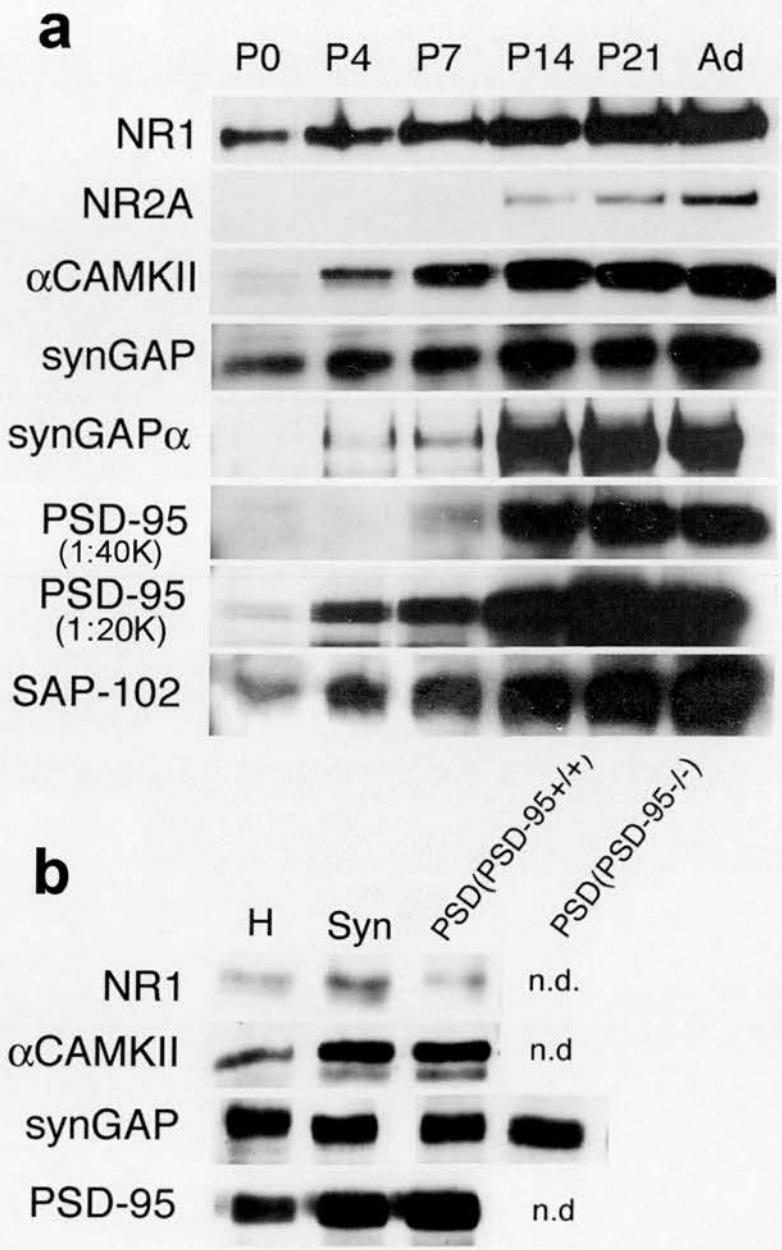

Figure 4.8: SynGAP still associates with the PSD in *Psd95*$^{-/-}$ mice. Western blot analysis of PSD components in homogenates of S1 cortex reveals a dramatic increase in PSD components during the first postnatal week (**a**). **b,** Western blot analysis of NR1, CaMKII, PSD95, and SynGAP in homogenates (H), synaptosomes (Syn), and PSDs isolated from S1 cortex of P7 WT mice as well as SynGAP expression in the PSD of P7 *Psd95*$^{-/-}$ mice. (n.d., not done).

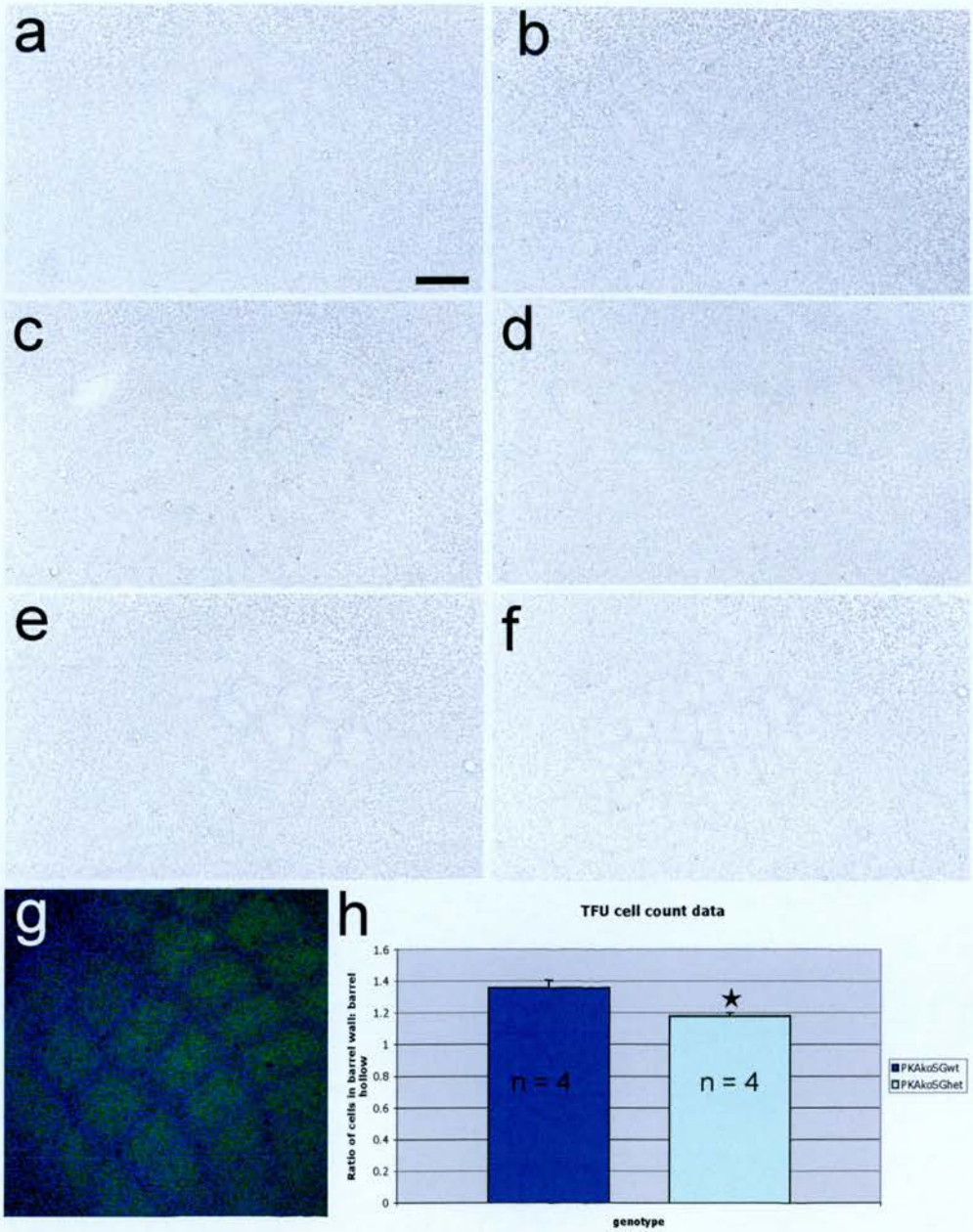

Figure 4.9: Cellular segregation is significantly reduced in *Prkar2β*$^{-/-}$*/Syngap*$^{+/-}$ mice relative to *Prkar2β*$^{-/-}$ mice. **a, b, and c, d,** Nissl stained adjacent tangential sections through layer IV of P7 *Prkar2β*$^{-/-}$*/Syngap*$^{+/-}$ reveal poorly segregated barrels in PMBSF and a complete lack of cellular segregation in more anterior regions of S1. **e - f,** Nissl stained adjacent tangential sections through layer IV of P7 *Prkar2β*$^{-/-}$. **g,** To quantify cellular segregation in layer 4 of *Prkar2β*$^{-/-}$*/Syngap*$^{+/+}$ and *Prkar2β*$^{-/-}$*/Syngap*$^{+/-}$, tangential sections through layer 4 were stained with Topro to label cell nuclei and SERT antibody to label TCA patches. **h,** The ratio of cells in the wall of barrel C2 versus the barrel C2 hollow is significantly reduced in *Prkar2β*$^{-/-}$*/Syngap+/-* mice relative to *Prkar2β*$^{-/-}$ mice (1.176 ± 0.04 versus 1.356 ± 0.1 respectively; p=0.0174). Scale bar: (in **a**) **a -f,** 200μm

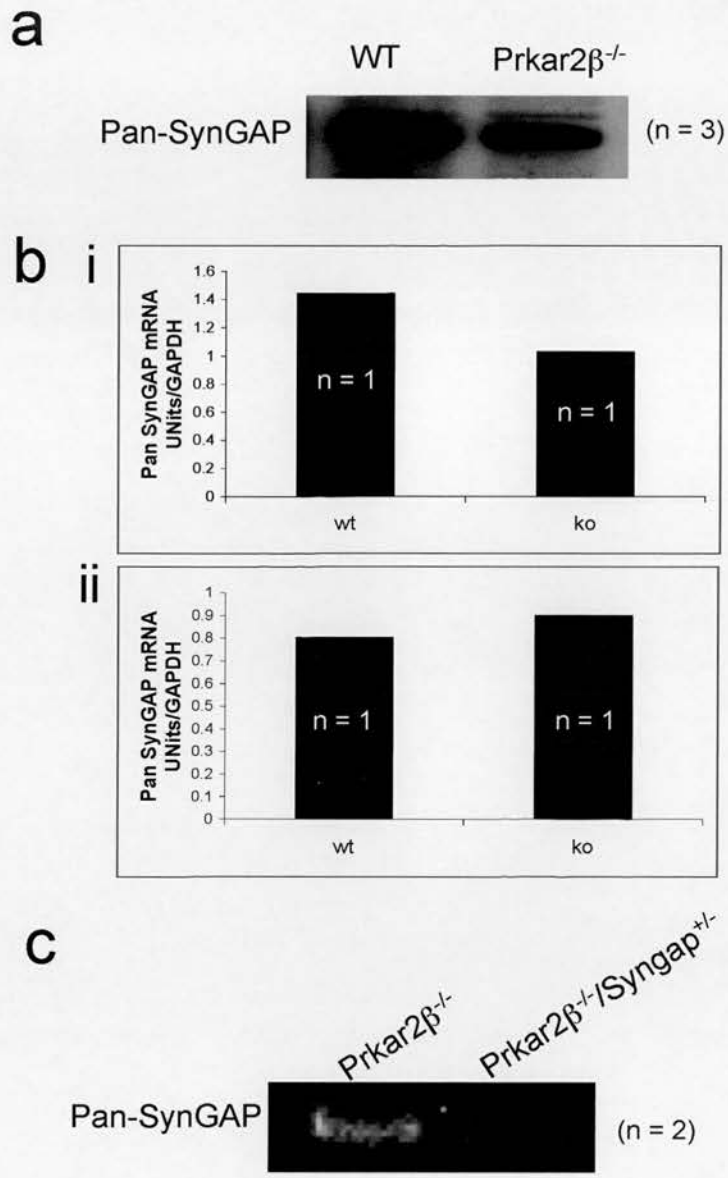

Figure 4.10: SynGAP expression is reduced in *Prkar2β*$^{-/-}$ mice. **a,** Western blot analysis of SynGAP protein levels in P7 WT and *Prkar2β*$^{-/-}$ mice reveals an approximately 40% reduction of SynGAP in *Prkar2β*$^{-/-}$ animals (n = 3). **b,** RTPCR experiment 1 (i; n=1) shows a similar decrease in Pan-SynGAP mRNA levels in *Prkar2β*$^{-/-}$ barrel cortex compared to wildtype, however experiment 2 (ii; n=1) does not show this decrease. **c,** Western blot showing clear reduction of SynGAP in *Prkar2β*$^{-/-}$*/Syngap*$^{+/-}$ mice compared to *Prkar2β*$^{-/-}$ mice (n = 2).

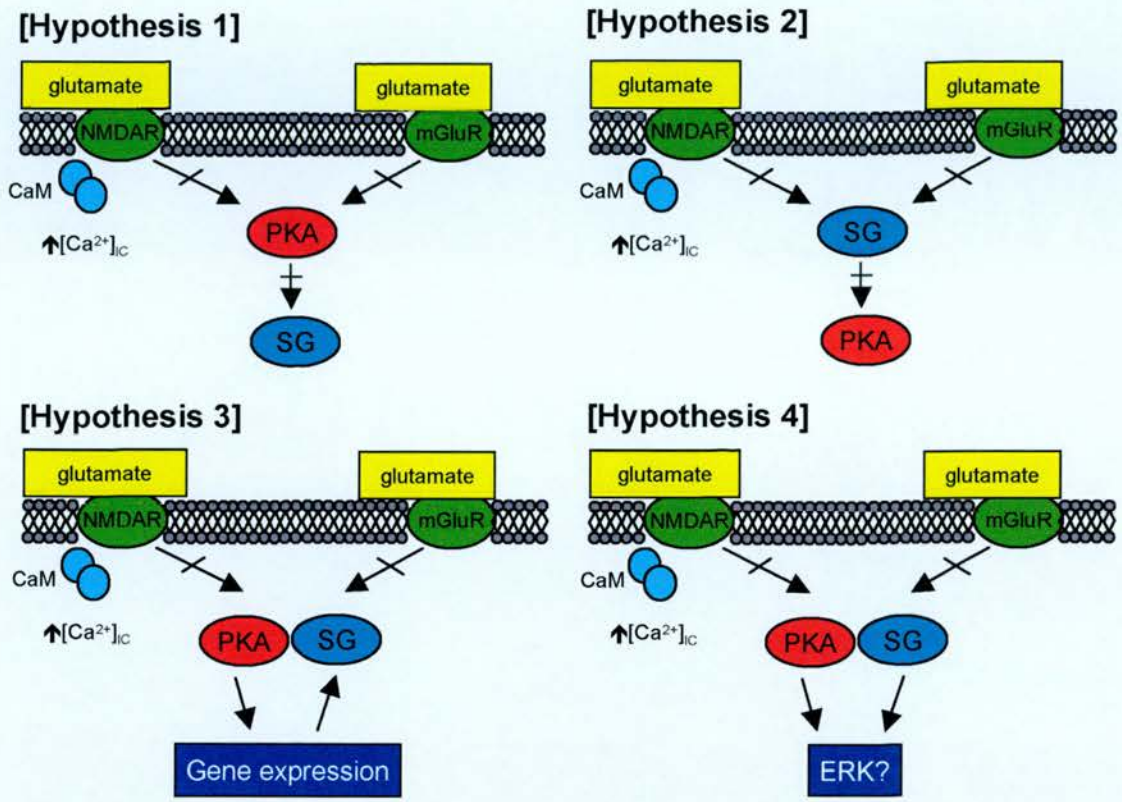

Figure 4.11: Four hypotheses of PKAR2β and SynGAP signaling in barrel development: (1) PKAR2β lies upstream of SynGAP within the PSD, and regulates SynGAP activity; (2) SynGAP lies upstream of PKAR2β within the PSD and regulates PKAR2β activity; (3) PKAR2β regulates gene expression that affects SynGAP or vice versa; and (4) PKAR2β and SynGAP signal via two distinct pathways but converge on a common target, for example on ERK, to affect barrel formation.

CHAPTER 5:

Investigation into the signaling pathways that PKAR2β and SynGAP mediate during barrel formation: experimental approaches & limitations

5.1 Introduction

A central approach taken by our laboratory to identify the intracellular pathways through which glutamate receptors regulate barrel development has been to screen the barrel cortex of previously generated transgenic mice with deletions in components of the PSD/NMDAR complex (Husi et al., 2001; Walikonis et al., 1998). The laboratory has now screened over 30 knockout mice of NMDAR associated proteins for defects in barrel development and several postsynaptic signaling molecules, PLCβ1, PKAR2β and SynGAP have been shown to play a role in barrel formation (Hannan et al., 2001; Watson et al., 2006; Barnett et al., 2006). There are limitations however of a solely transgenic anatomical approach to discover the intracellular pathways of barrel formation. The manufacture of transgenic mice is a lengthy process and although analysing anatomical changes in transgenic knockout mice can highlight particular molecules and candidate pathways to be involved in cortical differentiation, it cannot establish direct signaling effects.

In this thesis I have shown that PKAR2β (Chapter 3) and SynGAP (Chapter 4) regulate postsynaptic glutamatergic signaling during barrel formation (Watson et al., 2006; Barnett et al., 2006). Both of these molecules localise to the postsynaptic density (PSD) in S1 cortex during barrel development and transgenic mice that lack either PKAR2β or SynGAP fail to develop normal barrels compared to wild type animals (Chapters 3 and 4 respectively; Watson et al., 2006; Barnett et al., 2006). It has not yet been elucidated however, which receptor(s) activate PKAR2β and SynGAP, nor what effector molecules subsequently mediate barrel formation.

It is also unclear if PKAR2β and SynGAP signal via different or identical pathways, or converge on a common target. One approach for determining whether PKAR2β and SynGAP signal through the same or distinct barrel-signaling pathways was addressed in Chapter 4 and consisted of quantitative assessment of barrel segregation in Prkar2β/Syngap double transgenic mice relative to single transgenic knockout mice of these genes (see Chapter 4 for details). Unfortunately due to problems in animal generation a conclusive result relating to this has not yet been established.

In this chapter three alternative approaches for elucidating the glutamatergic signaling pathways upstream and downstream of PKAR2β and SynGAP in barrel formation are tested and discussed. They include:

[1] a pharmacological approach

[2] a phospho-proteomic approach, and

[3] a genomic approach

5.2 Methods

5.2.1 S1 cortical slice stimulation experiments

P7 WT and *Prkar2β*$^{-/-}$ mice were sacrificed by decapitation and their brains immediately dissected and placed into ice-cold oxygenated ACSF solution (119mM NaCl, 2.5mM KCl, 1.3mM $MgSO_4$, 1.0mM NaH_2PO_4, 26.2mM $NaHCO_3$, 11mM Glucose, 2.5mM $CaCl_2$). Both brain hemispheres were then sliced coronally (300μm) on a vibrotome in ice-cold oxygenated ACSF solution. The resultant coronal slices were examined under a light microscope, enabling clear discernment of the hippocampus. Four slices from each hemisphere containing the barrel cortex (identified by the hippocampus; where it extends medial/lateral, but does not curve ventrally) (see figure 2.1 in chapter 2) were chosen and the region of barrel cortex dissected from each of these slices. Slices from both hemispheres were then placed in 2 wells of an interface chamber that contained circulating (2-3ml/minute) oxygenated ACSF at room temperature for 2hours. After 2 hours, slices in one well were stimulated with oxygenated ACSF containing 100μM NMDA (gift from Seth Grants laboratory) for 5minutes. Both control and stimulated slices were then immediately snap-frozen onto dry ice and stored at –70°C. Levels of phospho-ERK expression in NMDA receptor stimulated slices compared to control slices was assessed by Western blot (see Chapter 2) using an anti-phospho-p44/42 Map Kinase antibody (Thr202/Tyr204) (1:2000; Cell Signaling Technology) and anti-PSD95 (1:10,000; Upstate) antibody as a loading control.

5.2.2 Pharmacological stimulation of primary cell culture

Wildtype (C57/BL6), *Syngap*$^{-/-}$, *Syngap*$^{+/-}$ and *Syngap*$^{+/+}$(MF1) primary cell cultures were set up from E18.5 old embryos and maintained for 10 or 14 days in vitro (DIV) as described in Chapter 2. To assess different stimulation paradigms, 14DIV wildtype cultures were treated with 6 different drug treatments at room temperature for 5minutes: [1] Mg^{2+} free growth media (GM), [2] GM (with Mg^{2+}), [3] Mg^{2+} free GM + 50μM Bicuculline, [4] GM with Mg^{2+} + 50μM Bicuculline, [5] Mg^{2+} free GM + 100μM NMDA + 20μM glycine, and [6] GM with Mg^{2+} + 100μM (or 20μM) NMDA + 20μM glycine. To examine the time-course for optimal Bicuculline stimulation, 14DIV wildtype cultures were treated with 50μM Bicuculline for 0, 4, 6 or 10 minutes. For all remaining primary culture experiments, one third of wells that contained 10 or 14DIV cortical cultures from one genotype were stimulated with 50μM Bicuculline (2ml; diluted in growth media) and another third of wells treated with 50μM Bicuculline + 50μM APV (2ml; diluted in growth media) for 6 minutes at room temperature. (NB: Growth media was changed in control wells). At 4, 6 or 10 minutes, all media (+/- drugs) was expirated from the cortical cultures and immediately replaced by ice-cold lysis buffer (containing 50mM HEPES pH7.5, 1% Triton X-100, 50mM NaCl, Protease Inhibitors (Roche) and Phosphatase Inhibitor cocktails I and II (Sigma P2850 and P5276)). Cell scrapers were then used in each well to extract the pharmacologically manipulated neurons. Lysed cells were transferred to eppendorf tubes, snap frozen on dry ice and stored at –70°C. Levels of phospho-ERK expression, in control, Bicuculline treated and Bicuculline + APV treated cultures were examined by Western blot using anti-phospho-p44/42 Map Kinase (Thr202/Tyr204) (1:2000; Cell Signaling Technology) and anti-p44/42 Map Kinase (1:2000; Cell Signaling) antibodies (see Chapter 2).

5.2.3 Large-scale biochemical screening of protein phosphorylation

P7 barrel cortices from 12 wildtype and 12 *Prkar2β*$^{-/-}$ animals were dissected in 320mM sucrose solution (pH 7.4, containing 1mM EDTA and 5mM Tris) and synaptosomes prepared as described in Chapter 2; two wildtype and two *Prkar2β*$^{-/-}$ synaptosome preparations were made, by pooling barrel cortices together from 6

animals of similar genotype. In collaboration with Kinexus™ Bioinformatics Corporation, two phospho-proteomic screens (KPSS1.3 and KPSS4.0) were performed on these wildtype and *Prkar2β*$^{-/-}$ synaptosome preparations containing 200μg of protein. Samples were resolved on single-lane SDS-PAGE gels followed by electrophoretic transfer to nitrocellulose membranes. The membranes were stained with Ponceau to examine whether protein was equally loaded and then probed with multiple phosphorylation-specific antibodies that had previously been validated by Kinexus™ for their potency and specificity in mouse. Antibodies bound to their target antigens on the membrane were detected by enhanced chemiluminescence (ECL) and resultant bands quantified using a 16-bit camera in combination with quantification software. Images of each sample were captured and the light signals from each image converted into digital data. An intensity profile for each band was then generated, by summing each pixel's intensity for a band. Bands were quantified by integrating the area underneath this profile curve to obtain the "trace quantity" of the band (units were intensity x millimetres). Important to note is that each sample's immunoblot was scanned at its maximum scan, to ensure that the signal for the strongest immunoreactive protein on the immunoblot was just below saturation. This ensured detection of minor immunoreactive proteins and accurate quantitation over a 2000-fold range of linearity. The resulting trace quantity for each band scanned at the maximum scan time was therefore termed the raw data because band intensity partially reflected the scan time. Due to the relationship between scan time and band intensity being linear over the quantifiable range of the signal intensity, the raw data from the scans was normalised to 60 seconds (counts per minute; CPM) for uniformity and comparison purposes.

5.2.4 Western Blotting

Immunoblot analysis was performed on P7 barrel cortex homogenate as described in Chapter 2. The following primary phospho-specific antibodies were used to incubate the blots overnight: Protein Kinase B alpha (Akt) (S473) (1:1000; Biosource), PKCalpha (S657) (1:1000; Upstate Biotechnology), Protein kinase C epsilon (S719) (1:1000; Upstate Biotechnology), Oncogene SRC (Y529) (1:1000; Biosource), Oncogene SRC (Y418) (1:1000; Biosource), Glycogen synthase kinase 3β (GSK3β)

(S9) (1:1000; Cell Signaling Technologies), PKCzeta (T410) / lambda (T403) (1:1000; Cell Signaling Technologies), Raf (S259) (1:1000; Cell Signaling Technologies), ERK1(T202/Y204)/ERK2 (T185/Y187) (1:1000; Biosource) and Type 1 protein phosphatase alpha (T320) (PP1a) (1:1000; Cell Signaling Technologies).

5.2.5 Gene Array

P7 barrel cortices from 6 wildtype and 6 *Prkar2β*$^{-/-}$ animals were dissected in ice-cold phosphate buffered saline (pH7.4 PBS, NaCl 137mM, KCL 2.7mM, NaH_2PO_4 1.4mM, Na_2HPO_4 4.3mM) and immediately frozen on dry ice and stored at –70°C. In collaboration with Professor Stanley McKnight, an affymetrix gene array experiment was then performed on the samples. First mRNA was isolated (as described in Chapter 2) and then mRNA from both individual and pooled biological samples was reverse transcribed and simultaneously labelled with fluorescent dyes, Cy3 and Cy5 for hybridization. Gene arrays were performed on the following combinations of samples and dyes (note: *Prkar2β*$^{-/-}$ animals had the following ID numbers: 710, 711, 760, 761, 784, 790):

1) Barrel cortex KO 710 Cy3 – WT (6 pooled dissections) Cy5
2) Barrel cortex KO 711 Cy5 – WT (6 pooled dissections) Cy3
3) Barrel cortex KO 711 + 761 Cy3 – WT (6 pooled dissections) Cy5
4) Barrel cortex KO 760 Cy3 – WT (6 pooled dissections) Cy5
5) Barrel cortex KO 760 Cy5 – WT (6 pooled dissections) Cy3
6) Barrel cortex KO 761 Cy5 – WT (6 pooled dissections) Cy3
7) Barrel cortex KO 784 Cy3 – WT (6 pooled dissections) Cy5
8) Barrel cortex KO 790 Cy3 – WT (6 pooled dissections) Cy5
9) Barrel cortex KO 790 Cy5 – WT (6 pooled dissections) Cy3

Both Cy3 and Cy5 dyes were used to label each WT and *Prkar2*β-/- sample to control for the efficacy of each dye binding to the chip. Following hybridization, laser light was used to excite these fluorescent dyes at wavelengths of 635nm and 532nm. Hybridization intensity (fluorescent emission) was scanned by a GenePix4000A machine and analysed by GenePix Pro 3.0.6.90 software. 19,550 genes in total were tested on the affymetrix gene array (see Appendix 13).

5.2.6 Real Time RT-PCR

Quantitative SYBRgreen RT-PCR was performed on an Opticon Monitor thermocycler machine to validate results obtained from the affymetrix gene array. P7 barrel cortices from 6 wildtype and 6 *Prkar2β*$^{-/-}$ animals were dissected in ice-cold phosphate buffered saline (pH7.4 PBS, NaCl 137mM, KCl 2.7mM, NaH_2PO_4 1.4mM, Na_2HPO_4 4.3mM) and immediately frozen on dry ice and stored at –70°C. mRNA was then isolated from these barrel cortices and cDNA synthesised as described in Chapter 2. In addition primers to the genes of interest were designed according to the guidelines explained in Chapter 2 and are listed below.

Gene	Forward Primer	Reverse Primer
OSBP1	ggtgacaggtgaagtgacag	cttctgcttcatggcctctc
ACF-7	acaaggtccatatgctgttg	gccactgctgtgttcacatc
MARK-1	ctgccgtctcatacaccaag	tgctaccgccagaatatacg
DUSP-21 (NO INTRON)*	accgttcgcatgatctactc	ccaaccataggtccaaggtc
RhoGAP-19	cagctggcaagatgtcagag	ttcttcttcgcggagtctgg
DOK-2 (NO INTRON)*	agagcgcagtgactggatac	ctgtggtggagctgctatac
BRD8	gcggagaagatggatattgc	tgccacatccagcacttcag
PDZK1	agaccgaactctcagcacag	attcctcggagaggcagttc
Serpin b6C	tcctcgtgaatgctgtctac	cagctcattgccaacatagg
Transthyretin	tgctgtagacgtggctgtaa	gccaagtgtcttccagtacg
Ndufb3	tgctggacatggacatgaac	caaagccgcccatgtatctc
Mdh1b	caggcgatctgattcaggag	cttccctaagtgcagacacc
Caspr (Cntnap1)	ggacgatgctaccagtcttg	ctcggatgtcacaatacacc
Parvalbumin	ccattctgaagggcttctcc	agcagtcagcgccacttagc
NR2C	gcgtcttctacatgctgttg	cgttgaagcagctgtagatg
MOG	cctgcagcacagactgagag	gtcttcggtgcagccagttg
MOBP	cctgccagaagactagattg	ccactcctgcatcatacttg
Nrap	cgagcgcttatacaggttgg	atccagcctgaagtcatagc
sprr2f (NO INTRON)*	gccttgtcctgagccatgtc	tcctgaagactgctgaagac
Efemp1	tggagagttctacctacgac	ctactgactgtcagcatctc
Nox4	tgtgaacatccagctgtacc	ctccaactgttttccctctg
Calpain 8	cgaccggtggagttcaagac	tgctgcacctggttgttgag
Titin Cap (NO INTRON)*	gaaggatgtgcaacgctctg	gaagtgcacggtggacattc
Zfh4	ccttcctccagtcattcttc	ctgcagcaaagatttggtgg
Pan Cdh8	gcatcattttgctgctcgtc	tcctccttcgtcgtcgtagc
Nkx1-2	ccttctctgtcttggacatc	agcttcctcctcctcctctg
Cea9	tcttaacctgctggctcttg	ttccgaggctcatgtctgtc

Table 5.1 : RTPCR primers designed for validating the affymetrix gene array The primers are all intron spanning except where stated * and are all written 5' to 3'.

1µl of cDNA was added to 24µl of mastermix containing: 0.5µl of each appropriate primer (12.5µM), 10.5µl double distilled water and 12.5µl of 2 x SYBRgreen RT-PCR mix (Qiagen). Two serial dilution series of P7 WT or KO cDNA and a blank control that contained no reverse transcriptase cDNA sythesis product was performed with each experiment (see Chapter 2). The Opticon Monitor RTPCR machine was programmed with an initial incubation at 95°C for 15 minutes and then 35 cycles of 94.0°C for 15 seconds, 55.0°C for 30seconds and 72.0°C for 30 seconds.

5.3 Results

5.3.1 Pharmacology: Regulation of ERK in R2β and SynGAP mutant mice upon glutamate receptor stimulation

To elucidate a role for ERK (hypothesised to be a common target of barrel signaling pathways - see Chapter 1 for more details) downstream of PKAR2β and SynGAP in barrel formation, two distinct pharmacological approaches were carried out: [1] a "slice stimulation" approach and [2] a "dissociated cortical neuron culture stimulation" approach.

To first investigate whether NMDAR activation regulates ERK phosphorylation via a PKAR2β-dependent mechanism in barrel development, slice stimulation experiments were performed using *Prkar2β*$^{-/-}$ and *Prkar2β*$^{+/-}$ (heterozygote) barrel cortex slices. Western blot densitometry analysis of pERK1 and pERK2 levels in P7 stimulated (100µM; NMDA) versus un-stimulated *Prkar2β*$^{-/-}$ and heterozygote S1 cortical slices (Fig. 5.1 A) show that upon NMDA activation, phosphorylated levels of ERK (represented in fig. 5.1 A as percentages of the un-stimulated pERK levels present) appear to be reduced in heterozygote animals but not *Prkar2β*$^{-/-}$ animals. Student t-tests however do not reveal a significant reduction in ERK1 and ERK2 phosphorylated levels in stimulated heterozygote slices (ERK1 HET 51.71±14.70% p=0.0973; ERK1 KO 78.08±5.81% p=0.237; ERK2 HET 45.19±10.14% p=0.0823; ERK2 KO 82.54±7.72% p=0.289), perhaps as a result of too few animals having been examined or one copy of the *Prkar2β* gene still remaining present in

heterozygote animals. Wildtype animals were not analysed due to an outbreak of MHV in the colony resulting in culling of the appropriate animals. No further slice stimulation experiments were carried out however because of methodological problems. The main limitation incurred was that the interface chamber only contained 2 wells so only 1 animal could be tested at a time and with just two treatments (un-stimulated and stimulated with NMDA). Therefore individual animals could never receive exactly the same conditions, which was not ideal and the accumulation of results was very slow. In addition, flooding of the interface chamber despite careful setting of a constant flow rate of ACSF happened frequently and caused many experiments to be abandoned. Therefore despite initially attractive advantages of the slice stimulation system: (1) it keeps cortical tissue intact and (2) the age of the tissue correlates directly to the age of the mouse sacrificed, it was decided more appropriate to move to a tissue culture system (see below) in order to investigate ERK further.

Interestingly though with respect to the slice stimulation data, the trend of reduced pERK levels in PKAR2β heterozygote slices upon NMDAR stimulation agrees with immunohistochemical data of pERK expression in layer IV of S1 in wildtype animals compared to *Prkar2β*$^{-/-}$ mice (Fig. 5.1 B, C respectively). Immunostaining for pERK (using an antibody that recognises both pERK1 and pERK2) in coronal sections through layer IV of S1 shows that pERK staining is punctate (shown by arrows) and labels dendrites, but qualitatively fewer immunoreactive puncta can be seen in a wildtype animal compared to a *Prkar2β*$^{-/-}$ animal (Fig. 5.1 B, C respectively). In summary the slice stimulation data suggests that upon NMDA activation a PKARβ pathway is activated and inhibits ERK phosphorylation.

To investigate ERK regulation downstream of PKAR2β and SynGAP in primary cortical cultures, a tissue culture system was set up that maintained healthy looking neurons until 14 days in vitro (DIV). Preliminary experiments were performed to generate a successful stimulation paradigm in culture. 14DIV wildtype cultures were treated with 6 different drug treatments at room temperature for 5minutes: [1] Mg^{2+} free growth media (GM), [2] GM (with Mg $^{2+}$), [3] Mg^{2+} free GM + 50μM Bicuculline, [4] GM with Mg^{2+} + 50μM Bicuculline, [5] Mg^{2+} free GM + 100μM

NMDA + 20μM glycine, and [6] GM with Mg^{2+} + 100μM NMDA + 20μM glycine. Western blot analysis of these six pharmacological conditions (Fig. 5.2 A), using an antibody specific to phosphorylated ERK, shows that application of Bicuculline in the presence of Mg^{2+} is the most effective treatment for inducing neuronal stimulation in 14 DIV cultures. Densitometry of pERK levels relative to PSD95, a protein that does not alter in expression level between *Prkar2β*$^{-/-}$ and *Prkar2β*$^{+/+}$ mice (Fig. 5.2 B), reveals that pERK1 and pERK2 levels are increased upon bicuculline treatment in growth media with Mg^{2+} (condition 4) but remain unchanged after any of the remaining five treatments (conditions 1,2,3,5 and 6) (Fig. 5.2 C). Bicuculline is a $GABA_A$ antagonist and specifically activates synaptic glutamate receptors (synaptic NMDARs and mGluRs). NMDA in contrast activates both synaptic and extrasynaptic NMDA receptors. Hardingham et al. (2002) showed that synaptic and extrasynaptic NMDA receptors have directly opposing effects on CREB function and neuronal fate in the hippocampus. Activation of both synaptic and extrasynaptic receptors in dissociated cortical cell cultures might also result in effects being opposed and cancelled out and explain for the lack of apparent stimulation upon NMDA application. Next, ERK regulation by glutamate receptor stimulation (bicuculline + Mg^{2+}) was characterised over time in order to optimise the stimulation protocol. 14DIV cultures were treated with Bicuculline for 0, 4, 6 and 10 minutes and western blot densitometry analysis of the pharmacologically manipulated neurons reveals that pERK levels peak at 6minutes (Fig. 5.3 A) and are suboptimal at 4 and 10 minutes. Finally, to examine whether the ERK regulation observed in wildtype neurons upon Bicuculline application results from synaptic NMDA receptor activation, Bicuculline + APV, an NMDAR antagonist was applied to the cultures for 6 minutes (Fig. 5.3B). Upon application of Bicuculline (-APV), neuronal pERK levels are increased relative to control cultures, but application of Bicuculline + APV block this stimulation effect (Fig. 5.3 B).

To examine (a) if SynGAP regulates ERK upon glutamate receptor stimulation and (b) if SynGAP regulates ERK due to synaptic NMDAR stimulation, *Syngap*$^{-/-}$, *Syngap*$^{+/-}$ and *Syngap*$^{+/+}$ 10DIV cultures were treated with the following 3 conditions: growth media, bicuculline (50μM), and bicuculline (50μM) + APV (50μM). The first set of data obtained however, summarised in Figure 5.4, is highly

variable and does not reveal any statistically significant results probably as a consequence. Important to note is that in this experiment, application of bicuculline to the *Syngap*$^{+/+}$ cultures does not appear to induce neuronal stimulation as previously shown in C57/Bl6 wildtype experiments. Two possible reasons for this difference are: [1] Syngap mice are on a different background strain (MF1) and [2] movement of the culture dish during the experiment may have resulted in high basal activity in the control wells to almost saturating levels. The graphs of individual animals treated with the 3 conditions (Appendix 10) suggest that the latter reason is the most probable because some *Syngap*$^{+/+}$ and *Syngap*$^{+/-}$ animals show neuronal stimulation upon Bicuculline application and others do not, perhaps reflecting variability in the levels of activity present in the control wells of each dish. The experiment was therefore repeated and movement of the culture dishes kept to a minimum and carefully monitored. To determine the health of the cultures, neurons were examined beneath a microscope 24 hours rather that just prior to pharmacological treatment. During the 6-minute drug treatment culture dishes were left in the culture hood at room temperature rather than returning them to the 37°C incubator. The resultant data (Fig. 5.5 and Appendix 11) demonstrates that bicuculline treatment does induce neuronal stimulation in *Syngap*$^{+/-}$ (control) neurons. In *Syngap*$^{+/-}$ cultures pERK levels significantly increase upon bicuculline application and bicuculline + APV treatment blocks this effect demonstrating that the regulation of ERK is NMDAR dependent. *Syngap*$^{-/-}$ cultures in contrast show high levels of basal activity (pERK2 levels are 54% higher) compared to *Syngap*$^{+/-}$ neurons and Bicuculline treatment does not result in further stimulation presumably because the basal activity in the culture has already reached saturating levels. The high basal levels are not believed to result from culture dish movement because *Syngap*$^{-/-}$ and *Syngap*$^{+/-}$ animals were plated blind to genotype with two animals per culture dish. Lastly, application of Bicuculline + APV to *Syngap*$^{-/-}$ cultures is seen to reduce pERK levels relative to Bicuculline application alone indicating that regulation of ERK in *Syngap*$^{-/-}$ cortical neurons is at least in part due to synaptic NMDAR activation (Fig. 5.5).

5.3.2 Proteomics: Changes in protein phosphorylation in R2β KO mice

To investigate potential targets downstream of PKAR2β in barrel formation, two large-scale protein phosphorylation screens of P7 wildtype and *Prkar2β*$^{-/-}$ synaptosome preparations were undertaken in collaboration with Kinexus^{TM} Bioinformatics Corporation (Vancover, Canada). The screens, illustrated in figures 5.6 and 5.7, comprise large western blots probed with multiple phosphorylation-site specific antibodies in each lane. In figures 5.6 and 5.7, the vertical red lines label each lane and the horizontal red lines mark each of the bands present that correspond to particular phosphorylation sites. Densitometry was performed on each of these bands detected as described in section 5.2.3 (raw data in Appendix 12) and left unnormalised to overall blot intensity because Ponceau staining revealed that equal protein was loaded on comparative wildtype and *Prkar2β*$^{-/-}$ immunoblots (200μg per blot) (data not shown). In summary the analysis shows 17 protein phosphorylation sites that are upregulated, 9 that are downregulated and 6 that remain unchanged in *Prkar2β*$^{-/-}$ synaptosomes compared to P7 WT synaptosomes (Figure 5.8).

To validate the results of the two Kinexus^{TM} screens (each representing n = 1), ten protein phosphorylation-sites of interest were chosen for small scale western blotting and include sites that were found upregulated, downregulated and unchanged on the Kinexus phosphorylation screens:

Upregulated - PKB/Akt1 S473, PKCα S657, SRC Y529 and PKCε S719

Downregulated - GSK3β S9, PP1a T320, PKCz/λ T410/T403

Unchanged - ERK1 T202/Y204 and Erk2 T185/Y187, SRC Y418 and Raf1 S259.

Preliminary small scale western blotting results (Fig. 5.9) confirm that PKCε S719 and PKB/Akt1 S473 are upregulated, GSK3β S9 is downregulated and ERK1 T202/Y204 and Erk2 T185/Y187 are unchanged in P7 *Prkar2β*$^{-/-}$ barrel cortex homogenate compared to wildtype controls. These five results are in agreement with the phosphorylation site specific regulation found on the large-scale screens. PKCz/λ T410/T403 however (Fig. 5.9) shows no qualitative difference at this site between P7 *Prkar2β*$^{-/-}$ and wildtype barrel cortex homogenate despite

downregulation (-41.6%) in the large-scale screens. Western blots for PKCα S657, PP1a T320, Raf1 S259, SRC Y529 and SRC Y418 did not work.

5.3.3 Genomics: Altered transcription of candidate genes in R2β KO mice

Western blot data (Fig. 5.12 A) reveals altered protein expression levels of several different synaptic molecules in *Prkar2β*$^{-/-}$ mice compared to wildtype littermate controls. It is unclear however whether these changes in protein expression result from altered translation or transcription. To investigate genes that show altered transcriptional regulation in *Prkar2β*$^{-/-}$ mice, a common oligonucleotide affymetrix gene array was performed in collaboration with Professor Stanley McKnight on P7 wildtype and *Prkar2β*$^{-/-}$ mRNA isolated from S1 cortical dissections. The affymetrix chip used examined 19,550 genes in total (Appendix 13). In summary, 1530 of these genes returned "no data", because the features (spots) either contained saturated pixels, or no features or bad features were found, and the data of 836 genes failed to replicate (n=1) impeding statistical analysis. However 1452 genes were found to be significantly up- or down- regulated ($p<0.05$) in P7 *Prkar2β*$^{-/-}$ samples compared to wildtype controls and 41 of these genes displayed at least 2-fold regulation. The gene array data (Fig. 5.12 B and Appendix 13) shows that the most downregulated gene in the *Prkar2β*$^{-/-}$ is mouse cAMP-dependent protein kinase type two beta regulatory subunit (*Prkar2β*) and the most upregulated gene is neo, in agreement with the insertion of a neocassette into the *Prkar2β*$^{-/-}$ on generation of the animal (Brandon et al., 1998).

The data returned of the 2-fold downregulated genes (Fig. 5.12 and Fig 5.13 B) contained RIKEN cDNA clones. To identify the RIKEN cDNA clone genes, the Mouse Genome Informatics (MGI) database (Jackson laboratories) was used to search the gene name from the appropriate Genbank code (Fig. 5.13 A and B). Further bioinformatics research was also used to classify many of the up- and down-2-fold-regulated genes into common categories and address whether any of these genes significantly regulated could be candidates for playing a role in barrel

formation. Figure 5.14 lists some of the 2-fold regulated genes and illustrates how they include cytoskeletal, signaling, scaffolding, cell adhesion and myelin-related molecules.

To validate the gene array data, 30 genes were first prioritised for confirmation (Fig 5.14). The prioritised genes include 17 statistically significant 2-fold-regulated genes, 7 genes of interest that lie on the borderline of 2-fold significance (*Acf7, Dusp21, NR2C, Pdzk1, Brd8, MOBP and MOG*), 1 gene of interest that is less than 2-fold regulated but is statistically significantly regulated (*Cadherin 8*) and 5 control non-regulated genes (other PKA subunits). To confirm the transcriptional regulation of these 30 genes, real time RT-PCR was carried out on 6 P7 wildtype and 6 P7 *Prkar2β*$^{-/-}$ mRNA samples isolated from S1 cortical dissections using primers specific to each of these genes. The RT-PCR data, normalised to two common housekeeping genes GAPDH and 18S, confirms the regulation of several, but not all the genes investigated (Fig. 5.15, 5.16 and 5.17). In summary, RTPCR data on the genes found upregulated on the array confirms that Parvalbumin and Cadherin 8 are statistically upregulated in *Prkar2β*$^{-/-}$ compared to wildtype S1 cortex and reveals that NR2C, Mobp and Mog that were on the borderline of 2-fold statistical upregulation on the array are also statistically upregulated (Fig. 5.15). However RTPCR shows no change in Cntnap (Caspr) regulation between *Prkar2β*$^{-/-}$ and wildtype S1 cortex (Fig. 5.15). In contrast, *Acf7*, *Osbp1*, *Mark1*, *Rhogap19*, *Dok2*, *Brd8*, *Pdzk1*, *Serpin6b*, *Efemp1*, *Transthyretin*, *Ndufb3* and *Mdh1b* are all downregulated in the *Prkar2β*$^{-/-}$ compared to wildtype S1 cortex on the gene array, but RTPCR data does not confirm the downregulation of any of these genes in *Prkar2β*$^{-/-}$ S1 cortex (Fig. 5.16). In fact *Serpin6b*, a gene involved in synaptogenesis, is found significantly upregulated when normalised to 18S ($p=0.009$) in *Prkar2β*$^{-/-}$ compared to wildtype S1 cortex (Fig. 5.16). Lastly, in agreement with the gene array data, *Prkar2α, Prkar1β, Prkacα* and *Prkacβ* all show no change in gene expression by RTPCR between *Prkar2β*$^{-/-}$ and wildtype S1 cortex when normalised to GAPDH (Fig. 5.17). Normalisation of the RTPCR data of these PKA subunit specific genes to 18S however, reveals a discrepancy between data normalised to GAPDH and data normalised to 18S. *Prkacα* appears significantly upregulated in *Prkar2β*$^{-/-}$ S1 cortex

when normalised against 18S. A similar discrepancy is seen when *Cadherin 8* expression is normalised to both GAPDH and 18S (Fig. 5.15).

5.4 Discussion

5.4.1 Advantages and disadvantages of in vitro pharmacological manipulation for elucidating the intracellular signaling pathways involved in barrel formation.

In vitro pharmacological experiments should provide an excellent tool for investigating direct targets and effectors in the signaling pathways that lead to barrel formation. Direct pharmacological activation of slices and cultured neurons, can be manipulated in numerous ways and the effects quantified by densitometry analysis of western blots. Many other techniques employed to study intracellular signaling pathways, for example immunoblotting, *in situ* hybridisation and anatomical segregation in layer IV of different transgenic mice, are non-quantitative, and western blotting alone, although quantitative, cannot provide evidence of a direct effect.

In reality however, problems were encountered with both slice and tissue culture stimulation experiments in this chapter. Both methods were performed to investigate whether NMDAR activation regulates ERK phosphorylation via PKAR2β and/or SynGAP dependent mechanisms in barrel formation. The advantages of performing the pharmacological manipulation in slices rather than tissue culture were that S1 cortex was used, the cortical tissue remained intact and the age of the tissue correlated precisely with the postnatal age of the animal (P7). The incubation chamber however kept flooding, and only one animal could be experimented on at a time due to only 2-wells, limiting proper controls and increasing variability. Preliminary data using this technique suggested that NMDAR stimulation of a PKARβ-dependent pathway leads to inhibition of ERK phosphorylation.

A tissue culture approach was next pursued; having the advantage of within experiment controls but the disadvantages of inappropriate cortical connections and

the stage of development being less well defined with respect to barrel development. The main limitation encountered with the pharmacological experiments in culture, was variability in the levels of basal stimulation. Possible reasons for the variability were that movement and the changing of media induced high levels of basal activity in the cultures. Improvements were made in the protocol to limit this problem however and resulted in preliminary data showing that glutamate receptor activation regulates ERK phosphorylation via a SynGAP-dependent mechanism in agreement with findings by Raumbaugh et al. (2006).

ERK and barrel formation

ERK has been hypothesised to play a role in barrel formation because it has the ability to integrate signals initiated from a variety of sources to produce coordinated cellular events (Rosenblum et al., 2000). ERK has also been targeted as a potential downstream target of PKAR2β- and SynGAP- mediated barrel development in this chapter because a PKA/ERK signaling pathway has previously been described to play a role in visual cortex plasticity (Cancedda et al., 2003) and SynGAP has been reported to negatively regulate the ERK pathway upon NMDAR stimulation in hippocampal neurons (Rumbaugh et al., 2006). Recent qualitative analysis of the barrel cortex in ERK1 knockout mice has shown that barrels develop normally (preliminary, unpublished data; Watson and Kind) in these mutant mice. Unfortunately, whether ERK plays a role in barrel development is still not clear however. ERK2 knockout mice have not been able to be analysed for a barrel phenotype because they are embryonic lethal. To further investigate if ERK is required for barrel development, conditional ERK knockout mice will have to be generated and analysed.

Only preliminary pharmacological data was obtained in the cortical cell culture system presented here, due to time and animal breeding limitations, but the results that were generated (following the improvements made in the protocol) indicate that the tissue culture pharmacological approach would be worth pursuing for future experiments. Future experiments would first focus on whether PKAR2β and SynGAP regulate ERK due to synaptic NMDAR (+/- APV) or mGluR5 (+/- MPEP) stimulation. Then it would be interesting to investigate the regulation of other

signaling pathways such as p38MAPK and PI3Kinase upon glutamate receptor stimulation.

5.4.2 Large-scale protein phosphorylation screening: a useful tool for identifying intracellular pathways involved in barrel formation?

The protein phosphorylation screens performed in this chapter in collaboration with Kinexus^{TM} Bioinformatics Corporation have identified numerous phosphorylation sites that are regulated in Prkar2β$^{-/-}$ mice compared to wildtype controls. An advantage of using the commercially available screens is that a relatively large number of phosphorylation sites can be rapidly analysed compared to small scale western blotting. The large-scale proteomic screening approach has therefore been a useful tool for focussing attention on particular proteins and specific phosphorylation sites for further investigation by small scale western blotting. Preliminary small scale western blotting has examined several of these phosphorylation sites of interest and has produced results that agree with the regulation found on the screens. Only one discrepancy was found but this could be explained by the fact that the small-scale immunoblotting experiments used cortical homogenate from *Prkar2β*$^{-/-}$ and wildtype mice compared to synaptosome preparations used for the Kinexus screens.

The phosphorylation sites regulated on the screens are not necessarily direct targets of PKAR2β. PKA phosphorylates serine and threonine residues, but this study has showed several regulated phosphorylation sites in the *Prkar2β*$^{-/-}$ sample that are tyrosine residues (Figure 5.8). To discover which kinases act at the specific phosphorylation sites highlighted in the Kinexus screens, bioinformatics research has been employed. Database mining using Pubmed Entrez (summarised in figures 5.10 and 5.11) has revealed that only one of the phosphorylation sites regulated on the Kinexus screens has previously been shown to be directly phosphorylated by PKA: GSK3β - S9. This bioinformatics research has clearly illustrated that PKAR2β must either play a role upstream of these molecules activating the kinase that regulates these phosphorylation sites or must act at another phosphorylation site on the molecule that affects phosphorylation levels at the regulated site. Combining the

Kinexus data with bioinformatics research investigating what kinases act at these sites should begin to highlight candidate molecules and pathways that PKAR2β may regulate during barrel formation. Several candidate molecules for a role in barrel formation that have been identified by Kinexus are described below.

SRC and barrel formation

The most upregulated protein phosphorylation site on the Kinexus screens was Oncogene Src Y529 (+92.3%). Bioinformatic analysis revealed that PKA activation normally causes activation of SRC via phosphorylation at Ser-17 and subsequently causes autophosphorylation at Tyr-416 and dephosphorylation at the Tyr-529 site (Schmitt and Stork, 2002). In a *PKA*$^{-/-}$ mutant however, this sequence of events may not occur causing a build up of inactive SRC and perhaps explaining why an upregulation of the Tyr-529 site in *Prkar2β*$^{-/-}$ synaptosomes is observed in the Kinexus™ screens. The barrel cortex of SRC mutant mice has been analysed by Seth Grants laboratory and preliminary data has revealed normal barrel map segregation using cytochrome oxidase staining (personal communication, Seth Grant). Cytochrome oxidase does not distinguish between the pre- and post-synaptic elements of barrel formation however, so further analysis of these mice using 5HTT immunohistochemistry and Nissl stain would be beneficial to assess whether SRC plays a role in barrel formation.

PKC and barrel formation

Several phosphorylation sites in several different isoforms of PKC have been found regulated (some up- and some down- regulated) on the Kinexus screens. Interestingly, PKC has recently been shown to regulate synaptic strength at thalamocortical synapses in layer 4 neonatal barrel cortex (Scott et al., 2007). Therefore changes in phosphorylation and PKC activity could result in abnormal plasticity and barrel cortex map development.

GSK3β and barrel formation

GSK3β-(S9) was the only regulated site identified by the large-scale screens to be directly phosphorylated by PKA. GSK3β is a potentially interesting candidate with respect to barrel development, because it is known to phosphorylate two

microtubule-associated proteins, Tau and MAP1B (Mandelkow et al., 1992; Guidato et al., 1996). If GSK3β-mediated Tau and MAP1B phosphorylation levels are altered, changes in microtubule stability and organisation might occur – a cellular process that could provide an important mechanism for rearrangements during barrel formation (Wagner et al., 1996; Goold et al., 1999).

In summary, large-scale protein-phosphorylation screens can rapidly highlight candidate proteins and intracellular pathways for further, more-detailed investigation into a role in barrel formation.

5.4.3 Do gene arrays provide the future to understanding the mechanisms of barrel development?

Gene arrays, like other large-scale screening methods, allow the rapid analysis of a large number of genes. The affymetrix gene array performed in this chapter in collaboration with Professor Stanley McKnight has been a useful tool for highlighting genes that are regulated in *Prkar2β*$^{-/-}$ barrel cortex compared to wildtype barrel cortex. The statistically upregulated genes confirmed by RTPCR: *Parvalbumin*, *Mobp*, *Mog*, *Nr2c* and *Cadherin 8* are all interesting candidates for a role in barrel formation.

Parvalbumin and barrel formation

RTPCR data shows that *Parvalbumin,* which encodes a calcium binding protein in a subset of GABAergic nonpyramidal neurons, is approximately 4-fold upregulated in P7 *Prkar2β*$^{-/-}$ S1 cortex. Parvalbumin expression usually emerges in a wildtype mouse during postnatal weeks two and three (Del Rio et al., 1994). Therefore significantly higher levels of *Parvalbumin* present in P7 *Prkar2β*$^{-/-}$ cortex, suggests a premature maturation of the GABAergic system in *Prkar2β*$^{-/-}$ animals. The emergence of parvalbumin- positive cells has also been shown to correspond with the onset of the critical period in visual cortex development (Del Rio et al., 1994). The RTPCR results presented in this chapter could therefore indicate that critical period

plasticity is altered in *Prkar2β*$^{-/-}$ animals, which in turn would affect barrel development.

Mobp and Mog and barrel formation

Mobp and *Mog* (upregulated 8-10 and 3-4 fold respectively) are genes that encode structural components of myelin and indicate a dysregulation in myelination, a process required for efficient flow of information between different brain areas. Since neural activity is known to be crucial for barrel development, altered communication between the whisker pad and S1 cortex could disrupt barrel formation.

NR2C and barrel formation

NR2C, an NMDAR subunit, has been confirmed by RTPCR to be 2-fold upregulated in *Prkar2β*$^{-/-}$ barrel cortex compared to wildtype barrel cortex. *Nr2c* has recently been shown to be the predominant NMDAR subunit in layer IV neurons of the barrel cortex (Binshtok et al., 2006). NR2C-containing NMDA receptors show decreased sensitivity to Mg2+ blockade (Monyer et al., 1992, 1994; Farrant et al., 1994; Momiyama et al., 1996) and their normal expression, starting at the end of the first postnatal week coincides with the end of the period when NMDA-dependent LTP (Crair and Malenka, 1995) and LTD (Feldman et al., 1998) can be evoked. Therefore increased NR2C levels in *Prkar2β*$^{-/-}$ mice at P7 could indicate earlier onset of NR2C expression and a shortened sensitive period in these mice causing disrupted barrel development.

Cadherin 8 and barrel formation

Cadherin 8 only appears to be approximately 0.5-fold upregulated in *Prkar2β*$^{-/-}$ mice compared to wildtype controls but it remains an interesting candidate for a role in barrel formation. Cadherin 8 is a cell-adhesion molecule that is highly expressed in the barrel cortex before TCAs invade the cortex (Gil et al., 2002). However at P3/4 TCAs invade layer 4 of the cortex and segregate into whisker related patches. In addition the TCAs release glutamate that inhibits cadherin 8 expression in the presumptive barrel hollows but leaves high cadherin 8 expression in the barrel walls and septa (Gil et al., 2002). Such differential adhesion combined with tangential

growth of the cortex has been hypothesised to be a cellular process by which barrels could form (see Chapter 1: section 1.3). Altered levels of cadherin 8 in *Prkar2β*$^{-/-}$ mice might disrupt this process resulting in impaired barrel formation as described in Chapter 3. The MGI database shows that Cadherin 8 knockout mice are available for future examination.

The Affymetrix gene array did not produce a definitive list of genes regulated in *Prkar2β*$^{-/-}$ mice because some genes of interest, for example *Syngap*, were not present on this commercially available chip. To screen all the genes of interest, a custom array would have to be produced. The array data obtained however (some of which has been validated), will certainly focus future work on specific molecules (for example, Parvalbumin and Cadherin 8) and will lend itself to high throughput screening of mutant mice for defects in barrel formation. It is important to note however that the gene array data does not yield any information about the cellular or laminar organisation of these regulated molecules so *in situ* hybridisation and immunohistochemical analysis (if antibodies are available) would also be performed in future work to examine the laminar expression and cellular specificity of these molecules.

Lastly, to perform gene arrays on other mutant mice with similar barrel defects, for example *Plcβ1*$^{-/-}$, *Syngap*$^{+/-}$ and *mGlur5*$^{-/-}$ mice could provide the future for investigating the mechanisms of barrel development because it could highlight common genes that are regulated in each of these mice that fail to form barrels, and perhaps highlight the key genes involved in barrel formation.

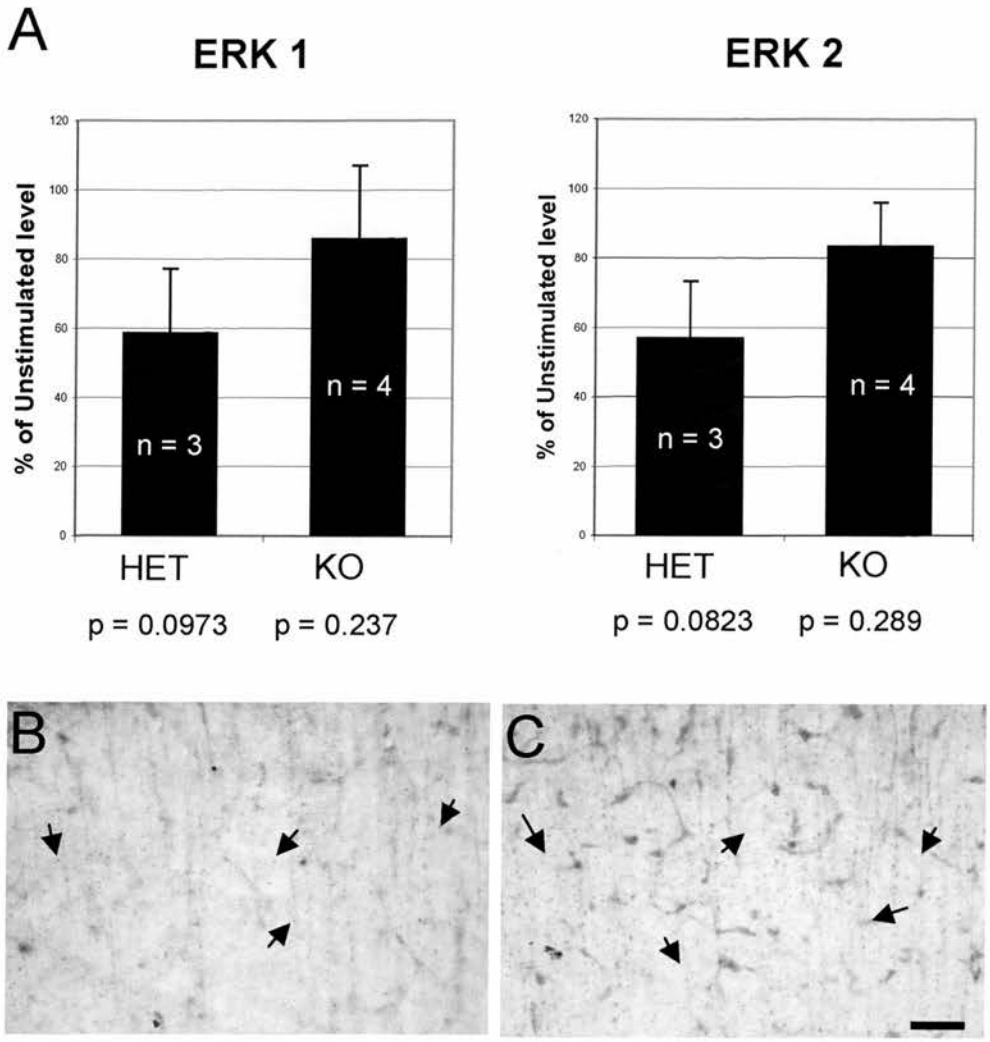

Figure 5.1: pERK regulation in *Prkar2β*$^{-/-}$ (KO) and control *Prkar2β*$^{+/-}$ (HET) S1 cortical slices **A,** Preliminary slice stimulation data indicates that upon NMDAR stimulation (100μM NMDA) pERK levels are reduced in HET but not KO P7 S1 cortical slices. Such a reduction is not yet shown to be statistically significant however (ERK1 HET 51.71±14.70% p=0.0973; ERK1 KO 78.08±5.81% p=0.237; ERK2 HET 45.19±10.14% p=0.0823; ERK2 KO 82.54±7.72% p=0.289). **B,** Immunoblotting for pERK through layer IV of S1 cortex in P7 *Prkar2β*$^{+/+}$ (**B**) and *Prkar2β*$^{-/-}$ (**C**) reveals that pERK labels dendrites (B,C; arrows) and that levels of pERK immunostaining is lower in P7 *Prkar2β*$^{+/+}$ compared to *Prkar2β*$^{-/-}$ barrel cortex (**C**). Scale bar (in **C**): **B, C,** 80μm

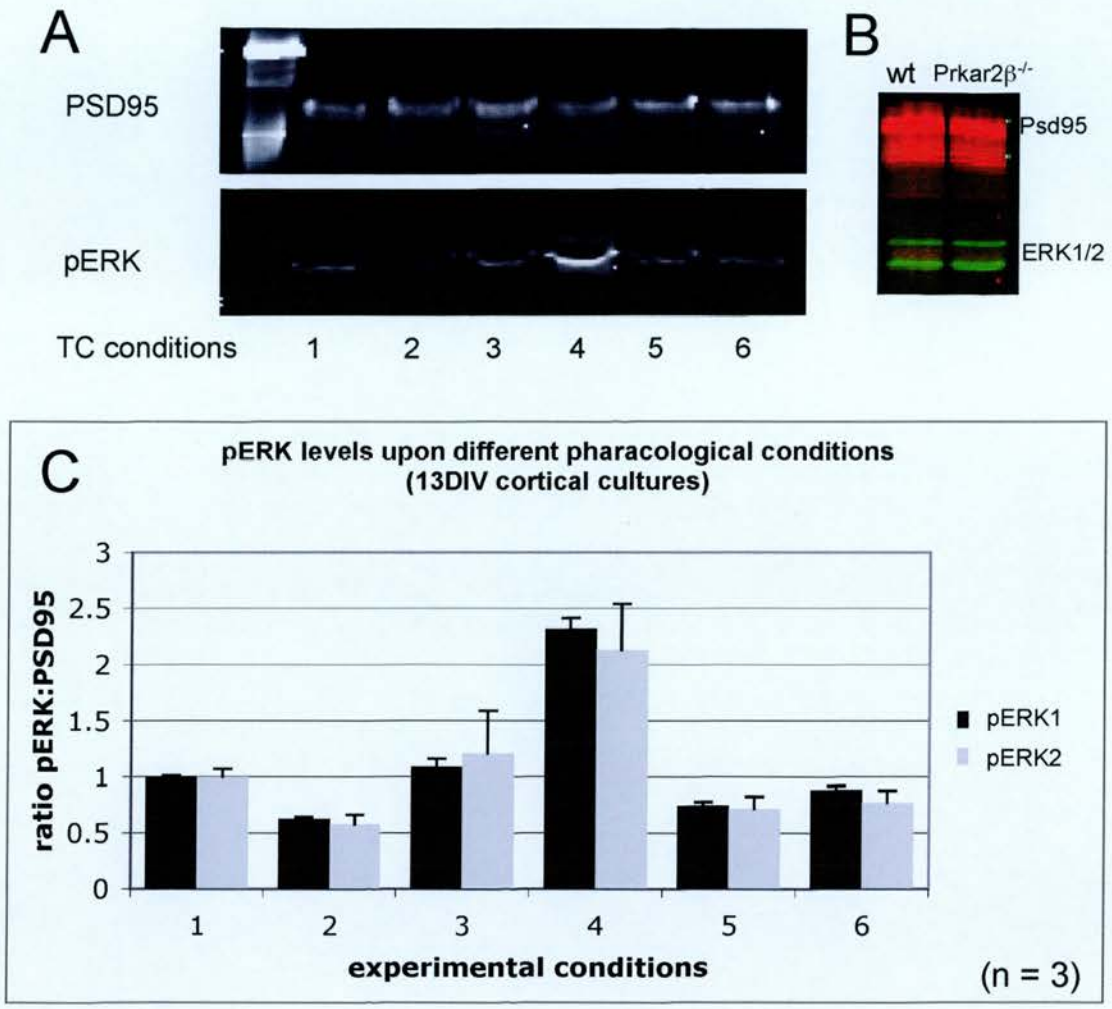

Figure 5.2: Assessment of different stimulation paradigms in 14DIV primary cortical culture. **A,** Representative western blot of pERK levels relative to PSD95 (loading control) in 14 DIV wildtype primary culture after 6 different pharmacological treatments: [1] Mg^{2+} free growth media (GM), [2] GM (with Mg^{2+}), [3] Mg^{2+} free GM + 50μM Bicuculline, [4] GM with Mg^{2+} + 50μM Bicuculline, [5] Mg^{2+} free GM + 100μM NMDA + 20μM glycine, and [6] GM with Mg^{2+} + 100μM NMDA + 20μM glycine, demonstrates that 50μM Bicuculline in the presence of Mg^{2+} induces neuronal stimulation **B,** Densitometry of pERK levels was performed relative to PSD95 (on the same blot), a protein that does not change expression levels between wt and Prkar2β$^{-/-}$ neurons. **C,** Graph of pERK1 and pERK2 levels in 14DIV wildtype primary culture treated with the 6 different pharmacological treatments listed above illustrates that 50μM Bicuculline (+Mg^{2+}) induces the best neuronal stimulation. Error bars = standard error.

A

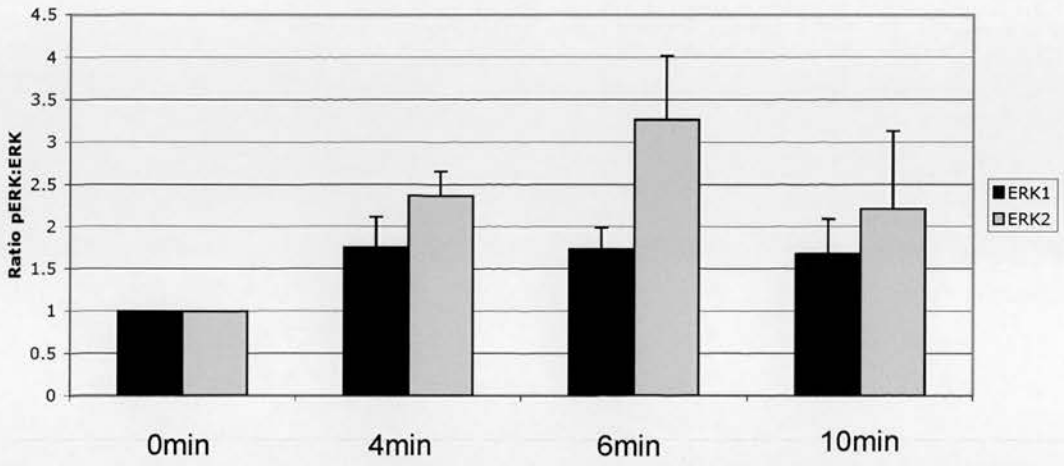

B

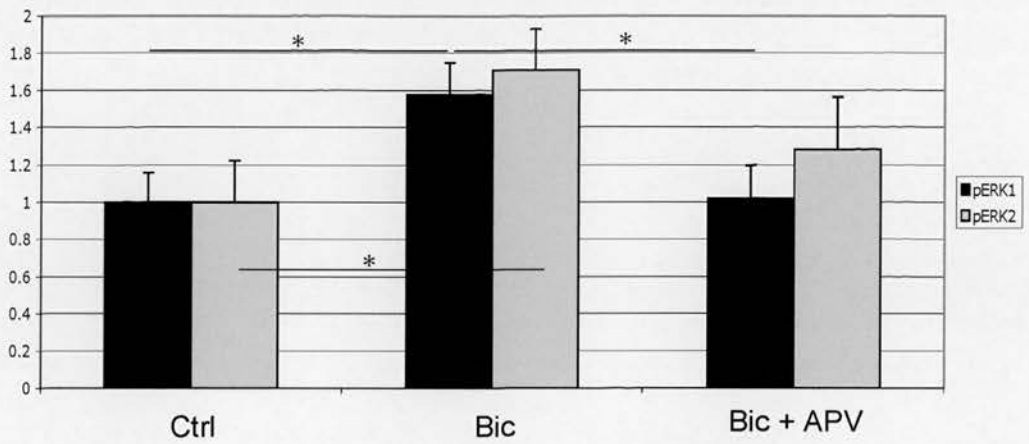

Figure 5.3: Characterisation of Bicuculline Stimulation in wildtype primary cortical cultures. **A,** A graphical representation (n = 2) of pERK1/2 levels upon Bic stimulation for 0, 4, 6 and 10 minutes shows that 6 minutes of Bicuculline treatment results in maximal neuronal stimulation. **B,** A graphical representation (n = 10) of wildtype (C57/Bl6) 14DIV cultures treated with either no drug, Bicuculline or Bicuculline + APV, shows that pERK levels (ratio of ERK levels) are upregulated upon glutamate receptor activation by Bicuculline treatment, and that this effect is blocked by APV an NMDAR antagonist (pERK1 ctrl - bic, p=0.02; pERK1 bic - apv, p= 0.05; pERK2 ctrl - bic, p=0.039). Error bars = standard error.

A

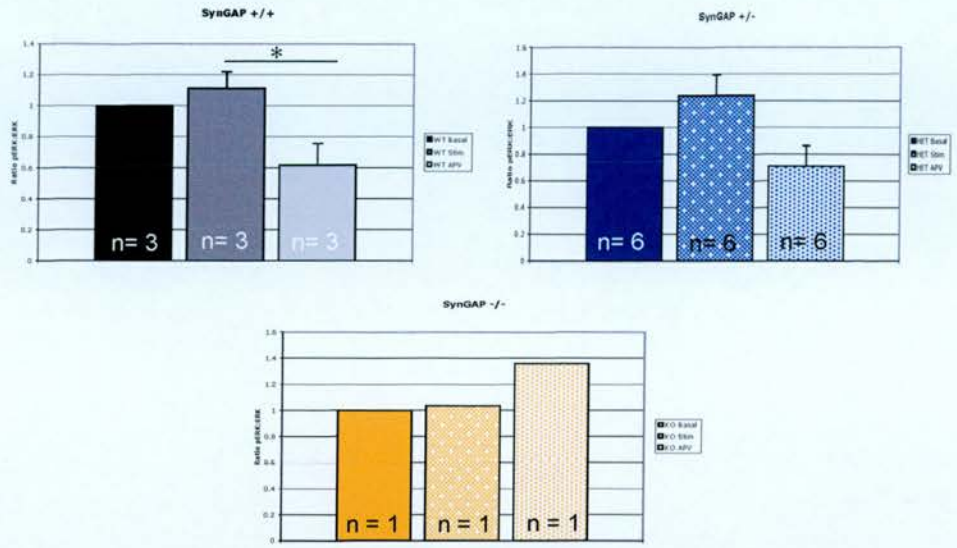

B

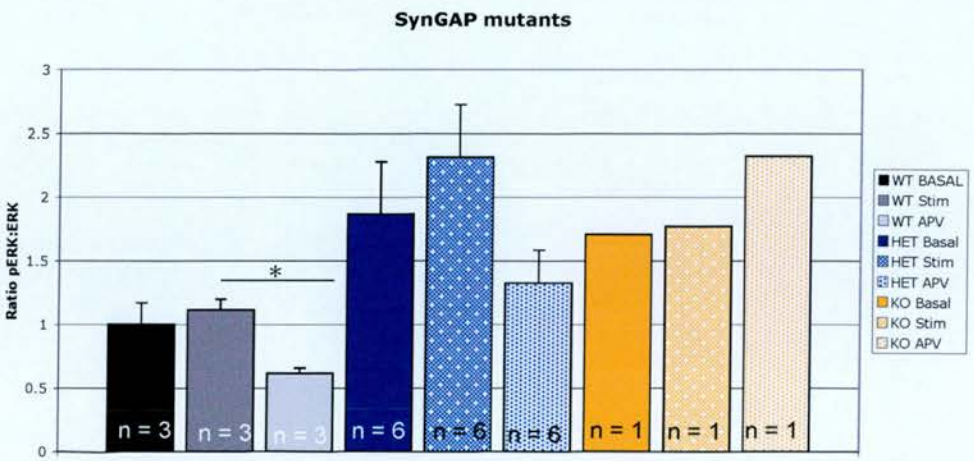

Figure 5.4: First set of SynGAP mutant cortical culture experiments. **A and B,** *Syngap*$^{+/+}$ (greyscale), *Syngap*$^{+/-}$ (bluescale) and *Syngap*$^{-/-}$ (yellowscale) 14DIV cultures treated with 3 conditions: no drug, 50μM Bicuculline, and 50μM Bicuculline + 50μM APV. The graphs show pERK2 levels (as a ratio of ERK2 levels) normalised to the control within each genotype in **A,** and normalised to the control in *Syngap*$^{+/+}$ in **B.** Within each genotype, cultures were not found to be significantly stimulated on the application of Bicuculline. However bicuculline + APV significantly reduced pERK2 levels in comparison to Bicuculline application in *Syngap*$^{+/+}$ cultures (p=0.0065). Error bars = standard error.

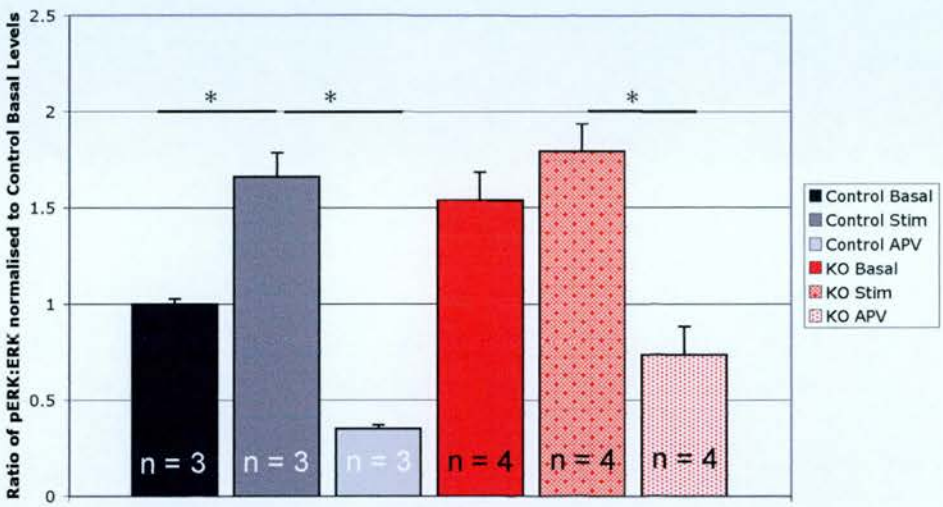

Figure 5.5: SynGAP mutant cortical culture data after modifications in the protocol. Basal pERK2 levels (as a ratio of ERK2 levels) are 54% higher in *Syngap*$^{-/-}$ compared to control *Syngap*$^{+/-}$ cultures. Glutamate receptor stimulation (50μM Bicuculline) significantly increases pERK2 levels in *SynGAP*$^{+/-}$ cultures (students t-test: p=0.0067) and to saturating levels in *Syngap*$^{-/-}$ cultures. Application of Bicuculline + APV to either *Syngap*$^{+/-}$ or *Syngap*$^{-/-}$ cultures blocks this effect (student t-tests: *Syngap*$^{+/-}$, p=0.00052; *Syngap*$^{-/-}$, p=0.0000657). Error bars = standard error.

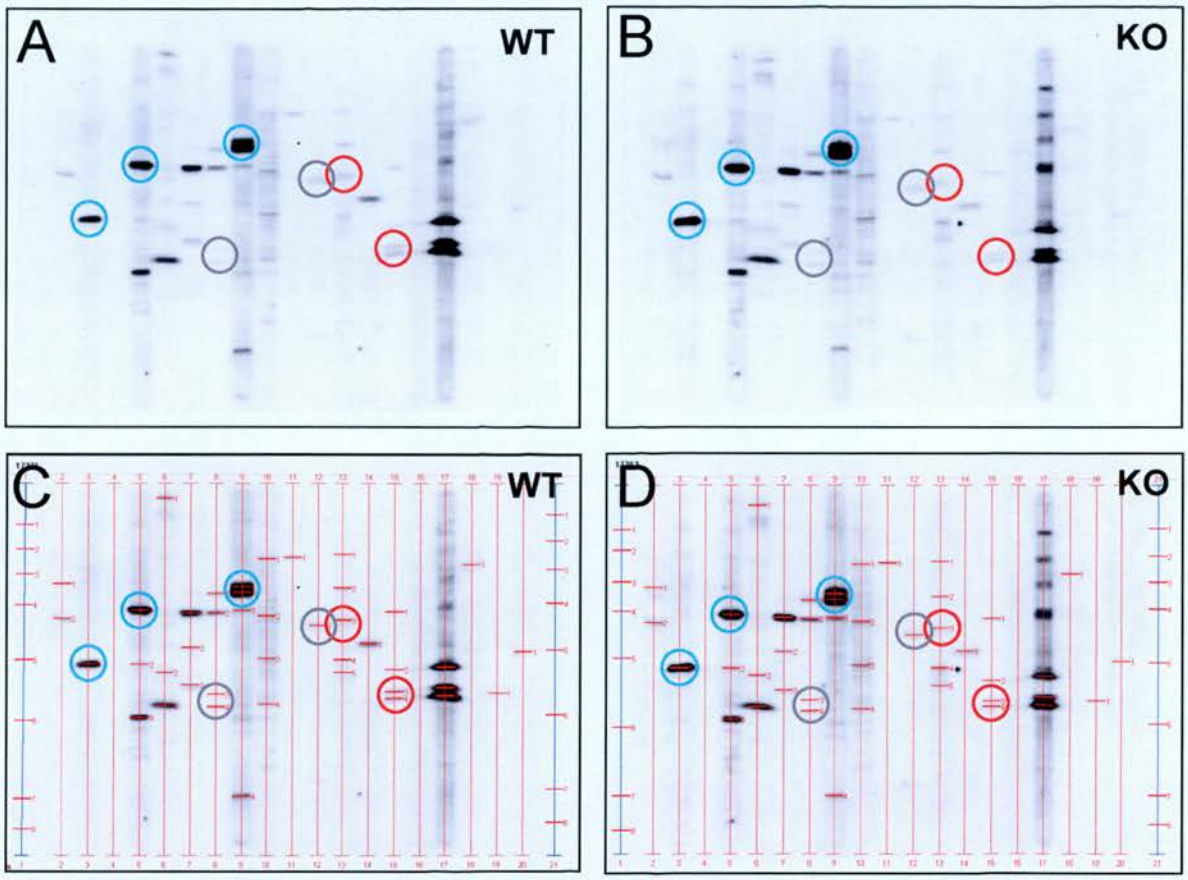

Figure 5.6: Phospho-proteomic screen KPSS1.3 performed in collaboration with Kinexus™ Bioinformatics Corporation. **A and B,** Western blot of *Prkar2β*$^{+/+}$ (**A**) and *Prkar2β*$^{-/-}$ (**B**) protein from synaptosome preparations probed with multiple phosphorylation specific antibodies in each lane. **C and D,** Copy of A and B respectively, marking the lanes and bands that correspond to the specific phosphorylation sites analysed. **A - D,** Circles label examples of upregulated (blue), downregulated (red) and non regulated (grey) phosphorylation sites in *Prkar2β*$^{-/-}$ synaptosome preparations compared to *Prkar2β*$^{+/+}$ control.

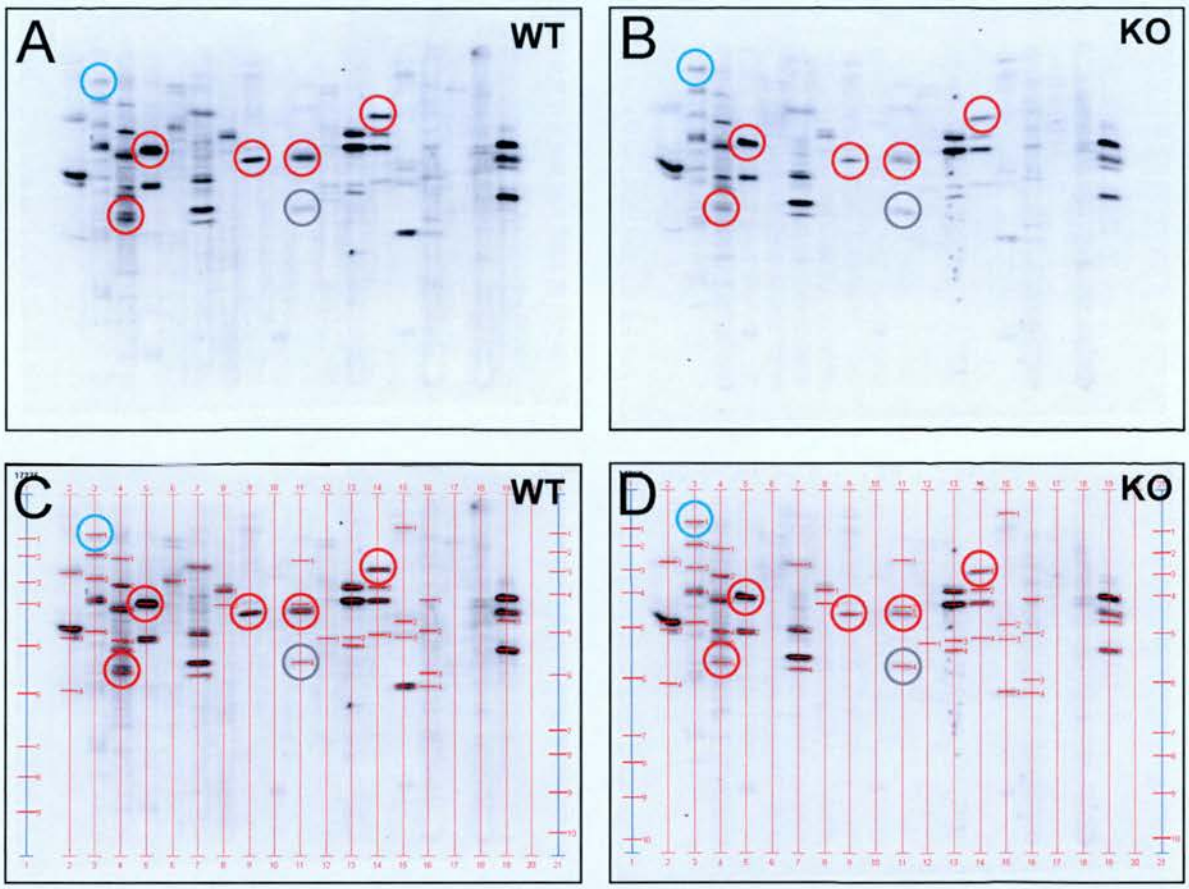

Figure 5.7: Phospho-proteomic screen KPSS4.0 performed in collaboration with Kinexus™ Bioinformatics Corporation. **A and B,** Western blot of *Prkar2β*$^{+/+}$ (**A**) and *Prkar2β*$^{-/-}$ (**B**) protein from synaptosome preparations probed with multiple phosphorylation specific antibodies in each lane. **C and D,** Copy of A and B respectively, marking the lanes and bands that correspond to the specific phosphorylation sites analysed. **A - D,** Circles label examples of upregulated (blue), downregulated (red) and non regulated (grey) phosphorylation sites in *Prkar2β*$^{-/-}$ synaptosome preparations compared to *Prkar2β*$^{+/+}$ control.

A

Name of Protein	Epitope	% change
Retinoblastoma 1	S780	- 41.0
PKCδ	T505	- 22.6
PKCzeta/lambda	T403/410	- 41.6
PKCα/β	T638	- 16.25
GSK3α	S21	- 25.8
GSK3α	Y279	- 30.2
GSK3β	S9	- 40.0
GSK3β	Y216	- 15.7
90kDa ribosomal S6K	S380	- 47.6
Syk	Y352	- 53.97
Lyn	Y507	- 49.02
PKC-related kinase 1	T778	- 34.1
PP1a	T320	- 65.2
AMPKa	T172	- 28.04
MKK3/6	S189/S207	- 40.0
MKK6	S207	- 43.9
PRK-1	T778	- 34.1

B

Name of Protein	Epitope	% change
Oncogene SRC	Y529	+ 92.3
PKCα	S657	+ 58.1
PKCα/β	T638/641	+ 46.8
PKCε	S719	+ 57.99
mTor	S2448	+ 31.8
IKKa	S181	+ 47.06
PKBα/Akt1	S473	+ 48.9
PDK1	S241	+ 14.6
S6 Kinase p70	T389	+ 18.1

C

Name of Protein	Epitope
Oncogene SRC	Y418
SAPK (40)	T183/Y185
SAPK (46)	T183/Y185
Oncogene Raf1	S259
ERK1/2	T202/Y204
MEK1/2	S217/S221

Figure 5.8: Phosphorylation sites found regulated in *Prkar2β*$^{-/-}$ compared to *Prkar2β*$^{+/+}$ S1 cortex in the large-scale screens (KPSS1.3 and KPSS4.0) performed in collaboration with Kinexus™. **A - C,** Protein phosphorylation sites downregulated (**A**), upregulated (**B**) and non regulated (**C**) in *Prkar2β*$^{-/-}$ compared to *Prkar2β*$^{+/+}$ S1 cortex.

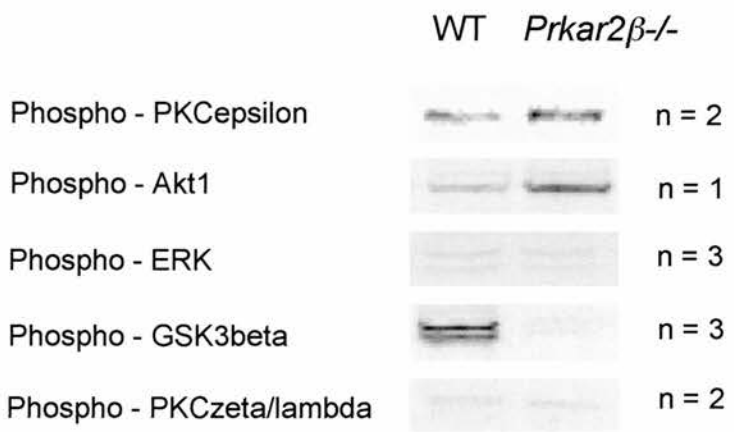

Figure 5.9: Small scale western blotting of several specific phosphorylation sites previously analysed on the large-scale Kinexus™ screens. Western blots show that PKCε S719 and PKB/Akt1 S473 are upregulated, GSK3β S9 is downregulated and ERK1 T202/Y204 and Erk2 T185/Y187 are unchanged in P7 *Prkar2β*$^{-/-}$ barrel cortex homogenate compared to wildtype controls and are in agreement with the phosphorylation site specific regulation found on the large-scale screens. In contrast PKCz/λ T410/T403 appears to show no qualitative difference between P7 *Prkar2β*$^{-/-}$ and wildtype barrel cortex homogenate whereas on the large-scale screens it is downregulated (-41.6%).

Molecule	PO_4 site	% regulated	Kinase	Reference
SRC	Y529	+ 92.3	Csk	Schmitt JM & Stork PJ, Mol Cell 2002: Jan;9(1):85-94
SRC	Y418	0	Csk/AVP	Obergfell A et al., J Cell Biol 2002: 157(2):265-75
PKCα	S657	+ 58.1	Syk	Kawakami T et al., Proc Natl Acad Sci 2003: 100(16):9470-5
SAPK	T183/Y185	0	T183-MST kinase & MKK7/Y185-MKK4	Glantschnig H et al., J Biol Chem 2002: 277(45):42987-96
PKCα/β	T638/641	+ 46.8		
S6 Kinase p70	T389	+ 18.1	Raf/Mek/Erk1&2	Iijima Y et al., J Biol Chem 2002: 277(25):23065-75
Erk 1	T202/Y204	0	GIP	Ehses et al., J Biol Chem 2002: 277(40):37088-97
Erk 2	T185/T187	0	Raf/Mek/Erk1&2	Marshall M. Mol Reprod Dev 1995: 42(4):493-9
PKCε	S719	+ 57.99		
Raf1	S259	- 17.2	PP1/PP2a	Dhillon AS et al., Mol Cell Biol 2002: 22(10):3237-46
PKCdelta	T505	- 51.8	PI3kinase/PDK-1	Cataldi A et al., J Cell Biochem 2003: 89(5):956-63
PKBα/Akt1	S473	+ 48.9	PI3kinase	Filippa et al., Mol Cell Biol 1999: 19(7):4989-5000
GSK3β	S9	- 40	PKA	Fang X et al., Proc Natl Acad Sci 2000: 97(22):11960-5
GSK3α	Y279	-30.2	PI3kinase-Akt pathway	Somervaille TC et al., 2001: 98(5):1374-81
GSK3β	Y216	- 15.7		
Retinoblastoma1	S780	- 43.4	Cdk4/D1 dependent	Pan W et al., Cancer Res 2001: 61(7):2885-91
MEK1/2	S217/S221	0	Raf1	Bondzi C et al., Oncogene 2000: 19(43):5030-3
MSK1/2	S376	- 21.5		
GSK3α	S21	- 25.8	PI3kinase-Akt pathway	Somervaille TC et al., 2001: 98(5):1374-81

Figure 5.10: Bioinformatics research into phosphorylation sites that were analysed on the KPPS1.3 screen, performed in collaboration with KinexusTM Bioinformatics Corporation. The table lists molecules that can act at each of the protein phosphorylation sites.

Molecule	PO_4 site	% regulated	Kinase	Reference
Retinoblastoma 1	S780	- 41	Cdk4/D1 dependent	Pan W et al., Cancer Res 2001: 61(7):2885-91
PDK1	S241	+ 14.6	autophosphorylated	Sato et al., J Biol Chem 2002: 277(42):39360-7
mTor	S2448	+ 31.8	PKB	Yoneza K et al., Curr Microbiol Immunol 2004: 279: 271-82
PKCdelta	T505	- 22	PI3kinase	Cataldi A et al., J Cell Biochem 2003: 89(5):956-63
GSK3α	S21	- 18.6	PI3K-Akt	Somervaille TC et al., Blood 2001: 98(5):1374-81
GSK3β	S9	- 39	PKA	Fang X et al., Proc Natl Acad Sci 2000: 97(22):11960-5
PKCz/lambda	T403/T410	- 41.6	PDK1 depedendent via PIP3	Standaert ML et al., Biochemistry 2001: 40(1):249-55
Erk 1	T202/Y204	0		Ehses JA et al., J Biol Chem 2002: 277(40):37088-97
Erk 2	T185/Y187	0	Raf/Mek/Erk1&2	Marshall M. Mol reprod Dev 1995: 42(4):493-9
p90RSK	S380	- 47.6	Mapk	Vik T & Ryder J Biochem Biophys Res Com 1997: 235(2):398
Syk	Y352	- 53.97		
Raf	S259	0	PP1/PP2A	Dillon AS et al., Mol Cell Biol 2002: 22(10):3237-46
Mapk/Erk	S217/S221	0	Raf1	Bondzi C et al., Oncogene 2000: 19(43):5030-3
Lyn	Y507	- 49.02	autophosphorylated	Donella-Deana A et al., Biochem 1998: 37(5):1438-46
P85 S6K2	T412	- 19.9	mTor	Yonezawa K et al., Curr T Microbiol Immun 2004: 279:271-82
MAPKAP	T334	0	P38 Mapk	Zu YL et al., Blood 1996: 87(12):5287-96
PRK1	T778	- 34.1		
PP1a	T320	- 65.2		
IKKa	S181	+ 47.06	Pkz	Lallena MJ et al., Mol Cell Biol 1999: 19(3):2180-8
MKK3/6	S189/S207	- 40	SGK1	Chun J et al., J Biochem (Tokyo) 2003: 133(1):103-8
MKK6	S207	- 43.9	SGK1	Chun J et al., J Biochem (Tokyo) 2003: 133(1):103-8
PKCα/β	T638	- 16.25		
AMPKa	T172	- 28.04		

Figure 5.11: Bioinformatics research into phosphorylation sites that were analysed on the KPPS4.0 screen, performed in collaboration with KinexusTM Bioinformatics Corporation. The table lists molecules that can act at each of the protein phosphorylation sites.

A

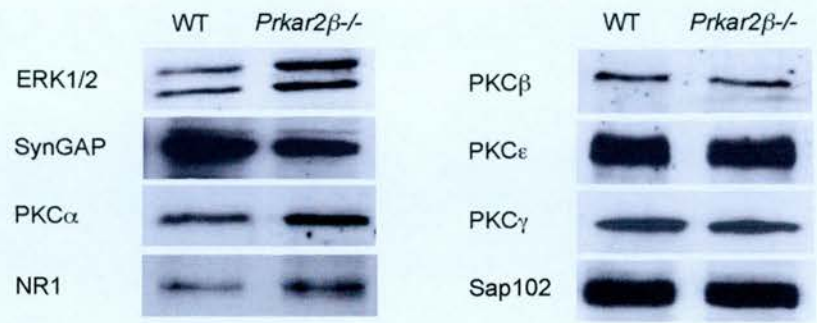

B

RIIB KO-WT normalized	WT	KO	t-test p-value	Genbank	Description
4.656 (2.7 to 10.57)	17.17 (10 to 21.48)	79.29 (53 to 116)	6.89E-05	AF179463	knockout allele constructed with PGKneo insertion; FMRP; contains neo-disrupted exon 5; alternatively spliced; modified fragile X mental retardation protein (Fmr1) mRNA, Fmr1-tm1Cgr allele, partial cds
4.364 (2.396 to 7.174)	20.79 (11.15 to 36.19)	97 (36 to 175)	0.0443	AF057367	ubiquitously transcribed tetratricopeptide repeat gene, Y chromosome
35.97 (4.5 to 91.09)	13.16 (10 to 22.04)	690.8 (45 to 1,897)	2.48E-06	M23377	neo gene
2.893 (2.1 to 4)	10.25 (10 to 10.75)	30.67 (21 to 40)	0.0293	Y13557	cea9 gene
2.648 (1.6 to 3.9)	16.83 (10 to 37.32)	45.75 (16 to 98)	0.0138	NM_011540	titin-cap
2.471 (2.011 to 3.102)	25.81 (14.19 to 46.33)	63.33 (34 to 112)	0.0187	NM_016782	contactin associated protein 1
2.394 (2.1 to 2.7)	11.35 (10 to 14.05)	27.33 (21 to 34)	0.00687	AY073370	olfactory receptor MOR268-2 gene, complete cds
2.265 (1.477 to 3.289)	14.78 (10 to 20.93)	35.5 (21 to 54)	0.0169	NM_025612	
2.181 (0.706 to 4.309)	54.05 (12.91 to 95.47)	151.7 (36 to 364)	0.0205	AF223362	NK1 transcription factor related, locus 2 (Drosophila)
2.142 (1.373 to 3.794)	22.86 (13.84 to 27.87)	55.75 (19 to 99)	0.0487	NM_008486	alanyl (membrane) aminopeptidase
2.13 (2 to 2.3)	10	21.33 (20 to 23)	0.00292	AB061519	calpain 8
2.102 (1.825 to 2.3)	40.16 (10 to 65.75)	80.67 (23 to 120)	0.00914	AY073555	olfactory receptor MOR256-11 gene, complete cds
2.02 (1.134 to 3.726)	18.11 (10.44 to 27.1)	44.4 (15 to 101)	0.0313	AK013561	parvalbumin
0.497 (0.393 to 0.596)	30.05 (20.14 to 43.24)	14.33 (12 to 17)	0.0294	NM_033601	B-cell leukemia/lymphoma 3
0.484 (0.316 to 0.678)	28.98 (20.66 to 37.95)	13.75 (12 to 15)	0.0212	NM_008733	nebulin-related anchoring protein
0.484 (0.243 to 0.997)	820.5 (194.6 to 1,645)	346 (79 to 716)	0.00459	BC009140	expressed sequence AW556797
0.48 (0.459 to 0.503)	21.74 (19.59 to 23.88)	10.5 (9 to 12)	0.039	NM_010071	downstream of tyrosine kinase 2
0.473 (0.471 to 0.476)	28.53 (27.33 to 29.74)	13.5 (13 to 14)	0.00429	AY073459	olfactory receptor MOR177-9 gene, complete cds
0.472 (0.142 to 1.601)	97.7 (26.81 to 234.3)	76 (9 to 375)	0.018	NM_023894	placenta specific homeobox 2
0.465 (0.338 to 0.703)	54.52 (34.24 to 109.3)	24 (12 to 37)	0.0235	BC023060	epidermal growth factor-containing fibulin-like extracellular matrix protein 1
0.463 (0.155 to 1.651)	283.6 (104.2 to 540.8)	140.3 (27 to 279)	0.0262	X59289	9 days embryo whole body cDNA, RIKEN full-length enriched library, clone:D030072M03 product:inactive X specific transcripts, full insert sequence
0.452 (0.379 to 0.496)	57.48 (22.19 to 105.6)	24.33 (11 to 40)	0.0123	NM_025597	RIKEN cDNA 2700033I16 gene
0.449 (0.433 to 0.472)	20.68 (13.51 to 25.41)	9.333 (6 to 12)	0.00103	NM_010293	glucokinase activity, related sequence 1
0.416 (0.389 to 0.444)	17.04 (13.51 to 20.56)	7 (6 to 8)	0.0477	AK006554	RIKEN cDNA 1700030K01 gene
0.412 (0.322 to 0.471)	52.62 (39.08 to 72.16)	22.33 (15 to 34)	0.0188	AK016763	RIKEN cDNA 4933411B03 gene
0.409 (0.354 to 0.548)	70.64 (56.53 to 87.51)	30.67 (20 to 48)	0.0258	AY073795	olfactory receptor MOR106-12 gene, complete cds
0.389 (0.372 to 0.406)	24.52 (22.16 to 26.87)	9.5 (9 to 10)	0.0295	NM_009139	chemokine (C-C motif) ligand 6
0.382 (0.373 to 0.39)	24.88 (24.15 to 25.61)	9.5 (9 to 10)	0.0154	AK007262	RIKEN cDNA 1700124B08 gene
0.353 (0.286 to 0.422)	21.16 (17.45 to 24.7)	7.667 (5 to 9)	0.0116	NM_007812	cytochrome P450, family 2, subfamily a, polypeptide 5
0.351 (0.192 to 0.504)	49.67 (22.14 to 119.8)	14.25 (10 to 23)	0.0167	AF282300	odorant receptor M15 gene, complete cds
0.35 (0.221 to 0.844)	34.12 (22.61 to 65.68)	12.25 (5 to 20)	0.0413	AF320347	G-protein coupled seven-transmembrane domain protein; odorant receptor ORZ6 (Orz6) gene, complete cds
0.346 (0.247 to 0.42)	82.51 (37.51 to 157.7)	25.33 (15 to 39)	0.0245	AK012919	RIKEN cDNA 2810047L02 gene
0.313 (0.307 to 0.32)	28.73 (28.12 to 29.35)	9	0.0118	AY073110	olfactory receptor MOR232-3 gene, complete cds
0.302 (0.269 to 0.347)	29.54 (27.21 to 31.73)	9 (8 to 11)	0.00378	AF425084	expressed sequence C76171
0.297 (0.246 to 0.336)	21.76 (16.28 to 25.21)	6.667 (4 to 8)	0.00626	NM_023865	RIKEN cDNA 9530002B09 gene
0.268 (0.253 to 0.284)	14.73 (11.84 to 17.63)	4 (3 to 5)	0.0271	NM_007974	coagulation factor II (thrombin) receptor-like 1
0.135 (0.0775 to 0.283)	258.2 (12.9 to 444.5)	38.33 (1 to 72)	2.34E-07	M68861	Mouse cAMP-dependent protein kinase type II beta regulatory subunit gene, exon 1
0.0945 (0.0854 to 0.113)	65.03 (44.34 to 93.72)	6 (5 to 8)	0.00141	NM_013697	transthyretin
0.0336 (0.01 to 4.3)	111.4 (10 to 366.3)	1.4 (-19 to 43)	0.0489	AF453686	ELKL motif serine-threonine protein kinase 3

Figure 5.12: Gene Array. **A,** Western blots showing altered protein expression levels of ERK1/2, SynGAP, PKCα and NR1 in P7 *Prkar2β*$^{-/-}$ synaptosomes relative to P7 wildtype synaptosomes (left panel) compared to no qualitative difference in expression levels of PKCβ, PKCε, PKCγ and Sap102 (right panel) in P7 *Prkar2β*$^{-/-}$ synaptosomes relative to P7 wildtype synaptosomes. The altered protein expression levels could be due to translation or transcription. **B,** The statistically significant 2-fold (or greater) upregulated (blue) and downregulated (grey) genes in P7 *Prkar2β*$^{-/-}$ S1 cortex identified by an Affymetrix gene array performed in collaboration with Professor Stanley McKnight.

A

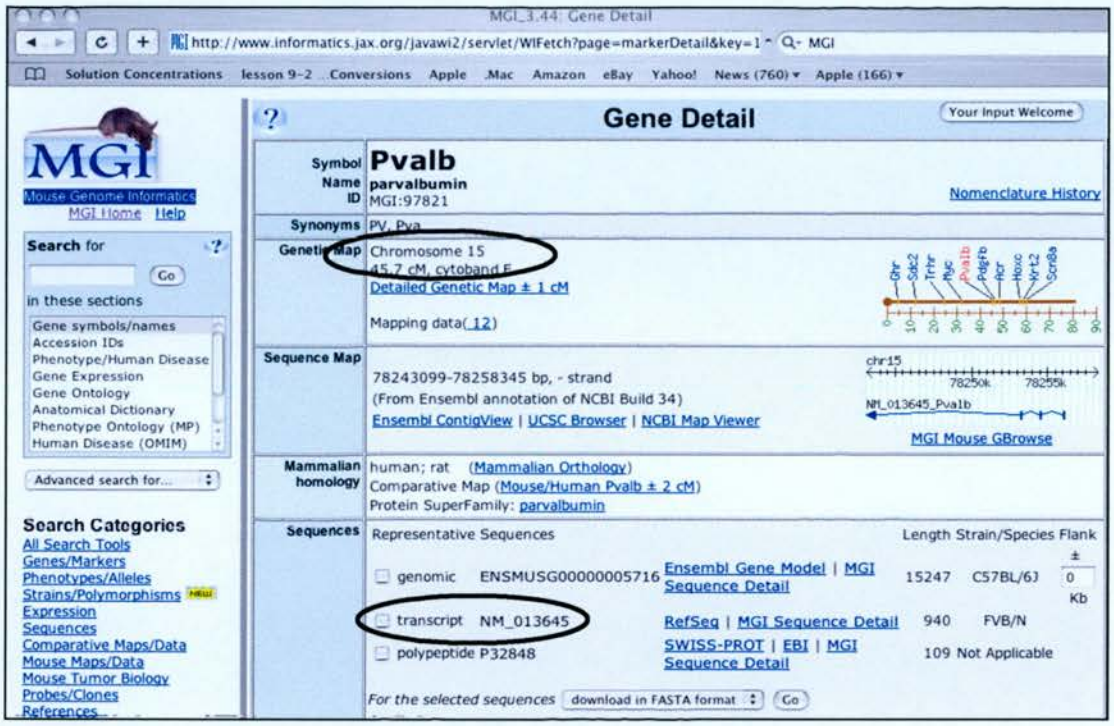

B

T-test	Transcript	Gene Name
2.34E-07	M68861	**Mouse cAMP-dependent protein kinase type II beta regulatory su**
0.00103	NM_010293	glucokinase activity, related sequence 1
0.00141	NM_013697	transthyretin
0.00344	BC003443	OSBP1 ERK regulator RIKEN cDNA 1110018F06 gene, mRNA (cDN
0.00378	AF425084	expressed sequence C76171 **serpin 6c**
0.00429	AY073459	olfactory receptor MOR177-9 gene, complete cds
0.00459	BC009140	expressed sequence AW556797 D15Mgi27
0.00626	NM_023865	RIKEN cDNA 9530002B09 gene component of extracellular space
0.0116	NM_007812	cytochrome P450, family 2, subfamily a, polypeptide 5
0.0118	AY073110	olfactory receptor MOR232-3 gene, complete cds
0.0123	NM_025597	RIKEN cDNA 2700033I16 gene Ndufb3
0.0154	AK007262	RIKEN cDNA 1700124B08 gene Malate dehydrogenase 1b
0.0167	AF282300	odorant receptor M15 gene, complete cds
0.0188	AK016763	RIKEN cDNA 4933411B03 gene RhoGAP
0.0212	NM_008733	nebulin-related anchoring protein Actin anchoring protein
0.0235	BC023060	epidermal growth factor-containing fibulin-like extracellular matrix prot
0.0245	AK012919	RIKEN cDNA 2810047L02 gene denticleless homolog
0.0258	AY073795	olfactory receptor MOR106-12 gene, complete cds
0.0262	X59289	9 days embryo whole body cDNA, XIST RIKEN full-length enriched l
0.0271	NM_007974	coagulation factor II (thrombin) receptor-like 1
0.0294	NM_033601	B-cell leukemia/lymphoma 3
0.0295	NM_009139	chemokine (C-C motif) ligand 6
0.039	NM_010071	downstream of tyrosine kinase 2
0.0413	AF320347	G-protein coupled seven-transmembrane domain protein; odorant re
0.0454	NM_011472	small proline-rich protein 2F
0.0477	AK006554	RIKEN cDNA 1700030K01 gene spata9
0.0482	NM_030708	zinc finger homeodomain 4 zfh-4
0.0489	AF453686	ELKL motif serine-threonine protein kinase 3 EMK/MARK1

Figure 5.13: Bioinformatics identification of the RIKEN cDNA clones included in the gene array data. **A,** The Mouse Genome Informatics database (Jackson Laboratories) that was used to identify the RIKEN cDNA clones from their unique Genbank identification codes. **B,** An annotated list of the genes found significantly 2-fold (or greater) downregulated in the P7 *Prkar2β*$^{-/-}$ S1 sample compared to wildtype control on the gene array.

Downregulated genes	Upregulated genes	Non-regulated genes
Acf7 (cytoskeletal) Nrap (cytoskeletal)	Cntnap1/Caspr (myelin) MOG (myelin) MBP (myelin)	PKAR1α (signaling) PKAR2α (signaling) PKAR1β (signaling) PKACα (signaling) PKACβ (signaling)
Osbp1 (signaling) Mark1/EMK/ELKL (signaling) Dusp21 (signaling) RhoGAP (signaling) Dok2 (signaling) Brd8 (signaling)	Calpain 8 (?) Titin-cap (?) Nkx1(?) Cea9 (?)	
Sprr2f (scaffolding) Pdzk1 (scaffolding)	Parvalbumin (GABAergic)	
Serpin 6b (cell adhesion) Efemp1 (cell adhesion)	NR2C (NMDAR subunit)	
Transthyretin (?) Ndufb3 (?) MDH1b (?) Nox4 (?)	Cadherin 8 (cell adhesion)	

Figure 5.14: Genes prioritised for validation by RTPCR: 17 genes that are significantly 2-fold-up- or down- regulated on the array, 7 genes of interest that lie on the borderline of 2-fold significance (Acf7, Dusp21, NR2C, Pdzk1, Brd8, MOBP and MOG), 1 gene of interest that is less than 2-fold regulated but is statistically significant (cadherin 8) and 5 control non-regulated genes (other PKA subunits).

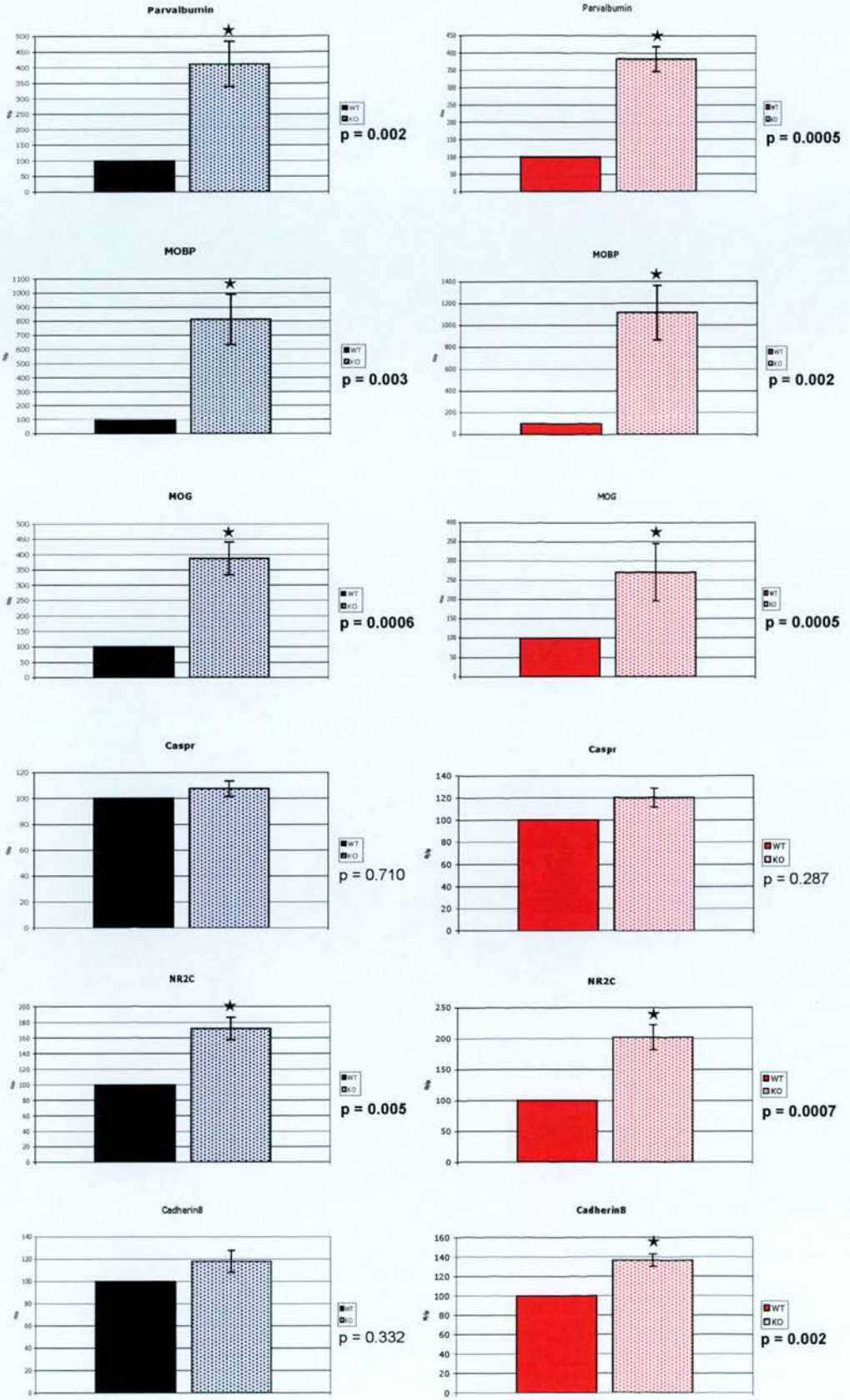

Figure 5.15: RTPCR analysis of genes that were shown to be 2 fold upregulated on the Affymetrix gene array. The RTPCR performed on 6 P7 wildtype and 6 P7 *Prkar2β*$^{-/-}$ mRNA samples isolated from S1 cortical dissections confirms that *Parvalbumin*, *Mobp*, *Mog*, *Nr2c* and *Cadherin* are upregulated. Caspr appears not to change between *Prkar2β*$^{-/-}$ and wildtype S1 cortex.

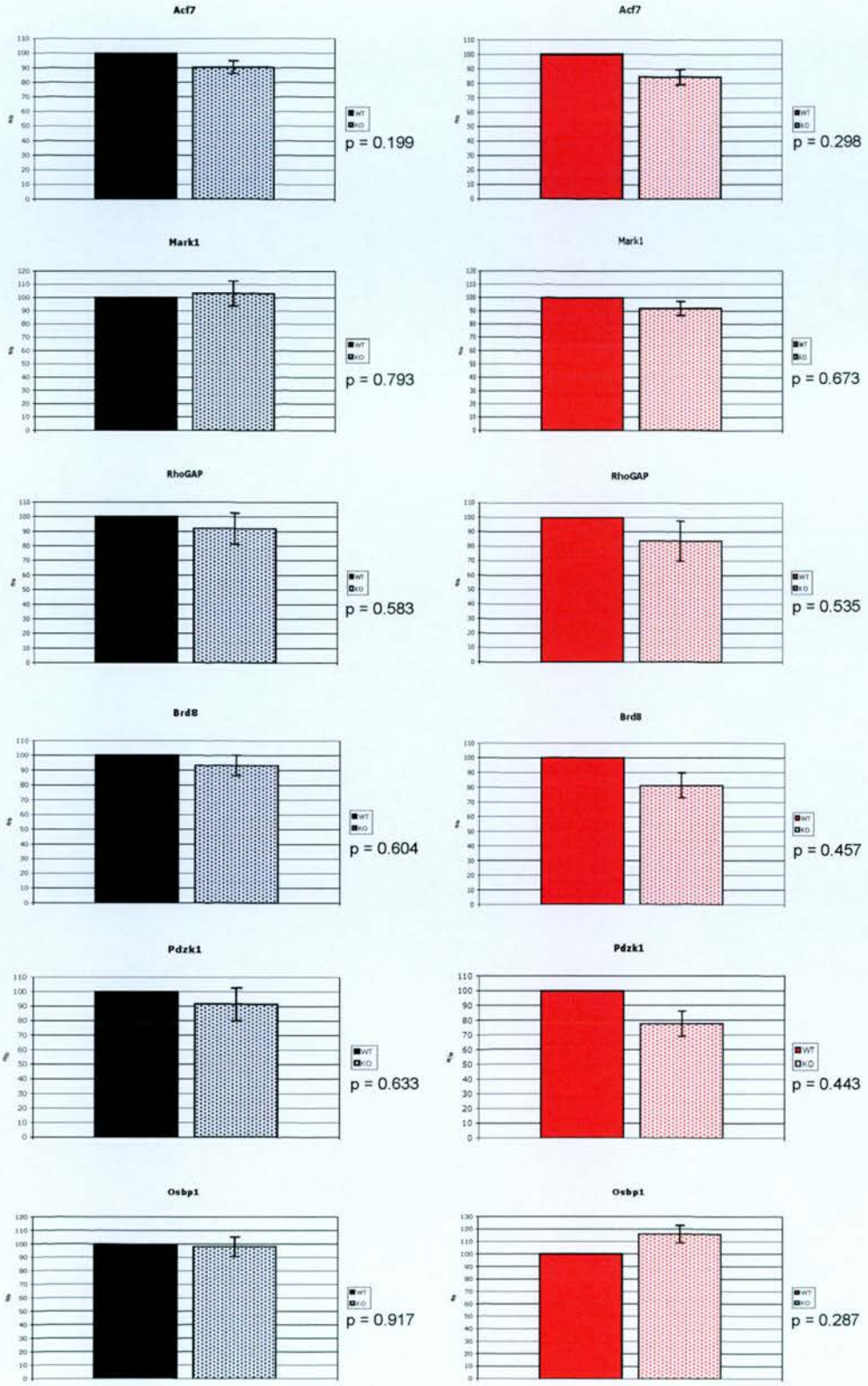

Figure 5.16: Continued on next page

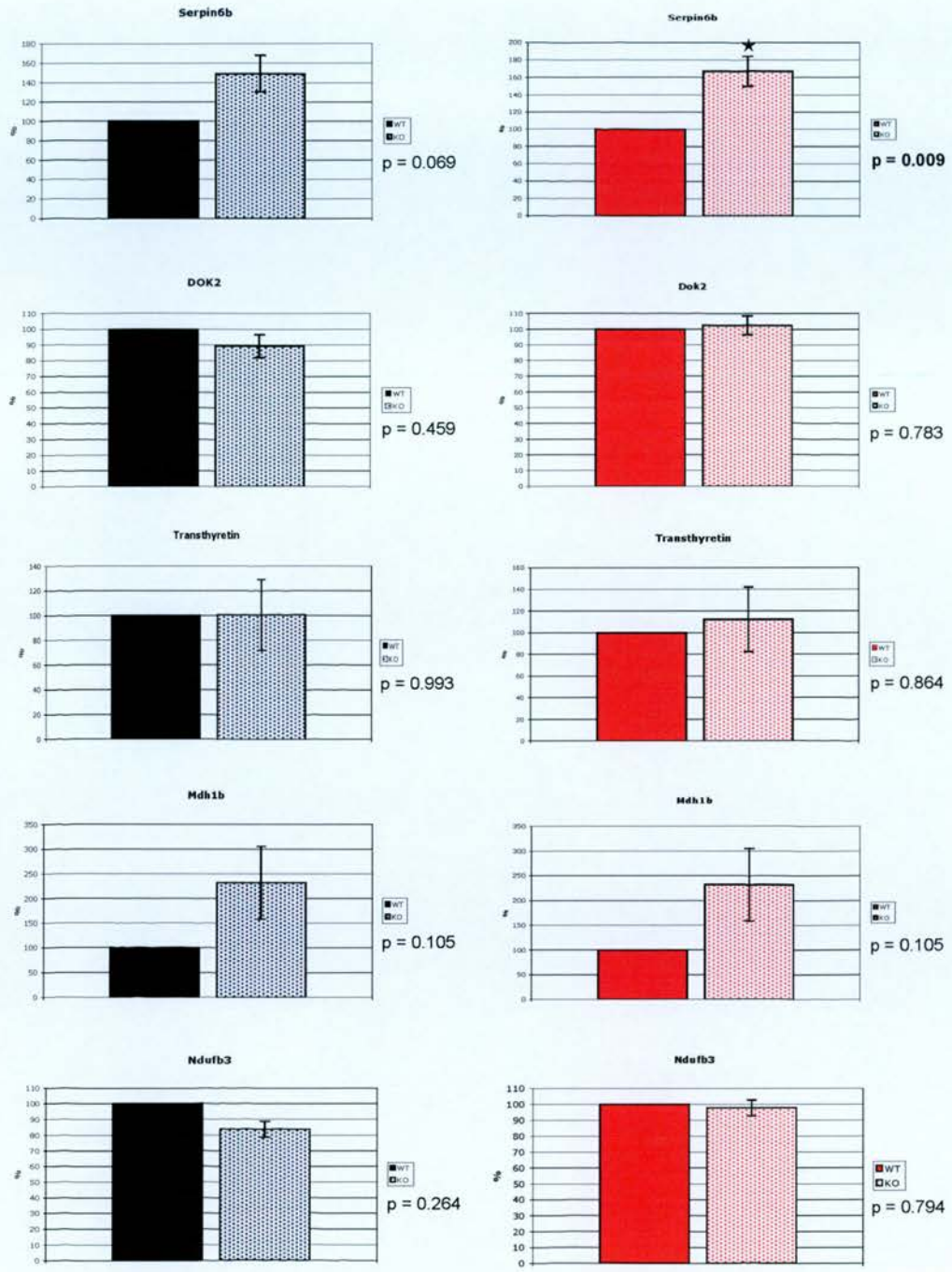

Figure 5.16: RTPCR analysis of genes that were shown to be 2 fold downregulated on the Affymetrix gene array. The RTPCR performed on 6 P7 wildtype and 6 P7 *Prkar2β*$^{-/-}$ mRNA samples isolated from S1 cortical dissections does not confirm the significant downregulation of any of these genes when normalised to either GAPDH (black graphs) or 18S (red graphs). Serpin6b, normalised to 18S is significantly up-regulated.

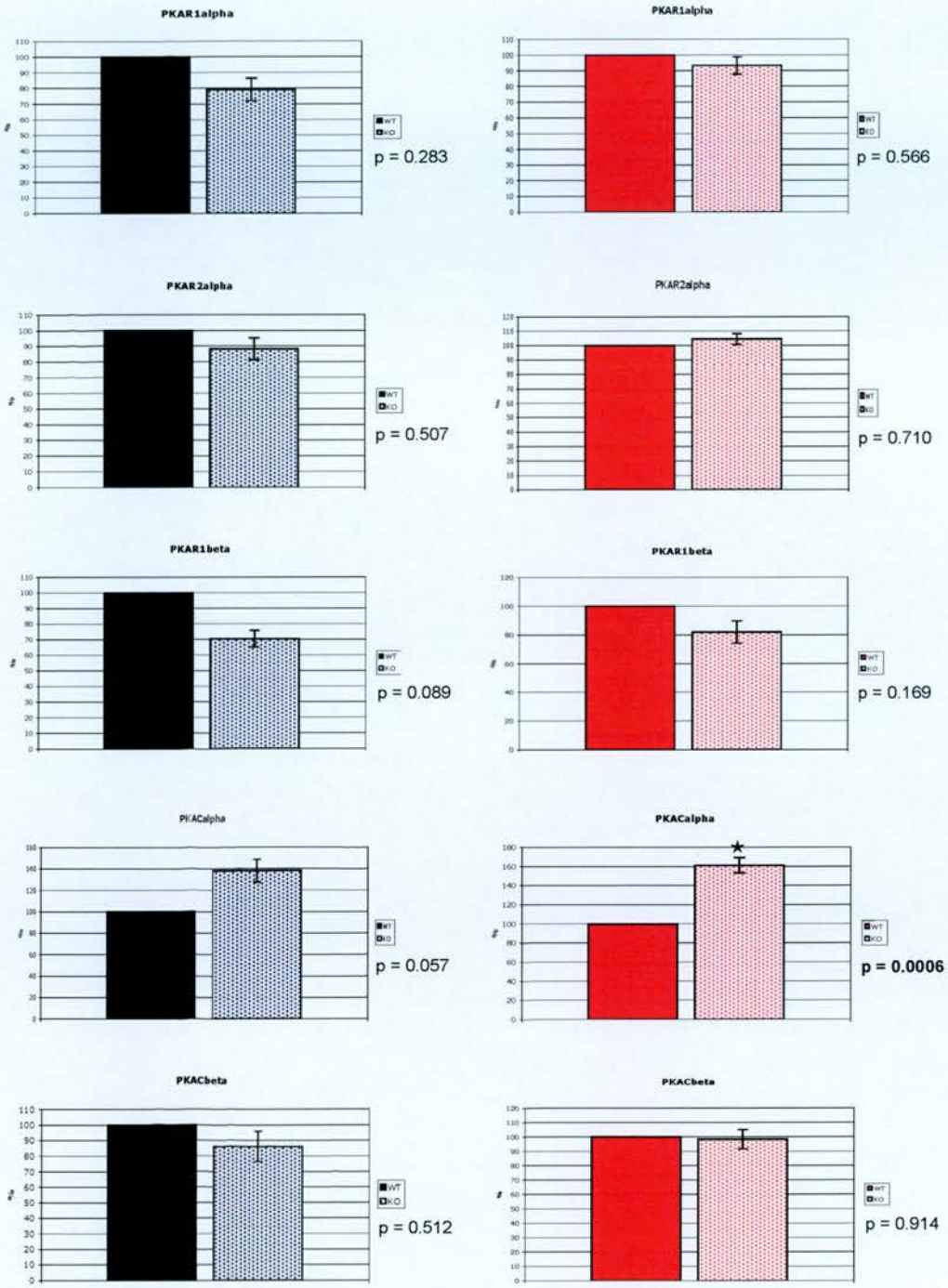

Figure 5.17: RTPCR analysis of genes found unregulated on the Affymetrix gene array. The RTPCR performed on 6 P7 wildtype and 6 P7 *Prkar2β*$^{-/-}$ mRNA samples isolated from S1 cortical dissections shows that *Prkar1α*, *Prkar2α*, *Prkar1β*, *Prkacα* and *Prkacβ*, are not transcriptionally regulated normalised to GAPDH (black graphs) but *Prkacα* is upregulated when normalised to 18S (red graph).

CHAPTER 6:
Concluding Remarks

6.1 The barrel cortex: a tool for studying the molecular basis of activity-dependent cortical differentiation

The mouse primary somatosensory cortex (S1) is an excellent system for studying the molecular basis of activity-dependent cortical development because it contains distinct cytoarchitectonic units in layer 4 called barrels that allow for easy assay of the effects of manipulating individual genes. Furthermore, both the presynaptic thalamocortical afferents and the postsynaptic layer 4 cells cluster to form a barrel, making the barrel system an extremely useful tool for distinguishing between pre- and post- synaptic events involved in cortical differentiation. Also, neurotransmitter activity (both presynaptic serotonergic and postsynaptic glutamatergic) has been shown previously to be crucial for the development of barrels since mice with deletions of mGluR5 (Hannan et al., 2001), and cortex specific NMDA receptors (Iwasato et al., 2000) lack barrels in S1 and 5HT1B also plays an important role (Salichon et al., 2001). How receptor activation affects the anatomical and functional features of the developing cortex though, is poorly understood. This thesis has taken advantage of the barrel system and recent transgenic, molecular and biochemical technology to begin elucidating the intracellular pathways through which postsynaptic glutamate receptors mediate their effects.

6.2 New insights into the molecular mechanisms of barrel development

Prior to this thesis only one intracellular signaling molecule, phospholipase-C-β1 (PLCβ1) had been identified to play a role in barrel development (Hannan et al., 2001). New research presented in this thesis however, has illustrated the involvement of two additional signaling molecules in barrel differentiation: PKAR2β and SynGAP (Chapter's 3 and 4 respectively). Mutant mice that lack *Prkar2β* develop poorly differentiated barrels in layer 4 of S1 cortex, and mice that lack *Syngap* completely fail to form barrels compared to wildtype littermate controls. Identification of these two intracellular molecules and detailed characterisation of their mutant barrel phenotypes has shed new light on the molecular basis of somatosensory cortex development. Immunoelectron microscopy has also shown that both PKAR2β and SynGAP localise to dendrites and dendritic spines in layer 4

of S1 and not presynaptic terminals, providing evidence that both these molecules play a role in the postsynaptic glutamatergic pathways important for barrel differentiation.

In addition, the biochemical pathways through which PKAR2β and SynGAP mediate barrel development downstream of mGluR5 or NMDA receptors are beginning to be elucidated. Chapter 5 of this thesis adopted three distinct approaches for gaining further insight into the intracellular signaling pathways involved in barrel formation. First, a pharmacological approach was used to investigate the activators and direct targets of PKAR2β and SynGAP in somatosensory cortex. Preliminary data obtained suggests that both PKAR2β and SynGAP regulate ERK upon glutamate receptor stimulation. Second, a large-scale protein phosphorylation screen examined the dynamics of various PSD proteins in a *Prkar2β*$^{-/-}$ compared to a wildtype animal and has highlighted numerous regulated phosphorylation sites. Together with bioinformatics research into what molecules act at these specific phosphorylation sites, this information is beginning to help us understand the molecular complexity underpinning barrel development and is highlighting certain biochemical pathways. Lastly, gene array analysis comparing *Prkar2β*$^{-/-}$ and wildtype somatosensory cortex was carried out to examine if transcriptional regulation contributes to the disrupted barrel development found in *Prkar2β*$^{-/-}$ mice. A number of genes were found 2-fold regulated on the array, and several of these results have been validated and the genes are being investigated as potential candidates for a role in barrel formation.

Finally, a role for AMPAR trafficking in barrel development was investigated in Chapter 3. Lu et al. (2003) proposed that AMPAR trafficking might be an important molecular mechanism for barrel map development because *Ac1*$^{-/-}$ (*barrelless*) mice show impairment of LTP/LTD type synaptic plasticity and reduced GluR phosphorylation and GluR insertion into the PSD. Chapter 3 demonstrated that *Prkar2β*$^{-/-}$ (Chapter 3) mutant mice also have reduced levels of GluRA at layer 4/TCA synapses compared to wildtype mice. Analysis of the barrel cortex in *GlurA*$^{-/-}$ mice however (Chapter 3) showed that these mice develop quantitatively normal barrels. Also preliminary analysis of *GlurB*$^{-/-}$ and *GlurC*$^{-/-}$ mice revealed qualitatively normal barrelfields in each of these mutant mice. Collectively this data

has indicated that the mechanism of AMPAR insertion into the PSD is not required for barrel development and that these two processes are genetically distinct from one another. Multiple AMPAR subunit knockout mice will have to be examined though to conclude that this is the case (see below; section 6.3).

6.3 Limitations of a transgenic approach to determine the signaling pathways for barrel cortex development

The analysis of transgenic mice with deletions in particular genes has provided some invaluable insight into specific molecules involved in barrel differentiation, but also has several important limitations. First, most of the transgenic mice analysed do not have mutations restricted to the barrel cortex, and therefore interpretation of positive results is complicated by the broader spatial and temporal expression pattern of the molecule under investigation. Second, a normal barrel phenotype in a particular transgenic animal does not necessarily mean that the protein in question is not involved in barrel cortex development. Compensation by other isoforms, or related proteins could mask a role for a protein in normal barrel development. For example, *GlurA*$^{-/-}$ mice show a normal barrel phenotype but this could be due to compensation by GluRB or GluRC. Combined double and triple transgenic mice could be used to distinguish between these possibilities. Thirdly, there are numerous mechanisms involved in development of the barrel cortex and conditions such as differences in background strain have been shown to sometimes affect the barrel phenotype of particular transgenic mutants, for example *mGlur5*$^{-/-}$ mice (Hannan et al., 2001) and *Maoa*$^{-/-}$ mice (Vitalis et al., 1998). And lastly, while deficits in the barrel cortex of transgenic mice not expressing a specific protein suggest the involvement of this protein in the normal development of the barrel cortex, they give little information about the in-vivo signaling pathways in which this protein is involved. Despite these limitations however, when combined with proper neuroanatomical, pharmacological and physiological techniques, the use of transgenic animals remains an effective tool for the initial identification of signaling pathways important for barrel development.

6.4 Biochemical assessment of the NRC/PSD during barrel development

Postsynaptic molecules NR1, mGluR5, PLCβ1, PKAR2β and SynGAP that are known to affect barrel development, are all found within the NMDA receptor complex (NRC), isolated by Husi et al. (2000). This has suggested that the NRC plays an important role in cortical differentiation. As a result, one approach taken by our laboratory to identify the second messenger pathways downstream of glutamate receptor activation involved in development and plasticity has been to screen mutants of NRC associated proteins for defects in cortical development as described throughout this thesis. Characterisation of the NRC and entire PSD in adult forebrain (Husi et al., 2000; Walikonis et al., 2000) has provided a large list of candidate molecules that could be acting downstream of NMDAR or mGluR5 signaling during cortical development. However the constituent proteins of the NRC/PSD are known to vary with activity, age and brain area (Okabe, 1999). In this thesis, western blot analysis of several PSD proteins throughout development (Fig.4.8) has illustrated that the NRC/PSD is highly dynamic during barrel development. The expression of most PSD proteins steadily increases throughout development from birth to adulthood (for example NR1 and SAP102), in agreement with synaptogenesis. However some proteins show more dynamic developmental expression profiles, being expressed at relatively low levels during the first postnatal week when barrels form, and then rapidly being upregulated at P14 and increasing into adulthood (for example SynGAPα and NR2A). Interestingly this second type of protein expression profile correlates well with the sharp increase in density of spines and glutamatergic synapses that occurs in S1 cortex at P14 (see figure 6.1) and also the critical periods for spine motility, receptor field properties and dendritic branching identified in layers 2/3 of the barrel cortex (see figure 6.2). In summary, it appears that there could be two general groups of proteins: those that are important for barrel formation and anatomical plasticity in the first postnatal week and those that are important for other aspects of barrel plasticity once whisking begins and drives increased sensory driven activity (see figures 6.1 and 6.2).

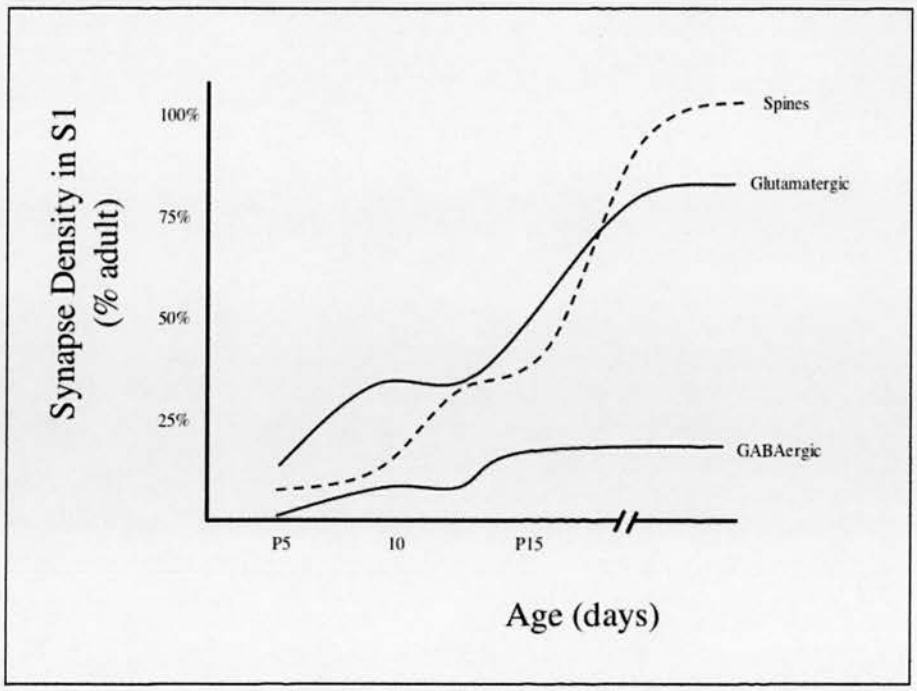

Figure 6.1: The development of spines and synapses in mouse S1 cortex. Glutamatergic synapse density increases rapidly between P6 to P8, slowly from P9 to P12 and sharply between P13 and P14, correlating with the onset of patterned whisking (White et al., 1997). GABAergic synapse density shows a similar trend at P10-P12. In adulthood, there are approximately 80% glutamatergic synapses and 20% GABAergic synapses.

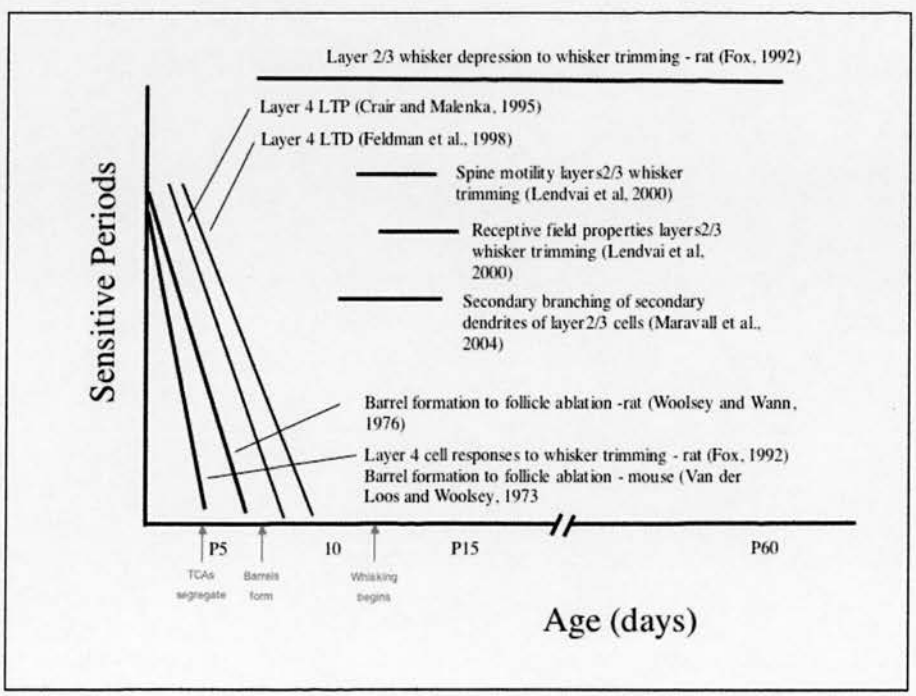

Figure 6.2: Critical periods in the barrel cortex. There are multiple different critical periods in rodent barrel cortex during development, however they appear to correlate with two distinct phases in development: before and after the onset of patterned whisking.

A major goal for the future that will undoubtedly aid dissection of the signaling pathways required for barrel development is to understand more fully the dynamic nature of the NRC because it is hypothesised that dynamic changes in NRC components, result in different patterns of composition within the complex and changes in the induction of plasticity (Grant and O'Dell, 2001). In order to advance understanding of NRC/PSD dynamics, a detailed knowledge of the protein composition of the NRC/PSD specifically in the barrel cortex and a study of its nature over the time period of barrel development is required. To identify novel PSD proteins in the developing barrel cortex, mass spectrometry should be performed on PSD preparations from P7 wildtype barrel cortex. Alongside this, the analysis of protein expression profiles throughout development will help to identify those components that are particularly significant during cortical development. In addition, synaptosome or PSD preparations from wildtype P7, P14 and adult barrel cortex could be sent to Kinexus^{TM} Bioinformatics Corporation (Vancouver, Canada) for their phosphatase and kinase screens to identify which phosphatases and which kinases are present at each of these developmental stages in the barrel cortex. Beyond these experiments it would then be interesting to investigate the effects caused by altering one component of the complex, on the regulation of other protein expression profiles. In this way, signaling pathways that lead to alterations in phenotypes could be constructed, enabling further understanding of which pathways are important in cortical development.

A huge limitation of the biochemical experiments suggested above however, is that the barrel cortex dissections from which PSD preparations would be isolated from in the laboratory, contain all six layers of the cortex (refer to 2.1.1) rather than just layer 4 containing the barrel synapses of interest. Resultant data would therefore reflect a global representation of synapse composition in layers 1-6 of S1 cortex. Dissection of cortical layer 4 alone is technically very difficult and also yields too small a quantity of tissue for protein fractionation and extraction. Furthermore, layer 4 dissections would still not exclusively contain TCA/layer 4 synapses because layer 4 also contains dendrites from cortical layers 2, 3 and 5. Another factor to consider is that in accordance with the dynamic nature of the NRC, it is possible that some molecules might be present in one synapse but not in others. This can certainly not

be determined using a biochemical approach, but could be addressed by looking at fluorescently tagged molecules in the synapses of layer 4 or by combining a biochemical approach with double label immunoelectron microscopy (Sans et al., 2000).

6.5 Examination of the cellular processes of barrel formation

Barrels develop as a result of four main processes, as described in Chapter 1: thalamocortical afferent segregation, cellular aggregation of layer 4 neurons, selective orientation of dendrites, and synapse formation and strengthening. Some mutant mice, like *Syngap*$^{-/-}$ mice, display a complete lack of barrel formation, whilst other mutant mice such as *Prkar2β*$^{-/-}$ and *Syngap*$^{+/-}$ mice display poorly differentiated barrels. These intermediate type barrel phenotypes require detailed methods for their analysis. In this thesis, cell counts were employed to analyse the degree of cellular segregation in mutant mice examined and the results obtained confirmed qualitative observations. A limiting factor of the cell counting method however was that the extent of cellular segregation was only measured in a single barrel of PMBSF, so variation such as a gradient of disruption across the barrelfield in S1 cortex was not taken into account quantitatively. To better assess cellular segregation throughout the barrelfield, density plot analysis might be a direction to pursue. In addition, to examine thalamocortical afferent segregation, this thesis has used immunohistochemistry for 5HT or 5HTT that provides a good overview of input segregation to the cortex. However for future analysis of mutant mice with a barrel phenotype, it would be useful to be able to investigate thalamocortical afferent morphology at the level of single axons. Single axon analysis, could be performed by injecting DiI into VpM of the thalamus.

6.6 The clinical implications of studying the molecular basis of activity-dependent cortical development

Finally, to end this thesis I'd like to reflect on the importance of conducting further research into the molecular mechanisms of barrel development. As previously explained, the anatomical and functional features of the developing cortex can be

permanently and extensively modified during a sensitive period in early childhood in response to activity (both spontaneous and sensory-evoked). To understand the molecular basis of this experience-dependent developmental plasticity in the mammalian cerebral cortex, will not only help us to understand how the mature nervous system is precisely constructed, but could also lead to the identification of fundamental defects that cause many developmental neurological disorders and childhood learning disabilities.

The NRC has been hypothesised to play an important role in cortical development and numerous links are frequently being discovered between the NRC and human mental retardation syndromes by finding gene products such as NF1, Rsk2 and L1, involved in mental retardation, present in the NMDAR complex (Weeber & Sweatt, 2002). The latest bioinformatics mining (Grant et al., 2005) revealed that over one-third of genes encoding NRC-associated proteins are important in human disease. Recent research from Mark Bear's laboratory has indicated that the primary defects in Fragile X mental retardation could result from alterations in mGluR5 signaling (Bear et al., 2004; Dolen and Bear, 2005). If this is proven to be the case, the knowledge could lead to powerful drug therapies being developed for patients. Also, SAP-102, a key MAGUK present in the NRC during cortical development has been discovered to be the gene disrupted in a form of familial X-linked mental retardation (Tarpey et al., 2004). If the biochemical pathways through which molecules such as SAP102 regulate normal development are elucidated, many novel treatments may be developed for a range of neurodevelopmental disorders.

Further insight into the extremely adaptable nature of the young brain may also have implications for treatment of adult neuronal degenerative diseases and adult mental retardation syndromes such as neurofibromatosis type 1 (NF1), and neural trauma. Perhaps in the future clinicians will be able to induce periods of heightened plasticity in mature brains that are experiencing disease or trauma to aid their recovery.

APPENDICES

Appendix 1:

Watson RF, Abdel-Majid RM, Barnett MW, Willis BS, Katsnelson A, Gillingwater TH, McKnight GS, Kind PC, Neumann PE (2006). Involvement of protein kinase A in patterning of the mouse somatosensory cortex. J Neurosci 26:5393-5401.

Development/Plasticity/Repair

Involvement of Protein Kinase A in Patterning of the Mouse Somatosensory Cortex

Ruth F. Watson,[1] Raja M. Abdel-Majid,[2] Mark W. Barnett,[1] Brandon S. Willis,[3] Alla Katsnelson,[1] Thomas H. Gillingwater,[1] G. Stanley McKnight,[3] Peter C. Kind,[1]* and Paul E. Neumann[2]*

[1]Centre for Integrative Physiology, Centre for Neuroscience, University of Edinburgh, Edinburgh EH8 9XD, United Kingdom, [2]Department of Anatomy and Neurobiology, Dalhousie University, Halifax, Nova Scotia, Canada B3H 1X5, and [3]Department of Pharmacology, University of Washington, Seattle, Washington 98195

Patterning of the mouse somatosensory cortex is unusually evident because of the presence of a "barrel field." Presynaptic serotonin and postsynaptic glutamate receptors regulate barrel formation, but little is known of the intracellular signaling pathways through which they act. To determine whether protein kinase A (PKA) plays a role in the development of the barrel field, we examined five viable PKA subunit-specific knock-out (KO) mouse lines for barrel field abnormalities. Barrels are present in these mice, but those lacking the RIIβ subunit display significantly reduced contrast between the cell densities of barrel hollows and sides compared with wild-type animals. Thalamocortical afferent segregation in the posterior medial barrel subfield appeared normal, suggesting a postsynaptic site of gene action for the RIIβ protein. Immunoelectron microscopy confirmed that RIIβ was selectively localized to dendrites and dendritic spines. Mice lacking RIIβ show reduced glutamate receptor A (GluRA) subunit insertion into the postsynaptic density in postnatal day 7 somatosensory cortex; however, GluRA KO mice developed normal barrels. Our results clearly demonstrate a role for postsynaptic PKA signaling pathways in barrel differentiation. They also demonstrate a clear dissociation between the regulation of GluRA trafficking by PKA and its role in barrel formation. Finally, although a role for PKA downstream of cAMP cannot be ruled out, these data suggest that PKA may not be the principle downstream target because none of the mutants showed a barrelless phenotype similar to that observed in adenylate cyclase type 1 KO mice. These results give insight into activity-dependent mechanisms that regulate barrel formation.

Key words: barrel; cAMP; protein kinase A; somatosensory cortex; development; NMDA receptor

Introduction

A fundamental concept of the structure and function of the cerebral cortex is arrangement of sensory and motor systems into distinct topographically defined domains. In the primary somatosensory cortex (SI) of rodents, periphery-related patterns of sensory receptors are recapitulated in layer IV as an array of multineuronal structures ("barrels") called the barrel field (Woolsey and Van der Loos, 1970). In barrels, neurons are arranged in cylindrical or oval-shaped rings that are separated from their neighbors by hypocellular "septa." In mice, cell-dense barrel walls surround a cell-sparse "hollow" that contains thalamocortical afferent (TCA) terminals (Woolsey and Van der Loos, 1970).

Postsynaptic glutamate signaling regulates barrel formation (Erzurumlu and Kind, 2001; Kind and Neumann, 2001). Genetic ablation of either metabotropic glutamate receptor 5 (mGluR5) (Hannan et al., 2001) or cortical NR1 (Iwasato et al., 2000), the essential subunit of the NMDA receptor, results in a complete loss of cellular segregation in layer IV despite at least partial segregation of TCAs. Serotonin signaling also regulates barrel formation (Gaspar et al., 2003). Overexpression of 5-HT causes a near-complete loss of barrels that can be rescued by ablation of presynaptic 5-HT_{1B} receptors (Salichon et al., 2001). Although much is known about the neurotransmitter receptors that regulate barrel formation, little is known of the intracellular signaling pathways through which they act.

Several findings suggest a role for cAMP-dependent protein kinase A (PKA) in barrel formation. PKA is present in both axon terminals and postsynaptic densities (PSDs) and can be regulated by 5-HT_{1B}, NMDA, and mGlu5 receptors. Furthermore, *adenylate cyclase type 1* (*Adcy1*) mutant mice are "barrelless," showing no TCA segregation or cellular segregation in layer IV (Welker et al., 1996; Abdel-Majid et al., 1998). Loss of adenylate cyclase type 1 (AC1) may cause a barrelless phenotype by altering 5-HT_{1B} regulation of cAMP/PKA activity in TCAs, thereby reducing glutamate release (Abdel-Majid et al., 1998; Laurent et al., 2002). Direct evidence for a presynaptic site of action for AC1 comes from the finding that TCA segregation and cortical cell clustering is normal in mice with a cortex-specific deletion of AC1 (Iwasato et al., 2005).

A postsynaptic role for PKA in barrel formation has also been hypothesized (Kind and Neumann, 2001). PKA is involved in

Received Oct. 12, 2005; revised March 23, 2006; accepted March 25, 2006.

This work was supported by the Medical Research Council of Great Britain (P.C.K.), the Wellcome Trust (P.C.K.), the Medical Research Council of Canada (Grant MA-14218 to P.E.N.), and the National Institutes of Health (G.S.M.). We thank Rolf Sprengel for supplying the GluRA KO mice.

*P.C.K. and P.E.N. contributed equally to this work.

Correspondence should be addressed to Peter C. Kind, Centre for Integrative Physiology, Centre for Neuroscience, University of Edinburgh, Hugh Robson Building, George Square, Edinburgh EH8 9XD, UK. E-mail: pkind@ed.ac.uk.

DOI:10.1523/JNEUROSCI.0750-06.2006

 0270-6474/06/265393-09$15.00/0

long-term potentiation (LTP) and long-term depression at developing TCA synapses (Lu et al., 2003), and it also plays a crucial role in developing visual cortex plasticity (Beaver et al., 2001; Fischer et al., 2004). PKA is a heterotetramer composed of two regulatory (R) and two catalytic (C) subunits. Four regulatory (*Prkar1a*, *Prkar1b*, *Prkar2a*, and *Prkar2b*) and two catalytic (*Prkaca* and *Prkacb*) subunit genes have been identified and disrupted by homologous recombination (Brandon et al., 1997). Loss of the RIα subunit in *Prkar1a* knock-out (KO) mice is an embryonic lethal condition (Amieux et al., 2002). To determine whether PKA plays a role in barrel formation, we examined the barrelfield morphology in the five viable PKA null mutant mice.

Materials and Methods

Animals. Targeting of embryonic stem cells, establishment of chimeras, and mouse lines carrying mutations in the Cα, Cβ, RIα, RIβ, and RIIβ PKA subunit genes have been described (Brandon et al., 1995, 1998; Qi et al., 1996, Skalhegg et al., 2002). For initial analysis of barrel phenotype, mice were maintained at University of Washington, Seattle. Ten-week-old mice, from different litters, homozygous for targeted disruptions of the PKA subunit genes RIβ ($n = 3$), RIIα ($n = 3$), RIIβ ($n = 8$), Cα ($n = 3$), and Cβ ($n = 3$) were given a lethal dose of sodium pentobarbitol and then were perfused transcardially with 0.1 M PBS, pH 7.4, followed by 4% chilled paraformaldehyde in 0.1 M PBS. Brains were postfixed for 24 h in the same fixative and transported to Dalhousie University for subsequent analysis. Brains were sectioned serially parallel to the pial surface overlying the SI at a thickness of 50 μm using a vibratome. Sections were mounted on gelatin-coated slides, dried overnight, and then stained either with cresyl violet (Nissl) stain or cytochrome oxidase (CO) histochemistry. CO histochemistry was performed as described by Wong-Riley (1979). After completion of the staining reaction, sections were rinsed, dehydrated through series of alcohol, cleared in xylene, and coverslipped. For further analysis of RIIβ KO mice, mice were maintained at the University of Edinburgh on a C57BL/6J background. GluRA KO mice (Zamanillo et al., 1999) were obtained from Dr. Rolf Sprengel (Max-Planck-Institut für medizinische Forschung, Heidelberg, Germany).

Histology and immunohistochemistry. Animals ranging in age from postnatal day 4 (P4) to adult were killed and perfused as above, then brains were removed and postfixed for at least 6 h in 4% paraformaldehyde, and then equilibrated overnight in 30% sucrose. Brains were sectioned (48 μm) on a freezing microtome either coronally to reveal cortical layers and thalamic nuclei or tangential to the pial surface to reveal a full barrel field. For tangential sections, cortices were dissected from the thalamus and the hippocampus and striatum removed. The cortex was then flattened on the freezing microtome stage with the pial surface facing up. Sections were either mounted on gelatin-coated slides and stained with cresyl violet or thionin to reveal cellular distribution or placed in primary antibodies, free floating overnight, to reveal the localization of PKA RIIβ, serotonin transporter (SERT), or GluRA. All immunohistochemistry was performed according to previously described protocols (Hannan et al., 2001; Vitalis et al., 2002) with the following exceptions. Two diluents were used for incubation of tissue in primary and secondary antibodies. Initially antibodies were diluted in PBS containing 0.2–0.5% Triton X-100. This protocol was changed to dilution in DMEM containing 5% fetal calf serum and 0.2–0.5% Triton X-100 because it reduces nonspecific background staining (Kind et al., 1994). Sections for immunohistochemistry were incubated overnight in rabbit anti-mouse PKA RIIβ (1:600–1:2000; Santa Cruz Biotechnology, Santa Cruz, CA), goat anti-rabbit GluRA (1:250; Upstate Biotechnology, Lake Placid, NY), or goat anti-rabbit SERT (1:2000; Calbiochem, La Jolla, CA), followed by biotinylated anti-rabbit antibodies. Visualization was performed using a Vectastain ABC kit (Vector Laboratories, Burlingame, CA) with DAB as the chromogen. In all cases, sections were dehydrated into xylene and coverslipped. For cell counts, 48 μm tangential sections were immunolabeled for SERT (as above), but visualized using an AlexaFluor 568-conjugated goat anti-rabbit secondary antibody (1:200; Invitrogen, San Diego, CA). To reveal nuclei, free-floating sections were then counterstained by incubating them for 30 min in a solution containing Topro (1:1000; Invitrogen). Sections were rinsed in PBS, mounted on gelatin-coated slides, and coverslipped in PBS–glycerol (3:1, w/v).

Area measurements. All area measurements were obtained from tangential sections stained with anti-SERT antibody as described above. Images were captured at magnifications of 31.25× (S1 cortex area), 62.5× [posterior medial barrel subfield (PMBSF) area], and 125× (C1 barrel area, cortical thickness and cortical layer thickness measurements) using a Leica (Nussloch, Germany) DMLB microscope, Leica 480 digital camera, and the Leica DMLB Image Manager version 4.0 program. Area measurements were then performed on the digitized images using Image Tool for Windows version 3.0 software (University of Texas Health Science Centre at San Antonio, San Antonio, TX). Each image measurement was calibrated using a 1 mm graticule (Graticules, Tonbridge, Kent, UK). Results are reported as mean ± SEM.

Cell counts. Sections stained with anti-SERT antibody and Topro were used for counting cells. Three to four adjacent sections containing the barrel-field representation were analyzed for each animal. From these sections, the position of individual barrels were determined, and a series of confocal images (Leica) of B3 and its neighboring barrels were taken with 7 μm intervals using the 10 and 20× objectives. Morphometric analysis was performed with the Leica software (TCNST). For each series of optical images, the section containing the clearer representation of the barrel of interest was used to start the analysis. On this selected section, three rectangles along the B2–B4 axis, one containing the B2–B3 wall, one the B3 hollow, and one the B3–B4 wall, were drawn to calculate the density of Topro-stained nuclei in each rectangle. Measurements were done on the selected section and on the two adjacent sections (upper and lower). From these data, the average density of Topro-stained nuclei in the walls and hollow of the chosen barrel was calculated. Results are reported as means of average densities ± SEM.

Immunoelectron microscopy. Animals for electron microscopy were perfused as above, except that 0.1% glutaraldehyde was included in the fixative. Fifty-millimeter-thick vibratome sections were placed in 1:200 dilution of anti-RIIβ antibody overnight at 4°C in the absence of detergent and reacted for DAB histochemistry as described above. They were then postfixed in 1% osmium tetroxide in 0.1 M phosphate buffer for 45 min. After dehydration through an ascending series of ethanol solutions and propylene oxide, all sections were embedded on glass slides in Durcupan resin. Regions of cortex (~1 × 1 mm^2) to be used for assessment were then cut out using a scalpel and glued onto a resin block for sectioning. Ultrathin sections (~70 nm) were cut and collected on Formvar-coated grids (Agar Scientific, Stansted, UK), stained with uranyl acetate and lead citrate in a LKB-Wallac (Gaithersburg, MD) Ultrostainer, and then assessed in a Philips CM12 transmission electron microscope. Negatives taken in the microscope were scanned onto a Macintosh G5 computer (Apple Computers, Cupertino, CA) using an Epson (Long Beach, CA) 4870 photo flat-bed scanner at 1200 dots per inch, before being prepared for presentation in Adobe Photoshop (Adobe Systems, San Jose, CA).

Protein kinase A activity. The area of the SI of 1-week-old wild-type (WT; $n = 3$) and RIIβ knock-out ($n = 4$) mice was excised and immediately immersed in liquid nitrogen. Protein homogenates were prepared in cold homogenization buffer (20 mM Tris, pH 7.6, 250 mM sucrose, 1 mM EGTA, 5 mM EDTA, 10 mM dithiothreitol, 5 mM magnesium acetate, 1% Triton X-100, 1 μg/ml leupeptine, 3 μg/ml aprotinin, 5 mM 4-(2-aminomethyl)benzenesulfonylfluoride hydrochloride, 0.1 mg/ml soybean trypsin inhibitor) using a Polytron, followed by brief sonication and centrifugation at 10,000 rpm at 4°C. Protein concentration was estimated using the Bradford assay (Bio-Rad, Hercules, CA), and samples were diluted to 2–3 mg of protein/ml. Total and basal cAMP-dependent protein kinase (PKA) activities were measured with Kemptide substrate as described previously (Clegg et al., 1987), in the presence and absence of 5 μM cAMP, respectively. Nonspecific kinase activity that remained in the presence of the PKA inhibitor PKI was subtracted from both basal and total PKA activity.

Synaptosome and PSD preparations. Synaptosome preparations were prepared according to the methods of Dunkley et al. (1986). We used a strong homogenization step leaving little if any membrane attached to

Figure 1. RIIβ KO mice show reduced segregation of neurons in SI cortex. ***A***, Western blot analysis of synaptosome preparations revealed immunoreactive protein for RI, RIIα, RIIβ, and C subunits. Although antibodies specific for each of the RI and C subunits were not used, this result indicates that several different PKA holoenzymes are present at synapses throughout postnatal development of the barrel cortex. Whether these subunits are in the presynaptic terminal or part of the postsynaptic density could not be determined using this preparation. ***B***, Digitized images of cresyl violet (Nissl)-stained sections of layer IV of the SI of adult wild-type mice and RIβ, RIIα, RIIβ, Cα, and Cβ null mutant (knock-out) mice. Barrels are present in PKA subunit-specific knock-out mice; however, mice lacking the RIIβ subunit have poorly differentiated barrels. Scale bar, 200 μm.

the postsynaptic density; therefore, it contains a presynaptic terminal and postsynaptic proteins associated with the PSD. Briefly, SI cortex was homogenized in a 320 mM sucrose solution (pH 7.4, containing 1 mM EDTA and 5 mM Tris) and poured onto Percoll gradients (3 ml layers of 24, 10, and 3% Percoll), which were centrifuged for 12 min at 15,000 rpm at 4°C. Synaptosomes were removed from between the 24 and 10% Percoll layers and spun for 30 min at 13,000 rpm in ice-cold 320 mM sucrose solution. The resulting synaptosome pellet was then resuspended and centrifuged in cold Krebs' buffer (containing NaCl, KCl, $MgSO_4$, glucose, $Na_2HPO_4 \cdot 12H_2O$, and HEPES) without Ca^{2+} at 13,000 rpm for 10 min, twice in succession. Synaptosomes were treated with lysis buffer [50 mM HEPES, pH 7.5, 1% Triton X-100, 50 mM NaCl containing protease inhibitors, phosphatase inhibitor mixtures I and II (P2850 and P5276; Sigma, St. Louis, MO)]. The PSD fraction was then pelleted by two successive centrifugations, in the presence or absence of Ca^{2+} (100 μm), at 36,800 × *g* for 45 min.

Western blotting. Mice were killed either by cervical dislocation or decapitation and SI cortices dissected from P4, P7, P14, P21, and adult mice were immediately frozen on dry ice and stored at −70°C. For developmental analysis, barrel cortices were homogenized in lysis buffer (50 mM HEPES, pH 7.5, 1% Triton X-100, 50 mM NaCl containing protease inhibitors, phosphatase inhibitor mixtures I and II). Protein concentrations were determined by Bradford assays, and immunoblot analysis was performed according to the methods of Kind et al. (1994). Briefly, 10 μg of protein were loaded per lane of each age on a 7 or 10% polyacrylamide gel with a 4% stacking gel. The proteins were then transferred to nitrocellulose membranes, which were then stained with amido black to confirm equal loading of protein. The blots were then incubated in primary antibody overnight [GluRA, 1:1000, Upstate Biotechnology; RIIβ, 1:600, Santa Cruz Biotechnology; PKA RI (RI), 1:500, BD Transduction Labs, San Diego, CA; PKAC (C), 1:1000, BD Transduction Labs; RIIα, 1:1000, BD Transduction Labs; synapse-associated protein-102 (SAP-102), 1:5000, Chemicon; PSD-95, 1:20,000, Upstate Biotechnology] at room temperature before being placed in secondary antibodies (anti-mouse IgG, 1:10,000; anti-rabbit IgG, 1:25,000; anti-goat IgG, 1:50,000; Sigma), coupled to HRP for 1–2 h. Proteins were visualized either using ECL reagents (Pierce, Rockford, IL) and XAR Kodak (Eastman Kodak, Rochester, NY) autoradiographic film or fluorescently coupled anti-rabbit (1:5000; Rockland, Gilbertsville, PA) or mouse (1:5000; Invitrogen) secondaries and visualized using the LiCor system. Densitometry was performed using either the Bio-Rad GS710 imager using the Bio-Rad Quantity One imaging software or the LiCor Odyssey imaging system and densitometry performed using NIH ImageJ software.

Analysis of gene expression using real-time reverse transcription-PCR. SI was dissected from P4, P7, P14, P21, and adult mice, frozen on dry ice, and stored at −70°C. Total RNA was extracted using an RNeasy mini-kit (Qiagen, Hilden, Germany) and an RNase-free DNase set (Qiagen). Total RNA was run on 0.8% agarose gel to ensure that RNA was not degraded (28S ribosomal band was well defined and double the intensity of 18S ribosomal band) or the sample was discarded. First-strand cDNA synthesis was performed as described by Barnett et al. (1998). Real-time reverse transcription-PCR (RT-PCR) was performed using MJ Research (Watertown, MA) DNA Engine Opticon and Quantitect SYBR green PCR kit (Qiagen). In each PCR reaction, 1 μl of cDNA was combined with gene-specific primers (0.5 μM) and 12.5 μl of QuantiTect SYBR green PCR master mix to a total volume of 25 μl. To compare expression levels at different developmental stages, a dilution series of control cDNA was made and assayed in each Opticon run. The dilution series was used from cDNA of the developmental stage predicted to give the highest expression of the gene product being amplified. Other controls performed in each run were RT and water blanks.

At the end of each run, melting curve analysis was performed between 60 and 90°C, single melting peak demonstrated specific product. OpticonMonitor analysis software (version 1.01) was used to compare amplification in experimental samples during the log-linear phase to the standard curve from the dilution series of control cDNA. Comparisons were displayed as histograms. 18S rRNA and glyceraldehyde-3-phosphate dehydrogenase were used as a loading control, and each bar was normalized to the level of 18S rRNA expression. The following primer sets specific for each PKA subunit were checked using basic local alignment search tool: RIIβ-forward (RIIβ-F), 5′-TAAACCGGTTCACAAGGCGTG-3′; RIIβ-reverse (RIIβ-R), 5′-GTTACCGACGCATCTTCCAAC-3′; RIIα-F, 5′-CGTCGTCGCCTTGGTCAATG-3′; RIIα-R, 5′-TGAGCAGAGATGCCGGCTTC-3′; RIα-F, 5′-TGGAGAGCTGGCTTTGATTTA-3′; RIα-R, 5′-GCTGTGCCCTCTAAAATGATG-3′; RIβ-F, 5′-GGGGAAACAGTCATACAGCAA-3′, RIβ-R, 5′-CTCCAGGGATTCTAGGATGGA-3′; Cα-F, 5′-GAATACAGCCCAGTTGGATCA-3′; Cα-R, 5′-CTCGCCACCAGCTACATACTC-3′; Cβ-F, 5′-GGGGAACACTGCGATCGCCAA-3′; Cβ-R, 5′-CCAGGGACGTATTCCATAACC-3′; 18S-F, 5′-GTGGAGCGATTTGTCTGGTT-3′; 18S-R, 5′-CAAGCTTATGACCCGCACTT-3′.

Results

Morphology of cortical barrelfield in PKA mutant mice

To determine which PKA subunits are present at synapses in the developing barrel cortex, we performed Western blot analysis on synaptosome preparations (Fig. 1*A*) from developing barrel cortices. These synaptosome preparations use a strong initial homogenization so they consist of presynaptic terminals with attached PSDs. Little, if any, postsynaptic membrane remains attached to the PSD. All PKA subunits were present in synaptosomes through barrel cortex development. As expected, because of the rapid increase in synaptogenesis between P4 and P21 (White et al., 1997; Spires et al., 2005), total protein isolated from synaptosomes increased approximately fivefold during this time (data not shown), and expression of PKA subunits also increased during this time period. mRNA for all six of the PKA subunits were examined in developing SI cortex at all ages examined by real-time quantitative RT-PCR (supplemental Fig. 1, available at www.jneurosci.org as supplemental material). Similar to the Western blot analysis, mRNA for all PKA subunits were present throughout postnatal development, although there was often discordance between protein and mRNA levels. This appears to be a common feature of PSD-associated molecules and may be because of the rapid turnover of synapses and hence synaptic proteins during development (Barnett et al., 2006). Using ANOVA and linear regression analysis, only *Prkar2b* and *Prkarca* showed significant trends in variation of expression levels with age.

Examination of the barrelfield using Nissl-stained sections revealed the presence of barrels in all five of the subunit-specific PKA knock-out mouse lines; however, one mutant line displayed defects in barrel morphology (Fig. 1*B*). In adult (10-week-old) RIIβ KO mice, barrels were hard to discern because the cell density appeared more uniform across septa and barrel hollows relative to the barrel sides than in WT animals or mice heterozygous for the RIIβ null mutation. All other subunit specific mutants revealed normal cellular segregation with clear barrel walls, hollow, and septas in PMBSF. All five subunit-specific PKA knock-out mouse lines displayed normal barrel-like patches in cytochrome oxidase-stained sections of the SI (data not shown).

To elucidate the cellular mechanisms by which RIIβ may be regulating barrel formation, we examined the expression pattern of the RIIβ protein through development. RIIβ is most strongly expressed in layer IV of the cortex of WT mice at P4 and P7 (Fig. 2*A*,*B*, respectively), where staining appears as diffuse neuropilar patches. That these patches correspond to the barrels was confirmed in tangential sections through layer IV at P7 where RIIβ is at highest levels in SI (Fig. 2*C*). No immunoreactive product was seen in brains from RIIβ KO mice, confirming the specificity of the antibody for the RIIβ protein (supplemental Fig. 2, available at www.jneurosci.org as supplemental material).

We then examined the precise nature of the defects present in the RIIβ null mutant mice at younger ages. Nissl-stained sections of 7-d-old WT and RIIβ KO mice revealed decreased cellular segregation similar to that found in adults (Fig. 2*D–G*). In PMBSF, barrel walls and hollows can be seen, but cellular segregation is reduced. No barrels are visible in the anterior snout (AS) region. The cell densities in barrel walls and hollows were calculated to permit quantitative analysis of the segregation of cells in the barrelfields of WT and RIIβ KO mice. Tangential sections were double-labeled by Topro staining (for nuclei) and SERT immunohistochemistry (for TCAs to identify barrel hollows) (supplemental Fig. 3*A*, available at www.jneurosci.org as supplemental material). Nuclei were counted in images of 7 μm optical sections obtained using the confocal microscope (supplemental Fig. 3*B*, available at www.jneurosci.org as supplemental material). The ratio of cell density in the barrel wall to that in the hollow was significantly less in RIIβ KO mice than in WT mice (supplemental Fig. 4, available at www.jneurosci.org as supplemental material), confirming our qualitative assessment. No differences in overall density of cells in layer IV were seen, indicating that cell death was unaltered in the RIIβ mutants.

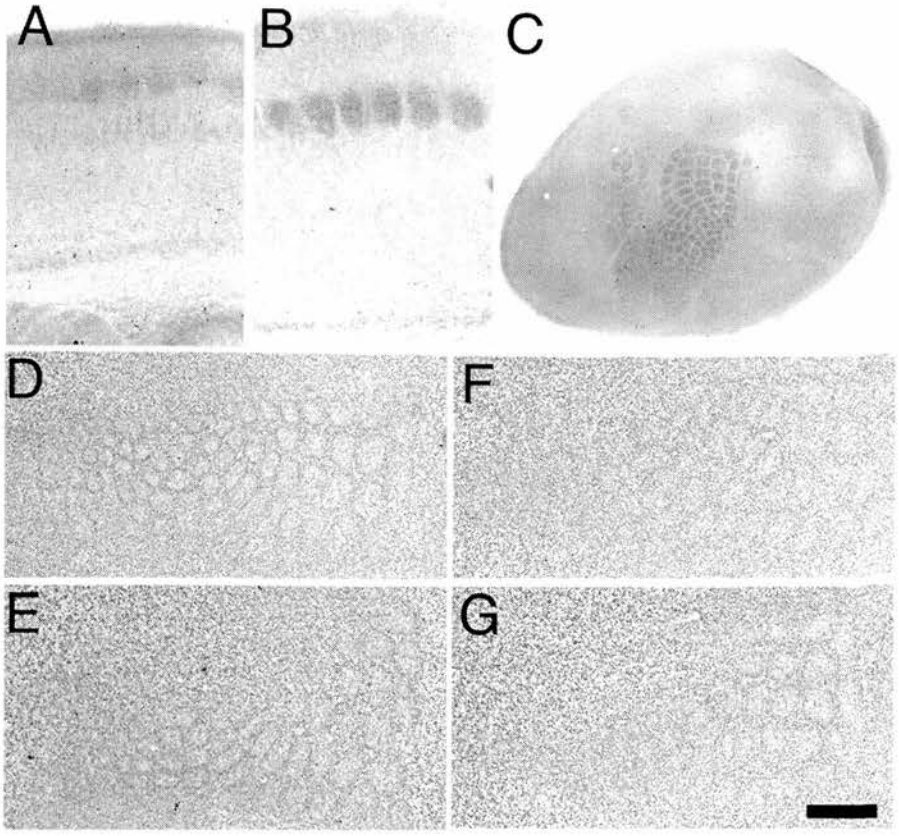

Figure 2. Decreased cellular segregation in PMBSF in RIIβ KO mice. ***A***, ***B***, Immunostaining for RIIβ in coronal sections of WT mice shows high levels of the protein in layer IV of SI cortex at both P4 (***A***) and P7 (***B***). A tangential section through layer IV (***C***) of P7 WT mice shows clear localization of RIIβ to barrel hollows. ***D–G***, Digitized images of pairs of adjacent Nissl-stained sections through layer IV of the SI of P7 WT (***D***, ***E***) and RIIβ KO (***F***, ***G***) mice are shown. In RIIβ KO mice, barrels can be seen in PMBSF; however, segregation of cells appears reduced and few barrels are visible in the anterior snout region. To quantify the degree of segregation in PMBSF, tangential sections through layer IV from P7 WT and RIIβ KO mice were stained with Topro to label nuclei and immunostained using anti-SERT antibodies to label TCAs (supplemental Fig. 3, available at www.jneurosci.org as supplemental material). Blind analysis of the cell densities of barrel walls and hollows (supplemental Fig. 4, available at www.jneurosci.org as supplemental material) showed a significant decrease in the wall-to-hollow ratio in RIIβ KO ($n = 5$) mice relative to that of WT ($n = 5$) mice (1.32 ± 0.03 vs 1.76 ± 0.05, respectively; $p = 0.0001$, 2-sample t test). Scale bar: (in ***G***) ***A***, ***B***, 250 μm; ***C***, 750 μm; ***D–G***, 200 μm).

Role of RIIβ in TCA segregation

To determine whether RIIβ plays a role in TCA segregation, we next examined CO and SERT staining in RIIβ KO mice. The normal pattern in WT and RIIβ KO mice contrasts markedly with the diffuse staining of the layer IV in barrelless ($Adcy1^{brl}$) mutant mice (Welker et al., 1996) (data not shown). The implication that segregation of TCAs in PMBSF is normal in RIIβ KO mice was confirmed with SERT immunohistochemistry (Fig. 3*A*,*B*). No difference in patch size and distribution of TCAs was seen in PMBSF in P7 mice. This qualitative assessment was confirmed by measuring the area of individual patches sizes and the overall size of PMBSF. No differences were found between WT and RIIβ KO mice in size of the PMBSF or in the size of individual TCA patches (supplemental Fig. 4, available at www.jneurosci.org as supplemental material). In the AS subregion, a different pattern emerged. RIIβ KO animals showed a clear reduction in TCA segregation (Fig. 3*A*,*B*; supplemental Fig. 5, available at www.jneurosci.org as supplemental material). Individual TCA patches became difficult to identify. Although TCA segregation was reduced within the AS, the major demarcations between AS and other subregions within SI were not disrupted (Fig. 3*A*,*B*, arrows), indicating that the loss of RIIβ impairs segregation within AS rather than causing a more general defect in TCA pathfinding. Hence, the barrel phenotype of the RIIβ KO mice is similar to those of the phospholipase C-β1 (PLC-β1), mGluR5,

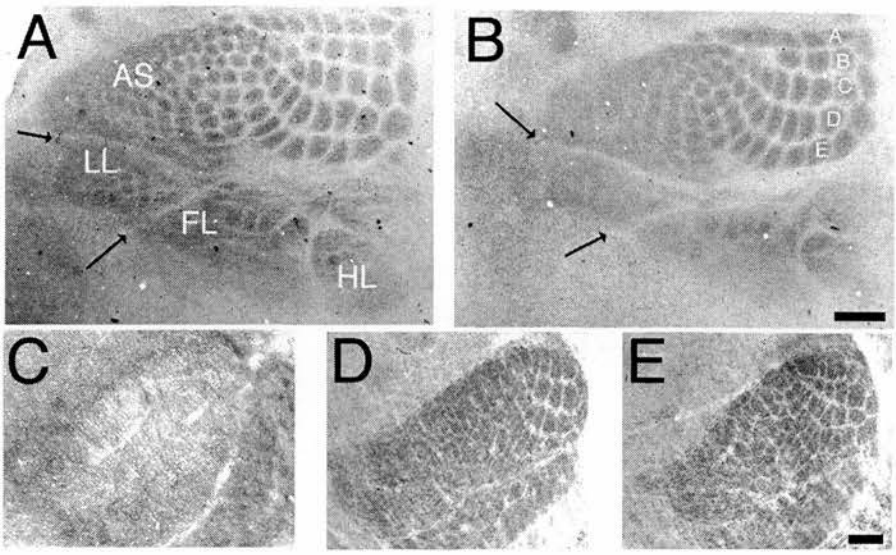

Figure 3. TCAs segregate normally in PMBSF but not in anterior snout regions in RIIβ KO mice. ***A***, ***B***, SERT immunohistochemical staining of tangential sections through layer IV at P7 reveals clear TCA patches in PMBSF in WT (***A***) and RIIβ KO (***B***) mice. In RIIβ KO mice, staining appears more uniform in the AS regions with only the largest, more dorsomedial, patches being visible. The demarcations between different subregions (arrows) of SI were clearly visible in both WT and RIIβ KO mice, indicating that the loss of segregation within AS is not a result of a general problem of TCA pathfinding in this region. LL, Lower lip; FL, forelimb; HL, hindlimb. The five main rows barrels representing the five rows of mystacial vibrissas on the facepad are labeled as A–E in ***B***. To assess TCA segregation in PMBSF, area measurements of PMBSF and TCA patches of barrels B2, B3, C2, C3, D2, and D3 were performed blind to genotype (supplemental Fig. 4, available at www.jneurosci.org as supplemental material) on five WT and six RIIβ KO P7 mice. No significant differences in any of these measurements were observed (PMBSF, $p = 0.66$; B2, $p = 0.30$; B3, $p = 0.43$; C2, $p = 0.36$; C3, $p = 0.39$; D2, $p = 0.55$; D3, $p = 0.47$). RIIβ is expressed in developing SI and VpM, but barreloids form normally in RIIβ KO mice. RIIβ is expressed at low levels in VpM and barreloids appear normal in RIIβ KO mice. ***C***, At P7, RIIβ immunostaining can be seen throughout VpM with highest levels in the inter-barreloid regions. ***D***, ***E***, Cytochrome oxidase staining of coronal sections through the VpM nucleus of P7 WT (***D***) and RIIβ KO (***E***) mice revealed clear barreloids even in the regions representing the anterior snout whiskers. Scale bar: (in ***B***) ***A***, ***B***, 200 μm; (in ***E***) ***C–E***, 80 μm.

and cortex-specific NR1 (Erzurumlu and Kind, 2001; Kind and Neumann, 2001) knock-out mice in that no cortical barrels are present despite at least partial segregation of TCAs. These findings are consistent with a postsynaptic role for PKA signaling in barrel formation.

Further support for a role for cortically expressed RIIβ in barrel development was provided by analysis of barreloid formation in the thalamic ventral posterior medial (VpM) nucleus that projects to SI. Immunohistochemistry for RIIβ reveals a diffuse staining throughout thalamus at P7. In VpM, the inter-barreloid regions are the most deeply stained with low levels of staining in the center of the barreloids (Fig. 3*C*). Barreloid segregation within VpM, examined using cytochrome oxidase histochemistry, in RIIβ KO mice ($n = 7$) appeared indistinguishable from that in WT mice (Fig. 3*D*,*E*).

RIIβ is expressed in the PSD of layer IV synapses

RIIβ associates with mature PSDs via its interaction with A-kinase anchor proteins (AKAPs). To determine whether RIIβ selectively associates with PSD in developing SI, we performed immunoelectron microscopy of layer IV of P14 SI cortex. RIIβ localizes to some, but not all, dendrites and dendritic spines (Fig. 4). The postsynaptic density was particularly strongly stained by the DAB reaction product. The absence of RIIβ at some synapses was not a result of poor antibody penetration, because immunopositive dendrites (Fig. 4*D*,*E*, asterisks) were visible adjacent to the immunonegative synapses. The RIIβ–AKAP–PSD-95 complex has been shown to associate with the PSD in a Ca^{2+}-dependent manner (Colledge et al., 2000; Snyder et al., 2005). To determine whether the association of RIIβ with the PSD is dependent on Ca^{2+} in developing SI, we isolated PSDs from P7 SI cortex in the presence or absence of 100 μm Ca^{2+} (Fig. 4*F*). In the presence of Ca^{2+}, RIIβ is in the soluble fraction, and in the absence of Ca^{2+}, it associates with the pellet fraction.

Expression of other subunits in RIIβ KO mice

The expression of PKA subunit genes and the activity of PKA in postnatal SI cortex were examined in P7 WT and RIIβ KO mice to determine whether there are any compensatory changes in PKA subunit expression in RIIβ KO mice. Western blots of homogenates from WT and RIIβ KO animals (Fig. 5*A*) did not detect differences in the levels of other PKA regulatory subunits. The level of C subunits was reduced by 35% in RIIβ KO mice compared with WT, but this difference was not significant [720 optical density units (ODU) ± 116, $n = 4$ vs 1107 ODU ± 180, $n = 4$; t test, $p = 0.12$] (supplemental Fig. 4, available at www.jneurosci.org as supplemental material). Reduced catalytic subunits in adult forebrain of RIIβ KO mice has been reported previously (Brandon et al., 1995, 1998). In agreement with the apparent lack of compensation by other subunits in the RIIβ KO mice and with the suggestion of lower levels of catalytic subunits, we found that total protein kinase A activity was reduced by 40% in SI of 1-week-old RIIβ knock-out mice relative to wild-type controls (t test, $p = 0.006$) (Fig. 5*B*). The higher basal PKA activity in RIIβ KO mice ($p = 0.0004$) may be because of constitutive activity of C subunits (Niswender et al., 2005).

RIIβ, the PSD, and GluRA

Previous findings from several laboratories have indicated a crucial role for PKA in regulating GluRA insertion into the PSD during plasticity (Malinow and Malenka, 2002). GluRA, an AMPA receptor subunit also known as GluR1, is present throughout SI cortex at both P4 (data not shown) and P7 (Fig. 6*A*,*B*). Specificity of the antibody was confirmed by the complete absence of staining in GluRA KO animals (supplemental Fig. 2, available at www.jneurosci.org as supplemental material). Staining was seen throughout the cortex and labels both neuronal soma and neuropil consistent with a synaptic localization. In layer IV (Fig. 6*B*), clear neuronal and neuropilar staining is visible; however, the neuropilar staining is somewhat reduced compared with other layers. GluRA is also expressed in developing VpM, but levels appear low compared with both cortex and the rest of the thalamus (Fig. 6*C*).

To determine whether loss of RIIβ would disturb the role of PKA in regulating GluRA insertion into the PSD during barrel formation, we examined the level of GluRA in synaptosome preparations from P7 SI cortex (Fig. 6*E*,*F*). There was a significant reduction in GluRA expression in RIIβ KO mice relative to WT animals but no reduction in the levels of PSD-95 (data not

shown) or SAP-102 (Fig. 6*F*; supplemental Fig. 4, available at www.jneurosci.org as supplemental material). To determine whether this disruption of the regulation of GluRA insertion could be responsible for the defects in barrel segregation observed in the RIIβ KO mice, we examined the barrel field of GluRA KO mice ($n = 4$) in Nissl-stained tangential sections through layer IV (Fig. 6*D*). Barrel segregation appeared normal with good segregation in both PMBSF and anterior snout whisker regions. These data indicate that although RIIβ-containing PKA holoenzymes regulate GluRA insertion in developing cortical synapses, this insertion does not appear to play a role in barrel development.

Discussion

One of the five viable PKA subunit-specific knock-out mouse lines examined here displayed poorly defined barrels. In mice lacking the RIIβ subunit, the contrast in cell density of the barrel hollows relative to the sides was dramatically reduced. Although there were defects in segregation of TCAs in the anterior snout whisker region, segregation of the TCAs in the PMBSF appeared normal. The finding that RIIβ KO mice had the poorest barrel morphology may not be surprising because they have the largest reported decrease in PKA activity and other signs of neurologic disorder (Brandon et al., 1997, 1998). PKA activity is reduced by 40% in the primary somatosensory cortex of 1-week-old RIIβ KO mice, with no evidence of compensation in the expression of other PKA regulatory subunits.

The site of gene action in RIIβ KO mice appears to be postsynaptic in barrel cortex because RIIβ was immunolocalized to dendrites and dendritic spines and because the barrelfield phenotype resembles that of PLC-β1 and cortex-specific NR1 KO mice (Iwasato et al., 2000; Hannan et al., 2001). The Ca^{2+}-dependent association of RIIβ with the PSD in SI indicates that it is acting downstream of glutamate receptor signaling to regulate barrel development. Finally, mice lacking RIIβ show reduced GluRA insertion into the PSD in P7 SI cortex; however, this reduction is unlikely to regulate barrel formation because GluRA KO mice develop normal barrels. Our results clearly demonstrate a role for postsynaptic PKA signaling pathways in barrel differentiation and are in complete agreement with previous studies showing that glutamate neurotransmission is critical for barrel formation (Fox et al., 1996; Iwasato et al., 2000; Hannan et al., 2001; Barnett et al., 2006).

We also conclude that RIIβ-containing PKA holoenzymes are not the downstream targets of AC1 in the pathway responsible for the barrelless (*Adcy1*^{brl}) trait, because the phenotype of RIIβ KO mice differs markedly from those of *Adcy1*^{brl} mutant (Welker et al., 1996; Abdel-Majid et al., 1998) and monoamine oxidase A (Cases et al., 1995, 1996) and SERT (Salichon et al., 2001) KO mice.

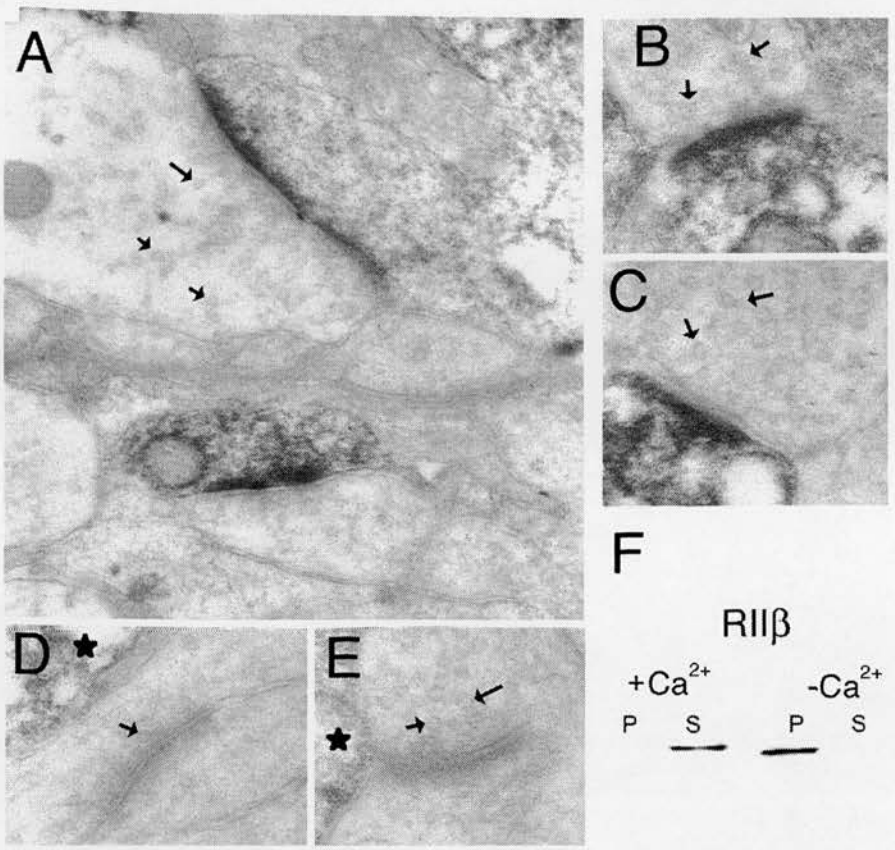

Figure 4. RIIβ is postsynaptic in developing SI cortex. ***A–C***, Electron micrographs of layer IV of P14 barrel cortex reveal dark RIIβ immunoreaction product within postsynaptic densities and dendrites (***A–C***), but not of presynaptic terminals. Synapses can be clearly identified by the presence of presynaptic vesicles (arrows) opposite an electron dense PSD. ***D***, ***E***, Not all synapses in layer IV are labeled; however, the presence of DAB reaction product in adjacent dendrites (asterisks) indicates that the absence of staining is not because of a lack of penetration of the antibody. ***F***, Western blot analysis demonstrates that the association of RIIβ with the PSD is regulated by Ca^{2+}. In the presence of 100 μM calcium, RIIβ is found in the soluble (S) fraction of synaptosome preparations. In the absence of Ca^{2+}, RIIβ is in the particulate (P) fraction (i.e., it is associated with the PSD).

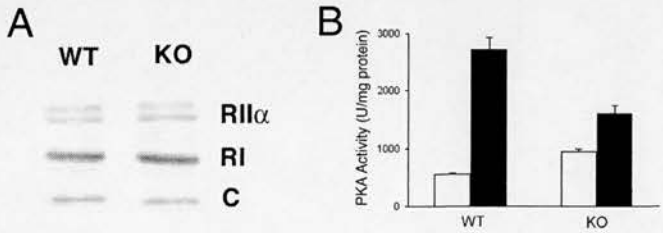

Figure 5. Protein expression of other PKA regulatory subunits in SI cortex of RIIβ KO mice. ***A***, Western blot analyses of homogenates from SI dissections from P7 mice show no significant difference in the levels of RI, RIIα, and C subunits between WT and RIIβ KO mice. Measurements of protein density expressed as optical density units confirm these qualitative assessments (supplemental Fig. 4, available at www.jneurosci.org as supplemental material; sample sizes are indicated above each bar). ***B***, Consistent with the observed lack of compensation of protein concentration, total protein kinase A activity in the SI of P7 RIIβ KO mice ($n = 4$) was lower than in P7 wild-type mice ($n = 3$). Basal and total enzyme activity in protein homogenates was measured in the absence (white bars) and presence (black bars) of 5 μM cAMP, respectively. U, Picomoles of inorganic orthophosphate transferred per minute. Error bars represent SEM.

The postsynaptic role of RIIβ in barrel formation

PKA regulatory subunits, through their interaction with AKAP, impart specificity of localization to PKA holoenzymes. RIIβ associates with the NMDA receptor in the postsynaptic density via an AKAP79/150–membrane-associated guanylate kinase scaffolding complex (Colledge et al., 2000; Snyder et al., 2005). Therefore, loss of RIIβ may lead to ectopic or constitutive PKA

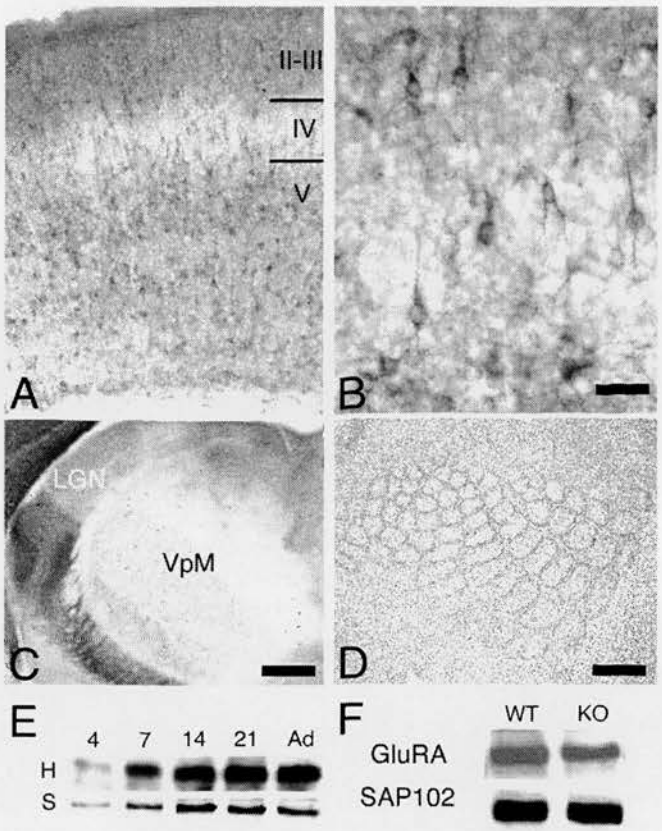

Figure 6. RIIβ regulates GluRA insertion independent of barrel formation. ***A***, GluRA immunolocalization in SI of P7 animals reveals staining throughout the cortex with highest levels in layers II/II and V. ***B***, Higher-magnification images through layer IV show clear immunopositive neurons and diffuse neuropilar staining. ***C***, Staining is also visible in P7 thalamus with lowest levels in VpM. ***E***, Western blot analysis demonstrated a rapid increase in the levels of GluRA in homogenates (H) and synaptosome (S) preparations during the first postnatal week, consistent with the rapid increase in synapses during this period. Ad, Adult. ***F***, To determine whether RIIβ is necessary for insertion of GluRA into the PSD, Western blot analyses of synaptosome preparations from SI of 7-d-old WT and RIIβ KO mice were performed. In each experiment, GluRA levels in RIIβ KO mice are normalized to WT levels. RIIβ KO mice have significantly less GluRA (74.4% $\pm$ 6.8; $n = 5$; 1-sample t test, $p = 0.006$) (supplemental Fig. 4, available at www.jneurosci.org as supplemental material) in synaptosomes than WT mice ($n = 5$; 100%). No differences in SAP-102 (***F***) or PSD-95 levels (data not shown) or in GluRA levels in homogenates (data not shown) were seen, indicating that the decrease in GluRA was not simply caused by a general decrease in PSD components in RIIβ KO mice. Nissl staining through layer IV of adult GluRA KO mice (***D***) reveals clear cellular segregation throughout the barrelfield, including in the anterior snout representations, indicating that neither GluRA insertion nor its presence are necessary for barrel formation. Scale bar: (in ***B***) ***A***, 140 μm; ***B***, 35 μm; ***C***, 250 μm; ***D***, 350 μm.

activity. In P7 mice, we found that loss of RIIβ results in a slight increase in basal PKA activity and a dramatic reduction in stimulated levels of PKA activity, indicating that there is an increase in free catalytic subunits in RIIβ KO mice but that total catalytic subunit concentrations may be lower. Although this expected reduction in catalytic subunit expression was not statistically significant in our P7 barrel cortex homogenates, Inan et al. (2006) found a reduction in P11 barrel cortex homogenates. Nonetheless, the key questions in defining the role of RIIβ-containing PKA holoenzymes in postsynaptic signaling pathways involved in barrel formation include the identity of the PKA activator(s), the relevant PKA phosphorylation substrate(s), and the mechanism(s) by which they influence barrel formation.

Our results showing a reduction in PSD-associated GluRA in the RIIβ KO mice identify RIIβ as the regulatory subunit that is responsible for regulating AMPA receptor insertion and synaptic plasticity in developing thalamocortical synapses (Lu et al., 2003). Our results are in agreement with those showing a role for PKA in ocular dominance plasticity (Beaver et al., 2001) and those showing phosphorylation of GluRA at a PKA-dependent site (Ser845) regulates GluRA insertion into the PSD in visual cortex (Heynen et al., 2003). More recently, RIIβ has been shown to regulate LTP at developing layer IV synapses in SI (Inan et al., 2006). PKA also phosphorylates GluRD receptors to regulate their insertion into the PSD (Carvalho et al., 1999; Esteban et al., 2003). We have been unable to detect significant GluRD levels in SI during barrel development (data not shown), in agreement with previous findings (Catania et al., 1995). We know of no evidence for phosphorylation of GluRB or GluRC by PKA.

The finding that GluRA KO mice develop normal barrels strongly suggests that although RIIβ does regulate GluRA insertion and barrel formation, these two events are not causally related. Our findings are also in good agreement with previous findings that dissociate barrel development from mechanisms that underlie synaptic plasticity. For example, after row C follicle ablation, the cells still cluster around the fused row of TCAs to form a "megabarrel" (Van der Loos and Woolsey, 1973). The clustering of layer IV cells despite the absence of the corresponding follicles strongly indicates that patterned release of glutamate, in a manner similar to that needed to induce synaptic plasticity, is unlikely to regulate barrel development. Similarly, in mice in which barrel formation is delayed by early overexpression of 5-HT, barrel formation takes place even in the absence of whisker follicles (Rebsam et al., 2005).

Activation of postsynaptic PKA in barrel formation

Both NMDA and mGluR5 glutamate receptors can activate PKA (Kind and Neumann, 2001). Our finding that association of RIIβ with the PSD is Ca^{2+} dependent is in good agreement with this hypothesis and previous findings showing a similar NMDA receptor-dependent association with the PSD in hippocampal neurons (Snyder et al., 2005). RIIβ-containing holoenzymes could be regulated by NMDA receptors through Ca^{2+}/CaM-dependent adenylyl cyclases. AC1 and AC8 are both expressed in layer IV neurons during barrel development (Nicol et al., 2005); however, neither AC8 KO mice (Abdel-Majid et al., 1998) nor cortex-specific AC1 KO mice (Iwasato et al., 2005) have obvious defects in barrel development. Perhaps these adenylyl cyclases can compensate for each other to regulate cellular segregation in layer IV.

The Ca^{2+} signal need not come from the NMDA receptor. mGluR5 can also increase release of Ca^{2+} from intracellular stores via the activation of PLC-β1 and subsequent generation of IP_3 (Hannan et al., 2001). In fact, the similarity of the phenotypes of PLC-β1 and RIIβ KO mice suggests that RIIβ activation may be downstream of mGluR5 activation of PLC-β1 in mediating barrel development.

Alternatively, PKA may be activated by other ACs or by a cAMP-independent mechanism. Regulation of Ca^{2+}/CaM-independent adenylyl cyclases by mGluR5 may be the key pathway in RIIβ-mediated barrel development. Both AC4 (Defer et al., 2000) and AC9 (Antoni et al., 1998) are expressed in cortical neurons, and their activities are regulated by G_q, the principal G-protein associated with mGluR5. In addition, a cAMP-independent form of type II PKA activation has been identified recently (Ma et al., 2005), raising the possibility that RIIβ-containing holoenzymes may be regulating barrel development independent of adenylyl cyclases.

cAMP signaling in the presynaptic terminal in barrel formation

The barrelless phenotype in Adcy1 mutant mice revealed the involvement of cAMP intracellular signaling pathways in patterning of the mouse SI cortex (Welker et al., 1996; Abdel-Majid et al., 1998). The hypothesis that the site of gene action of *Adcy1*^{brl} is presynaptic was confirmed recently in somatosensory cortex using cortex-specific AC1 KO mice (Iwasato et al., 2005). It appears to have a similar presynaptic role in retinal ganglion cell projections (Nicol et al., 2006). Low AC1 activity in TCA presynaptic terminals, either because of a loss-of-function *Adcy1* mutation or increased stimulation of 5-HT$_{1B}$ serotonin receptors, causes a barrelless phenotype, perhaps by suppressing glutamate transmission (Abdel-Majid et al., 1998; Salichon et al., 2001; Gaspar et al., 2003). We found no evidence that PKA is the principal target of AC1 in presynaptic signaling pathways involved in barrel formation, but the lack of a phenotype in most of the PKA mutant mice examined may reflect compensation between subunits in individual subunit KOs, as has been found in other tissue (Brandon et al., 1995, 1997, 1998; Amieux et al., 2002). Or RIα may be a key regulatory subunit; however, the embryonic lethality of these KO mice (Amieux et al., 2002) prevented their analysis.

Alternatively, PKA may not be the principal downstream target of cAMP generated by AC1. Other possible targets of cAMP signaling are cAMP-regulated guanine nucleotide exchange factors (Kawasaki et al., 1998) and cyclic-nucleotide-gated (CNG) channels (Kaupp, 1995; Zimmerman, 1995). In *Caenorhabditis elegans*, sensory axons of CNG channel (*tax-2* and *tax-4* mutants) terminate in inappropriate regions, bypassing their normal site of termination (Coburn et al., 1998). The fact that barrelless mice display excessive lateral growth of TCAs in layer IV (Welker et al., 1996) is consistent with the hypothesis that low levels of cAMP in TCAs would be associated with low CNG channel activity.

We and others have shown previously that the process of TCA segregation can be genetically dissociated from the process of cellular segregation in layer IV. Whereas the former is dependent on 5-HT$_{1B}$ receptor signaling, likely via AC1, the latter is dependent on glutamate receptor signaling via RIIβ-containing PKA holoenzymes, PLC-β1, and SynGAP. Furthermore, although RIIβ regulates GluRA insertion and synaptic plasticity, its regulation of cellular segregation is independent of these changes in synaptic strength.

References

Abdel-Majid RM, Leong WL, Schalkwyk LC, Smallman DS, Wong ST, Storm DR, Fine A, Dobson MJ, Guernsey DL, Neumann PE (1998) Loss of adenylyl cyclase I activity disrupts patterning of mouse somatosensory cortex. Nat Genet 19:289–291.

Amieux PS, Howe DG, Knickerbocker H, Lee DC, Su T, Laszlo GS, Idzerda RL, McKnight GS (2002) Increased basal cAMP-dependent protein kinase activity inhibits the formation of mesoderm-derived structures in the developing mouse embryo. J Biol Chem 277:27294–27304.

Antoni FA, Palkovits M, Simpson J, Smith SM, Leitch AL, Rosie R, Fink G, Paterson JM (1998) Ca^{2+}/calcineurin-inhibited adenylyl cyclase, highly abundant in forebrain regions, is important for learning and memory. J Neurosci 18:9650–9661.

Barnett MW, Old RW, Jones EA (1998) Neural induction and patterning by fibroblast growth factor, notochord and somite tissue in *Xenopus*. Dev Growth Differ 40:47–57.

Barnett MW, Watson RF, Vitalis T, Porter K, Komiyama NH, Stoney PN, Gillingwater TH, Grant SGN, Kind PC (2006) SynGAP regulates pattern formation in the trigeminal system of mice. J Neurosci 26:1355–1365.

Beaver CJ, Ji Q, Fischer QS, Daw NW (2001) Cyclic AMP-dependent protein kinase mediates ocular dominance shifts in cat visual cortex. Nat Neurosci 4:159–163.

Brandon EP, Gerhold KA, Qi M, McKnight GS, Idzerda RL (1995) Derivation of novel embryonic stem cell lines and targeting of cyclic AMP-dependent protein kinase genes. Recent Prog Horm Res 50:403–408.

Brandon EP, Idzerda RL, McKnight GS (1997) PKA isoforms, neural pathways, and behaviour: making the connection. Curr Opin Neurobiol 7:397–403.

Brandon EP, Logue SF, Adams MR, Qi M, Sullivan SP, Matsumoto AM, Dorsa DM, Wehner JM, McKnight GS, Idzerda RL (1998) Defective motor behavior and neural gene expression in RIIβ-protein kinase A mutant mice. J Neurosci 18:3639–3649.

Carvalho AL, Kameyama K, Huganir RL (1999) Characterization of phosphorylation sites on the glutamate receptor 4 subunit of the AMPA receptors. J Neurosci 19:4748–4754.

Cases O, Seif I, Grimsby J, Gaspar P, Chen K, Pournin S, Muller U, Aguet M, Babinet C, Shih JC, De Maeyer E (1995) Aggressive behavior and altered amounts of brain serotonin and norepinephrine in mice lacking MAOA. Science 268:1763–1766.

Cases O, Vitalis T, Seif I, De Maeyer E, Sotelo C, Gaspar P (1996) Lack of barrels in the somatosensory cortex of monoamine oxidase A-deficient mice: role of a serotonin excess during the critical period. Neuron 16:297–307.

Catania MV, Tolle TR, Monyer H (1995) Differential expression of AMPA receptor subunits in NOS-positive neurons of cortex, striatum, and hippocampus. J Neurosci 15:7046–7061.

Clegg CH, Correll LA, Cadd GG, McKnight GS (1987) Inhibition of intracellular cAMP-dependent protein kinase using mutant genes of the regulatory type I subunit. J Biol Chem 262:13111–13119.

Coburn CM, Mori I, Ohshima Y, Bargmann CI (1998) A cyclic nucleotide-gated channel inhibits sensory axon outgrowth in larval and adult *Caenorhabditis elegans*: a distinct pathway for maintenance of sensory axon structure. Development 125:249–258.

Colledge M, Dean RA, Scott GK, Langeberg LK, Huganir RL, Scott JD (2000) Targeting of PKA to glutamate receptors through a MAGUK-AKAP complex. Neuron 27:107–119.

Defer N, Best-Belpomme M, Hanoune J (2000) Tissue specificity and physiological relevance of various isoforms of adenylyl cyclase. Am J Physiol Renal Physiol 279:F400–F416.

Dunkley PR, Jarvie PE, Heath JW, Kidd GJ, Rostas JA (1986) A rapid method for isolation of synaptosomes on Percoll gradients. Brain Res 372:115–129.

Erzurumlu RS, Kind PC (2001) Neural activity: sculptor of "barrels" in the neocortex. Trends Neurosci 24:589–595.

Esteban JA, Shi SH, Wilson C, Nuriya M, Huganir RL, Malinow R (2003) PKA phosphorylation of AMPA receptor subunits controls synaptic trafficking underlying plasticity. Nat Neurosci 6:136–143.

Fischer QS, Beaver CJ, Yang Y, Rao Y, Jakobsdottir KB, Storm DR, McKnight GS, Daw NW (2004) Requirement for the RIIβ isoform of PKA, but not calcium-stimulated adenylyl cyclase, in visual cortical plasticity. J Neurosci 24:9049–9058.

Fox K, Schlaggar BL, Glazewski S, O'Leary DD (1996) Glutamate receptor blockade at cortical synapses disrupts development of thalamocortical and columnar organization in somatosensory cortex. Proc Natl Acad Sci USA 93:5584–5589.

Gaspar P, Cases O, Maroteaux L (2003) The developmental role of serotonin: news from mouse molecular genetics. Nat Rev Neurosci 4:1002–1012.

Hannan AJ, Blakemore C, Katsnelson A, Vitalis T, Huber KM, Bear M, Roder J, Kim D, Shin HS, Kind PC (2001) PLC-beta1, activated via mGluRs, mediates activity-dependent differentiation in cerebral cortex. Nat Neurosci 4:282–288.

Heynen AJ, Yoon BJ, Liu CH, Chung HJ, Huganir RL, Bear MF (2003) Molecular mechanism for loss of visual cortical responsiveness following brief monocular deprivation. Nat Neurosci 6:854–862.

Inan M, Lu HC, Albright MJ, She WC, Crair MC (2006) Barrel map development relies on PKARIIβ-mediated cAMP signaling. J Neurosci, 26:4338–4349.

Iwasato T, Datwani A, Wolf AM, Nishiyama H, Taguchi Y, Tonegawa S, Knopfel T, Erzurumlu RS, Itohara S (2000) Cortex-restricted disruption of NMDAR1 impairs neuronal patterns in the barrel cortex. Nature 406:726–731.

Iwasato T, Lee LJ, Ando R, Saito YM, Kanki H, Muglia LJ, Erzurumlu RS, Itohara S (2005) Calcium-stimulated adenylyl cyclase in cortical excita-

tory neurons is not essential for barrel formation in the mouse somatosensory cortex. Soc Neurosci Abstr 31:716.5.

Kaupp UB (1995) Family of cyclic nucleotide gated ion channels. Curr Opin Neurobiol 5:434–442.

Kawasaki H, Springett GM, Mochizuki N, Toki S, Nakaya M, Matsuda M, Housman DE, Graybiel AM (1998) A family of cAMP-binding proteins that directly activate Rap1. Science 282:2275–2279.

Kind P, Blakemore C, Fryer H, Hockfield S (1994) Identification of proteins down-regulated during the postnatal development of the cat visual cortex. Cereb Cortex 4:361–375.

Kind PC, Neumann PE (2001) Plasticity: downstream of glutamate. Trends Neurosci 24:553–555.

Laurent A, Goaillard JM, Cases O, Lebrand C, Gaspar P, Ropert N (2002) Activity-dependent presynaptic effect of serotonin 1B receptors on the somatosensory thalamocortical transmission in neonatal mice. J Neurosci 22:886–900.

Lu HC, She WC, Plas DT, Neumann PE, Janz R, Crair MC (2003) Adenylyl cyclase I regulates AMPA receptor trafficking during mouse cortical 'barrel' map development. Nat Neurosci 6:939–947.

Ma Y, Pitson S, Hercus T, Murphy J, Lopez A, Woodcock J (2005) Sphingosine activates protein kinase A type II by a novel cAMP-independent mechanism. J Biol Chem 280:26011–26017.

Malinow R, Malenka RC (2002) AMPA receptor trafficking and synaptic plasticity. Annu Rev Neurosci 25:103–126.

Nicol X, Muzerelle A, Bachy I, Ravary A, Gaspar P (2005) Spatiotemporal localization of the calcium-stimulated adenylate cyclases, AC1 and AC8, during mouse brain development. J Comp Neurol 486:281–294.

Nicol X, Muzerelle A, Rio JP, Metin C, Gaspar P (2006) Requirement of adenylate cyclase 1 for the ephrin-A5-dependent retraction of exuberant retinal axons. J Neurosci 26:862–872.

Niswender CM, Willis BS, Wallen A, Sweet IR, Jetton TL, Thompson BR, Wu C, Lange AJ, McKnight GS (2005) Cre recombinase-dependent expression of a constitutively active mutant allele of the catalytic subunit of protein kinase A. Genesis 43:109–119.

Qi M, Zhuo M, Skalhegg BS, Brandon EP, Kandel ER, McKnight GS, Idzerda RL (1996) Impaired hippocampal plasticity in mice lacking the Cbeta1 catalytic subunit of cAMP-dependent protein kinase. Proc Natl Acad Sci USA 93:1571–1576.

Rebsam A, Seif I, Gaspar P (2005) Dissociating barrel development and lesion-induced plasticity in the mouse somatosensory cortex. J Neurosci 25:706–710.

Salichon N, Gaspar P, Upton AL, Picaud S, Hanoun N, Hamon M, De Maeyer E, Murphy DL, Mossner R, Lesch KP, Hen R, Seif I (2001) Excessive activation of serotonin (5-HT) 1B receptors disrupts the formation of sensory maps in monoamine oxidase a and 5-HT transporter knock-out mice. J Neurosci 21:884–896.

Skalhegg BS, Huang Y, Su T, Idzerda RL, McKnight GS, Burton KA (2002) Mutation of the Calpha subunit of PKA leads to growth retardation and sperm dysfunction. Mol Endocrinol 16:630–639.

Snyder EM, Colledge M, Crozier RA, Chen WS, Scott JD, Bear MF (2005) Role for A kinase-anchoring proteins (AKAPS) in glutamate receptor trafficking and long term synaptic depression. J Biol Chem 280:16962–16968.

Spires TL, Molnar Z, Kind PC, Cordery PM, Upton AL, Blakemore C, Hannan AJ (2005) Activity-dependent regulation of synapse and dendritic spine morphology in developing barrel cortex requires phospholipase C-beta1 signalling. Cereb Cortex 15:385–393.

Van der Loos H, Woolsey TA (1973) Somatosensory cortex: structural alterations following early injury to sense organs. Science 179:395–398.

Vitalis T, Cases O, Gillies K, Hanoun N, Hamon M, Seif I, Gaspar P, Kind P, Price DJ (2002) Interactions between TrkB signaling and serotonin excess in the developing murine somatosensory cortex: a role in tangential and radial organization of thalamocortical axons. J Neurosci 22:4987–5000.

Welker E, Armstrong-James M, Bronchti G, Ourednik W, Gheorghita-Baechler F, Dubois R, Guernsey DL, Van der Loos H, Neumann PE (1996) Altered sensory processing in the somatosensory cortex of the mouse mutant barrelless. Science 271:1864–1867.

White EL, Weinfeld L, Lev DL (1997) A survey of morphogenesis during the early postnatal period in PMBSF barrels of mouse SmI cortex with emphasis on barrel D4. Somatosens Mot Res 14:34–55.

Wong-Riley M (1979) Changes in the visual system of monocularly sutured or enucleated cats demonstrable with cytochrome oxidase histochemistry. Brain Res 171:11–28.

Woolsey TA, Van der Loos H (1970) The structural organization of layer IV in the somatosensory region (SI) of mouse cerebral cortex. The description of a cortical field composed of discrete cytoarchitectonic units. Brain Res 17:205–242.

Zamanillo D, Sprengel R, Hvalby O, Jensen V, Burnashev N, Rozov A, Kaiser KM, Koster HJ, Borchardt T, Worley P, Lubke J, Frotscher M, Kelly PH, Sommer B, Andersen P, Seeburg PH, Sakmann B (1999) Importance of AMPA receptors for hippocampal synaptic plasticity but not for spatial learning. Science 284:1805–1811.

Zimmerman AL (1995) Cyclic nucleotide gated channels. Curr Opin Neurobiol 5:296–303.

Appendix 2:

PKAR2β RTPCR genotyping protocol

Number of samples to be genotyped: 1

Number used to calculate Master Mix: 1.2

Master Mix:

Reagent	µl/rxn	µlth is mix
ddH20	6.275	7.53
10x ABI Buffer	0.9	1.08
dNTPs (25mM each)	0.36	0.432
50mM MgCl2	0.63	0.756
Ref. Dye (1:500)	0.135	0.162
Amp Taq	0.1	0.12
R2β for (10uM)	0.1	0.12
R2β rev (10uM)	0.1	0.12
R2β hybrid (10uM)	0.1	0.12
Neo for (10uM)	0.1	0.12
Neo rev (10uM)	0.1	0.12
Neo hybrid (10uM)	0.1	0.12

Program R2β : 95 for 2minutes, (95 for 30seconds, 56 for 60 seconds) x 40

R2β WT allele runs under FAM

R2β KO (neo) allele runs under VIC

Appendix 3

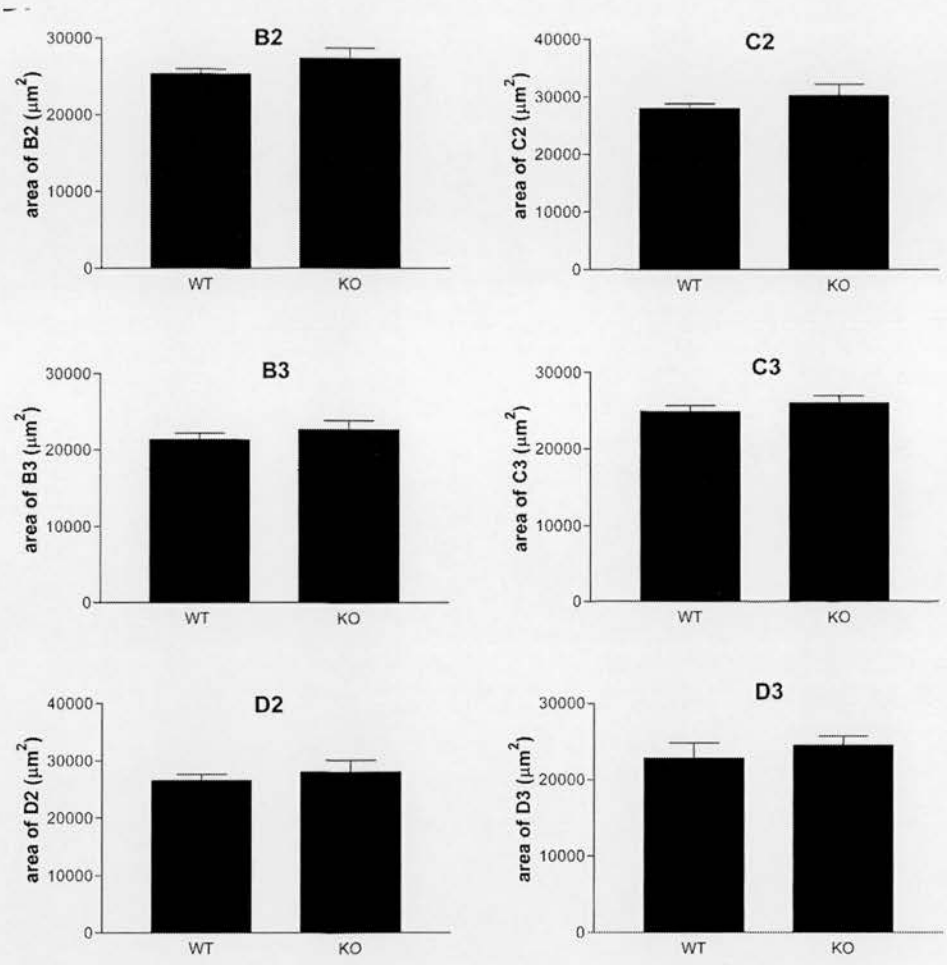

Appendix 3: Normal TCA patch size in the PMBSF of *Prkar2β-/-* mice. To assess TCA distribution in *Prkar2β-/-* mice , TCA patch size was calculated of barrels B2, B3, C2, C3, D2, and D3 from WT and *Prkar2β-/-* animals and no significant difference was found between genotypes.

Appendix 4

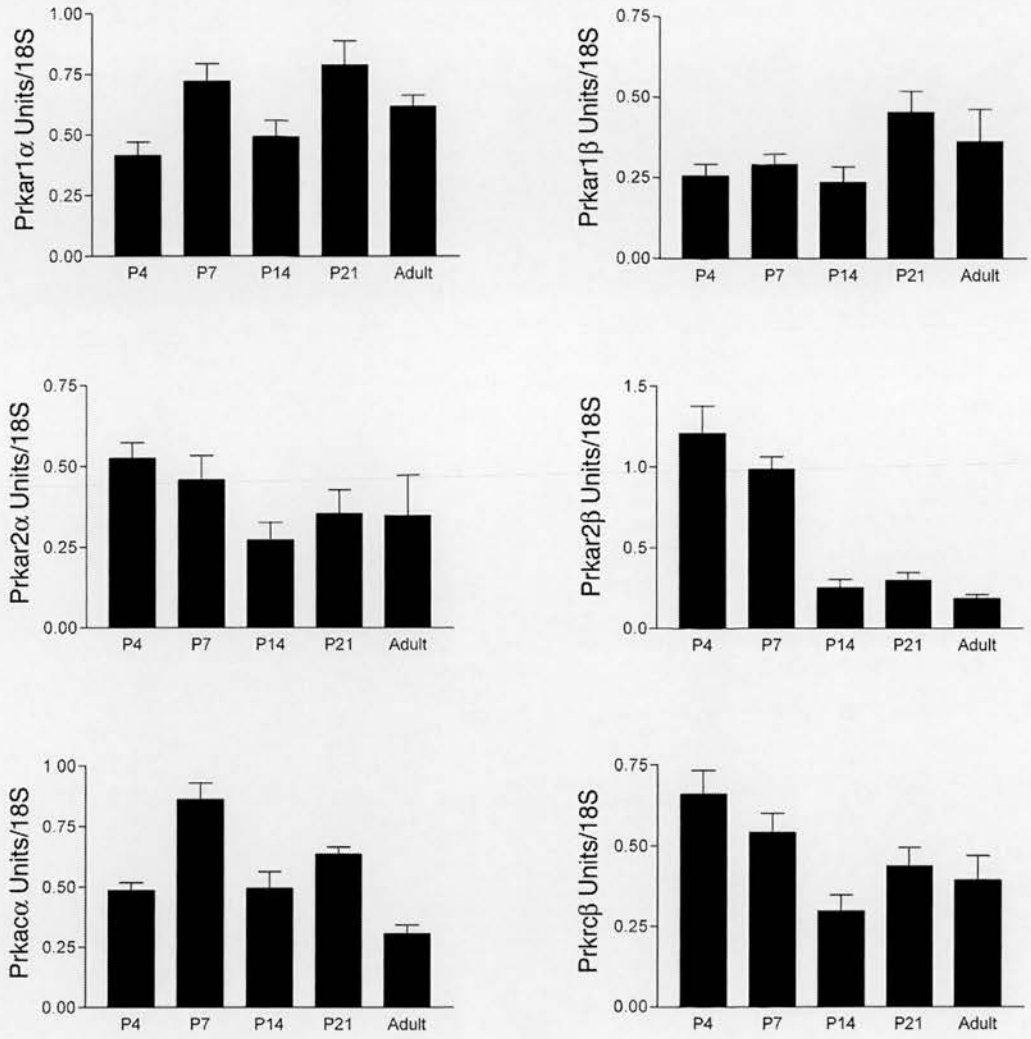

Appendix 4: Developmental mRNA expression profiles of each PKA subunit. All PKA subunits are present throughout barrel cortex development. PKA subunit R2β appears to be the most developmentally regulated subunit, expressed high during the first postnatal week and then dramatically reduced between P7 and P14 before remaining at low levels into adulthood.

Appendix 5

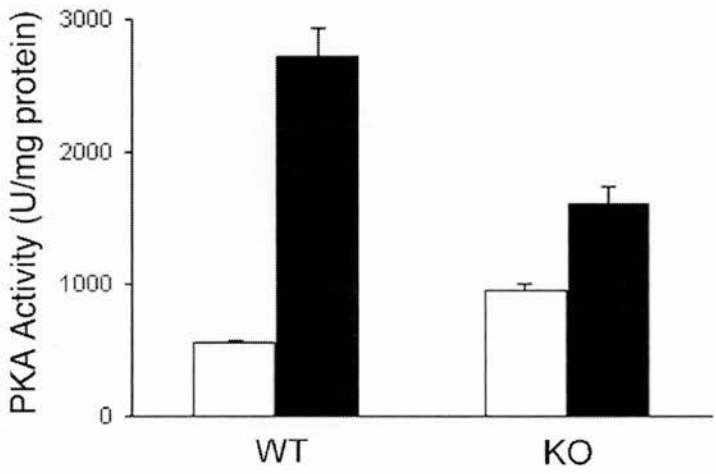

Appendix 5: Total protein kinase A activity is reduced in *Prkar2β-/-* mice. Basal and total enzyme activity was measured from homogenates of P7 *Prkar2β-/-* S1 cortex in the absence (white bars) and presence (black bars) of 5um cAMP, respectively. U, Picomoles of inorganic orthophosphate transferred per minute. Error bars represent SEM. (Watson et al., 2006)

Appendix 6:

Barnett MW, Watson RF, Vitalis T, Porter K, Komiyama NH, Stoney PN, Gillingwater TH, Grant SG, Kind PC (2006) Synaptic Ras GTPase activating protein regulates pattern formation in the trigeminal system of mice. J Neurosci 26:1355-1365.

Development/Plasticity/Repair

Synaptic Ras GTPase Activating Protein Regulates Pattern Formation in the Trigeminal System of Mice

Mark W. Barnett,[1]* Ruth F. Watson,[1]* Tania Vitalis,[1,2]* Karen Porter,[1,3]* Noboru H. Komiyama,[1,3] Patrick N. Stoney,[1] Thomas H. Gillingwater,[1] Seth G. N. Grant,[1,3] and Peter C. Kind[1]

[1]Centre for Integrative Physiology and Centre for Neuroscience Research, University of Edinburgh, Edinburgh EH8 9XD, United Kingdom, [2]Unité 106, Institut National de la Santé et de la Recherche Médicale, Hopital de la Salepetriere, Batiment de Pediatrie, 75013 Paris, France, and [3]Genes to Cognition Programme, Wellcome Trust Sanger Institute, Cambridge CB10 1SA, United Kingdom

The development of ordered connections or "maps" within the nervous system is a common feature of sensory systems and is crucial for their normal function. NMDA receptors are known to play a key role in the formation of these maps; however, the intracellular signaling pathways that mediate the effects of glutamate are poorly understood. Here, we demonstrate that SynGAP, a synaptic Ras GTPase activating protein, is essential for the anatomical development of whisker-related patterns in the developing somatosensory pathways in rodent forebrain. Mice lacking SynGAP show only partial segregation of barreloids in the thalamus, and thalamocortical axons segregate into rows but do not form whisker-related patches. In cortex, layer 4 cells do not aggregate to form barrels. In *Syngap*$^{+/-}$ animals, barreloids develop normally, and thalamocortical afferents segregate in layer 4, but cell segregation is retarded. SynGAP is not necessary for the development of whisker-related patterns in the brainstem. Immunoelectron microscopy for SynGAP from layer 4 revealed a postsynaptic localization with labeling in developing postsynaptic densities (PSDs). Biochemically, SynGAP associates with the PSD in a PSD-95-independent manner, and *Psd-95*$^{-/-}$ animals develop normal barrels. These data demonstrate an essential role for SynGAP signaling in the activity-dependent development of whisker-related maps selectively in forebrain structures indicating that the intracellular pathways by which NMDA receptor activation mediates map formation differ between brain regions and developmental stage.

Key words: SynGAP; barrels; NMDA receptors; somatosensory; development; PSD-95

Introduction

Sensory cortices are organized into topographic maps whereby the pattern of the peripheral receptors is faithfully recapitulated onto the cortical surface via thalamocortical afferents (TCAs). Within these topographic maps, structural and functional specializations occur, such as the whisker-related modules, the "barrels," of the rodent somatosensory cortex (Woolsey and Van der Loos, 1970; Killackey and Belford, 1979). Initially, TCAs overlap tangentially in layer 4 and subsequently segregate into whisker-related clusters (Rebsam et al., 2002) in a process that is modulated by presynaptic serotonin signaling (Gaspar et al., 2003). Subsequently, cortical neurons form cellular aggregates around the TCA clusters (Woolsey and Van der Loos, 1970) in a process that is regulated by glutamate neurotransmission (Erzurumlu and Kind, 2001; Kind and Neumann, 2001). Mice lacking the metabotropic glutamate receptor 5 (mGluR5) or cortical NMDA receptors (NMDARs) fail to form barrels despite at least partial segregation of TCAs (Iwasato et al., 2000; Hannan et al., 2001). Similarly, activity-dependent changes in neuronal phenotype in response to altered sensory activity are dependent on NMDAR activation (Schlaggar et al., 1993; Fox et al., 1996; Datwani et al., 2002).

The characterization of the postsynaptic density (PSD) and NMDA receptor complex has provided a framework for identifying candidate proteins regulated by glutamate receptors that may be involved in the cellular processes mediating barrel formation (Husi et al., 2000; Walikonis et al., 2000). One such protein is SynGAP, a synaptic GTPase activating protein that regulates small G-proteins (Ras, Rab, and Rap) (Chen et al., 1998; Kim et al., 1998; Krapivinsky et al., 2004; Tomoda et al., 2004). SynGAP binds to the NMDA receptor via its association with membrane associated guanylate kinases (MAGUKs), including PSD-95 and synapse-associated protein 102 (SAP-102) and negatively regulates the extracellular-regulated kinase (ERK) signaling cascade (Komiyama et al., 2002). ERK regulates numerous forms of plasticity, including the critical period plasticity in rodent visual cortex, long-term potentiation (LTP), and learning and memory (Di Cristo et al., 2001; Adams and Sweatt, 2002). It also regulates cytoskeletal rearrangements, synaptogenesis, dendritic morphology, and cellular migration (Ho et al., 2001; Adams and Sweatt, 2002). Thus, SynGAP may represent a key link from NMDARs to downstream pathways regulating barrel development.

A single gene encodes SynGAP, although the mRNA can be spliced to give several distinct proteins, the functions of which are

Received March 1, 2005; revised Nov. 30, 2005; accepted Dec. 8, 2005.

This work was supported by the Wellcome Trust (P.C.K.), the Wellcome Trust Genes to Cognition Programme (S.G.N.G.), and the Medical Research Council UK (P.C.K.).

*M.W.B., R.F.W., T.V., and K.P. contributed equally to this work.

Correspondence should be addressed to Peter Kind, Division of Biomedical and Clinical Laboratory Sciences, University of Edinburgh, Hugh Robson Building, George Square, Edinburgh EH8 9XD, UK. E-mail: pkind@ed.ac.uk.

DOI:10.1523/JNEUROSCI.3164-05.2006

 0270-6474/06/261355-11$15.00/0

not clear (Li et al., 2001). It is expressed throughout the cortex, hippocampus, and thalamus of postnatal mice, suggesting a role in developmental plasticity (Porter et al., 2005). SynGAP homozygous null mutant mice die perinatally (Komiyama et al., 2002; Kim et al., 2003; Vazquez et al., 2004), although some live to postnatal day 5 (P5) to P7 (Kim et al., 2003); heterozygotes are viable. The brains of *Syngap*$^{-/-}$ mice appear grossly normal, and the cause of death is not clear. *Syngap*$^{+/-}$ mice show a significant reduction in LTP) and a shift in the plasticity frequency function (Komiyama et al., 2002; Kim et al., 2003) and defects in spatial learning (Komiyama et al., 2002). Cultured hippocampal neurons lacking SynGAP show precocious spine and synapse formation, and spines are significantly larger than normal (Vazquez et al., 2004).

Materials and Methods

Breeding and genotyping of transgenic mice. Syngap heterozygous mating pairs on the MF1 background were used to derive wild-type (WT), heterozygous, and homozygous pups for experimental analysis. PCR genotyping from purified genomic DNA was performed as described previously (Komiyama et al., 2002). All animals were treated in accordance with the UK Animal Scientific Procedures Act (1986).

Biochemistry. Mice were killed either by cervical dislocation or decapitation, and S1 cortices dissected from P0, P4, P7, P14, P21, and adult mice were immediately frozen on dry ice and stored at −70°C. For developmental analysis, barrel cortices were homogenized in lysis buffer (50 mM HEPES, pH 7.5, 1% Triton X-100, 50 mM NaCl containing protease inhibitors, phosphatase inhibitor cocktails I and II) (P2850 and P5276; Sigma, Poole, UK). Protein concentrations were determined by Bradford assays, and immunoblot analysis was performed according to the methods of Kind et al. (1994). Briefly, 10 μg of protein was loaded per lane of each age on a 7 or 10% polyacrylamide gel with a 4% stacking gel. The proteins were then transferred to nitrocellulose membranes, which were then stained with amido black to confirm equal loading of protein. The blots were then incubated in primary antibody [calcium calmodulin-dependent protein kinase II (CaMKII), 1:1000 (Promega, Madison, WI); PSD-95, 1:20,000 (Upstate Biotechnology, Lake Placid, NY); pan-SynGAP, 1:4000 (Affinity BioReagents, Golden, CO); SynGAPα, 1:2000 (Upstate Biotechnology); SAP-102, 1:5000 (Santa Cruz Biotechnology, Santa Cruz, CA; Chemicon, Temecula, CA; Alomone Labs, Jerusalem, Israel; or Synaptic Systems, Gottingen, Germany); NR2A, 1:2000 (Chemicon); NR1, 1:10,000 (Santa Cruz Biotechnology)] overnight at room temperature before being placed in secondary antibodies (anti-mouse IgG 1:10,000, anti-rabbit IgG 1:25,000, anti-goat IgG 1:50,000; Sigma) coupled to HRP for 1–2 h. Proteins were visualized using ECL reagents (Amersham Biosciences, Piscataway, NJ) and XAR Kodak (Rochester, NY) autoradiographic film.

Synaptosome and PSD fractionation. Synaptosome preparations were prepared according to the methods of Dunkley et al. (1986). Briefly, S1 cortex was homogenized in a 320 mM sucrose solution (pH 7.4, containing 1 mM EDTA and 5 mM Tris) and then poured onto Percoll gradients (3 ml layers of 24, 10, and 3% Percoll) that were centrifuged for 12 min at 15,000 rpm at 4°C. Synaptosomes were removed from between the 24 and 10% Percoll layers and spun for 30 min at 13,000 rpm in ice-cold 320 mM sucrose solution. The resulting synaptosome pellet was then resuspended and centrifuged in cold minus Ca^{2+} Krebs buffer (containing NaCl, KCl, $MgSO_4$ glucose, $Na_2HPO_4{\cdot}12H_20$, and HEPES) at 13,000 rpm for 10 min, twice in succession. Synaptosomes were treated with lysis buffer [50 mM HEPES, pH 7.5, 1% Triton X-100, 50 mM NaCl containing protease inhibitors, phosphatase inhibitor cocktails I and II (Sigma P2850 and P5276)]. The PSD fraction was then pelleted by two successive centrifugations at 36,800 × *g* for 45 min.

Tissue preparation for histology. Mice were anesthetized with an overdose of sodium pentobarbital (Euthanal; 200 mg/kg, i.p.) and were perfused with PB followed by 4% (w/v) paraformaldehyde in 0.1 M phosphate buffer. The brains were removed, fixed overnight in 4% paraformaldehyde, and cryoprotected overnight in 30% (w/v) sucrose. The brains were sectioned on a freezing microtome either coronally or tangentially to the pial surface at 48 μm. For tangential sections, cortices were dissected from the thalamus, and the hippocampus and striatum were removed. The cortex was then flattened on the freezing microtome stage with the pial surface facing up.

Histology. 5-Bromo-4-chloro-3-indolyl-β-D-galactopyranoside (X-Gal) staining was performed as described previously (Porter et al., 2005). At least three animals at each age from at least two separate litters were used for X-Gal staining. Thionin (Nissl) and cytochrome oxidase (CO) staining was performed as described previously (Hannan et al., 2001). For 5-HT and serotonin transporter (5-HTT) immunohistochemistry, sections were incubated overnight in rat anti-mouse 5-HT (1:10 to 1:20; Harlan Sprague Dawley, Indianapolis, IN) or rabbit anti-mouse 5-HTT (1:2000; Calbiochem, La Jolla, CA), respectively, diluted in PBS containing 0.2–0.5% Triton X-100 or DMEM containing 5% fetal calf serum and 0.2–0.5% Triton X-100. Visualization of 5-HT was then performed as described previously (Vitalis et al., 2002). Sections reacted for calretinin (1:3000; Swant, Bellinzona, Switzerland) and cAMP-dependent protein kinase A regulatory subunit IIβ (PKARIIβ) (1:600; Santa Cruz Biotechnology, Santa Cruz, CA) were incubated overnight in antibody diluted in DMEM containing 5% fetal calf serum and 0.2–0.5% Triton X-100. Visualization was performed using a Vectastain ABC kit (Vector Laboratories, Burlingame, CA). To reveal barrels, flattened sections were mounted on slides, dried overnight, and stained with cresyl violet acetate (0.5%). In both cases, sections were dehydrated into xylene and coverslipped. For propidium iodide (PI) staining, free-floating sections were collected serially in PBS and incubated for 30 min in a solution containing 1:1000 propidium iodide (Invitrogen, San Diego, CA). Sections were rinsed in PBS, mounted on gelatin-coated slides, and coverslipped in PBS-glycerol (3:1; w/v). To reveal SynGAP protein localization, 48 μm frozen sections were incubated free-floating overnight at room temperature in a 1:200 to 1:600 dilution of rabbit anti-mouse pan-SynGAP antibodies (1:4000; Affinity BioReagents) in DMEM containing 5% fetal calf serum and 0.2% Triton X-100. Signal was then amplified by incubation in biotinylated goat anti-rabbit secondary antibody and streptavidin-coupled HRP.

Measurements. All analyses were performed blind to genotype. No difference in cortical thickness or neocortical area was observed in mice between P5 and P7; therefore, animals at these ages were combined for analysis. Cortical thickness measurements in posterior medial barrel subfield (PMBSF) were obtained from Nissl-stained 48 μm coronal sections equivalent to between −1.82 and −1.94 mm posterior and between 2.8 and 3.2 mm lateral to bregma (Franklin and Paxinos, 1997). Additional cortical thickness measurements in the anterior snout region were obtained from Nissl-stained 48 μm coronal sections equivalent to between −0.94 and −1.06 mm posterior and between 3.0 and 3.4 mm lateral to bregma. In all cases, adjacent sections stained with 5-HTT were used to confirm the location within PMBSF or the anterior snout region. Layer 4 thickness and layer 5/6 thickness measurements were obtained in identical sections stained with anti-PKARIIβ and anti-calretinin antibodies, respectively. All area measurements were obtained from tangential sections stained with anti-5-HTT or anti-5HT antibodies. Images were analyzed at a final magnification of 40× (S1 cortex area), 80× (PMBSF area), and 160× (C1 barrel area, cortical thickness and cortical layer thickness measurements) using a Leica DMLB microscope and the Leica DMLB Image Manager version 4.0 program. All linear and area measurements were performed using the Image Tool for Windows version 3.0 software (University of Texas Health Science Centre at San Antonio, San Antonio, TX). Each image measurement was calibrated using a 1 mm graticule (Graticules, Tonbridge, Kent).

Cell counts. Sections were viewed with a Leica confocal microscope. Three to four adjacent sections containing the barrel-field representation were analyzed for each animal. From these sections, the position of individual barrels were determined, and a series of confocal images of B3 and its neighboring barrels were taken with 7 μm intervals using the 10 and 20× objectives. Morphometric analysis was performed with the Leica software (TCNST). For each series of optical images, the section containing the clearer representation of the barrel of interest was used to start the analysis. All analysis was performed blind to genotype. On this selected

section, three rectangles along the B2–B4 axis, one containing the B2–B3 wall, one the B3 hollow, and one the B3–B4 wall were drawn to calculate the density of propidium-stained nuclei in each rectangle. Within each animal, rectangle size remained constant but varied slightly between animals to ensure that its outer limits were restricted to the structure (barrel wall or hollow) of interest. Each rectangle was 60–70 × 80 μm, and in all cases, the rectangle was restricted to the structure (i.e., barrel wall or hollow) being measured. Counts were then normalized to the area of the rectangle being measured. Measurements were done on the selected section and on the two adjacent sections (upper and lower). From these data, the average density of propidium-stained nuclei in the walls and hollow of the chosen barrel was calculated. Measures are means of average densities ± SEM (P8, wild type, $n = 8$; *Syngap*$^{+/-}$, $n = 8$). Average differences in nuclear densities taken from walls and hollows of the wild-type and *Syngap*$^{+/-}$ groups were statistically different (Student's t test; $^{*}p < 0.01$).

Electron microscopy. Animals for electron microscopy were perfused as above, except that 0.1% glutaraldehyde was included in the fixative. Vibratome sections, 50-μm-thick, were placed in 1:200 dilution of rabbit anti-mouse SynGAP overnight at 4°C in the absence of detergent and reacted for DAB histochemistry as described above. They were then post-fixed in 1% osmium tetroxide in 0.1 M phosphate buffer for 45 min. After dehydration through an ascending series of ethanol solutions and propylene oxide, all sections were embedded on glass slides in Durcupan resin. Regions of cortex (~1 × 1 mm) to be used for assessment were then cut out using a scalpel and glued onto a resin block for sectioning. Ultrathin sections (~70 nm) were cut and collected on formvar-coated grids (Agar Scientific, Stansted, UK), stained with uranyl acetate and lead citrate in a LKB Ultrostainer, and then assessed in a Philips CM12 transmission electron microscope. Negatives taken in the microscope were scanned onto an Apple Macintosh G5 computer using an Epson 4870 Photo flatbed scanner at 1200 dpi, before being prepared for presentation in Adobe Photoshop (Adobe Systems, San Jose, CA).

Analysis of gene expression using real-time reverse transcription-PCR. The barrel cortex was dissected from mice between P0 and adult, frozen on dry ice, and stored at −70°C. Total RNA was extracted using an RNeasy mini-kit (Qiagen) and an RNase-Free DNase set (Qiagen). Total RNA was run on 0.8% agarose gel to ensure that RNA was not degraded (28S ribosomal band was well defined and double the intensity of 18S ribosomal band) or the sample was discarded. First-strand cDNA synthesis was performed as described by Barnett et al. (1998). Real-time reverse transcription (RT)-PCR was performed using MJ Research DNA Engine Opticon and Quantitect SYBR Green PCR kit (Qiagen). In each PCR, 1 μl of cDNA was combined with gene-specific primers (0.5 μM) and 12.5 μl of QuantiTect SYBR Green PCR Master Mix to a total volume of 25 μl. To compare expression levels at different developmental stages, a dilution series of control cDNA was made and assayed in each Opticon run. The dilution series was used from cDNA of the developmental stage predicted to give the highest expression of the gene product being amplified. Other controls performed in each run were RT and water blanks.

At the end of each run, melting curve analysis was performed between 60 and 90°C, and single melting peak demonstrated specific product. OpticonMonitor analysis software (version 1.01) was used to compare amplification in experimental samples during the log-linear phase to the standard curve from the dilution series of control cDNA. Comparisons were displayed as histograms. 18S rRNA and glyceraldehyde-3-phosphate dehydrogenase were used as a loading control, and each bar was normalized to the level of 18S rRNA expression. Primer sets used were pan-*Syngap*-F 5′-CGAAGTGCTGACCATGAC-3′, pan-*Syngap*-R 5′-CGGCTGTTGTCCTTGTTG-3′, 18S-F 5′-GTGGAGCGATTTGTCTGGTT-3′, and 18S-R 5′-CAAGCTTATGACCCGCACTT-3′.

Analysis of SynGAP splice variant expression. Ventral posterior medial nucleus (VpM) and layer IV of S1 cortex were dissected from P8 C57BL/6 mice in PBS and immediately frozen on dry ice. Total RNA was extracted using an RNeasy mini kit (Qiagen) and dissolved in RNase-free dH2O. RNA quality was verified by visualization on an agarose gel. cDNA synthesis was performed as done by Barnett et al. (1998), and PCR was performed with primers that detect all known Syngap 3′ isoforms (Li et al., 2001; Kim et al., 1998). The resulting PCR products were electrophoretically separated on an agarose gel, extracted, and ligated into P-GEM-T Easy Vector (Promega) and transformed into JM109 competent cells. Plasmid DNA was extracted using a Quiagen mini-prep kit, and the insert was sequenced by MWG (Ebersberg, Germany).

Results

SynGAP is necessary for barrel formation

Previous reports have demonstrated that *Syngap*$^{-/-}$ mice die within 48 h of birth (Komiyama et al., 2002; Vazquez et al., 2004), although one report showed mice living as late as P7. We observed a propensity for *Syngap*$^{-/-}$ mice to die when part of large litters, however, when competition between littermates is reduced, either as a result of naturally small litters or deliberate culling of littermates, we have been able to maintain homozygous knockout animals to 1 week of age.

To determine whether SynGAP plays a role in the general development and lamination of the cortex, we examined the expression of several layer-specific markers including 5-HTT, PKA-RIIβ, and calretinin in the barrel field in P5–P7 *Syngap*$^{-/-}$, *Syngap*$^{+/-}$, and *Syngap*$^{+/+}$ mice (Fig. 1). Qualitatively, no difference was seen in the laminar expression patterns of these proteins in *Syngap*$^{+/-}$ or *Syngap*$^{-/-}$ mice relative to littermate control animals. Quantitatively we examined the following: (1) cortical thickness in coronal Nissl sections through both PMBSF and the anterior snout whiskers region; (2) areas of neocortex, S1, and PMBSF in flattened sections labeled with 5-HTT; (3) radial thickness of TCA terminals in coronal sections labeled with 5-HTT in sections through both PMBSF and the anterior snout whiskers region; (4) radial thickness of layers 1–4 and 5–6 in calretinin-labeled sections through both PMBSF and the anterior snout whiskers region; and (5) area of B1–B3, C1–C3, and D1–D3 barrels in *Syngap*$^{+/+}$ and *Syngap*$^{+/-}$ animals (Figs. 1*m*, 2*f*) (supplemental Fig. 1, available at www.jneurosci.org as supplemental material). No significant difference was present between WT and heterozygous animals indicating that the cortex develops normally in these mice. In comparison with *Syngap*$^{+/+}$ and *Syngap*$^{+/-}$ animals, *Syngap*$^{-/-}$ mice demonstrate a small reduction in cortical thickness in PMBSF and the anterior snout region. The decrease in cortical thickness affected all layers. These results (summarized in supplemental Table 1, available at www.jneurosci.org as supplemental material) are in good agreement with the reduction in body weight and brain size reported previously (Kim et al., 2003; Vasquez et al., 2004).

To determine whether SynGAP plays a role in the development of the primary somatosensory cortex, we examined the distribution of TCAs and soma of layer 4 neurons in *Syngap*$^{+/+}$ ($n = 4$ for both TCAs and cell distribution) and *Syngap*$^{-/-}$ ($n = 5$) mice. Nissl staining in flattened sections through layer 4 of P6/7 *Syngap*$^{-/-}$ mice demonstrates a complete loss of cellular segregation into barrels in layer 4 (Fig. 2*b*). Supplemental Figure 2 (available at www.jneurosci.org as supplemental material) shows three adjacent sections through layer 4 of another *Syngap*$^{-/-}$ mouse. No barrels are visible in any section. Wild-type littermate control animals demonstrate a normal cellular aggregation in layer 4 (Fig. 2*a*). To elucidate the locus of the defect in *Syngap*$^{-/-}$ mice, we examined the state of TCA segregation using 5-HT immunohistochemistry in *Syngap*$^{-/-}$, *Syngap*$^{+/-}$, and *Syngap*$^{+/+}$ mice (Figs. 1*g–i*, 2*c–e*). Serotonin immunoreactivity in coronal sections through the posteromedial barrel subfield of P6/P7 animals revealed TCAs were restricted to layer 4 in all three genotypes (Fig. 1*g–i*). In tangential sections through layer 4 of *Syngap*$^{-/-}$ animals (Fig. 2*e*), however, TCAs segregated into rows but not into individual whisker-related patches,

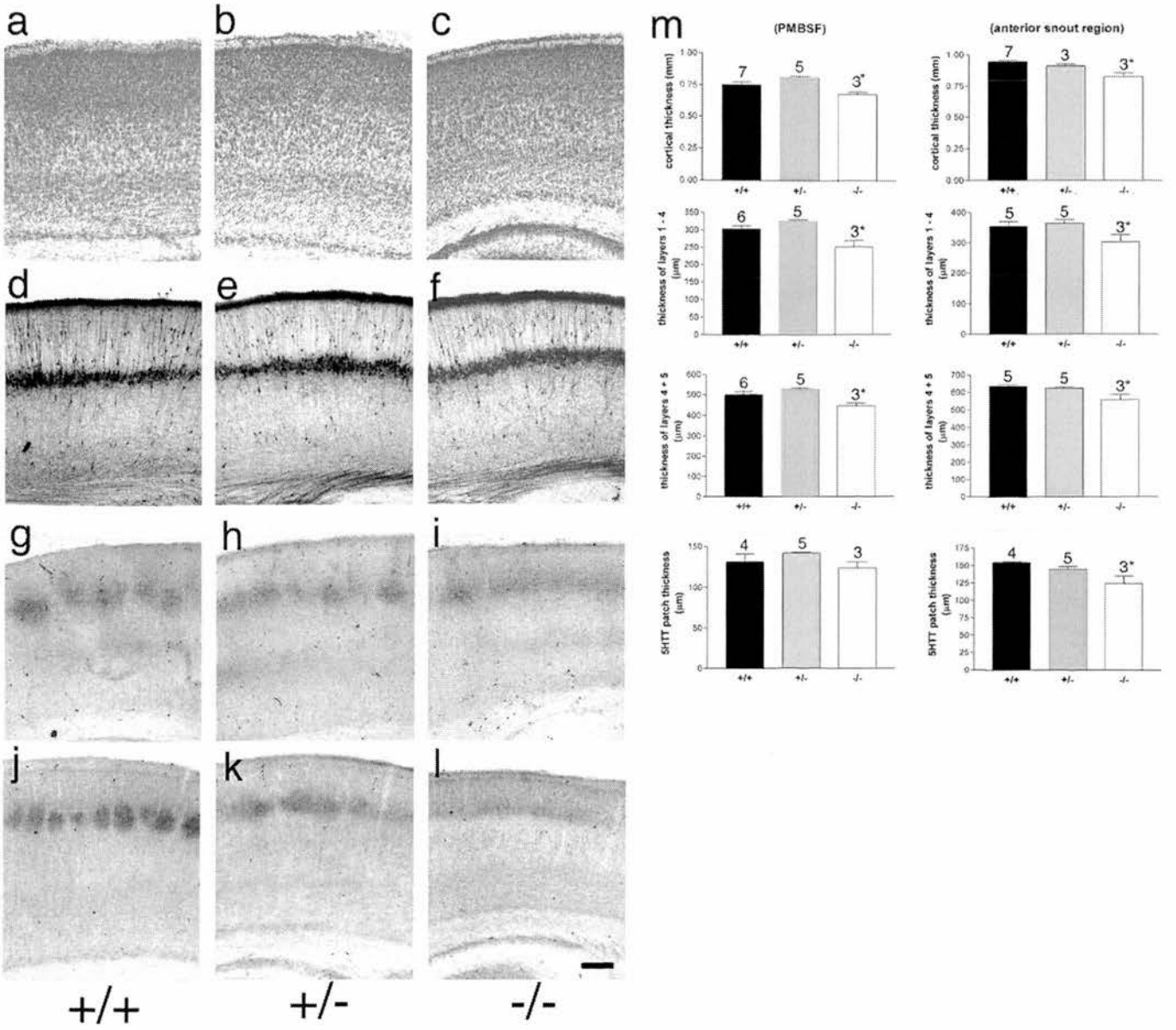

Figure 1. Normal cortical lamination in *Syngap* $^{+/-}$ and *Syngap* $^{-/-}$ mice. Coronal sections through S1 cortex of P6/7 *Syngap* $^{+/+}$ (***a***, ***d***, ***g***, ***j***), *Syngap* $^{+/-}$ (***b***, ***e***, ***h***, ***k***), and *Syngap* $^{-/-}$ (***c***, ***f***, ***i***, ***l***) mice stained for Nissl substance (***a–c***), calretinin (***d–f***), 5-HTT (***g–i***), and PKA RIIβ (***j–l***). No qualitative difference in pattern of staining is visible between genotypes with the exception of the lack of segregation of TCAs seen in the *Syngap* $^{-/-}$ animals. Quantitative analysis of cortical thickness, radial thickness of TCA terminals, layer 5/6 thickness, and layer 1–4 thickness was also calculated (***m***). In all cases, there was no significant difference between *Syngap* $^{+/+}$ and *Syngap* $^{+/-}$ animals. There was a significant decrease in *Syngap* $^{-/-}$ compared with *Syngap* $^{+/+}$ and *Syngap* $^{+/-}$ animals in all parameters measured except 5-HTT terminal zone thickness in PMBSF. A complete numerical account of these data is presented in supplemental Table 1 (available at www.jneurosci.org as supplemental material). Scale bar, 250 μm. Error bars represent SE.

indicating that while TCAs terminate correctly in the radial dimension but fail to segregate into a barrel-like pattern. In contrast, wild-type and *Syngap* $^{+/-}$ littermates showed normal segregation of TCAs in layer 4 (Fig. 2*c*,*d*). A small decrease in the size of S1 or PMBSF was seen in *Syngap* $^{-/-}$ animals compared with WT and *Syngap* $^{+/-}$ animals; this decrease was small and was not significant in the former (Fig. 2*f*) (supplemental Table 1, available at www.jneurosci.org as supplemental material). Therefore, decrease in area of S1 and/or PMBSF cannot account for the loss of segregation seen in *Syngap* $^{-/-}$ animals. Interestingly, despite the reduced tangential TCA segregation in S1, the segregation of TCAs between cortical areas appears normal (i.e., V1, S1, S2, and A1 are all easily identifiable). Even subregions of S1 such as the PMBSF and the anterior snout, lower lip, forepaw, and hindpaw representations are all identifiable, indicating that the effects in S1 do not arise from a general defect in TCA pathfinding.

The complete lack of barrels, despite partial segregation of TCAs, suggested a role for cortically expressed SynGAP in barrel formation. To gain additional insight into the role of SynGAP, we examined the *Syngap* heterozygotes in more detail (Fig. 3). P8 *Syngap* $^{+/-}$ mice (Fig. 3*b*,*d*) demonstrated reduced segregation in PMBSF compared with age-matched wild-type mice (Fig. 3*a*,*c*). To quantify the change in segregation, tangential sections through layer 4 from eight wild-type and eight *Syngap* $^{+/-}$ mice were labeled with PI and labeled nuclei were visualized using the confocal microscope. All eight *Syngap* $^{+/-}$ mice showed reduced segregation compared with wild-type controls. In 7 μm optical sections, PI-labeled nuclei were counted in both the barrel wall

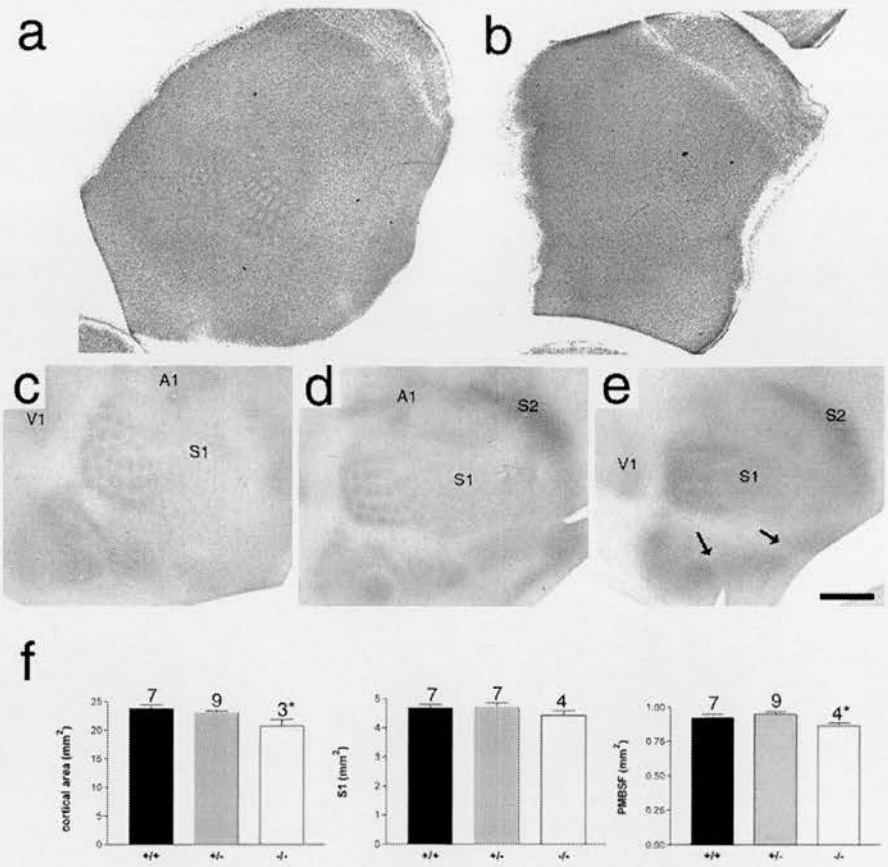

Figure 2. Lack of barrel formation in *Syngap*$^{-/-}$ mice. Nissl staining of flattened sections through layer 4 of P6.5 *Syngap*$^{+/+}$ (***a***) and *Syngap*$^{-/-}$ (***b***) mice showing a complete absence of cellular aggregation in *Syngap*$^{-/-}$ mice. Flattened sections through layer 4 of *Syngap*$^{+/+}$ (***c***), *Syngap*$^{+/-}$ (***d***), and *Syngap*$^{-/-}$ (***e***) mice were immunostained for 5-HT to reveal the distribution of TCAs. Clear segregation of primary visual (V1), somatosensory (S1), and auditory (A1) as well as secondary somatosensory (S2) cortical areas can be seen in all three genotypes indicating no general defect in TCA pathfinding in *Syngap* mutants. Within S1, the representation of different body regions (PMBSF and the anterior snout, lower lip, forepaw, and hindpaw representations) are also clearly defined (arrows). However, within the anterior snout, no TCA segregation is visible and, within PMBSF, TCAs can be seen segregating into rows, but patches corresponding to individual whiskers fail to form. Scale bar (in ***e***): ***a***, ***b***, 1 mm; ***c–e***, 800 μm. Quantification of neocortical area, area of S1, and PMBSF in *Syngap*$^{+/+}$, *Syngap*$^{+/-}$, and *Syngap*$^{-/-}$ animals revealed a small but significant decrease in neocortical area and area of PMBSF in *Syngap*$^{-/-}$ animals. The area of S1 was reduced in *Syngap*$^{-/-}$ animals, although this decrease was not significant. No significant difference between *Syngap*$^{+/+}$ and *Syngap*$^{+/-}$ was seen in any these measurements. In addition, there was no significant difference in the area of individual TCA patches of PMBSF barrels in *Syngap*$^{+/+}$ compared with *Syngap*$^{+/-}$ mice (supplemental Fig. 1, available at www.jneurosci.org as supplemental material). Error bars represent SE.

and barrel hollow of barrel B3 (Fig. 3*e*). The mean number of cells in the wall of the B3 barrel was 32.7 ± 2.8 per 500 μm^2 in *Syngap*$^{+/+}$ and was significantly reduced to 26.6 ± 0.13 in *Syngap*$^{+/-}$ mice (Student's *t* test; $p < 0.01$). Analysis of cell density in the barrel hollows revealed a significant increase in the *Syngap*$^{+/-}$ (23.8 ± 1.7) compared with *Syngap*$^{+/+}$ (21.1 ± 2.8) mice ($p < 0.01$). In *Syngap*$^{+/+}$, the ratio of PI-labeled nuclei in the barrel wall to barrel hollow was 1.73 ± 0.16. In contrast, this ratio was significantly reduced in *Syngap*$^{+/-}$ mice to 1.25 ± 0.13 ($p < 0.01$) (Fig. 3*f*). The decrease in wall-to-hollow ratio reflects an increase in the number of neurons in the barrel hollow and a decrease in the number in the barrel wall (Fig. 3*f*). No difference in the overall number of barrel neurons was observed. This reduction in barrel segregation in *Syngap*$^{+/-}$ mice is not attributable to a delay in barrel formation, because it is visible at all ages examined (data not shown). Furthermore, the decrease in cortical cell segregation did not result from a decrease in TCA segregation, because TCA patch formation appears normal in *Syngap*$^{+/-}$ animals (Fig. 2*d*). To address this issue quantitatively, we measured the area of PMBSF and individual TCA patches identified with 5-HTT immunoreactivity in normal compared with WT animals (Fig. 2*f*). (supplemental Fig. 1, available at www.jneurosci.org as supplemental material). PMBSF size and TCA patch sizes were not significantly different between *Syngap*$^{+/+}$ and *Syngap*$^{+/-}$ animals indicating normal TCA patch segregation.

SynGAP is needed for barreloid but not barrelette formation

In the trigeminal pathway, the segregation into whisker-specific modules also occurs within the brainstem and thalamus where they are referred to as barrelettes and barreloids, respectively. The incomplete segregation of TCAs in *Syngap*$^{-/-}$ mice raised the possibility that SynGAP plays a role in the segregation of barreloids in the VpM of the thalamus. CO histochemistry in wild-type mice showed clear segregation of barreloids at both P4 and P7 (Fig. 4*a* and *d*, respectively). In contrast, *Syngap*$^{-/-}$ showed reduced segregation at P4 and P7 (Fig. 4*c* and *f*, respectively). Patches of CO label are visible in the dorsolateral region of VpM corresponding to the large whisker representations; however, no segregation is visible in the regions receiving input from whiskers on the anterior snout. In P7 *Syngap*$^{+/-}$ mice (Fig. 4*e*), barreloid segregation was indistinguishable from *Syngap*$^{+/+}$ animals. At P4, barreloids were visible in the *Syngap*$^{+/-}$ animals; however, segregation does not appear as complete as in WT mice (Fig. 4*b* and *a*, respectively). These data indicate that reduced levels of SynGAP may result in a delay in barreloid formation. No delay in TCA segregation in layer 4 has been observed (data not shown). In contrast to the developmental pattern in the barreloids, CO staining revealed normal formation of barrelettes in both the principal nucleus (Fig. 4*g*,*h*) of the trigeminal complex (PrV) and the subnucleus interpolaris (SpI) (Fig. 4*i*,*j*) of P4 *Syngap*$^{+/-}$ (Fig. 4*g*,*i*) and *Syngap*$^{-/-}$ (Fig. 4*h*,*j*) mice. The normal formation of whisker-related structures in these brainstem nuclei is in good agreement with the lack of SynGAP expression in the developing trigeminal nuclei (see below).

The smaller body weight and cortical size of *Syngap*$^{-/-}$ animals raises the possibility that the lack of barrels in these animals results from general ill health or defects in brain development. We find this possibility very unlikely for several reasons. First, general ill health does not prevent TCA or barrel segregation (Vongdokmai, 1980). For example, mice lacking trkB show reduced body and brain weight and, similar to *Syngap*$^{-/-}$ mice, die during the first postnatal week. Despite their general ill health, we have shown that TCAs segregate normally in layer 4, and barrels are indistinguishable from wild-type controls (Vitalis et al., 2002). Second, barrelettes form normally in the trigeminal brain-

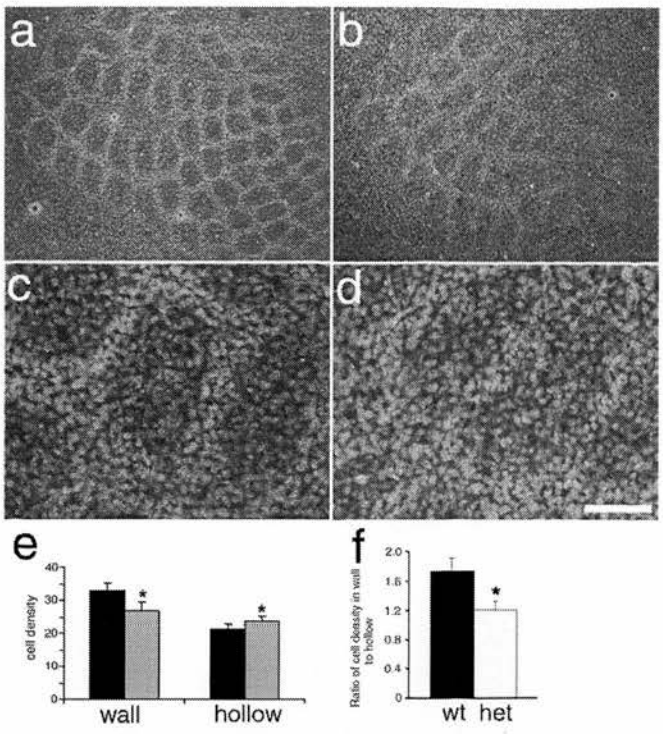

Figure 3. Reduced barrel segregation in *Syngap*$^{+/-}$ mice. Propidium iodide staining showing neuronal distribution in flattened sections from WT (***a***, ***c***) and *Syngap*$^{+/-}$ (***b***, ***d***) mice showing a clear reduction in the ratio of cells in the barrel wall to barrel hollow in *Syngap*$^{+/-}$ mice. Cell counts revealed a significant decrease ($p < 0.01$) in the density of barrel wall neurons and a significant increase ($p < 0.01$) in the density of barrel hollow neurons in *Syngap*$^{+/-}$ (gray bars) compared with *Syngap*$^{+/-}$ (black bars) animals (***e***). The barrel wall to hollow ratio is significantly reduced ($p < 0.01$) from 1.8 in WT mice to 1.2 in *Syngap*$^{+/-}$ mice (***f***). The reduction in this ratio appears to be caused by a change in the distribution of cells rather than an overall change in the number of cells (***f***). Scale bar (in ***d***): ***a***, ***b***, 250 μm; ***c***, ***d***, 70 μm. Error bars represent SE. het, Heterozygotes.

stem nuclei of *Syngap*$^{-/-}$ mice where SynGAP is not expressed strongly, suggesting the lack or decrease in barrel or barreloid segregation is specific to the lack of SynGAP. Third, cortical development appears normal in all features, apart from TCA segregation and barrel formation in S1. We observe no general problem with TCA pathfinding; TCAs stop in layer 4 of S1 and also form their typical segregation into sensory areas. Even within S1, the segregation of body regions occurs normally as the representation of the forepaw, hindpaw, lower jaw, anterior snout, and PMBSF can all be clearly demarcated (Fig. 2). The only defects observed are within PMBSF and anterior snout regions of S1. Fourth, levels of cytochrome oxidase activity appear normal in VpM and cortex in *Syngap*$^{-/-}$ animals, again suggesting no general defect in activity levels in cortex (Fig. 4) (data not shown). Finally, *Syngap*$^{+/-}$ animals show clear deficits in barrel development despite being indistinguishable from the WT littermates in general health and other aspects of brain development examined.

Postnatal development of SynGAP expression in the somatosensory pathway

The analysis of the mutant mice indicates a temporal and spatial requirement for SynGAP in the development of the trigeminal system. To identify the cells expressing *Syngap*, we examined the spatiotemporal expression profile of *Syngap* in *Syngap*$^{+/-}$ animals, taking advantage of the presence of the insertion of the gene encoding β-galactosidase (β-gal) into the *Syngap* locus (Komiyama et al., 2002). It should be noted that because there is an internal ribosomal entry site upstream of the β-galactosidase gene, translation of the protein would not be effected by regulatory sequences in the 3′ and 5′ untranslated regions of the mRNA. Hence, X-Gal expression is more likely to reflect the expression profile of *Syngap* mRNA rather than SynGAP protein. To validate the *LacZ* reporter, we examined the levels of *Syngap* mRNA using real-time RT-PCR with primers specific for the conserved GAP domain (supplemental Fig. 3*b*, available at www.jneurosci.org as supplemental material). These results were consistent with the X-Gal histochemistry as *Syngap* mRNA levels peaked during the second postnatal week in the barrel cortex before being dramatically reduced in the adult. In addition, because lacZ does not contain any SynGAP peptide sequences, including those for localization to dendrites, staining will accurately report on the cells in which SynGAP is normally transcribed and not the localization of SynGAP protein. Hence, X-Gal staining appears as one or several cytoplasmic inclusions and was not seen in dendrites or axons.

In barrel cortex, X-Gal staining clearly reveals a regionalized pattern of *Syngap* expression throughout development (Fig. 5) (supplemental Fig. 3, available at www.jneurosci.org as supplemental material). At P0, *Syngap* expression was located throughout the dorsal thalamus with high levels in both the dorsal lateral geniculate nucleus and ventrobasal complex (VB) (supplemental Fig. 3, available at www.jneurosci.org as supplemental material). No X-Gal staining was observed in the ventral thalamus indicating a selective expression in projection nuclei of the thalamus. X-Gal staining remained high throughout the dorsal thalamus at P4 (Fig. 5*c*), including within VB, where it increased dramatically by P8 (Fig. 5*d*). Staining remained high until P14 before decreasing at P21 (supplemental Fig. 3, available at www.jneurosci.org as supplemental material). No staining was seen in any region of the adult thalamus.

Throughout cortical development, X-Gal expression appeared in a pattern consistent with a neuronal localization. It was not found in the white matter, suggesting it is not present in oligodendrocytes. Furthermore, no X-Gal-positive cells were visible in layer 1, and no double-labeled cells were seen when sections were stained with the astrocyte marker GFAP, strongly suggesting it is not present in astrocytes (data not shown). At P0 in the somatosensory cortex, X-Gal expression appeared as a thin dense band at the bottom of the cortical plate (supplemental Fig. 3, available at www.jneurosci.org as supplemental material). The ventricular zone, subventricular zone, intermediate zone, and upper layers of the cortical plate showed little or no staining. At P4, *Syngap* expression was clearly present through the granular and supragranular layers of the cortex (Fig. 5*b*). Little staining was observed in the infragranular layers, although a thin band of cells can be seen at the bottom of layer 6. During the second postnatal week, X-Gal staining was present throughout the cortical plate with highest levels in layer 4, where clear staining was seen in the barrel walls (Fig. 5*a*). By P35, the density of labeled cells had decreased and in the adult two thin bands of label remained in upper layer 2 and at the layer 4/5 boundary (supplemental Fig. 3, available at www.jneurosci.org as supplemental material).

Immunohistochemical distribution of SynGAP protein in S1 cortex and VpM was in good agreement with the results obtained for X-Gal staining (Fig. 5*e–g*). At P7 (Fig. 5*e*,*f*), SynGAP is expressed throughout S1 with highest staining in the layer 4 and the supragranular layers. Patchy label representing barrels is clearly present in layer 4 corresponding to high expression in barrels

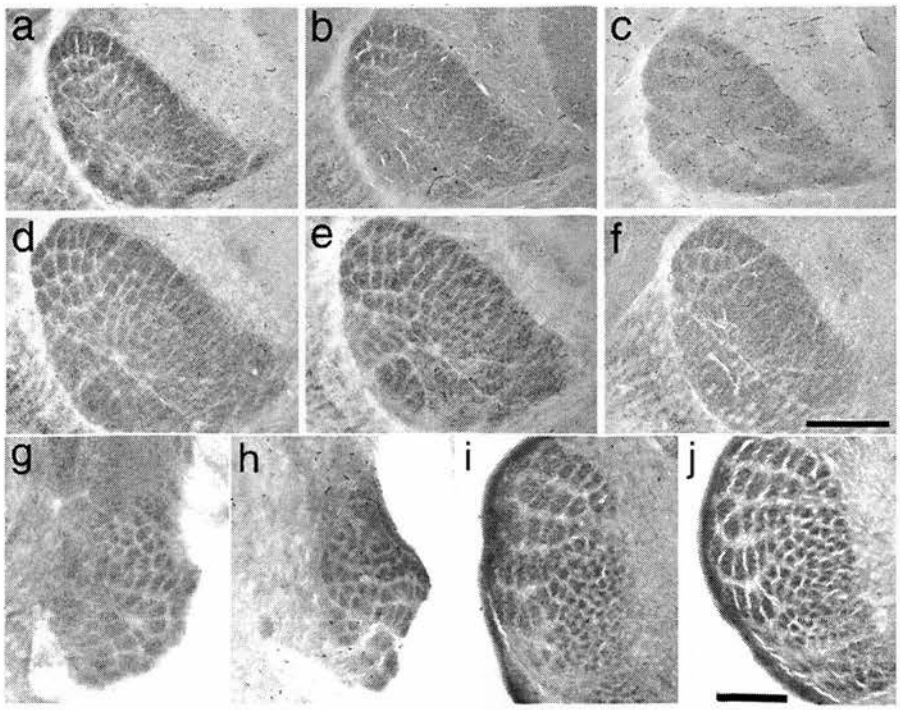

Figure 4. Reduced barreloid segregation in *Syngap*$^{-/-}$ mice. Cytochrome oxidase staining in VpM of thalamus to reveal barreloids in *Syngap*$^{+/+}$ (***a***, ***d***), *Syngap*$^{+/-}$ (***b***, ***e***), and *Syngap*$^{-/-}$ (***c***, ***f***) mice at P4 (***a–c***) and P7 (***d–f***). Barreloids can be clearly seen in all genotypes at both P3/4 and P7; however, segregation is clearly reduced in *Syngap*$^{-/-}$ mice ($n = 5$) at both ages relative to *Syngap*$^{+/+}$ ($n = 8$) and *Syngap*$^{+/-}$ ($n = 12$) mice, especially in the anterior snout representations. Coronal section through the brainstem trigeminal complex stained for cytochrome oxidase in P3/4 control (***g***, ***i***; $n = 10$) and *Syngap*$^{-/-}$ (***h***, ***j***; $n = 6$) mice showing normal barrelette formation in PrV (***g***, ***h***) and Spl (***i***, ***j***). Scale bars: (in ***f***) ***a–f***, 350 μm; (in ***j***) ***g***, ***h***, 225 μm; (in ***j***) ***i***, ***j***, 250 μm.

(Fig. 5*f*). SynGAP is also expressed in the barreloids in good agreement with its role in barreloid segregation (Fig. 5*g*).

To determine the subcellular localization of SynGAP, we performed immunoelectron microscopy on layer 4 from P14 barrel cortex (Fig. 5*h–j*). SynGAP immunoreactivity can be clearly seen in postsynaptic densities abutting presynaptic terminals containing synaptic vesicles. SynGAP was also seen throughout dendritic shafts; however, a precise subcellular localization was prevented because of the large amount of DAB reaction product. Reaction product was never seen in the axons or presynaptic terminals. A postsynaptic localization for SynGAP in cortex is in good agreement with previous findings from several groups showing SynGAP selectively associates with PSD in cultured hippocampal neurons. To further examine the likely localization of SynGAP during barrel development, we examined the expression of *Syngap* splice variants during barrel cortex development. *Syngap* is a heteromeric mRNA consisting of three known N-terminal (a, b, c) and seven known C-terminal (α1, 2, β1–4, γ) splice variants (Li et al., 2001). *SynGAPα1* is the isoform of SynGAP originally characterized by Kim et al. (1998) and Chen et al. (1998). In cultured cerebellar neurons, SynGAPα2 was shown to localize to axons (Tomoda et al., 2004). To determine whether SynGAPα2 was present in developing VpM and hence could localize to TCAs, we examined the expression of the mRNA encoding the SynGAP isoforms in layer 4 and VpM of P8 mice. Using primers designed to amplify all known 3′ isoforms of the *Syngap* gene, we used PCR to amplify, clone, and sequence *Syngap* mRNAs from layer 4 cells and VpM. Of the 17 *Syngap* cDNAs cloned from VpM, none encoded sequence for *Syngapα2*, indicating that the axon-associated form of *Syngap* is not present in the VpM cells during barrel development (data not shown).

SynGAP interactions with PSD-95 and H-Ras

The family of MAGUK proteins that interact with the NMDAR include PSD-95, PSD-93/Chapsyn-110, and SAP102. Each contains three PDZ domains, of which the first two bind to the C termini of NR2 subunits. The third PDZ domain of PSD-95 and SAP-102 binds to the C terminus of SynGAP. To explore whether PSD-95 was the specific MAGUK protein responsible for regulating SynGAP, we examine the barrel phenotype of adult ($n = 3$) and P7 ($n = 7$) *Psd-95*$^{-/-}$ mutant mice (Migaud et al., 1998). There was no abnormality detected (Fig. 6*c*). The lack of any discernible alteration in barrel pattern in the *Psd-95*$^{-/-}$ animals raised the possibility that SynGAP may be associating with the PSD in a PSD-95-independent manner. To examine this possibility, we isolated PSDs from barrel cortex taken from wild-type and *Psd-95*$^{-/-}$ animals at P7 (Fig. 7*b*). A 135 kDa band corresponding to the SynGAP protein was clearly visible in both synaptosomes and PSD fractions of wild-type and *Psd-95*$^{-/-}$ animals. We also examined the developmental profile of PSD component proteins in S1 cortex homogenates and in synaptosomal fractions from P7 S1 cortex (Fig. 7*a*). SynGAP, NR1, and SAP-102 were all present in neonatal homogenates of barrel cortex and increased their expression levels into adulthood. In contrast, NR2A was barely detectable in homogenates of barrel cortex at P7, increased dramatically by P14 and continued to increase gradually into adulthood. PSD-95 is expressed throughout the first postnatal week and then increases dramatically from P14 to adulthood. This increase in PSD-95 expression was so dramatic that two separate concentrations of primary antibody were needed to clearly analyze the low and high end of the developmental expression. PSD-95 was highly enriched in synaptosomes at P7; however, the presence of PSD-95 was not necessary for SynGAP association with the PSD. These data indicate that PSD-95 is not the key MAGUK for mediating SynGAP function during barrel formation; instead, this function may reside in either SAP102, other MAGUKs, or via MAGUK-independent interactions.

Our results examining the *Syngap* splice variants expressed during cortical development are in good agreement with these biochemical findings. SynGAPα1 is the C-terminal splice variant that contains the QTRV sequence necessary for binding to the PDZ domain of PSD-95. Interestingly, of the 13 clones analyzed from layer 4 of barrel cortex, Syngapα1 was not found. One of 13 clones encoded a protein that differed by only two amino acids from SynGAPα1 and contained the coding region for the QTRV sequence. It also coded for the peptide sequence recognized by the SynGAPα1-specific antibody. To determine the relative abundance of SynGAPα1 protein in the developing barrel cortex, we compared the developmental profile of SynGAPα1 to all SynGAPs using a pan-SynGAP antibody, the epitope of which lies in

the GAP domain (Fig. 7*a*). Both pan-SynGAP and SynGAPα1 levels increase dramatically during the second postnatal week; however, unlike pan-SynGAP, very little SynGAPα1 is present during the first postnatal week. These data strongly suggest that the principal isoforms of SynGAP present during barrel formation are not those that bind directly to the MAGUKs.

In vitro studies show that SynGAP hydrolyzes H-Ras-GTP to H-Ras-GDP (Chen et al., 1998). If H-Ras is the key effector for SynGAP, then H-Ras mutants may show a barrel phenotype. We detected no overt phenotype in the barrel cortex of either adult ($n = 3$) (Fig. 6*b*) or P7 ($n = 5$) *H-Ras* homozygous null mice. The absence of an *in vivo* effector role for H-Ras in the cortex is consistent with previous data in the hippocampus (Komiyama et al., 2002). The presence of other Ras isoforms in the barrel cortex may provide the physiological substrate for SynGAP.

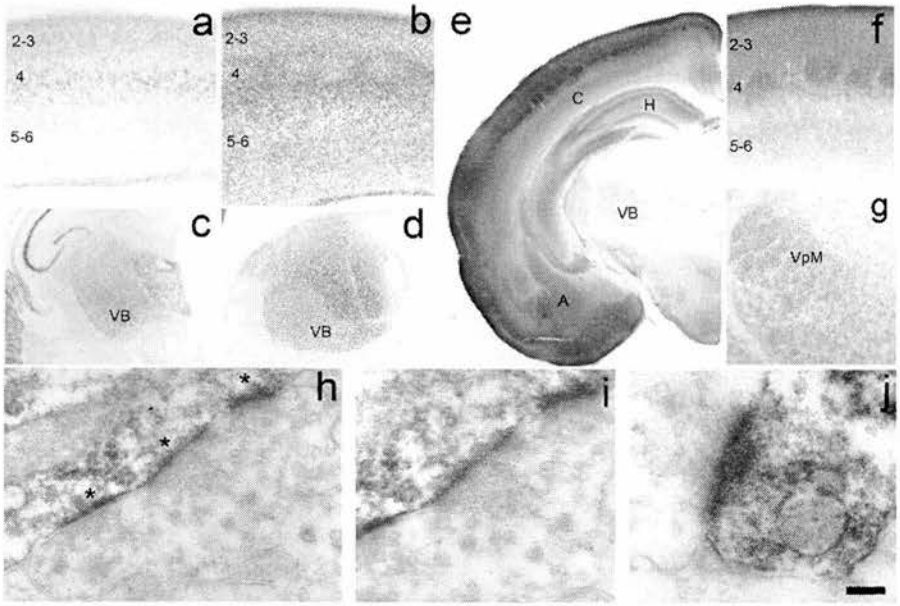

Figure 5. SynGAP expression in the developing cortex and thalamus. Histochemistry for β-galactosidase to reveal the expression profile of *Syngap* in the S1 (***a***, ***b***) and thalamus (***c***, ***d***) at P4 (***a***, ***c***) and P8 (***b***, ***d***). For a complete developmental series, see supplemental Figure 2 (available at www.jneurosci.org as supplemental material). In cortex, β-gal is first expressed at P0 in layer 4 of the developing cortical plate. By P4, staining can be seen throughout the supragranular layers as well as layer 4 and the upper region of layer 5. It is also present in a thin strip of cells located at the bottom of the cortical plate (***a***). By P8, staining can be seen throughout the cortical plate, and the barrels are clearly distinguished in layer 4 (***c***). By adulthood, staining has been dramatically reduced and can only be seen at the layer 4/5 border and in layer 1. A similar developmental profile can be seen in the VB and throughout the dorsal thalamus with strong staining visible at P4 (***c***) and P8 (***d***) and reduced expression in adults. Immunohistochemical localization of SynGAP protein at P7 (***e–g***) is in good agreement with β-gal localization. Low-power images show high levels of SynGAP in the cortex (C), hippocampus (H), and amygdaloid complex (A) with lower levels in the VB of the thalamus. In S1 (***f***), SynGAP levels are highest in layer 4, and the supragranular layers and barrels can be clearly seen. Expression is just starting to appear in the infragranular layers, although a dense band of label can be seen at the layer 4/5 border. The immunohistochemical localization therefore is in good agreement with the large increase in X-Gal staining between P4 and P7. In thalamus, SynGAP is expressed throughout the VB. Electron microscopy analysis of SynGAP expression in layer 4 at P14 reveals a postsynaptic localization for SynGAP (***h–j***). DAB reaction product can be clearly seen as dark labeling in the PSD (asterisks) opposing presynaptic terminals containing synaptic vesicles. In ***h***, three PSDs in tandem on the shaft of a dendrite are clearly visible. Higher magnification of the middle synapse in ***h*** shows clear amalgamation of presynaptic vesicles abutting the SynGAP-positive PSD. Clear presynaptic vesicles are also seen in ***j***. Reaction product was never seen in axons or axon terminals. Scale bar (in ***j***): ***a***, ***b***, 200 μm; ***c***, ***d***, 400 μm; ***e***, 775 μm; ***f***, 150 μm; ***g***, 275 μm; ***h***, 250 nm; ***i***, 175 nm; ***j***, 100 nm.

Discussion

NMDA receptors play a critical role in the development of the somatosensory cortex (Schlaggar et al., 1993; Fox et al., 1996; Iwasato et al., 2000; Datwani et al., 2002). The intracellular pathways through which NMDARs signal to initiate these morphological changes are not clear. We show that SynGAP, a component of the mature NMDA receptor complex (Chen et al., 1998; Kim et al., 1998, 2003; Komiyama et al., 2002), is expressed in the developing PSD and regulates S1 cortical development. Mice lacking SynGAP show an absence of barrels and only partial formation of barreloids in VpM. Thalamocortical axons segregate into rows, but individual whisker-related clusters do not form. *SynGAP*$^{+/-}$ animals also show reduced barrel segregation but normal clustering of TCA and normal barreloid formation. Barrel development is normal in *Psd-95*$^{-/-}$ animals. SynGAP maintains its association with the PSD in P7 S1 cortex in the absence of PSD-95. These data demonstrate a crucial role for SynGAP in the organization of sensory maps selectively in forebrain structures. They also highlight the heterogeneity of intracellular pathways used by different brain regions at different developmental stages.

SynGAP in barreloid and barrel formation

SynGAP was initially identified as a Ras-GAP (Chen et al., 1998; Kim et al., 1998), the activity of which is regulated by NMDA receptor stimulation in hippocampus (Komiyama et al., 2002; Oh et al., 2004). Our findings suggest that SynGAP is also downstream of NMDA receptor activation during trigeminal pathway development. SynGAP associates with the PSD in developing S1. Furthemore, the phenotype resulting from the loss of NMDA receptors or SynGAP are very similar. In cortex, NMDA receptors and SynGAP are necessary for barrel formation but not for the development of cortical layers or cell type (Messersmith et al., 1997; Iwasato et al., 2000). In *Syngap*$^{-/-}$ mice, cortical lamination, radial distribution of calretinin-positive interneurons, distribution of PKARIIβ, and radial termination of TCAs are similar to WT mice. Barreloid formation is also dependent on NMDARs (Iwasato et al., 1997) and SynGAP. In contrast, we found no role for SynGAP in barrelette formation, although NMDARs are required (Li et al., 1994; Iwasato et al., 1997). These observations suggest that NMDA receptor-dependent development uses different signaling proteins in different neuronal populations to achieve very similar cellular outcomes (e.g., axon segregation). These findings are also in agreement with previous studies showing that mGluR5 signaling via PLC-β1 is critical in barrel formation (Hannan et al., 2001) but not for barreloid and barrelette formation (our unpublished observations).

The finding that TCAs in *Syngap*$^{-/-}$ mice form rows but not individual patches raises the possibility that the cortical defect in *Syngap*$^{-/-}$ mice is secondary to thalamic defects. However, two main findings indicate a cortical role for SynGAP during barrel formation in addition to its role in the thalamus. First, a significant reduction in barrel segregation was seen in *Syngap*$^{+/-}$ animals despite normal segregation of TCAs into whisker-related patches. Second, in *Syngap*$^{-/-}$ mice, TCAs segregate into rows, but no barrels form around these rows. In contrast, in WT mice,

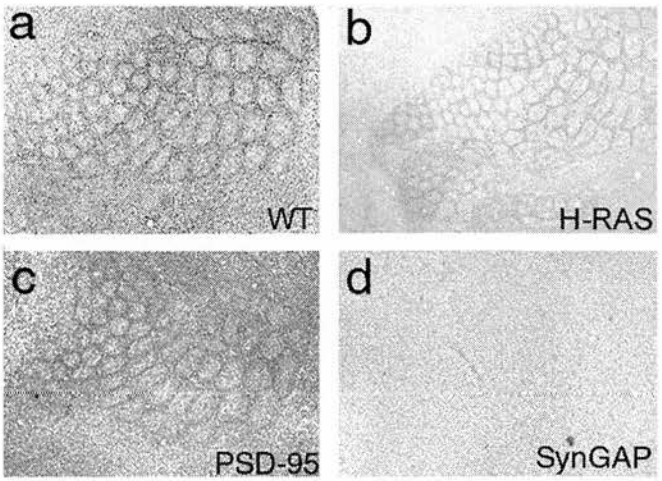

Figure 6. Normal barrel formation in mice lacking PSD-95 and H-Ras. Nissl staining in flattened sections through layer 4 of WT (***a***), H-Ras (***b***), PSD-95 (***c***), and SynGAP (***d***) mutant mice.

the soma of layer 4 neurons cluster around the row of TCAs that forms after cauterization of row C follicles to form one large barrel (Van der Loos and Woolsey, 1973). If barrel formation is independent of cortically expressed SynGAP, a large barrel would be expected to form around the rows of TCAs in *Syngap*$^{-/-}$ mice; this result was never observed.

It is not yet clear whether the incomplete segregation of TCAs into rows results from the loss of SynGAP in the cortex or thalamus. In *CxNR1*$^{-/-}$ mice, TCAs form rudimentary patches, and there is a significant decrease in TCA complexity within layer 4 (Lee et al., 2005), indicating that cortically derived signals regulate TCA elaboration independently of axon segregation. NMDA receptors similarly regulate axon dynamics in *Xenopus* tectum (Ruthazer et al., 2003). NMDA receptors may be regulating axon branch dynamics via SynGAP-regulated release of a retrograde signal. Alternatively, the loss of TCA segregation in *Syngap*$^{+/-}$ animals could arise from a cell-autonomous defect in the thalamic neurons that prevents terminal segregation in the cortex. Distinguishing between these two possibilities awaits examination of mice with a cortex-specific *Syngap* deletion.

Association of SynGAP with the PSD

SynGAP has been demonstrated to associate with the PSD via PSD-95 (Chen et al., 1998; Kim et al., 1998). However, we have shown that *Psd-95*$^{-/-}$ mice develop normal barrels, and SynGAP remains associated with the developing PSD in these mice. The apparent discrepancy between these findings may be resolved by the recent finding that in adult hippocampus, SynGAP is preferentially associated with NR2B receptors via an interaction with SAP-102 (Kim et al., 2005). It is also consistent with previous studies examining the developmental and spatial expression profiles of these PSD components (Porter et al., 2005). During development, NMDA receptors are predominantly NR2B containing and associated with SAP-102; NR2A and PSD-95 are expressed later in development and may displace NR2B/SAP-102 complexes from the PSD (Shi et al., 1997; Sans et al., 2000; Yoshii et al., 2003; Van Zundert et al., 2004). In S1, we found high levels of both PSD-95 and SAP-102 in the developing PSD, and their increase correlates well with the rapid increase in synapse formation in rodent S1 (Micheva and Beaulieu, 1996; White et al., 1997; Spires et al., 2004). However, PSD-95 levels increase more dramatically with age and therefore more closely parallel the NR2A

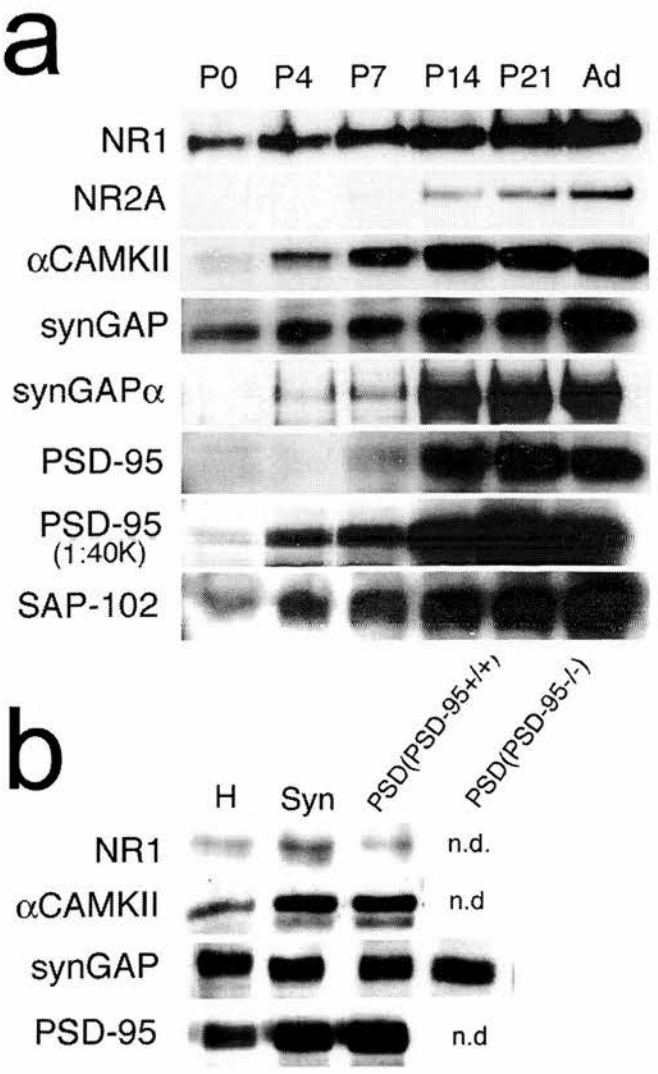

Figure 7. SynGAP still associates with the PSD in *Psd-95*$^{-/-}$ mice. Western blotting for PSD components in homogenates of S1 cortex reveals a dramatic increase in PSD components during the first postnatal week (***a***). ***b***, Western blotting for NR1, CaMKII, PSD-95, and SynGAP (Syn) in homogenates, synaptosomes, and PSDs isolate from S1 of P7 WT mice as well as SynGAP expression in the PSD of P7 *Psd-95*$^{-/-}$ mice. n.d., Not done.

development expression profile. These findings suggest that, during barrel development, SynGAP may be associating with NR2B-containing receptors via SAP-102 and not PSD-95.

Alternatively, SynGAPs association with the PSD in developing S1 cortex may be independent of MAGUKs. Analysis of the C-terminal isoforms of SynGAP in layer 4 revealed a preponderance of SynGAP splice variants that do not contain the MAGUK-binding consensus sequence (Li et al., 2001). Thus, in developing S1, SynGAP may be associating with the PSD in a MAGUK-independent manner as has been described previously (Vazquez et al., 2004), possibly via its Plecktrin homology (PH) or C2 domains.

Pathways downstream of SynGAP

SynGAP has been shown to regulate the activation of ERK-mitogen-activated protein kinase (MAPK) through its role as a Ras-GAP (Komiyama et al., 2002). Furthermore, the Ras-ERK-MAPK pathway has been demonstrated to control numerous developmental processes, including synaptic plasticity, cell prolif-

eration, survival, migration, and differentiation (Gille and Downward, 1999; Di Cristo et al., 2001; Adams and Sweatt, 2002; Sweatt, 2004). These findings indicate that SynGAP maybe regulating barrel formation by regulating ERK activation and are in good agreement with previous work demonstrating a role for ERK-MAPK in visual cortical development as well as in NMDAR-dependent LTP in visual cortex (Di Cristo et al., 2001) and hippocampus (Winder et al., 1999) and performance on spatial learning tasks (Bozon et al., 2003). These results strongly indicate a conservation of signaling pathways for various forms of plasticity in a variety of brain areas at various developmental ages.

We have shown previously that mGluR5 signaling through PLC-β1 is crucial for barrel formation (Hannan et al., 2001). Because mGluR activation is also capable of regulating ERK activation (Choe and Wang, 2001; Berkeley and Levey, 2003; Gallagher et al., 2004), it is possible that ERK may be a common downstream target of multiple signaling pathways initiated from mGluR5 and NMDA receptors during cortical neuronal development. Interestingly, mGluR5$^{-/-}$ mice also show segregation of TCAs into rows, similar to the *Syngap*$^{-/-}$ mice, raising the possibility that mGluR5 may regulate SynGAP activity, possibly via PLC-β1 stimulated Ca^{2+} release from endoplasmic reticulum and subsequent CaMKII activity. A similar integrative role for ERK has been proposed previously (Watabe et al., 2000; Adams and Sweatt, 2002). This could explain why loss of any of the pathways leading to ERK regulation results in a disruption of barrel development.

It is also possible that SynGAP may be regulating pathways that are Ras dependent but ERK independent. In support of this possibility *Syngap*$^{+/-}$ mice showed defects in LTP induction using pairing protocols and 100 Hz stimulation (Komiyama et al., 2002), two forms of LTP induction that are ERK independent in wild-type slices (Winder et al., 1999; Watabe et al., 2000). Furthermore, Ras can regulate the activity of PI3-kinase (Sanna et al., 2002), which plays a crucial role in certain types of synaptic plasticity (Kelly and Lynch, 2000; Sanna et al., 2002; Opazo et al., 2003). Alternatively, SynGAP may be a GTPase for other non-RAS small G-proteins. For example, SynGAP has recently been shown to regulate Rab-5 activity (Tomoda et al., 2004) and Rab-5 has been shown to regulate the actin cytoskeleton during the formation of "circular ruffles" and three-dimensional migration (Lanzetti et al., 2004).

The mechanisms by which activity and, more specifically, glutamate neurotransmission, mediates early cortical development and map formation will be crucial to understand normal brain development and the cellular events that underlie many forms of mental retardation and possibly provide treatments for adult neurodegenerative diseases. We have shown that SynGAP plays a crucial role in the anatomical development of maps in the primary somatosensory cortex of mice and hence may be crucial in establishing the complex neuronal circuitry that mediates normal cortical function.

References

Adams JP, Sweatt JD (2002) Molecular psychology: roles for the ERK MAP kinase cascade in memory. Annu Rev Pharmacol Toxicol 42:135–163.

Barnett MW, Old RW, Jones EA (1998) Neural induction and patterning by fibroblast growth factor, notochord and somite tissue in *Xenopus*. Dev Growth Differ 40:47–57.

Berkeley JL, Levey AI (2003) Cell-specific extracellular signal-regulated kinase activation by multiple G protein-coupled receptor families in hippocampus. Mol Pharmacol 63:128–135.

Bozon B, Kelly A, Josselyn SA, Silva AJ, Davis S, Laroche S (2003) MAPK, CREB and zif268 are all required for the consolidation of recognition memory. Philos Trans R Soc Lond B Biol Sci 358:805–814.

Chen HJ, Rojas-Soto M, Oguni A, Kennedy MB (1998) A synaptic Ras-GTPase activating protein (p135 synGAP) inhibited by CaM kinase II. Neuron 20:895–904.

Choe ES, Wang JQ (2001) Group I metabotropic glutamate receptor activation increases phosphorylation of cAMP response element-binding protein, Elk-1, and extracellular signal-regulated kinases in rat dorsal striatum. Brain Res Mol Brain Res 94:75–84.

Datwani A, Iwasato T, Itohara S, Erzurumlu RS (2002) NMDA receptor-dependent pattern transfer from afferents to postsynaptic cells and dendritic differentiation in the barrel cortex. Mol Cell Neurosci 21:477–492.

Di Cristo G, Berardi N, Cancedda L, Pizzorusso T, Putignano E, Ratto GM, Maffei L (2001) Requirement of ERK activation for visual cortical plasticity. Science 292:2337–2340.

Dunkley PR, Jarvie PE, Heath JW, Kidd GJ, Rostas JA (1986) A rapid method for isolation of synaptosomes on Percoll gradients. Brain Res 372:115 129.

Erzurumlu RS, Kind PC (2001) Neural activity: sculptor of "barrels" in the neocortex. Trends Neurosci 24:589–595.

Fox K, Schlaggar BL, Glazewski S, O'Leary DD (1996) Glutamate receptor blockade at cortical synapses disrupts development of thalamocortical and columnar organization in somatosensory cortex. Proc Natl Acad Sci USA 93:5584–5589.

Franklin KBJ, Paxinos G (1997) The mouse brain in stereotaxic coordinates. San Diego: Academic.

Gallagher SM, Daly CA, Bear MF, Huber KM (2004) Extracellular signal-regulated protein kinase activation is required for metabotropic glutamate receptor-dependent long-term depression in hippocampal area CA1. J Neurosci 24:4859–4864.

Gaspar P, Cases O, Maroteaux L (2003) The developmental role of serotonin: news from mouse molecular genetics. Nat Rev Neurosci 4:1002–1012.

Gille H, Downward J (1999) Multiple ras effector pathways contribute to G(1) cell cycle progression. J Biol Chem 274:22033–22040.

Hannan AJ, Blakemore C, Katsnelson A, Vitalis T, Huber KM, Bear M, Roder J, Kim D, Shin HS, Kind PC (2001) Phospholipase C-β1, activated via mGluRs, mediates activity-dependent differentiation in cerebral cortex. Nat Neurosci 4:282–288.

Ho W, Uniyal S, Meakin SO, Morris VL, Chan BM (2001) A differential role of extracellular signal-regulated kinase in stimulated PC12 pheochromocytoma cell movement. Exp Cell Res 263:254–264.

Husi H, Ward MA, Choudhary JS, Blackstock WP, Grant SG (2000) Proteomic analysis of NMDA receptor-adhesion protein signaling complexes. Nat Neurosci 3:661–669.

Iwasato T, Erzurumlu RS, Huerta PT, Chen DF, Sasaoka T, Ulupinar E, Tonegawa S (1997) NMDA receptor-dependent refinement of somatotopic maps. Neuron 19:1201–1210.

Iwasato T, Datwani A, Wolf AM, Nishiyama H, Taguchi Y, Tonegawa S, Knopfel T, Erzurumlu RS, Itohara S (2000) Cortex-restricted disruption of NMDAR1 impairs neuronal patterns in the barrel cortex. Nature 406:726–731.

Kelly A, Lynch MA (2000) Long-term potentiation in dentate gyrus of the rat is inhibited by the phosphoinositide 3-kinase inhibitor, wortmannin. Neuropharm 39:643–651.

Killackey HP, Belford GR (1979) The formation of afferent patterns in the somatosensory cortex of the neonatal rat. J Comp Neurol 183:285–304.

Kim JH, Liao D, Lau LF, Huganir RL (1998) SynGAP: a synaptic RasGAP that associates with the PSD-95/SAP90 protein family. Neuron 20:683–691.

Kim JH, Lee HK, Takamiya K, Huganir RL (2003) The role of synaptic GTPase-activating protein in neuronal development and synaptic plasticity. J Neurosci 23:1119–1124.

Kim MJ, Dunah AW, Wang YT, Sheng M (2005) Differential roles of NR2A- and NR2B-containing NMDA receptors in Ras-ERK signaling and AMPA receptor trafficking. Neuron 46:745–760.

Kind PC, Neumann PE (2001) Plasticity: downstream of glutamate. Trends Neurosci 24:553–555.

Kind P, Blakemore C, Fryer H, Hockfield S (1994) Identification of proteins down-regulated during the postnatal development of the cat visual cortex. Cereb Cortex 4:361–375.

Komiyama NH, Watabe AM, Carlisle HJ, Porter K, Charlesworth P, Monti J,

Strathdee DJ, O'Carroll CM, Martin SJ, Morris RG, O'Dell TJ, Grant SG (2002) SynGAP regulates ERK/MAPK signaling, synaptic plasticity, and learning in the complex with postsynaptic density 95 and NMDA receptor. J Neurosci 22:9721–9732.

Krapivinsky G, Medina I, Krapivinsky L, Gapon S, Clapham DE (2004) SynGAP-MUPP1-CaMKII synaptic complexes regulate p38 MAP kinase activity and NMDA receptor-dependent synaptic AMPA receptor potentiation. Neuron 43:563–574.

Lanzetti L, Palamidessi A, Areces L, Scita G, Di Fiore PP (2004) Rab5 is a signalling GTPase involved in actin remodelling by receptor tyrosine kinases. Nature 429:309–314.

Lee LJ, Iwasato T, Itohara S, Erzurumlu RS (2005) Exuberant thalamocortical axon arborization in cortex-specific NMDAR1 knockout mice. J Comp Neurol 485:280–292.

Li W, Okano A, Tian QB, Nakayama K, Furihata T, Nawa H, Suzuki T (2001) Characterization of a novel synGAP isoform, synGAP-beta. J Biol Chem 276:21417–21424.

Li Y, Erzurumlu RS, Chen C, Jhaveri S, Tonegawa S (1994) Whisker-related neuronal patterns fail to develop in the trigeminal brainstem nuclei of NMDAR1 knockout mice. Cell 76:427–437.

Messersmith EK, Feller MB, Zhang H, Shatz CJ (1997) Migration of neocortical neurons in the absence of functional NMDA receptors. Mol Cell Neurosci 9:347–357.

Micheva KD, Beaulieu C (1996) Quantitative aspects of synaptogenesis in the rat barrel field cortex with special reference to GABA circuitry. J Comp Neurol 373:340–354.

Migaud M, Charlesworth P, Dempster M, Webster LC, Watabe AM, Makhinson M, He Y, Ramsay MF, Morris RG, Morrison JH, O'Dell TJ, Grant SG (1998) Enhanced long-term potentiation and impaired learning in mice with mutant postsynaptic density-95 protein. Nature 396:433–439.

Oh JS, Manzerra P, Kennedy MB (2004) Regulation of the neuron-specific Ras GTPase-activating protein, synGAP, by Ca^{2+}/calmodulin-dependent protein kinase II. J Biol Chem 279:17980–17988.

Opazo P, Watabe AM, Grant SG, O'Dell TJ (2003) Phosphatidylinositol 3-kinase regulates the induction of long-term potentiation through extracellular signal-related kinase-independent mechanisms. J Neurosci 23:3679–3688.

Porter K, Komiyama NH, Vitalis T, Kind PC, Grant SGN (2005) Differential expression of two NMDA receptor interacting proteins, PSD-95 and SynGAP during mouse development. EJN 21:351–362.

Rebsam A, Seif I, Gaspar P (2002) Refinement of thalamocortical arbors and emergence of barrel domains in the primary somatosensory cortex: a study of normal and monoamine oxidase a knock-out mice. J Neurosci 22:8541–8552.

Ruthazer ES, Akerman CJ, Cline HT (2003) Control of axon branch dynamics by correlated activity in vivo. Science 301:66–70.

Sanna PP, Cammalleri M, Berton F, Simpson C, Lutjens R, Bloom FE, Francesconi W (2002) Phosphatidylinositol 3-kinase is required for the expression but not the induction or maintenance of long-term potentiation in the hippocampal CA1 region. J Neurosci 22:3359–3365.

Sans N, Petralia RS, Wang YX, Blahos Jr J, Hell JW, Wenthold RJ (2000) A developmental change in NMDA receptor-associated proteins at hippocampal synapses. J Neurosci 20:1260–1271.

Schlaggar BL, Fox K, O'Leary DD (1993) Postsynaptic control of synaptic plasticity in developing somatosensory cortex. Nature 364:623–626.

Shi J, Aamodt SM, Constantine-Paton M (1997) Temporal correlations between functional and molecular changes in NMDA receptors and GABA neurotransmission in the superior colliculus. J Neurosci 17:6264–6276.

Spires TL, Molnar Z, Kind PC, Cordery PM, Upton AL, Blakemore C, Hannan AJ (2004) Activity-dependent regulation of synapse and dendritic spine morphology in developing barrel cortex requires phospholipase C-β1 signalling. Cereb Cortex 15:385–393.

Sweatt JD (2004) Mitogen-activated protein kinases in synaptic plasticity and memory. Curr Opin Neurobiol 14:311–317.

Tomoda T, Kim JH, Zhan C, Hatten ME (2004) Role of Unc51.1 and its binding partners in CNS axon outgrowth. Genes Dev 18:541–558.

Van der Loos H, Woolsey TA (1973) Somatosensory cortex: structural alterations following early injury to sense organs. Science 179:395–398.

Van Zundert B, Yoshii A, Constantine-Paton M (2004) Receptor compartmentalization and trafficking at glutamate synapses: a developmental proposal. Trends Neurosci 27:428–437.

Vazquez LE, Chen HJ, Sokolova I, Knuesel I, Kennedy MB (2004) synGAP regulates spine formation. J Neurosci 24:8862–8872.

Vitalis T, Cases O, Gillies K, Hanoun N, Hamon M, Seif I, Gaspar P, Kind PC, Price DJ (2002) Interactions between TrkB-signalling and serotonin excess in the developing murine somatosensory cortex: a role in tangential and radial organisation of thalamocortical axons. J Neurosci 22:4987–5000.

Vongdokmai R (1980) Effect of protein malnutrition on development of mouse cortical barrels. J Comp Neurol 191:283–294.

Walikonis RS, Jensen ON, Mann M, Provance Jr DW, Mercer JA, Kennedy MB (2000) Identification of proteins in the postsynaptic density fraction by mass spectrometry. J Neurosci 20:4069–4080.

Watabe AM, Zaki PA, O'Dell TJ (2000) Coactivation of β-adrenergic and cholinergic receptors enhances the induction of long-term potentiation and synergistically activates mitogen-activated protein kinase in the hippocampal CA1 region. J Neurosci 20:5924–5931.

White EL, Weinfeld L, Lev DL (1997) A survey of morphogenesis during the early postnatal period in PMBSF barrels of mouse SmI cortex with emphasis on barrel D4. J Comp Neurol Somatosens Mot Res 14:34–55.

Winder DG, Martin KC, Muzzio IA, Rohrer D, Chruscinski A, Kobilka B, Kandel ER (1999) ERK plays a regulatory role in induction of LTP by theta frequency stimulation and its modulation by beta-adrenergic receptors. Neuron 24:715–726.

Woolsey DH, Van der Loos H (1970) The structural organization of layer 4 in the somatosensory region (SI) of the mouse cerebral cortex. Brain Res 17:205–242.

Yoshii A, Sheng MH, Constantine-Paton M (2003) Eye opening induces a rapid dendritic localization of PSD-95 in central visual neurons. Proc Natl Acad Sci USA 100:1334–1339.

Appendix 7

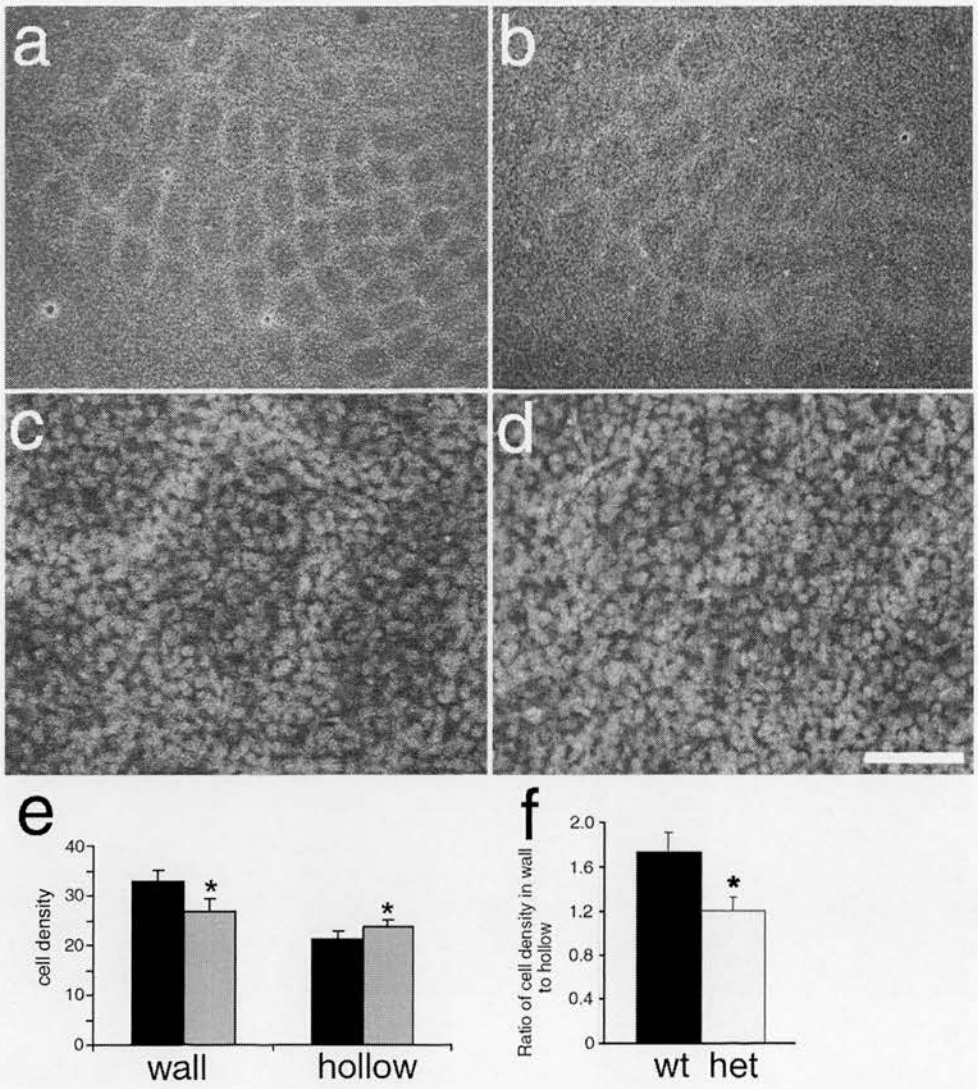

Appendix 7: Reduced cellular segregation in the barrelfield of *Syngap+/-*mice. **a - d,** Propidium iodide staining showing neuronal distribution in flattened tangential sections from WT (**a, c**) and *Syngap+/-* (**b, d**) mice. The images show a clear reduction in the ratio of cells in the barrel wall to barrel hollow in *Syngap+/-* mice (**d**) compared to WT animals (**c**). **e, f,** Cell counts demonstrated a significant decrease ($p<0.01$) in the density of barrel wall neurons and a significant increase ($p<0.01$) in the density of barrel hollow neurons in *Syngap+/-* mice (grey bars) compared to *Syngap+/+* (black bars) mice (**e**). Overall the ratio of cells in barrel B3 wall to barrel B3 hollow is significantly reduced ($p<0.01$) from 1.8 in WT mice to 1.2 in *Syngap+/-* mice (**f**). Scale bar (in **d**): **a, b,** 250μm; **c, d,** 70μm. Error bars represent SE.

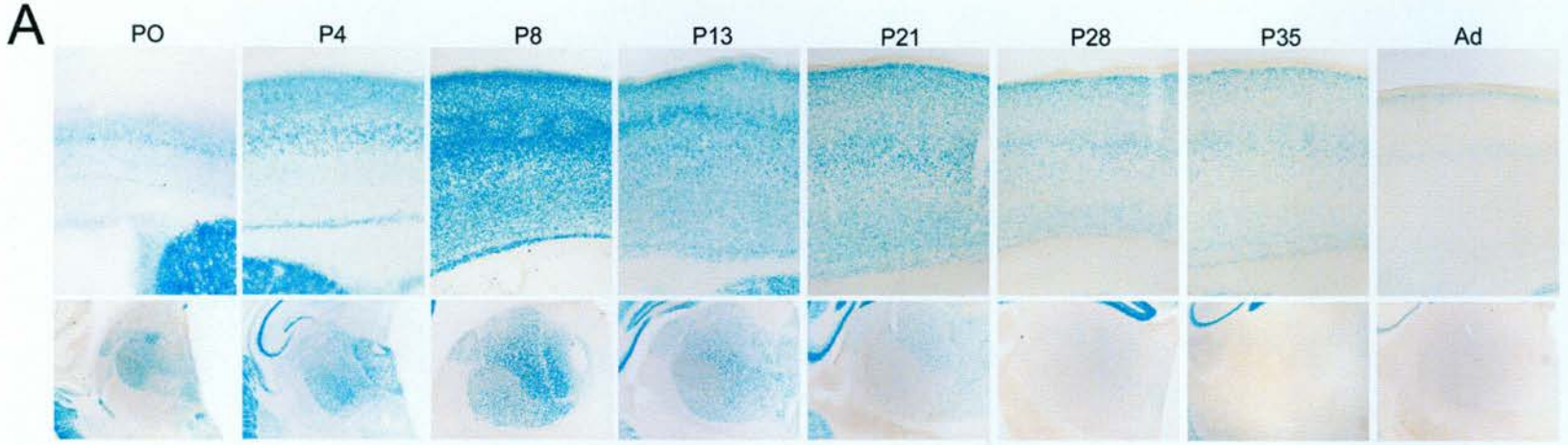

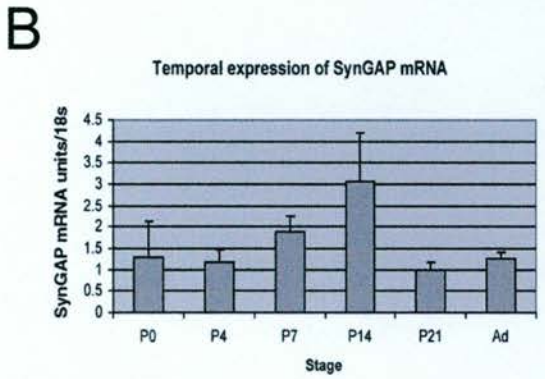

Appendix 8: *Syngap* expression throughout development in S1 and VB. The spatiotemporal expression profile of *Syngap* was examined by taking advantage of the fact that a gene encoding β-gal was inserted into the *Syngap* locus (Komiyama et al., 2002). β-gal staining should reflect levels of *Syngap* mRNA expressed in cells because β-gal transcription is driven by the *Syngap* promoter and translation is driven by an IRES sequence. **A,** In cortex at birth, X-gal staining is seen as a thin dense band at the bottom of the cortical plate. By P4, *Syngap* is clearly expressed through the granular and supragranular layers, but not in the infragranular layers. Between P8 and P21, *Syngap* is highly expresseed thoughout the entire cortex with intense staining in layer IV in bands. From P21 into adulthood, *Syngap* expression is reduced and only two thin bands in upper layer 3 and at the layer 4/5 boundary remain. In thalamus,, X-gal staining is present throughout the dorsal thalamus at birth. *Syngap* expression then increases dramatically in VB between P4 and P8, peaks at P14. Then levels of *Syngap* expression decrease into adulthood when X-gal staining is no longer visible. **B,** Quantitative RT-PCR analysis of *Syngap* mRNA levels in S1 preparations show that *SynGAP* expression peaks during the second postnatal week.

Appendix 9

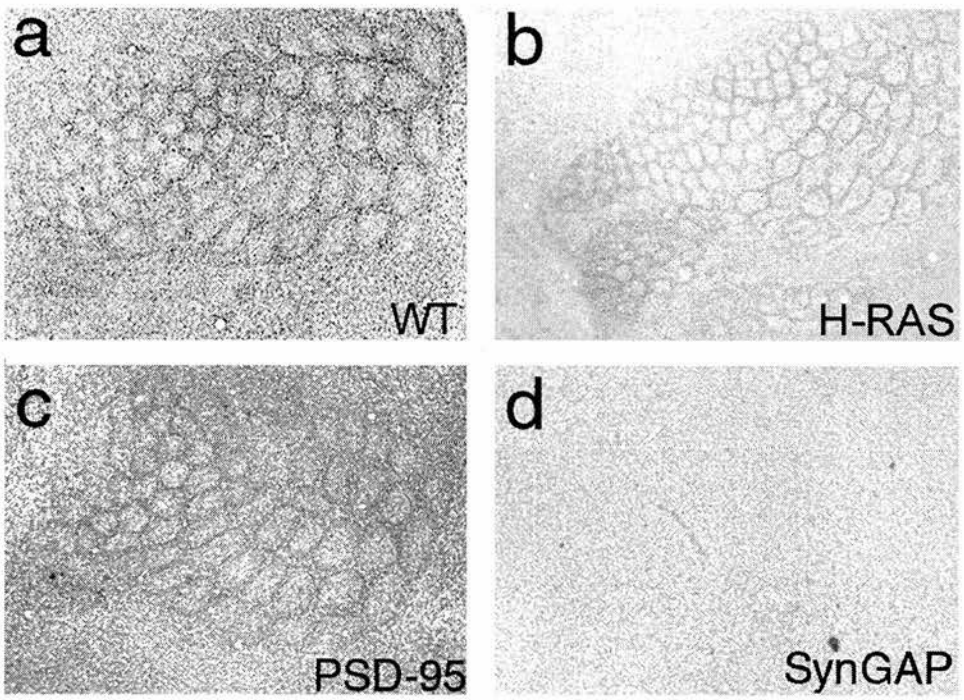

Appendix 9: Barrels form normally in layer IV of mice lacking PSD95 and H-Ras. **a - d,** Nissl stained tangential sections through layer IV of WT (**a**), H-Ras (**b**), PSD95 (**c**), and SynGAP (**d**) mutant mice (Watson et al., 2006).

Appendix 10

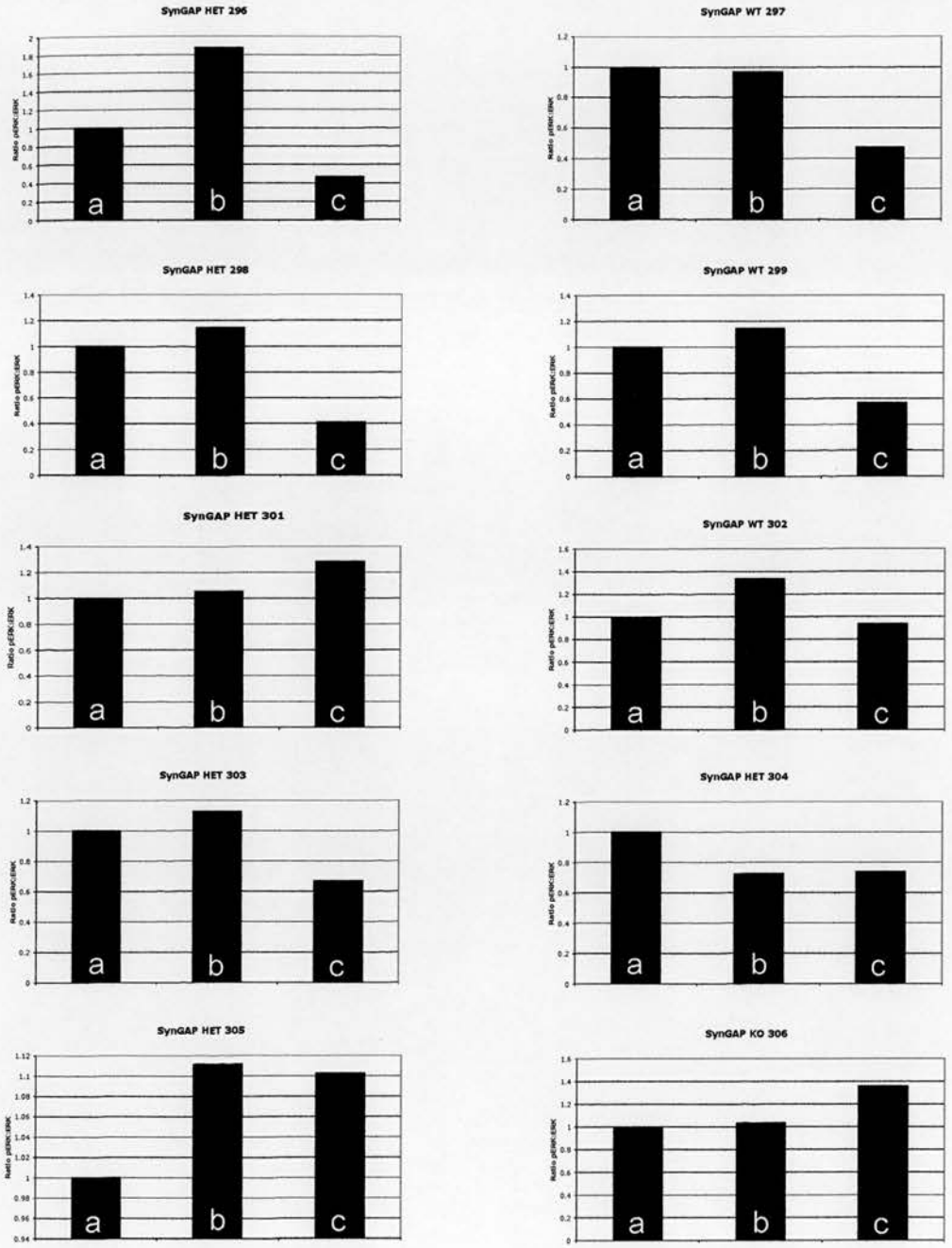

Appendix 10: First set of pharmacological tissue culture experiments using Syngap mutant mice. The graphs represent cortical cell cultures from individual animals (Syngap wt, het and ko mice) treated with 3 different conditions: (a) control - growth media; (b) 50μM Bicuculline diluted in growth media; and c) 50μM Bicuculline + 50μM APV diluted in growth media. The results are highly variable with high levels of basal activity in some of the control wells.

Appendix 11

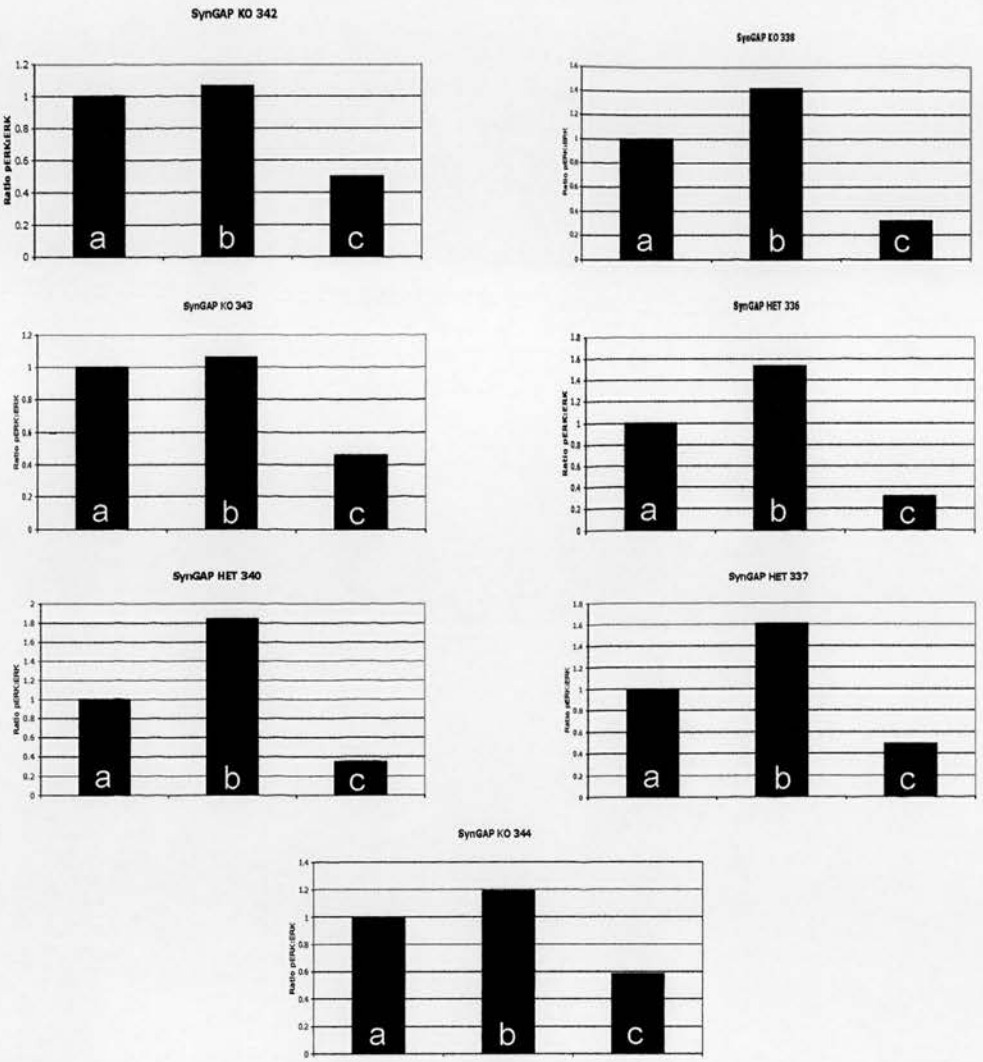

Appendix 11: Second set of pharmacological tissue culture experiments using Syngap mutant mice. The graphs represent cortical cell cultures from individual animals (Syngap het and ko mice) treated with 3 different conditions: (a) control - growth media; (b) 50μM Bicuculline diluted in growth media; and c) 50μM Bicuculline + 50μM APV diluted in growth media. The results are less variable than the first set of pharmacological data in tissue culture. SynGAP hets consistently show activation upon bicuculline application and SynGAP ko cultures consistently show higher levels of basal activity.

Appendix 12:

Kinexus™ Bioinformatics Corporation protein phosphorylation screens - data from KPSS1.3 and KPSS 4.0 screens (burnt on the CD that can be found inside the back cover of this thesis)

Appendix 13:

Affymetrix gene array data (burnt on the CD that can be found inside the back cover of this thesis)

REFERENCES

References

Abbas L (2003) Synapse formation: let's stick together. Curr Biol 13:R25-27.

Abdel-Majid RM, Leong WL, Schalkwyk LC, Smallman DS, Wong ST, Storm DR, Fine A, Dobson MJ, Guernsey DL, Neumann PE (1998) Loss of adenylyl cyclase I activity disrupts patterning of mouse somatosensory cortex. Nat Genet 19:289-291.

Adams JP, Sweatt JD (2002) Molecular psychology: roles for the ERK MAP kinase cascade in memory. Annu Rev Pharmacol Toxicol 42:135-163.

Al-Ghoul WM, Miller MW (1989) Transient expression of Alx-50 immnoreactivity in developing rat neocortex: a marker for naturally occurring neuronal cell death? Brain Res 481(2):361-367

Amieux PS, Cummings DE, Motamed K, Brandon EP, Wailes LA, Le K, Idzerda RL, McKnight GS (1997) Compensatory regulation of RIalpha protein levels in protein kinase A mutant mice. J Biol Chem 272:3993-3998.

Amieux PS, McKnight GS (2002) The essential role of RI alpha in the maintenance of regulated PKA activity. Ann N Y Acad Sci 968:75-95.

Amieux PS, Howe DG, Knickerbocker H, Lee DC, Su T, Laszio GS, Idzerda RL, McKnight GS (2002) Increased basal cAMP-dependent protein kinase activity inhibits the formation of mesoderm-derived structures in the developing mouse embryo. J Biol Chem. 277(30):27294-304

Anderson SA, Kaznowski CE, Horn C, Rubenstein JL, McConnell SK (2002) Distinct origins of neocortical projection neurons and interneurons in vivo. Cereb Cortex 7:702-709

Anderson SA, Eisenstat DD, Sji L, Rubenstein JL (1997) Interneuron migration from basal forebrain to neocortex: dependence on Dlx genes. Science 278:474-476

Antoni FA, Palkovits M, Simpson J, Smith SM, Leitch AL, Rosie R, Fink G, Paterson JM (1998) Ca2+/calcineurin-inhibited adenylyl cyclase, highly abundant in forebrain regions, is important for learning and memory. J Neurosci 18:9650-9661.

Barnett MW, Watson RF, Vitalis T, Porter K, Komiyama NH, Stoney PN, Gillingwater TH, Grant SG, Kind PC (2006) Synaptic Ras GTPase activating protein regulates pattern formation in the trigeminal system of mice. J Neurosci 26:1355-1365.

Bates CA, Killackey HP (1985) The organization of the neonatal rat's brainstem trigeminal complex and its role in the formation of central trigeminal patterns. J Comp Neurol 240:265-287.

Bayer SA and Altman J (1991) Neocortical Development. New York: Raven

Bear MF, Huber KM, Warren ST (2004) The mGluR theory of fragile X mental retardation. Trends Neurosci 27:370-377.

Bear MF, Malenka RC (1994) Synaptic plasticity: LTP and LTD. Curr Opin Neurobiol 4:389-399.

Beaver CJ, Ji Q, Fischer QS, Daw NW (2001) Cyclic AMP-dependent protein kinase mediates ocular dominance shifts in cat visual cortex. Nat Neurosci 4:159-163.

Bengel D, Murphy DL, Andrews AM, Wichems CH, Feltner D, Heils A, Mossner R, Westphal H, Lesch KP (1998) Altered brain serotonin homeostasis and locomotor insensitivity to 3, 4-methylenedioxymethamphetamine ("Ecstasy") in serotonin transporter-deficient mice. Mol Pharmacol 53:649-655.

Bennett-Clarke CA, Leslie MJ, Chiaia NL, Rhoades RW (1993) Serotonin 1B receptors in the developing somatosensory and visual cortices are located on thalamocortical axons. Proc Natl Acad Sci U S A 90:153-157.

Berkeley JL, Levey AI (2003) Cell-specific extracellular signal-regulated kinase activation by multiple G protein-coupled receptor families in hippocampus. Mol Pharmacol 63:128-135.

Binschtok AM, Fleidervish IA, Sprengel R, Gutnick MJ (2006) NMDA receptors in layer 4 spiny stellate cells of the mouse barrel cortex contain the NR2C subunit. J Neurosci 26(2):708-715

Bishop KM, Garel S, Nakagawa Y, Rubenstein JL, O'Leary DD (2003) Emx1 and Emx2 cooperate to regulate cortical size, lamination, neuronal differentiation, development of cortical efferents, and thalamocortical pathfinding. J Comp Neurol 457:345-360

Bishop KM, Rubenstein JL, O'Leary DD (2002) Distinct actions of Emx1, Emx2, and Pax6 in regulating the specification of areas in the developing neocortex. J Neurosci 22:7637-7638

Bishop KM, Goudreau G, O'Leary DD (2000) Regulation of area identity in the mammalian neocortex by Emx2 and Pax6. Science 288:344-349

Bliss TV, Collingridge GL (1993) A synaptic model of memory: long-term potentiation in the hippocampus. Nature 361:31-39.

Bozon B, Kelly A, Josselyn SA, Silva AJ, Davis S, Laroche S (2003) MAPK, CREB and zif268 are all required for the consolidation of recognition memory. Philos Trans R Soc Lond B Biol Sci 358:805-814.

Brandon EP, Idzerda RL, McKnight GS (1997) PKA isoforms, neural pathways, and behaviour: making the connection. Curr Opin Neurobiol 7:397-403.

Brandon EP, Logue SF, Adams MR, Qi M, Sullivan SP, Matsumoto AM, Dorsa DM, Wehner JM, McKnight GS, Idzerda RL (1998) Defective motor behavior and neural gene expression in RIIbeta-protein kinase A mutant mice. J Neurosci 18:3639-3649.

Brandon EP, Zhuo M, Huang YY, Qi M, Gerhold KA, Burton KA, Kandel ER, McKnight GS, Idzerda RL (1995) Hippocampal long-term depression and depotentiation are defective in mice carrying a targeted disruption of the gene encoding the RI beta subunit of cAMP-dependent protein kinase. Proc Natl Acad Sci U S A 92:8851-8855.

Brown KE, Arends JJ, Wasserstrom SP, Zantua JB, Jacquin MF, Woolsey TA (1995) Developmental transformation of dendritic arbors in mouse whisker thalamus. Brain Res Dev Brain Res 86:335-339.

Bulfone A, Smiga SM, Shimamura K, Peterson A, Puelles L, Rubenstein JLR (1995) T-brain-1: A homolog of brachyury whose expression defines molecularly distinct domains within the cerebral cortex. Neuron 15:63:78

Cadd G, McKnight GS (1989) Distinct patterns of cAMP-dependent protein kinase gene expression in mouse brain. Neuron 3:71-79.

Cancedda L, Putignano E, Impey S, Maffei L, Ratto GM, Pizzorusso T (2003) Patterned vision causes CRE-mediated gene expression in the visual cortex through PKA and ERK. J Neurosci 23:7012-7020.

Cases O, Lebrand C, Giros B, Vitalis T, De Maeyer E, Caron MG, Price DJ, Gaspar P, Seif I (1998) Plasma membrane transporters of serotonin, dopamine, and norepinephrine mediate serotonin accumulation in atypical locations in the developing brain of monoamine oxidase A knock-outs. J Neurosci 18:6914-6927.

Cases O, Seif I, Grimsby J, Gaspar P, Chen K, Pournin S, Muller U, Aguet M, Babinet C, Shih JC, et al. (1995) Aggressive behavior and altered amounts of brain serotonin and norepinephrine in mice lacking MAOA. Science 268:1763-1766.

Cases O, Vitalis T, Seif I, De Maeyer E, Sotelo C, Gaspar P (1996) Lack of barrels in the somatosensory cortex of monoamine oxidase A-deficient mice: role of a serotonin excess during the critical period. Neuron 16:297-307.

Catania MV, Tolle TR, Monyer H (1995) Differential expression of AMPA receptor subunits in NOS-positive neurons of cortex, striatum, and hippocampus. J Neurosci 15:7046-7061.

Chan CH, Godinho LN, Thomaidou D, Tan SS, Gulisano M, Parnavelas JG (2001) Emx1 is a marker for pyramidal neurons of the cerebral cortex. Cereb Cortex 11:1191-1198

Chen HJ, Rojas-Soto M, Oguni A, Kennedy MB (1998) A synaptic Ras-GTPase activating protein (p135 SynGAP) inhibited by CaM kinase II. Neuron 20:895-904.

Chiaia NL, Fish SE, Bauer WR, Bennett-Clarke CA, Rhoades RW (1992) Postnatal blockade of cortical activity by tetrodotoxin does not disrupt the formation of vibrissa-related patterns in the rat's somatosensory cortex. Brain Res Dev Brain Res 66:244-250.

Chiaia NL, Fish SE, Bauer WR, Figley BA, Eck M, Bennett-Clarke CA, Rhoades RW (1994) Effects of postnatal blockade of cortical activity with tetrodotoxin upon the development and plasticity of vibrissa-related patterns in the somatosensory cortex of hamsters. Somatosens Mot Res 11:219-228.

Choe ES, Wang JQ (2001) Group I metabotropic glutamate receptors control phosphorylation of CREB, Elk-1 and ERK via a CaMKII-dependent pathway in rat striatum. Neurosci Lett 313:129-132.

Choe ES, Wang JQ (2001) Group I metabotropic glutamate receptor activation increases phosphorylation of cAMP response element-binding protein, Elk-1, and extracellular signal-regulated kinases in rat dorsal striatum. Brain Res Mol Brain Res 94:75-84.

Colledge M, Dean RA, Scott GK, Langeberg LK, Huganir RL, Scott JD (2000) Targeting of PKA to glutamate receptors through a MAGUK-AKAP complex. Neuron 27:107-119.

Colledge M, Scott JD (1999) AKAPs: from structure to function. Trends Cell Biol 9:216-221.

Constantine-Paton M, Cline HT, Debski E (1990) Patterned activity, synaptic convergence, and the NMDA receptor in developing visual pathways. Annu Rev Neurosci 13:129-154.

Crair MC, Malenka RC (1995) A critical period for long-term potentiation at thalamocortical synapses. Nature 375:325-328.

Creutzfeldt OD (1977) Generality of the functional structure of the neocortex. Naturwissenschaften 64:507-517.

Cullen PJ, Lockyer PJ (2002) Integration of calcium and Ras signalling. Nat Rev Mol Cell Biol 3:339-348.

Cybulska-Klosowicz A, Zakrzewska R, Pyza E, Kossut M, Schachner M (2004) Reduced plasticity of cortical whisker representation in adult tenascin-C-deficient mice after vibrissectomy. Eur J Neurosci 20:1538-1544.

Datwani A, Iwasato T, Itohara S, Erzurumlu RS (2002) NMDA receptor-dependent pattern transfer from afferents to postsynaptic cells and dendritic differentiation in the barrel cortex. Mol Cell Neurosci 21:477-492.

De Felipe J, Marco P, Fairen A, Jones EG (1997) Inhibitory synaptogenesis in mouse somatosensory cortex. Cereb Cortex 7:619-634

Defer N, Best-Belpomme M, Hanoune J (2000) Tissue specificity and physiological relevance of various isoforms of adenylyl cyclase. Am J Physiol Renal Physiol 279:F400-416.

Del Rio JA, De Lecea L, Ferrer I, Soriano E (1994) The development of parvalbumin-immunoreactivity in the neocortex of the mouse. Dev Brain Res 81:247-259

Desai AR, McConnell (2000) Progressive restriction in fate potential by neural progenitors during cerebral cortical development. Development 127:2863-2872

Di Cristo G, Berardi N, Cancedda L, Pizzorusso T, Putignano E, Ratto GM, Maffei L (2001) Requirement of ERK activation for visual cortical plasticity. Science 292(5525):2337-2340

Dolen G, Bear MF (2005) Courting a cure for fragile X. Neuron 45:642-644.

Donoghue MJ, Rakic P (1999) Molecular gradients and compartments in the embryonic primate cerebral cortex. Cereb Cortex 9:586-600

Dudek SM, Bear MF (1989) A biochemical correlate of the critical period for synaptic modification in the visual cortex. Science 246:673-675.

Dudek SM, Bowen WD, Bear MF (1989) Postnatal changes in glutamate stimulated phosphoinositide turnover in rat neocortical synaptoneurosomes. Brain Red Dev Brain Res 47:123-128

Dunkley PR, Jarvie PE, Heath JW, Kidd GJ, Rostas JA (1986) A rapid method for isolation of synaptosomes on Percoll gradients. Brain Res 372:115-129.

Ebrahimi-Gaillard A, Guitet J, Garnier C, Roger M (1994) Topographic distribution of efferent fibers originating from homotopic or heterotopic transplants: heterotopically transplanted neurons retain some of the developmental characteristics corresponding to their site of origin. Brain Res Dev Brain Res 77:271-283.

Ebrahimi-Gaillard A, Roger M (1996) Development of spinal cord projections from neocortical transplants heterotopically placed in the neocortex of newborn hosts is highly dependent on the embryonic locus of origin of the graft. J Comp Neurol 365:129-140.

Erzurumlu RS, Kind PC (2001) Neural activity: sculptor of 'barrels' in the neocortex. Trends Neurosci 24:589-595.

Esteban JA, Shi SH, Wilson C, Nuriya M, Huganir RL, Malinow R (2003) PKA phosphorylation of AMPA receptor subunits controls synaptic trafficking underlying plasticity. Nat Neurosci 6:136-143.

Fagni L, Worley PF, Ango F (2002) Homer as both a scaffold and transduction molecule. Sci STKE 2002:RE8.

Farrant M, Feldmeyer D, Takahashi T, Cull-Candy SG (1994) NMDA-receptor channel diversity in the developing cerebellum. Nature 368:335-339.

Feldman DE, Nicoll RA, Malenka RC, Isaac JT (1998) Long-term depression at thalamocortical synapses in developing rat somatosensory cortex. Neuron 21:347-357.

Feldman DE, Nicoll RA, Malenka RC, Isaac JT (1998) Long-term depression at thalamocortical synapses in developing rat somatosensory cortex. Neuron 21:347-357.

Finlay BL, Slattery M (1983) Local differences in the amount of early cell death in neocortex predict adult local specializations. Science 219:1349-1351.

Fischer QS, Beaver CJ, Yang Y, Rao Y, Jakobsdottir KB, Storm DR, McKnight GS, Daw NW (2004) Requirement for the RIIbeta isoform of PKA, but not calcium-stimulated adenylyl cyclase, in visual cortical plasticity. J Neurosci 24:9049-9058.

Flavell SW, Cowan CW, Kim TK, Greer PL, Lin Y, Paradis S, Griffith EC, Hu LS, Chen C, Greenberg ME (2006) Activity-dependent regulation of MEF2 transcription factors suppresses excitatory synapse number. Science 311:1008-1012.

Fox K (1992) A critical period for experience-dependent synaptic plasticity in rat barrel cortex. J Neurosci 12:1826-1838.

Fox K, Schlaggar BL, Glazewski S, O'Leary DD (1996) Glutamate receptor blockade at cortical synapses disrupts development of thalamocortical and columnar organization in somatosensory cortex. Proc Natl Acad Sci U S A 93:5584-5589.

Frantz GD, Bohner AP, Akers RM, McConnell SK (1994) Regulation of the POU domain gene SCIP during cerebral cortical development. J Neurosci 14:472-485

Frantz GD, Weimann JM, Levin ME, McConnell SK (1994) Otx1 and Otx2 define layers and regions in developing cerebral cortex and cerebellum. J Neurosci 14:5725-5740

Frappe I, Roger M, Gaillard A (1999) Transplants of fetal frontal cortex grafted into the occipital cortex of newborn rats receive a substantial thalamic input from nuclei normally projecting to the frontal cortex. Neuroscience 89:409-421.

Fukuchi-Shimogori T, Grove EA (2001) Neocortex patterning by the secreted signaling molecule FGF8. Science 294:1071-1074.

Fukuchi-Shimogori T, Grove EA (2003) Emx2 patterns the neocortex by regulating FGF positional signaling. Nat Neurosci 6:825-831.

Gaillard A, Nasarre C, Roger M (2003) Early (E12) cortical progenitors can change their fate upon heterotopic transplantation. Eur J Neurosci 17:1375-1383.

Gaillard A, Roger M (2000) Early commitment of embryonic neocortical cells to develop area-specific thalamic connections. Cereb Cortex 10:443-453.

Gallagher SM, Daly CA, Bear MF, Huber KM (2004) Extracellular signal-regulated protein kinase activation is required for metabotropic glutamate receptor-dependent long-term depression in hippocampal area CA1. J Neurosci 24:4859-4864.

Garnier C, Arnault P, Ebrahimi-Gaillard A, Letang J, Roger M (1995) The topographic distribution of the efferents from neocortical neurons is not only dependent upon where in the neocortex the cells develop. A transplantation study within one single neocortical region. Brain Res Dev Brain Res 89:1-10.

Garnier C, Arnault P, Roger M (1997) Development of the striatal projection from embryonic neurons from the lateral or medial frontal cortex grafted homo- or heterotopically into the medial frontal cortex of newborn rats. Neurosci Lett 235:41-44.

Gaspar P, Cases O, Maroteaux L (2003) The developmental role of serotonin: news from mouse molecular genetics. Nat Rev Neurosci 4:1002-1012.

Gil OD, Needleman L, Huntley GW (2002) Developmental patterns of cadherin expression and localisation in relation to compartmentalised thalamocortical terminations in rat barrel cortex. J Comp Neurol 453:372-388

Gilbert SF (2000) Developmental Biology – 6th edition. Sinauer Associates

Gille H, Downward J (1999) Multiple ras effector pathways contribute to G(1) cell cycle progression. J Biol Chem 274:22033-22040.

Gilles K, Price D (1993) The fates of cells in the developing cerebral cortex of normal and methylazoxymethanol acetate-lesioned mice. Eur J Neurosci 5:73-84

Glantz SB, Amat JA, Rubin CS (1992) cAMP signaling in neurons: patterns of neuronal expression and intracellular localization for a novel protein, AKAP 150, that anchors the regulatory subunit of cAMP-dependent protein kinase II beta. Mol Biol Cell 3:1215-1228.

Goold RG, Owen R, Gordon-Weeks PR (1999) Glycogen synthase kinase 3beta phosphorylation of microtubule-associated protein 1B regulates the stability of microtubules in growth cones. J Cell Sci 112:3373-3384

Gotz M, Sommer L (2005) Cortical development: the art of generating cell diversity. Development 132:3327-3332

Gotz M, Hartfuss E, Malatesta P (2002) Radial glial cells as neuronal precursors: a new perspective role on the correlation of morphology and lineage restriction in the developing cerebral cortex of mice. Brain Res Bull 57(6):777-88

Grant SGN, Marshall, Page KL, Cumiskey MA, Armstrong JD (2005) Synapse proteomics of multiprotein complexes: en route from genes to nervous system diseases. Hum Mol Genet 14: 225-234

Grant SG, O'Dell TJ (2001) Multiprotein complex signaling and the plasticity problem. Curr Opin Neurobiol 11:363-368.

Greenberg SM, Bernier L, Schwartz JH (1987) Distribution of cAMP and cAMP-dependent protein kinases in Aplysia sensory neurons. J Neurosci 7:291-301.

Greenberg SM, Castellucci VF, Bayley H, Schwartz JH (1987) A molecular mechanism for long-term sensitization in Aplysia. Nature 329:62-65.

Greenough WT, Chang FL (1988) Dendritic pattern formation involves both oriented regression and oriented growth in the barrels of mouse somatosensory cortex. Brain Res 471:148-152.

Grewal SS, Horgan AM, York RD, Withers GS, Banker GA, Stork PJ (2000) Neuronal calcium activates a Rap1 and B-Raf signalling pathway via the cyclic adenosine monophosphate-dependent protain kinase. J Biol Chem 275(5):3722-8

Guidato S, Tsai LH, Woodgett J, Miller CC (1996) Differential cellular phosphorylation of neurofilament heavy side-arms by glycogen synthase kinase-3 and cyclin-dependent kinase-5. J Neurochem 66:1698-1706.

Guillemot F (2005) Cellular and molecular control of neurogenesis in the mammalian telencephalon. Curr Opin Cell Biol 17:639-647.

Hamasaki T, Leingartner A, Ringstedt T, O'Leary DD (2004) Emx2 regulates size and positioning of the primary sensory and motor areas in neocortex by direct specification of cortical progenitors. Neuron 43(3):359-72

Hamori J, Savy C, Madarasz M, Somogyi J, Takacs J, Verley R, Farkas-Bargeton E (1986) Morphological alterations in subcortical vibrissal relays following vibrissal follicle destruction at birth in the mouse. J Comp Neurol 254:166-183.

Hand PJ (1982) Plasticity of the rat cortical barrel system. In: Changing concepts of the nervous system (Morison AR, Strick PL, eds) pp49-68 New York; Academic

Hannan AJ, Blakemore C, Katsnelson A, Vitalis T, Huber KM, Bear M, Roder J, Kim D, Shin HS, Kind PC (2001) PLC-beta1, activated via mGluRs, mediates activity-dependent differentiation in cerebral cortex. Nat Neurosci 4:282-288.

Hannan AJ, Kind PC, Blakemore C (1998) Phospholipase C-beta1 expression correlates with neuronal differentiation and synaptic plasticity in rat somatosensory cortex. Neuropharmacology 37:593-605.

Hardingham N, Fox K (2006) The role of nitric oxide and GluR1 in presynaptic and postsynaptic components of neocortical potentiation. J Neurosci 26:7395-7404.

Harris KM (1999) Calcium from internal stores modifies dendritic spine shape. Proc Natl Acad Sci U S A 96:12213-12215.

Harris RM, Woolsey TA (1982) Dendritic plasticity in mouse barrel cortex following postnatal vibrissae follicle damage. J Comp Neurol 196(3):357-76

Hayashi H (1980) Distributions of vibrissae afferent fiber collaterals in the trigeminal nuclei as revealed by intra-axonal injection of horseradish peroxidase. Brain Res 183:442-446.

Henderson TA, Woolsey TA, Jacquin MF (1992) Infraorbital nerve blockade from birth does not disrupt central trigeminal pattern formation in the rat. Brain Res Dev Brain Res 66:146-152.

Heumann D, Leuba G, Rabinowicz T (1978) Postnatal development of the mouse cerebral neocortex. IV. Evolution of the total cortical volume, of the population of neurons and glial cells. J Hirnforsch 19:385-393.

Heumann D, Leuba G (1983) Neuronal death in the development and aging of the cerebral cortex of the mouse. Neuropathol Appl Neurobiol 9(4):297-311

Hevner RF, Miyashita-Lin E, Rubenstein JL (2002) Cortical and thalamic axon pathfinding defects in Tbr1, Gbx2, and Pax6 mutant mice: evidence that cortical and thalamic axons interact and guide each other. J Comp Neurol 447:8-17.

Heynen AJ, Yoon BJ, Liu CH, Chung HJ, Huganir RL, Bear MF (2003) Molecular mechanism for loss of visual cortical responsiveness following brief monocular deprivation. Nat Neurosci 6:854-862.

Hillen M (2006) Mechanisms Underlying the Postnatal Development of Primary Somatosensory Cortex. University of Edinburgh. Ref Type: Thesis / Dissertation

Ho W, Uniyal S, Meakin SO, Morris VL, Chan BM (2001) A differential role of extracellular signal-regulated kinase in stimulated PC12 pheochromocytoma cell movement. Exp Cell Res 263:254-264.

Howe DG, Wiley JC, McKnight GS (2002) Molecular and behavioural effects of a null mutation in all PKA C beta isoforms. Mol Cell Neurosci 20(3):515-24

Husi H, Grant SG (2001) Proteomics of the nervous system. Trends Neurosci 24:259-266.

Husi H, Grant SG (2001) Isolation of 2000-kDa complexes of N-methyl-D-aspartate receptor and postsynaptic density 95 from mouse brain. J Neurochem 77:281-291.

Husi H, Ward MA, Choudhary JS, Blackstock WP, Grant SG (2000) Proteomic analysis of NMDA receptor-adhesion protein signaling complexes. Nat Neurosci 3:661-669.

Inan M, Lu HC, Albright MJ, She WC, Crair MC (2006) Barrel map development relies on protein kinase A regulatory subunit II beta-mediated cAMP signaling. J Neurosci 26:4338-4349.

Isaac JT, Crair MC, Nicoll RA, Malenka RC (1997) Silent synapses during development of thalamocortical inputs. Neuron 18:269-280.

Iwasato T, Datwani A, Wolf AM, Nishiyama H, Taguchi Y, Tonegawa S, Knopfel T, Erzurumlu RS, Itohara S (2000) Cortex-restricted disruption of NMDAR1 impairs neuronal patterns in the barrel cortex. Nature 406:726-731.

Iwasato T, Erzurumlu RS, Huerta PT, Chen DF, Sasaoka T, Ulupinar E, Tonegawa S (1997) NMDA receptor-dependent refinement of somatotopic maps. Neuron 19:1201-1210.

Iwasato T, Lee L, Ando R, Saito YM, Kanki H, Muglia LJ, Erzurumlu RS, Itohara S (2005) Calcium-stimulated adenylyl cyclase in cortical neurons is not essential for barrel formation in the mouse somatosensory cortex. Society for Neurosciences Abstract 2005 (716.5)

Jacquin MF, Rhoades RW (1987) Development and plasticity in hamster trigeminal primary afferent projections. Brain Res 428:161-175.

Kandel ER, Schwartz JH and Jeesl TM (2000) TheAnatomical Organisation of the Central Nervous System. In Principles of Neural Science. (New York: McGraw-Hill, Health Professions Division) pp.317-336

Katnelson A (2002) Genetic and Epigenetic factors in the Development of the Somatosensory cortex. Oxford University. Ref Type: Thesis/Dissertation

Kennedy MB (1993) The postsynaptic density. Curr Opin Neurobiol 3:732-737.

Kennedy MB (1997) The postsynaptic density at glutamatergic synapses. Trends Neurosci 20:264-268.

Killackey HP (1973) Anatomical evidence for cortical subdivisions based on vertically discrete thalamic projections from the ventral posterior nucleus to cortical barrels in the rat. Brain Res 51:326-331.

Kim JH, Lee HK, Takamiya K, Huganir RL (2003) The role of synaptic GTPase-activating protein in neuronal development and synaptic plasticity. J Neurosci 23:1119-1124.

Kim JH, Liao D, Lau LF, Huganir RL (1998) SynGAP: a synaptic RasGAP that associates with the PSD-95/SAP90 protein family. Neuron 20:683-691.

Kind P, Blakemore C, Fryer H, Hockfield S (1994) Identification of proteins downregulated during the postnatal development of the cat visual cortex. Cereb Cortex 4:361-375.

Kind PC, Kelly GM, Fryer HJ, Blakemore C, Hockfield S (1997) Phospholipase C-beta1 is present in the botrysome, an intermediate compartment-like organelle, and Is regulated by visual experience in cat visual cortex. J Neurosci 17:1471-1480.

Kind PC, Neumann PE (2001) Plasticity: downstream of glutamate. Trends Neurosci 24:553-555.

Klemke RL, Cai S, Giannini AL, Gallagher PJ, de Lanerolle P, Cheresh DA (1997) Regulation of cell motility by mitogen-activated protein kinase. J Cell Biol 137:481-492.

Kneusel I, Elliot A, Chen HJ, Mansuy IM, Kennedy MB (2005) A role for SynGAP in regulating neuronal apoptosis. Eur J Neurosci 21(3):611-621

Komiyama NH, Watabe AM, Carlisle HJ, Porter K, Charlesworth P, Monti J, Strathdee DJ, O'Carroll CM, Martin SJ, Morris RG, O'Dell TJ, Grant SG (2002) SynGAP regulates ERK/MAPK signaling, synaptic plasticity, and learning in the complex with postsynaptic density 95 and NMDA receptor. J Neurosci 22:9721-9732.

Krapivinsky G, Medina I, Krapivinsky L, Gapon S, Clapham DE (2004) SynGAP-MUPP1-CaMKII synaptic complexes regulate p38 MAP kinase activity and NMDA receptor-dependent synaptic AMPA receptor potentiation. Neuron 43:563-574.

Krueger JS, Keshamouni VG, Atanaskova N, Reddy KB (2001) Temporal and quantitative regulation of mitogen-activated protein kinase (MAPK) modulates cell motility and invasion. Oncogene 20:4209-4218.

Lanzetti L, Palamidessi A, Areces L, Scita G, Di Fiore PP (2004) Rab5 is a signalling GTPase involved in actin remodelling by receptor tyrosine kinases. Nature 429:309-314.

Laurent A, Goaillard JM, Cases O, Lebrand C, Gaspar P, Ropert N (2002) Activity-dependent presynaptic effect of serotonin 1B receptors on the somatosensory thalamocortical transmission in neonatal mice. J Neurosci 22:886-900.

Lavdas AA, Grigoriou M, Pachnis V, Parnavelas JG (1999) The medial ganglionic eminence gives rise to a population of early neurons in the developing cerebral cortex. J Neurosci 19:7881-7888

Lebrand C, Cases O, Adelbrecht C, Doye A, Alvarez C, El Mestikawy S, Seif I, Gaspar P (1996) Transient uptake and storage of serotonin in developing thalamic neurons. Neuron 17:823-835.

Lebrand C, Cases O, Wehrle R, Blakely RD, Edwards RH, Gaspar P (1998) Transient developmental expression of monoamine transporters in the rodent forebrain. J Comp Neurol 401:506-524.

Lee LJ, Iwasato T, Itohara S, Erzurumlu RS (2005) Exuberant thalamocortical axon arborization in cortex-specific NMDAR1 knockout mice. J Comp Neurol 485:280-292.

Lemmon MA, Falasca M, Ferguson KM, Schlessinger J (1997) Regulatory recruitment of signalling molecules to the cell membrane by pleckstrin-homology domains. Trends in Cell Biol 7:237-242

Lemmon MA and Ferguson KM (2001) Molecular determinants in pleckstrin homology domains that allow specific recognition of phosphoinositides. Biochemical Society Transactions 29(4):377-384

Lendvai B, Stern EA, Chen B, Svoboda K (2000) Experience-depedndent plasticity of dendritic spines in the developing rat barrel cortex in vivo. Nature 404(6780):876-81

Li W, Okano A, Tian QB, Nakayama K, Furihata T, Nawa H, Suzuki T (2001) Characterization of a novel synGAP isoform, synGAP-beta. J Biol Chem 276:21417-21424.

Li Y, Erzurumlu RS, Chen C, Jhaveri S, Tonegawa S (1994) Whisker-related neuronal patterns fail to develop in the trigeminal brainstem nuclei of NMDAR1 knockout mice. Cell 76:427-437.

Lopez-Bendito G, Molnar Z (2003) Thalamocortical development: how are we going to get there? Nat Rev Neurosci 4:276-289.

Lu HC, Gonzalez E, Crair MC (2001) Barrel cortex critical period plasticity is independent of changes in NMDA receptor subunit composition. Neuron 32:619-634.

Lu HC, She WC, Plas DT, Neumann PE, Janz R, Crair MC (2003) Adenylyl cyclase I regulates AMPA receptor trafficking during mouse cortical 'barrel' map development. Nat Neurosci 6:939-947.

Ludvig N, Ribak CE, Scott JD, Rubin CS (1990) Immunocytochemical localization of the neural-specific regulatory subunit of the type II cyclic AMP-dependent protein kinase to postsynaptic structures in the rat brain. Brain Res 520:90-102.

Luo X, Persico AM, Lauder JM (2003) Serotonergic regulation of somatosensory cortical development: lessons from genetic mouse models. Dev Neurosci 25:173-183.

Ma PM (1993) Barrelettes--architectonic vibrissal representations in the brainstem trigeminal complex of the mouse. II. Normal post-natal development. J Comp Neurol 327:376-397.

Ma PM, Woolsey TA (1984) Cytoarchitectonic correlates of the vibrissae in the medullary trigeminal complex of the mouse. Brain Res 306:374-379.

Ma PM, Woolsey TA (1983) Cytoarchitectonic organization of the brainstem trigeminal nuclei in the mouse: correlation with vibrissal inputs and postnatal development. Soc. Neurosci Abstr 9:922

Ma Y, Pitson S, Hercus T, Murphy J, Lopez A, Woodcock J (2005) Sphingosine activates protein kinase A type II by a novel cAMP-independent mechanism. J Biol Chem 280:26011-26017.

Mackarehtschian K, Lau CK, Caras I, McConnell SK (1999) Regional differences in the developing cerebral cortex revealed by Ephrin A5 expression. Cereb Cortex 9:601-610

Malatesta P, Hartfuss E, Gotz M (2001) Characterisation of CNS precursor subtypes and radial glia. Dev Biol 229(1):15-30

Malenka RC, Nicoll RA (1993) NMDA-receptor-dependent synaptic plasticity: multiple forms and mechanisms. Trends Neurosci 16:521-527.

Malinow R, Malenka RC (2002) AMPA receptor trafficking and synaptic plasticity. Annu Rev Neurosci 25:103-126.

Man HY, Wang Q, Lu WY, Ju W, Ahmadian G, Liu L, D'Souza S, Wong TP, Taghibiglou C, Lu J, Becker LE, Pei L, Liu F, Wymann MP, MacDonald JF, Wang YT (2003) Activation of PI3-kinase is required for AMPA receptor insertion during LTP of mEPSCs in cultured hippocampal neurons. Neuron 38:611-624.

Mandelkow EM, Drewes G, Biernat J, Gustke N, Van Lint J, Vandenheede JR, Mandelkow E (1992) Glycogen synthase kinase-3 and the Alzheimer-like state of microtubule-associated protein tau. FEBS Lett 314:315-321.

Maravall M, Koh IY, Lindquist WB, Svoboda K (2004) Experience-depedndent changes in basal dendritic branching of layer2/3 pyramidal neurons during a critical period for developmental plasticity in rat barrel cortex. Cereb Cortex 14(6):655-664

Marin O, Rubenstein JL (2003) Cell Migration in the forebrain. Annu Rev Neurosci 26:441-483

McCasland JS, Bernardo KL, Probst KL, Woolsey TA (1992) Cortical local circuit axons do not mature after early deafferentation. Proc Natl Acad Sci U S A 89:1832-1836.

McConnell SK, Kaznowski CE (1991) Cell cycle dependence of laminar determination in developing cerebral cortex. Science 254:282-285

Micheva KD, Beaulieu C (1995) Postnatal development of GABA neurons in the rat somatosensory barrel cortex: a quantitative study. Eur J Neurosci 7:419-430.

Micheva KD, Beaulieu C (1996) Quantitative aspects of synaptogenesis in the rat barrel field cortex with special reference to GABA circuitry. J Comp Neurol 373:340-354.

Miller MW (1995) Effect of pre- or postnatal exposure to ethanol on the total number of neurons in the principal sensory nucleus of the trigeminal nerve: cell proliferation and neuronal death. Alcohol Clin Exp Res 19:1359-1363.

Miyashita-Lin EM, Hevner R, Wassarman KM, Martinez S, Rubenstein JL (1999) Early neocortical regionalization in the absence of thalamic innervation. Science 285:906-909.

Momiyama A, Feldmeyer D, Cull-Candy SG (1996) Identification of a native low-conductance NMDA channel with reduced sensitivity to Mg2+ in rat central neurones. J Physiol 494 (Pt 2):479-492.

Monyer H, Burnashev N, Laurie DJ, Sakmann B, Seeburg PH (1994) Developmental and regional expression in the rat brain and functional properties of four NMDA receptors. Neuron 12:529-540.

Monyer H, Sprengel R, Schoepfer R, Herb A, Higuchi M, Lomeli H, Burnashev N, Sakmann B, Seeburg PH (1992) Heteromeric NMDA receptors: molecular and functional distinction of subtypes. Science 256:1217-1221.

Munoz A, Liu XB, Jones EG (1999) Development of metabotropic glutamate receptors from trigeminal nuclei to barrel cortex in postnatal mouse. J Comp Neurol 409:549-566.

Nadarajah B, Parnavelas J (2002) Modes of neuronal migration in the developing cerebral cortex. Nat Rev Neurosci 3:423-432

Neuman T, Keen A, Zuber MX, Kristjansson GI, Gruss P, Nornes HO (1993) Neuronal expression of regulatory helix-loop-helix factor Id2 gene in mouse. Dev Biol 160:186-195

Nguyen VA, Gao B (1999) Cross-talk between alpha(1B)-adrenergic receptor (alpha(1B)AR) and interleukin-6(IL-6) signalling pathways. Activation of alpha(1B)AR inhibits il-6-activated STAT3 in hepatic cells by a p42/44 mitogen-activated protein kinase-dependent mechanism. J Biol Chem 274(50):35492-8

Nicol X, Muzerelle A, Bachy I, Ravary A, Gaspar P (2005) Spatiotemporal localization of the calcium-stimulated adenylate cyclases, AC1 and AC8, during mouse brain development. J Comp Neurol 486:281-294.

Nicol X, Muzerelle A, Rio JP, Metin C, Gaspar P (2006) Requirement of adenylate cyclase 1 for the ephrin-A5-dependent retraction of exuberant retinal axons. J Neurosci 26:862-872.

Niswender CM, Willis BS, Wallen A, Sweet IR, Jetton TL, Thompson BR, Wu C, Lange AJ, McKnight GS (2005) Cre recombinase-dependent expression of a constitutively active mutant allele of the catalytic subunit of protein kinase A. Genesis 43:109-119.

O'Leary DD, Ruff NL, Dyck RH (1994) Development, critical period plasticity, and adult reorganizations of mammalian somatosensory systems. Curr Opin Neurobiol 4:535-544.

Oh JS, Manzerra P, Kennedy MB (2004) Regulation of the neuron-specific Ras GTPase-activating protein, synGAP, by Ca2+/calmodulin-dependent protein kinase II. J Biol Chem 279:17980-17988.

Okabe S, Kim HD, Miwa A, Kuriu T, Okado H (1999) Continual remodeling of postsynaptic density and its regulation by synaptic activity. Nat Neurosci 2:804-811.

Oohira A, Katoh-Semba R, Watanabe E, Matsui F (1994) Brain development and multiple molecular species of proteoglycan. Neurosci Res 20:195-207

Opazo P, Watabe AM, Grant SG, O'Dell TJ (2003) Phosphatidylinositol 3-kinase regulates the induction of long-term potentiation through extracellular signal-related kinase-independent mechanisms. J Neurosci 23:3679-3688.

Orban PC, Chapman PF, Brambilla R (1999) Is the Ras-MAPK signalling pathway necessary for long-term memory formation? Trends Neurosci 22:38-44.

Parnavelas JG (2000) The origin and migration of cortical neurons: new visitas. Trends Neurosci 23:126-131

Parnavelas JG, Nadarajah B (2001) Radial glial cells: are they really glia? Neuron 31:881-884

Peng J, Kim MJ, Cheng D, Duong DM, Gygi SP, Sheng M (2004) Semiquantitative proteomic analysis of rat forebrain postsynaptic density fractions by mass spectrometry. J Biol Chem 279:21003-21011.

Persico AM, Mengual E, Moessner R, Hall FS, Revay RS, Sora I, Arellano J, DeFelipe J, Gimenez-Amaya JM, Conciatori M, Marino R, Baldi A, Cabib S, Pascucci T, Uhl GR, Murphy DL, Lesch KP, Keller F (2001) Barrel pattern formation requires serotonin uptake by thalamocortical afferents, and not vesicular monoamine release. J Neurosci 21:6862-6873.

Petralia RS, Sans N, Wang YX, Wenthold RJ (2005) Ontogeny of postsynaptic density proteins at glutamatergic synapses. Mol Cell Neurosci 29:436-452.

Phillips GR, Huang JK, Wang Y, Tanaka H, Shapiro L, Zhang W, Shan WS, Arndt K, Frank M, Gordon RE, Gawinowicz MA, Zhao Y, Colman DR (2001) The presynaptic particle web: ultrastructure, composition, dissolution, and reconstitution. Neuron 32:63-77.

Pierret T, Lavallee P, Deschenes M (2000) Parallel streams for the relay of vibrissal information through thalamic barreloids. J Neurosci 20:7455-7462.

Pilpel Y, Segal M (2004) Activation of PKC induces rapid morphological plasticity in dendrites of hippocampal neurons via Rac and Rho-dependent mechanisms. Eur J Neurosci 19:3151-3164.

Polleux F, Giger RJ, Ginty DD, Kolodkin AL, Ghosh A (1998) Patterning of cortical efferent projections by semaphorin-neuropilin interactions. Science 282:1904-1906

Porter K, Komiyama NH, Vitalis T, Kind PC, Grant SG (2005) Differential expression of two NMDA receptor interacting proteins, PSD-95 and SynGAP during mouse development. Eur J Neurosci 21:351-362.

Price DJ and Willshaw DJ (2000) Mechanisms of cortical development. Monographs of the Physiological Society 48:9-48 Oxford; New York, Oxford University Press

Rakic P (1972) Mode of cell migration to the superficial layers of fetal monkey neocortex. J Comp Neurol 145:61-83.

Ravary A, Muzerelle A, Darmon M, Murphy DL, Moessner R, Lesch KP, Gaspar P (2001) Abnormal trafficking and subcellular localization of an N-terminally truncated serotonin transporter protein. Eur J Neurosci 13:1349-1362.

Ravary A, Muzerelle A, Herve D, Pascoli V, Ba-Charvet KN, Girault JA, Welker E, Gaspar P (2003) Adenylate cyclase 1 as a key actor in the refinement of retinal projection maps. J Neurosci 23:2228-2238.

Rebsam A, Seif I, Gaspar P (2002) Refinement of thalamocortical arbors and emergence of barrel domains in the primary somatosensory cortex: a study of normal and monoamine oxidase a knock-out mice. J Neurosci 22:8541-8552.

Rebsam A, Seif I, Gaspar P (2005) Dissociating barrel development and lesion-induced plasticity in the mouse somatosensory cortex. J Neurosci 25:706-710.

Redies C, Takeichi M (1993) Expression of N-cadherin mRNA during development of the mouse brain. Dev Dyn 197:26-39

Reid SN, Daw NW, Gregory DS, Flavin H (1996) cAMP levels increased by activation of metabotropic glutamate receptors correlate with visual plasticity. J Neurosci 16:7619-7626.

Rhoades RW, Chiaia NL, Mooney RD, Klein BG, Renehan WE, Jacquin MF (1987) Reorganization of the peripheral projections of the trigeminal ganglion following neonatal transection of the infraorbital nerve. Somatosens Res 5:35-62.

Rice DS, Curran T (2001) Role of the reelin signaling pathway in central nervous system development. Annu Rev Neurosci 24:1005-1039.

Rice FL, Van der Loos H (1977) Development of the barrels and barrel field in the somatosensory cortex of the mouse. J Comp Neurol 171:545-560.

Rigot V, Lehmann M, Andre F, Daemi N, Marvaldi J, Luis J (1998) Integrin ligation and PKC activation are required for migration of colon carcinoma cells. J Cell Sci 111(20):3119-27

Rizo J, Sudhof TC (1998) C2-domains, structure and function of a universal Ca2+-binding domain. J Biol Chem 273:15879-15882.

Rosenblum K, Futter M, Jones M, Hulme EC, Bliss TV (2000) ERKI/II regulation by the muscarinic acetylcholine receptors in neurons. J Neurosci 20:977-985.

Rubin CS (1994) A kinase anchor proteins and the intracellular targeting of signals carried by cyclic AMP. Biochim Biophys Acta 1224(3):467-79

Rudhard Y, Kneussel M, Nassar MA, Rast GF, Annala AJ, Chen PE, Tigaret CM, Dean I, Roes J, Gibb AJ, Hunt SP, Schoepfer R (2003) Absence of Whisker-related pattern formation in mice with NMDA receptors lacking coincidence detection properties and calcium signaling. J Neurosci 23:2323-2332.

Rumbaugh G, Adams JP, Kim JH, Huganir RL (2006) SynGAP regulates synaptic strength and mitogen-activated protein kinases in cultured neurons. Proc Natl Acad Sci 103:4344-4351

Sala C, Futai K, Yamamoto K, Worley PF, Hayashi Y, Sheng M (2003) Inhibition of dendritic spine morphogenesis and synaptic transmission by activity-inducible protein Homer1a. J Neurosci 23:6327-6337.

Salichon N, Gaspar P, Upton AL, Picaud S, Hanoun N, Hamon M, De Maeyer E, Murphy DL, Mossner R, Lesch KP, Hen R, Seif I (2001) Excessive activation of serotonin (5-HT) 1B receptors disrupts the formation of sensory maps in monoamine oxidase a and 5-ht transporter knock-out mice. J Neurosci 21:884-896.

Sans N, Petralia RS, Wang YX, Blahos J, 2nd, Hell JW, Wenthold RJ (2000) A developmental change in NMDA receptor-associated proteins at hippocampal synapses. J Neurosci 20:1260-1271.

Scheffzek K, Ahmadian MR, Wittinghofer A (1998) GTPase-activating proteins: helping hands to complement an active site. Trends Biochem Sci 23:257-262.

Schlaggar BL, Fox K, O'Leary DD (1993) Postsynaptic control of plasticity in developing somatosensory cortex. Nature 364:623-626.

Schlaggar BL, O'Leary DD (1991) Potential of visual cortex to develop an array of functional units unique to somatosensory cortex. Science 252:1556-1560.

Schlaggar BL, O'Leary DD (1993) Patterning of the barrel field in somatosensory cortex with implications for the specification of neocortical areas. Perspect Dev Neurobiol 1:81-91.

Schmitt JM, Stork PJ (2002) PKA phosphorylation of Src mediates cAMP's inhibition of cell growth via Rap1. Mol Cell 9:85-94.

Scott HL, Braud S, Bannister NJ, Isaac JT (2007) Synaptic strength at the thalamocortical input to layer IV neonatal barrel cortex is regulated by protein kinase C. Neuropharmacology 52:185-192.

Shi J, Aamodt SM, Constantine-Paton M (1997) Temporal correlations between functional and molecular changes in NMDA receptors and GABA neurotransmission in the superior colliculus. J Neurosci 17:6264-6276.

Simons DL and Land PW (1987) Early experience of tactile stimulation influences organisation of somatic sensory cortex. Nature 326: 694-697

Skalhegg BS, Huang Y, Su T, Idzerda RL, McKnight GS, Burton KA (2002) Mutation of the Calpha subunit of PKA leads to growth retardation and sperm dysfunction. Mol Endocrinol 16(3):630-9

Skalhegg BS, Tasken K, Hansson V, Huitfeldt HS, Jahnsen T, Lea T (1994) Location of cAMP-dependent protein kinase type I with the TCR-CD3 complex. Science 263:84-87.

Skaliora I, Singer W, Betz H, Puschel AW (1998) Differential patterns of semaphorin expression in the developing rat brain. Eur J Neurosci 10:1215-1229

Snyder EM, Colledge M, Crozier RA, Chen WS, Scott JD, Bear MF (2005) Role for A kinase-anchoring proteins (AKAPS) in glutamate receptor trafficking and long term synaptic depression. J Biol Chem 280:16962-16968.

Spires TL, Molnar Z, Kind PC, Cordery PM, Upton AL, Blakemore C, Hannan AJ (2005) Activity-dependent regulation of synapse and dendritic spine morphology in developing barrel cortex requires phospholipase C-beta1 signalling. Cereb Cortex 15:385-393.

Steffan H, Van der Loos H (1980) Early lesions of mouse vibrissal follicles: their influence on dendrite orientation in the cortical barrelfield. Exp Brain Res 40(4):419-31

Steindler DA, Settles D, Erickson HP, Laywell ED, Yoshiki A, Faissner A, Kusakabe M (1995) Tenascin knockout mice: barrels, boundary molecules, and glial scars. J Neurosci 15:1971-1983.

Suzuki SC, Inoue T, Kimura Y, Tanaka T, Takeichi M (1997) Neuronal circuits are subdivided by differential expression of type-II classic cadherins in postnatal mouse brains. Mol Cell Neurosci 9:433-447

Sweatt JD (2001) The neuronal MAP kinase cascade: a biochemical signal integration system subserving synaptic plasticity and memory. J Neurochem 76:1-10.

Sweatt JD (2004) Mitogen-activated protein kinases in synaptic plasticity and memory. Curr Opin Neurobiol 14:311-317.

Tarpey P, Parnau J, Blow M, Woffendin H, Bignell G, Cox C, Cox J, Davies H, Edkins S, Holden S, Korney A, Mallya U, Moon J, O'Meara S, Parker A, Stephens P, Stevens C, Teague J, Donnelly A, Mangelsdorf M, Mulley J, Partington M, Turner G, Stevenson R, Schwartz C, Young I, Easton D, Bobrow M, Futreal PA, Stratton MR, Gecz J, Wooster R, Raymond FL (2004) Mutations in the DLG3 gene cause nonsyndromic X-linked mental retardation. Am J Hum Genet 75:318-324

Thomas GM, Huganir RL (2004) MAPK cascade signalling and synaptic plasticity. Nat Rev Neurosci 5:173-183.

Tojima T, Kobayashi S, Ito E (2003) Dual role of cyclic AMP-dependent protein kinase in neuritogenesis and synaptogenesis during neuronal differentiation. J Neurosci Res 74(6):829-37

Tomoda T, Kim JH, Zhan C, Hatten ME (2004) Role of Unc51.1 and its binding partners in CNS axon outgrowth. Genes Dev 18:541-558.

Upton L, Katnelson A, Blakemore C, Hannan AJ, Kind PC (in preparation 2007) Normal dendritic complexity and orientation are not sufficient to form barrels in mouse primary somatosensory cortex.

Vanderklish PW, Edelman GM (2002) Dendritic spines elongate after stimulation of group 1 metabotropic glutamate receptors in cultured hippocampal neurons. Proc Natl Acad Sci U S A 99:1639-1644.

Van der Loos (1976) Barreloids in mouse somatosensory thalamus. Neurosci Letters 2:1-6

Van der Loos H and Woolsey TA (1973) Somatosensory cortex: structural alterations following early injury to sense organs. Science 179(71):395-398

Van Zundert, Yoshii A, Constantine-Paton M (2004) Receptor compartmentalization and trafficking at glutamate synapses: a developmental proposal. Trends Neurosci 27:428-437

Vasquez LE, Chen HJ, Sokolova I, Kneusel I and Kennedy MB (2004) SynGAP Regulates Spine Formation. J Neurosci 24(40):8862-8872

Vitalis T, Cases O, Callebert J, Launay JM, Price DJ, Seif I, Gaspar P (1998) Effects of monoamine oxidase A inhibition on barrel formation in the mouse somatosensory cortex: determination of a sensitive developmental period. J Comp Neurol 393:169-184.

Vitalis T, Cases O, Gillies K, Hanoun N, Hamon M, Seif I, Gaspar P, Kind P, Price DJ (2002) Interactions between TrkB signaling and serotonin excess in the developing murine somatosensory cortex: a role in tangential and radial organization of thalamocortical axons. J Neurosci 22:4987-5000.

Vongdokmai R (1980) Effect of protein malnutrition on development of mouse cortical barrels. J Comp Neurol 191:283-294.

Vossler MR, Yao H, York RD, Pan MG, Rim CS, Stork PJ (1997) cAMP activates MAP kinase and Elk-1 through a B-Raf- and Rap1-dependent pathway. Cell 89:73-82.

Wagner U, Utton M, Gallo JM, Miller CC (1996) Cellular phosphorylation of tau by GSK3beta influences tau binding to microtubules and microtubule organisation. J Cell Sci 109:1537-1543

Waite PM, Cragg BG (1982) The peripheral and central changes resulting from cutting or crushing the afferent nerve supply to the whiskers. Proc R Soc Lond B Biol Sci 214:191-211.

Walikonis RS, Jensen ON, Mann M, Provance DW, Jr., Mercer JA, Kennedy MB (2000) Identification of proteins in the postsynaptic density fraction by mass spectrometry. J Neurosci 20:4069-4080.

Waltereit R, Weller M (2003) Signaling from cAMP/PKA to MAPK and synaptic plasticity. Mol Neurobiol 27:99-106.

Wang X, Tang X, Li M, Marshall J, Mao Z (2005) Regulation of neuroprotective activity of myocyte-enhancer factor 2 by cAMP-protein kinase A signaling pathway in neuronal survival. J Biol Chem 280:16705-16713.

Wassarman KM, Lewandoski M, Campbell K, Joyner AL, Rubenstein JL, Martinez S, Martin GR (1997) Specification of the anterior hindbrain and establishment of a normal mid/hindbrain organizer is dependent on Gbx2 gene function. Development 124:2923-2934

Watabe AM, Zaki PA, O'Dell TJ (2000) Coactivation of beta-adrenergic and cholinergic receptors enhances the induction of long-term potentiation and synergistically activates mitogen-activated protein kinase in the hippocampal CA1 region. J Neurosci 20(16):5924-31

Watanabe M, Nakamura M, Sato K, Kano M, Simon MI, Inoue Y (1998) Patterns of expression for the mRNA corresponding to the four isoforms of phospholipase C beta in mouse brain. Eur J Neurosci 10:2016-2025

Watanabe E et al (1996) A membrane-bound heparan sulfate proteoglycan that is transiently expressed on growing axons in the rat brain. J Neurosci Res 44:84-96

Watson RF, Abdel-Majid RM, Barnett MW, Willis BS, Katsnelson A, Gillingwater TH, McKnight GS, Kind PC, Neumann PE (2006) Involvement of protein kinase A in patterning of the mouse somatosensory cortex. J Neurosci 26:5393-5401.

Weeber EJ, Sweatt JD (2002) Molecular neurobiology of human cognition. Neuron 33:845-848.

Welker E, Armstrong-James M, Bronchti G, Ourednik W, Gheorghita-Baechler F, Dubois R, Guernsey DL, Van der Loos H, Neumann PE (1996) Altered sensory processing in the somatosensory cortex of the mouse mutant barrelless. Science 271:1864-1867.

Welker E, Van der Loos H (1986) Quantitative correlation between barrel-field size and the sensory innervation of the whiskerpad: a comparative study in six strains of mice bred for different patterns of mystacial vibrissae. J Neurosci 6:3355-3373.

White EL (1979) Thalamocortical synaptic relations: a review with emphasis on the projections of specific thalamic nuclei to the primary sensory areas of the neocortex. Brain Res 180:275-311

White EL, Weinfeld L, Lev DL (1997) A survey of morphogenesis during the early postnatal period in PMBSF barrels of mouse SmI cortex with emphasis on barrel D4. Somatosens Mot Res 14:34-55.

Wichterle H, Turnbull DH, Nery S, Fishell G, Alvarez-Buylla A (2001) In utero fate mapping reveals distinct migratory pathways and fates of neurons born in the mammalian basal forebrain. Development 128:3759-3771

Wiesel TN, Hubel DH (1963) Effects of visual deprivation on morphology and physiology of cells in the cats lateral geniculate body. J Neurophysiol 26:978-993

Wiesel TN, Hubel DN (1963) Single-cell responses in srtiate cortex of kittens deprived of vision in one eye. J Neurophysiol 26:1003-1017

Winder DG, Martin KC, Muzzio IA, Rohrer D, Chruscinski A, Kobilka B, Kandel ER (1999) ERK plays a regulatory role in induction of LTP by theta frequency stimulation and its modulation by beta-adrenergic receptors. Neuron 24:715-726.

Woolsey TA, Dierker ML, Wann DF (1975) Mouse SmI cortex: qualitative and quantitative classification of golgi-impregnated barrel neurons. Proc Natl Acad Sci U S A 72:2165-2169.

Woolsey TA, Van der Loos H (1970) The structural organization of layer IV in the somatosensory region (SI) of mouse cerebral cortex. The description of a cortical field composed of discrete cytoarchitectonic units. Brain Res 17:205-242.

Woolsey TA, Wann JR (1976) Areal changes in mouse cortical barrels following vibrissal damage at different postnatal ages. J Comp Neurol 170:53-66.

Xiao B, Tu JC, Worley PF (2000) Homer: a link between neural activity and glutamate receptor function. Curr Opin Neurobiol 10:370-374.

Yamakodo M (1985) Postnatal development of barreloid neuropils in the ventrobasal complex of mouse thalamus: a histochemical study for cytochrome oxidase. No To Shinkei 37:497-506

Yoshii A, Sheng MH, Constantine-Paton M (2003) Eye opening induces a rapid dendritic localization of PSD-95 in central visual neurons. Proc Natl Acad Sci U S A 100:1334-1339.

Zamanillo D, Sprengel R, Hvalby O, Jensen V, Burnashev N, Rozov A, Kaiser KM, Koster HJ, Borchardt T, Worley P, Lubke J, Frotscher M, Kelly PH, Sommer B, Andersen P, Seeburg PH, Sakmann B (1999) Importance of AMPA receptors for hippocampal synaptic plasticity but not for spatial learning. Science 284:1805-1811.

Zantua JB, Wasserstrom SP, Arends JJ, Jacquin MF, Woolsey TA (1996) Postnatal development of mouse "whisker" thalamus: ventroposterior medial nucleus (VPM), barreloids, and their thalamocortical relay neurons. Somatosens Mot Res 13:307-322.